Investigations into extracellular ATP signalling and FB1-induced cell death in Arabidopsis thaliana.

TOME, DANIEL,FILIPE,ARAUJO

Investigations into extracellular ATP signalling and FB1-induced cell death in *Arabidopsis thaliana*.

Daniel Filipe de Araújo e Tomé

Thesis submitted in accordance with requirements of
Durham University for the degree of Doctor of Philosophy.

School of Biological and Biomedical Sciences
Durham University

2011

Abstract

Extracellular ATP (eATP) is an important signalling molecule involved in regulation of plant growth and development, interactions with other organisms and responses to several environmental stimuli. The molecular targets mediating the physiological effects of eATP in plants remain to be identified. The work presented in this thesis focuses on identifying the signalling components that underlie the physiological roles of eATP in plants, with a strong emphasis on cell death control.

An *Arabidopsis thaliana* (*Arabidopsis)* cell culture system combined with 2-dimensional difference in-gel electrophoresis (2D-DIGE) and mass spectrometry was used to identify proteins differentially expressed following ATP treatment. Twenty four putative cell death proteins were identified using the cell death-inducing toxin Fumonisin B1 (FB1) in combination with an ATP reversal filter. The potential role of these candidates in eATP-regulated cell death was tested using a variety of cell death assays on *Arabidopsis* T-DNA insertion KO mutants. The mitochondrial ATP synthase β-subunit, AT5G08690, was shown to be a novel cell death gene.

The early effects of eATP on global protein and transcript abundance were also investigated. 2D-DiGE identified 53 proteins differentially regulated by ATP and bioinformatic analysis revealed new effects of eATP on general metabolism. Re-examination of a previously acquired DNA chip experiment that used ATP and FB1 treatments identified 10 genes that are differentially expressed within minutes by eATP that can be used as molecular markers.

2D-DiGE proteomics was also used to investigate the specific toxic effects of FB1 on *Arabidopsis*. A subset of proteins that were specifically regulated by FB1 treatment were tested for a role in FB1-induced cell death using cell death assays on *Arabidopsis* T-DNA insertion KO mutants. The UDP-glucose pyrophosphorylase, AT3G03250, was identified as a cell death gene responsive to FB1.

Table of Contents

Declaration

No material contained herein has been previously submitted for any other degree. Except where specifically acknowledged, all material is the work of the author.

Statement of Copyright

List of Figures

List of Tables

Abbreviations

1D	one-dimensional
2DE	2-Dimensional polyacrylamide gel electrophoresis
ABC	ATP Binding Cassette
ADP	adenosine 5' diphosphate
AMP	adenosine 5' monophosphate
AMP-PCP	adenosine 5'-[(β,γ)-methyleno] triphosphate
APS	ammonium persulphate
Arabidopsis	*Arabidopsis thaliana*
ATP	adenosine 5'triphosphate
ATPaseβ	ATP synthase β-subunit
AU	arbitrary unit
BLAST	basic local alignment search tool
bp	base pairs
BSA	Bovine Serum Albumin
BVA	biological variation analysis
cAMP	cyclic adenosine 3'-5'-monophosphate
CCD	charge-coupled device
cDNA	complementary deoxyribonucleic acid
CHAPS	3-[(3-cholamidopropyl) dimethylammonio]-1-propanesulfonate
cm	centimetre
Col-0	*Arabidopsis thaliana* ecotype Columbia-0
CyDye	cyanine dye
DAVID	Database for Annotation and Visualization of Integrated Discovery
DIA	difference in-gel analysis
DiGE	difference in-gel electrophoresis
DMF	dimethylformamide
DMSO	dimethylsulphoxide
dNTP	deoxynucleoside triphosphate
DNA	deoxyribonucleic acid
DTT	dithiothreitol
ECM	extracellular matrix
EDTA	ethylenediaminetetra-acetic acid
eARP's	eATP-regulated proteins
eATP	Extracellular ATP
EtBr	ethidium bromide
FB1	Fumonisin b_1
g	acceleration due to gravity
gDNA	genomic DNA
GO	Gene Ontology
HCl	hydrochloric acid
HR	Hypersensitive Response
IEF	isoelectric focusing
IPG	immobilised pH gradient
KB	kilobases
KDa	kilo daltons
KEGG	Kyoto Encyclopaedia of Genes and Genomes
KO	knock-out
LB	lysis buffer

M	molar
MALDI-ToF	matrix-assisted laser desorption ionisation time-of-flight
mg	milligrams
ml	millilitre
mm	millimetre
mM	millimolar
MOWSE	Molecular Weight Search
MQ	Milli-Q
mRNA	messenger ribonucleic acid
MS	mass spectrometry
MSMO	Murashig and Skoog basal salts with minimum organics
MS/MS	tandem mass spectrometry
MTT	methyl thiazolyl blue tetrazolium
MW	molecular weight
m/z	mass to charge ratio
n	number of replicates
nahG	salicylate hydroxylase gene expressing
nm	nanometre
NO	nitric oxide
NASC	Nottingham Arabidopsis Stock Centre
OD	optical density
p	significance value
P2X	ionotropic purinoreceptors
P2Y	metabotropic purinoreceptors
PA	Phosphatidic acid
PAMP	pathogen-associated molecular patterns
PCD	Programmed Cell Death
PCR	polymerase chain reaction
pH	hydrogen potential
pI	isoelectric point
PMF	Peptide Mass Fingerprinting
PMT	photon multiplier tube
ppm	parts per million
PR	pathogenesis-related
PSI	pounds per square inch
PTM	post-translational modification
RNA	ribonucleic acid
ROS	Reactive Oxygen Species
RPM	revolutions per minute
SA	salicylic acid
SDS	sodium dodecyl sulphate
SDS-PAGE	sodium dodecyl sulphate polyacrylamide gel electrophoresis
SE	standard error
sqRT-PCR	semi-quantitative reverse-transcriptase coupled polymerase chain reaction
TAE	tris-acetate EDTA
TAIR	The Arabidopsis Information Resource
TEMED	N,N,N',N'-tetramethylethylenediamine
TFA	trifluor acetic acid
Tris	2-amino, 2-(hydroxymethyl) propane 1,3-diol
TSP	Total soluble protein

T-DNA	transfer-DNA
UDP	uridine diphosphate
UGP1	UDP-glucose pyrophosphorylase 1
UTR	untranslated region of a coding mRNA
UTP	uridine triphosphate
UV	ultraviolet
v/v	volume to volume
VPE	vacuolar processing enzyme
w/v	weight to volume
W	watts
µg	micro grams
µl	micro litre
µM	micro molar
µS	micro Siemens

List of Publications

Tomé, D.F.A.§, Chivasa, S.§, Hamilton, J.M., and Slabas, A.R. (2011). Proteomic analysis of extracellular ATP-regulated proteins identifies ATP synthase β–subunit as a novel plant cell death regulator. *Molecular and Cellular Proteomics.* 10(3): M110.003905.

Chivasa, S., Tomé, D.F.A., Murphy, A.M., Hamilton, J.M., Lindsey, K., Carr, J.P., and Slabas, A.R. (2009). Extracellular ATP is a regulator of pathogen defence in plants. *Plant Signalling and Behaviour*. 4:11, 1-3.

Acknowledgments

I am very grateful to Prof. Antoni R. Slabas for his constructive criticism, committed support, and general guidance throughout my Ph.D. His contributions were a good learning experience in helping me grow as a scientist.

I would like to thank the Portuguese Fundação para a Ciência e Tecnologia for awarding me the Ph.D. grant SFRH/BD/28814/2006 that made my Ph.D. possible to pursue.

I would like to thank present and past members of Lab 4/5 for help with preparing reagents, general lab work and for making my Ph.D. experience an enjoyable one. I would like to express my sincere thanks to Dr. Bill Simon and Joanne Robson for help with MALDI-TOF MS protein identification analyses which constituted an important part of my Ph.D.

In particular, I am indebted to Dr. Stephen Chivasa, one of the kindest and most intelligent scientists I have ever met, for invaluable help with 2D-DiGE, general proteomics, experimental design and scientific writing skills. His motivation and love for science no doubt played a part in my choice to pursue a career science. I also wish to thank Dr. John Hamilton for help with multiple aspects of molecular biology, cell death assays, and all the fun times outside the lab. In addition, I extend my sincere thanks to him for giving me access the DNA chip experiment he performed in conjunction with Dr. Stephen Chivasa, Dr. Sean Coughlan and Prof Toni Slabas.

I would like to thank departmental colleagues André, Vipul, Prashant, Vanja, Margarida, Andrei, Tim, Alex, Noha, Claire and Gosia who have become good friends over the years. A special thanks to Bekir for initiating SemiBar in the department, a very enjoyable event that has been running ever since.

Finally, I would like to thank my family and loved ones (you know who you are) for all the love and support during these years, and especially Tanja for all the best reasons in the world.

Chapter 1 Introduction

Plants are sessile organisms exposed to a constantly changing environment during their life cycle. Adaptation requires plants to perceive their surroundings by utilizing a multitude of mechanisms at their disposal. This can involve interaction between receptors present at the plasma membrane that are activated following binding to their respective ligands in the extracellular surface of a cell. Intracellular signalling is initiated and mediates changes in metabolism in response to a ligand. Plants have evolved to sense many types of ligands. These include proteins and their derivatives, carbohydrates and hormones. Recently, extracellular ATP (eATP) has been has been found on the extracellular surface of plant cells and reported to have similar properties to other ligands. Very little is currently known about eATP in plants, although its functions have been well studied in animals, particularly in mammals.

1.1 Discovery of extracellular ATP in animals

The first reports suggesting a physiological role for eATP were the results of experiments in animal systems almost 50 years prior to reports in plants. The first indication that ATP might have an extracellular function came as early as 1929, when experiments involving injection of muscle extracts into guinea pig found that adenosine modulates heart beat (Drury and Szent-Gyorgyi 1929). Later experiments found that ATP is released from undamaged cells upon antidromic stimulation of the rabbit's great auricular nerve, suggesting a role in neurotransmission (Holton 1959). This idea eventually gave rise to the concept of purinergic signalling as the basis for smooth muscle responses to autonomic nerve stimulation that was not blocked by adrenergic receptor antagonists, where eATP could act as a signalling molecule akin to a neurotransmitter (Burnstock 1972). Every neurotransmitter must have degradation and recycling systems to prevent over-stimulation. Released eATP is maintained at low levels through the action of ecto-ATPases, ecto-ADPases and ecto-5'-nucleotidases that break down ATP into adenosine and phosphate that are readily taken up by the cell (Komoszynski and Wojtczak 1996). The final piece of the eATP puzzle was placed when the first ATP receptor was cloned in the early 90's from neural cells (Lustig *et al.,* 1993). The concept of eATP as a signalling molecule became established and this effectively initiated a field that has been expanding ever since, driven mostly by research in animals.

1.2 Release of intracellular ATP

ATP is a molecule not normally found outside of living cells, prompting research into the possible mechanisms that account for its release from living cells. In eukaryotes, ATP is produced inside living cells primarily in the mitochondria via the ATP synthase complex that converts the proton motive force between the mitochondrial matrix and inter-membrane space into chemical energy in the form of phosphodiester bonds between the 3 phosphate groups in ATP (Garrett and Grisham 2010). It is also produced in small quantities during glycolysis by means of substrate level phosphorylation and in plants in the chloroplast during photosynthesis. ATP is highly negatively charged molecule as a consequence of its three negatively charged phosphate groups. Due to its physical characteristics it cannot freely diffuse across the plasma membrane (Chaudry 1982) and therefore can accumulate to high levels inside cells. For many years it was believed that damaged or dead cells with compromised plasma membranes were the main source of ATP release. When ATP was found to be released from neural cells, it was eventually discovered that it is released through synaptic vesicles in the synapse similarly to other neurotransmitters (Bodin and Burnstock 2001). Apart from excitatory tissues, ATP is now known to be released by most types of non-excitatory tissues under resting conditions, as a result of pharmacological stimuli and during mechanical stress (Lazarowski *et al.,* 2003). Three different mechanisms of ATP release have been described in animals. ATP can be secreted by vesicular release (Sorensen and Novak 2001), via plasma membrane maxi-anion channels (Dutta *et al.,* 2004) or transported across the plasma membrane utilizing the ATP Binding Cassette (ABC) multidrug resistant efflux pump P-glycoprotein in symport with a variety of toxic compounds (Abraham *et al.,* 1993). These different mechanisms could all be present in the same cell but primarily utilized under different stimuli. Research into the possible involvement of eATP in physiological responses has yielded numerous roles in many different organisms, especially animals. The functions of eATP in animals and unicellular organisms will be briefly discussed before looking at the current state of knowledge of the eATP field in plants.

1.3 Physiological roles of eATP in animals

The role of eATP in animals is well understood, but very little is known about it in other organisms and in particular in plants. The effects of eATP were initially characterized in animal tissue over 80 years ago (Drury *et al.,* 1929) so it is not surprising that most of its signalling roles and mode of action were obtained from the animal field. Similarly to established neurotransmitters, it was believed that some sort of receptor for eATP existed

as a means to channel signalling initiated at the external surface of the plasma membrane to the inside of the cell where it can affect metabolism. The first eATP receptor was cloned and characterized from mouse neuroblastoma cells (Lustig *et al.,* 1993). It is now known that purinergic signalling is mediated by plasma membrane purinoreceptors and conveys most of the physiological effects of eATP-signalling in animals, although some responses are not mediated by them, such as intracellular acidification of human bronchial epithelium cells (Urbach *et al.,* 2002). Extracellular ATP-mediated purinergic signalling is now known to control several physiological roles in many animal tissues such as the central nervous system, immune system, liver, lungs, kidneys, genital systems and skeletal muscles [reviewed in (Burnstock 2009)].

1.4 Purinoreceptors in animals

In animals, eATP can modulate different physiological processes by initiating signalling events through different membrane receptors. The broadest group of cell-surface nucleotide receptors are called P2 purinoceptors. The letter 'P' indicates that they are activated by purines and by pyrimidines in some cases, and the number '2' discriminates them from G protein-coupled P1 receptors that are specifically activated by adenosine. Extracellular ATP activates ionotropic (P2X) and metabotropic receptors (P2Y) upon binding to their extracellular surface (Figure 1.1). The literature on purinoreceptor structure, pharmacology and physiology is very vast, so it will only be briefly discussed below with particular emphasis of eATP-specific purinoreceptors.

1.4.1 P2X ionotropic receptors

There are 7 distinct P2X receptor subunits: $P2X_1$, $P2X_2$, $P2X_3$, $P2X_4$, $P2X_5$, $P2X_6$ and $P2X_7$ that have protein sequences ranging from 388 to 595 amino acids long (North 2002) and can have distinct tissue localization (Knight 2009). P2X receptors form channels by grouping the same subunits (homomeric channels) or by grouping different subunits together (heteromeric channels). P2X receptors contain intrinsic pores that switch conformation from closed to open upon binding ATP, allowing cations (Na^+, K^+ and Ca^{2+}) to flow into the cell within milliseconds. It is not clear how the energy transferred from ATP binding changes the conformation of each specific P2X, although lysine residues K_{68}, K_{70} and K_{309} are thought to play a significant role in the human $P2X_1$ as well as lysine residues K_{69}, K_{71} in the case of $P2X_2$ (North 2002). Although P2Xs activate cation influx, they do not appear to be redundant and bear specific signalling roles (Chessell *et al.,* 2005).

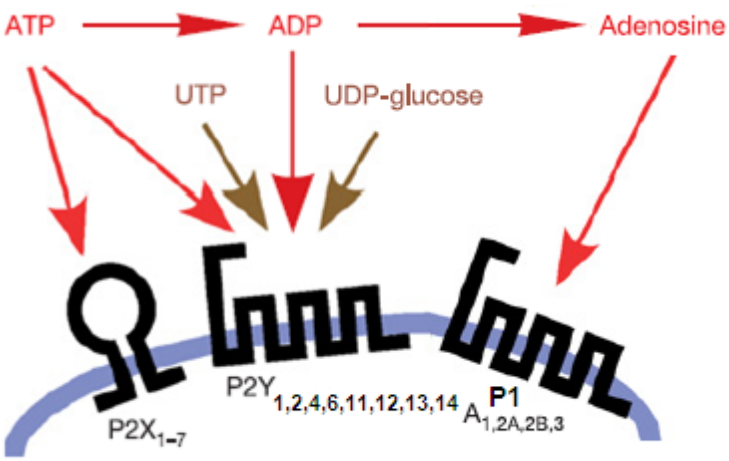

Figure 1.1 Receptors for extracellular nucleotides in mammals. ATP is hydrolyzed in the extracellular space to ADP and then to adenosine by several ecto-enzymes. Seven P2X receptors have been characterized and these are activated specifically by ATP binding. Eight P2Y receptors have been characterized and are activated by different ligands apart from ATP such as ADP, UTP and UDP-glucose. Adenosine activates four distinct P1 receptors (A1, A2A, A2B and A3). Adapted from Khakh and Burnstock (2009).

The influx of cations is a key signalling step, because it changes the overall transmembrane potential as well as local ion concentrations. Much of the current research on P2X's focuses on identifying cell specificity of each receptor and which receptor type mediates a specific response at the cell level, tissue level or whole organism level.

In the central nervous system, significant amounts of ATP are released during repetitive stimulation of neurons (Wieraszko and Seifert 1984). It is therefore not surprising that all types of P2X receptors subunits are present in these cells. The functional role of P2X receptors in the central nervous system might be related to their ability to trigger Ca^{2+} influx. In sensory nerve pathways, the change in membrane potential brought about by P2X activation initiates electrical impulses that mediate several neural responses, such as the sensation of pain (Tsuda *et al.,* 2003; Chessell *et al.,* 2005) and taste (Finger *et al.,* 2005). P2X receptors can also modulate downstream signalling responses such as mitogen-activated protein kinase (MAPK) signalling and gene expression changes in genes involved in inflammation responses (Potucek *et al.,* 2006).

Of specific interest are $P2X_7$ receptors, which appear to play a role in cell death activation. $P2X_7$ receptors differ from other P2X in their long C-terminal region containing several protein-protein interaction motifs, have relatively high eATP requirements for activation (≥ 100 μM) and high affinity to the non-hydrolysable ATP analogue 2',3'-(benzoyl-4-benzoyl)-ATP (North 2002). Evidence for a link with cell death activation came from initial reports suggested $P2X_7$ stimulation triggers membrane permeabilization, that results in uptake of large molecules like fluorescent dyes ethidium bromide (EtBr) and YO-PRO-1 (North, 2002), and membrane blebbing, a morphological marker of apoptosis, in human embryonic kidney cells expressing the rat $P2X_7$ receptor (Virginio *et al.,* 1999). Unknown signalling mediated by $P2X_7$ receptors rather than direct mechanistic action from them appears to be how $P2X_7$ receptors modulate these responses (Elliott *et al.,* 2005). Recently, several reports have linked $P2X_7$ receptors with apoptotic cell death regulation in the immune system (Chen and Brosnan 2006) and epithelia cells (Gorodeski 2009).

1.4.2 P2Y metabotropic receptors

Mammalian P2Y receptors are coupled to intracellular second-messenger systems through heteromeric G-proteins that are found in most mammalian tissues, especially in the central nervous system. Signalling from the exterior of the cell is commenced when the agonist binds to the exterior surface of P2Y, stimulating an exchange of guanosine diphosphate

(GDP) for guanosine triphosphate (GTP) on the G-protein subunit Gα of the heterotrimer complex, consisting of subunits Gα, Gβ and Gγ, in the internal surface of the plasma membrane. This results in the dissociation of the heterotrimer into Gα and a Gβγ subunit dimer. Once free, Gα and the Gβγ initiate downstream signalling events. Unlike P2X receptors, P2Y have 7 transmembrane domains and physically interact with G-proteins (Abbracchio *et al.,* 2006). Eight P2Y have been characterized and are divided into two distinct families based on specific properties of their downstream signalling mechanism (Harden *et al.,* 2010). $P2Y_1$, $P2Y_2$, $P2Y_4$, $P2Y_6$, and $P2Y_{11}$ initiate second messenger signalling via the G-protein $G\alpha_q$ and activate phospholipase C (PLC). PLC breaks down phosphatidylinosytol 4,5-bisphosphate to form inositol 1,4,5-trisphosphate, that stimulates the release of calcium from intracellular stores, and diacylglycerol, that activates protein kinase C. $P2Y_{12}$, $P2Y_{12}$, $P2Y_{14}$ initiate second messenger signalling via the G-protein $G\alpha_{i/o}$ and inhibit adenlyate cyclise activity and cAMP-mediated secondary messenger signalling. In contrast to P2X receptors, which are all specifically activated by ATP, P2Y receptors are activated by ATP, ADP, UTP and UDP-glucose. For example, $P2Y_2$ is equally activated by ATP and UTP. Only $P2Y_{11}$ is specifically activated by ATP and its non-hydrolysable analogues (Communi *et al.,* 1997) and its role in mediating eATP signalling will be discussed in more detail.

$P2Y_{11}$ is unique among P2Y purinoreceptors as it is the only one that is activated specifically by ATP and the only P2Y receptor to have an intron in its DNA coding sequence (Communi *et al.,* 2001). Activation of $P2Y_{11}$ stimulates downstream activation of PLC, production of inositol 1,4,5-trisphosphate and elevation of cytosolic calcium (White and McGeown 2003). It is also responsible for ATP-mediated elevation of cAMP via G-protein $G\alpha_s$ (Qi *et al.,* 2001). $P2Y_{11}$ has signalling roles in differentiation of certain human cell types. For example, $P2Y_{11}$ is present in human HL-60 cells and is upregulated following treatments that induce cellular differentiation, such as granulocytic differentiation mediated by the granulocyte colony-stimulating factor (Communi *et al.,* 2001). Interestingly, ATP has been shown to specifically induce differentiation of HL-60 cells into neutrophil-like cells (Packham *et al.,* 1996) and this is mediated by downstream increases in cAMP concentrations as a result of $P2Y_{11}$ activity (Conigrave *et al.,* 1998). ATP has also been shown to modulate differentiation of human dendritic cells via $P2Y_{11}$ activity (Wilkin *et al.,* 2001). Some signal transduction processes initiate nuclear gene expression. Among the $G\alpha_s$-linked receptors, only $P2Y_{11}$ is known to activate gene

expression via activation of the cAMP response element-binding transcription factor (CREB), resulting in upregulation of specific proteins, such as thrombospondin-1 (Marteau *et al.,* 2005), and specific cytokines such as interleukin 12 (Wilkin *et al.,* 2001) in human dendritic cells. Most of the effects of eATP signalling, at least in mammals, are now known to be mediated by purinoreceptors.

1.4.3 Purinoreceptors in other organisms

The effects of purines have been documented on a wide range of organisms. Until recently, P2 receptors were thought to be restricted to vertebrates (Burnstock 2009), however they have now been identified in several lower organisms. A P2X receptor bearing 25.8% to 36.6% sequence identity to human P2Xs, depending on which P2X is used in making the comparison, has been identified in the trematode worm *Schistosoma mansoni* (Agboh *et al.,* 2004). Recently an intracellular P2X receptor was identified in the social amoeba *Dictyostelium discoideum* (Fountain *et al.,* 2007). It was found to be located in the membranes of contractile vacuoles and is thought to be directly involved in osmoregulation instead of purinergic signalling. Later, a plasma membrane ionotropic receptor was identified also in *Dictyostelium discoideum* suggesting that this organism has purinergic signalling (Ludlow *et al.,* 2008). More recently, a purinoreceptor (named *OtP2X*) similar to ionotropic receptors has been identified in the unicellular algae *Ostreococcus tauri* (Fountain *et al.,* 2008). Expression of *OtP2X* protein in human HEK293 cells resulted in appearance of a functional ATP-gated channel. However, experiments designed to identify the function of *OtP2X* in native *Ostreococcus tauri* have failed to show what this receptor modulates (Fountain *et al.,* 2008). *OtP2X* provides evolutionary clues that purinoreceptors might be present in plants, because *Ostreococcus tauri* is very close to the evolutionary origin of photosynthetic plants (Derelle *et al.,* 2006).

1.5 Extracellular ATP in unicellular organisms

Few studies have addressed the effects of eATP in unicellular organisms. This might have been the result of sceptical views from the scientific community that the release of a high energy compound, such as ATP, could not be beneficial to unicellular organisms. Many species of gram-positive and gram-negative bacteria actively secrete ATP into the surrounding medium upon attachment to a new substrate (Ivanova *et al.,* 2006). Ivanova and co-workers (2006) surveyed 86 heterotrophic bacteria for release of ATP during attachment to either a hydrophilic or a hydrophobic substrate. Levels as high as 10 μM of

eATP were measured in the surrounding bacterial medium. It is not clear if eATP plays a role during attachment or is a consequence of the change in metabolism as bacteria start to produce a biofilm. eATP levels have also been found to modulate antibiotic production and morphology in the filamentous soil bacteria *Streptomyces* (Li *et al.,* 2008). A glucose-dependent ATP efflux has been documented in yeast (Boyum and Guidotti 1997). This efflux was not a result of non-specific permeability of the plasma membrane or cell lysis but its biological significance is not clear. In unicellular ciliates *Paramecium* and *Tetrahymena*, eATP is known to depolarize the plasma membrane and elicit a behaviour response termed the avoidance response, where the cells swim away from high concentrations of eATP in a zigzag fashion (Hennessey 2005). The mechanism appears to require the activity of an ATP receptor, since ATP was found to be physically bound to the plasma membrane and animal ATP receptor antagonists altered the physiological response of the ciliates to ATP. In the amoeba *Dictyostelium discoideum,* eATP can elicit external calcium influx. It was initially believed that eATP initiated this response via extracellular kinase-mediated phosphorylation of plasma membrane proteins (Parish and Weibel 1980), but it was later shown that direct eATP binding to plasma membrane calcium channels mediated the calcium influx (Ludlow *et al.,* 2008). The understanding of eATP effects is still poorly understood in unicellular organisms compared to animal systems, especially mammals.

1.6 Extracellular ATP in plants

1.6.1 Early research

As ATP was being proposed as an extracellular signal molecule in animals (Burnstock 1972), research being performed on plants demonstrated that exogenously applied ATP produced physiological changes. In the 1970's, it was shown that addition of extracellular ATP resulted in a faster closing of the Venus flytrap (Jaffe 1973), stimulated the production of endonucleases in *Avena* leaves (Udvardy and Farkas 1973) and stimulated potassium uptake in maize (Lüttge *et al.,* 1974). These studies did not show that the observed effects of ATP addition could derive from a signalling role of eATP. Instead, they hypothesized that ATP was providing cellular energy or chelating divalent cations rather than directly performing a signalling role. With hindsight, it is now clear that these studies were the first to show evidence for a signalling role of eATP in plants.

1.6.2 eATP is a true biological phenomenon in plants

eATP has now been shown to exist in the extracellular matrix (ECM) of plants. It was first detected using the firefly luciferase assay in the leaf surface of *Arabidopsis thaliana* (henceforth *Arabidopsis)* seedlings grown in sterile conditions (Thomas *et al.,* 2000). There were some concerns about this report because if cells had been accidentally damaged during collection of leaf surface fluid, contamination of intracellular ATP could account for the ATP detected. Later, it was confirmed that eATP originates from inside of undamaged living cells. Chivasa and co-workers (Chivasa *et al.,* 2005a) showed that *Arabidopsis* cell cultures treated with radiolabel inorganic phosphate, $[^{32}P]H_3PO_4$, secrete radiolabel eATP to the cell media within 1 hour. Finally, live imaging of eATP in the tips of growing root hairs was achieved by treating *Medicago* roots with a cellulose binding domain-luciferase fusion construct (Kim *et al.,* 2006b).

There are now many examples of where eATP has been detected in the ECM of living plants, pointing towards a ubiquitous nature of ATP release. During normal growth and development, eATP is spontaneously released to the ECM from a variety of plant tissues. eATP has been detected in *Arabidopsis* cell cultures (Chivasa *et al.,* 2005a), in growing root hairs of *Medicago* (Kim *et al.,* 2006b), in growing fibres of cotton (*Gossypium hirsutum*) ovule cultures (Clark *et al.,* 2010a) and in growing pollen tubes of *Arabidopsis* (Wu *et al.,* 2007). eATP is also released as a response to abiotic and biotic stress stimuli. eATP is released following osmotic stress of 300 mM and 100 mM NaCl in *Arabidopsis* seedlings (Jeter *et al.,* 2004; Kim *et al.,* 2009). Touch and mechanical stress also stimulates ATP release to the ECM in *Arabidopsis* seedlings (Jeter *et al.,* 2004) and in *Arabidopsis* root tips (Weerasinghe *et al.,* 2009). Severe mechanical stress can result in wounding of cells and passive release of intracellular ATP in the ECM. This was suggested from studies in *Arabidopsis* using oligogalacturonic acid (Jeter *et al.,* 2004) and confirmed in a later study to have a physiological role in generating reactive oxygen species [ROS (Song *et al.,* 2006)]. Plant pathogens and their elicitors also stimulate ATP release. The fungal polysaccharide chitin is capable of eliciting high amounts of ATP release in *Medicago* roots (Kim *et al.,* 2006b). In *Salvia miltiorrhiza* hairy roots cultures, ATP release was observed following treatment with a polysaccharide fraction of yeast extract (Wu *et al.,* 2008a). Similarly to chitin, this showed that an unknown polysaccharide elicitor(s) from yeast can trigger ATP release. Recently, the mycotoxin beauvericin, produced by several fungal species that infect major crop plants, was also found to elicit ATP release from

wheat seedling before they died (Srobarova *et al.,* 2009). Apart from passive ATP release via cell lysis, these studies show that plants must have tightly regulated mechanisms for controlling the release of ATP during specific situations they encounter during growth and development.

1.6.3 ATP release mechanisms in plants

The presence and controlled release of ATP in the ECM indicates that plants must possess specific release mechanisms. Although eATP can arise following wounding (Song *et al.,* 2006), this release is uncontrolled and should not be considered a specific mechanism. Release mechanisms were suspected to be similar to animals' and they are now known to exist in plants. Members of the ABC the *mdr1* P-glycoprotein, is a integral membrane transporter that is known to mediate toxin efflux in animal tumour cells (Gottesman and Pastan 1988) and this mechanism is coupled with ATP efflux (Abraham *et al.,* 1993). The P-glycoprotein might also mediate ATP efflux in yeast (Boyum *et al.,* 1997). The plant homologue of *mdr1*, *atPGP1*, was cloned into yeast and yeast cells overexpressing this protein displayed increase eATP release into the medium (Thomas *et al.,* 2000). *Arabidopsis* plants overexpressing this gene showed higher concentrations of eATP and were more resistant to cycloheximide (Thomas *et al.,* 2000). Although, P-glycoprotein appears to mediate a simport efflux of toxins and ATP, the release of ATP might be a consequence of the specific mechanism of toxin efflux by ABC transporters rather than the ultimate goal of these transporters. The physiological significance of this mechanism in non-toxin resistance context is unclear.

In plants, ATP can also be released through vesicular exocytosis. Studies of rapidly expanding tissues have provided evidence that exocytosis is probably the most important release mechanism. Studies in *Medicago* using the cellulose binding domain-luciferase fusion construct showed that eATP was present in higher concentrations at the tips of rapidly growing root hairs (Kim *et al.,* 2006b). The plasma membrane of root hairs expands through fusion of intracellular vesicles that release their contents into the ECM upon fusion with the plasma membrane. Treatment of roots with Brefeldin A, a general inhibitor of vesicular transport, resulted in a reduction of eATP concentrations (Kim *et al.,* 2006b). The shoot tip of *Arabidopsis* seedling is also an area of active growth where eATP levels similar to root tips have been measured (Weerasinghe *et al.,* 2009), and these high levels might be the result of ATP release via vesicle fusion with the plasma membrane. The physiological significance of ATP secretion via exocytosis and ABC transporters on

calcium influx was directly tested in *Arabidopsis* seedlings harbouring reconstituted aequorin (Tanaka *et al.,* 2010). Brefeldin A treatment successfully blocked calcium influx whereas 1-naphthylphthalamic acid, an inhibitor of ABC transporters belonging to the multidrug resistance-like P-glycoprotein subclass, had no effect (Tanaka *et al.,* 2010). This clearly showed that exocytosis is an important ATP release mechanism in plants.

1.6.4 Physiological eATP concentrations in plants

Although ATP exists in the plant ECM, the actual concentrations that plants encounter during growth and development are still unknown. This is an important question because it will allow the identification of concentrations that are physiologically meaningful from excessive ones that are unlikely to occur *in vivo*. It will also allow a more critical view on the results already in the literature obtained with a wide range of nucleotide concentrations. Several eATP concentrations have been measured using the luciferase assay from different plant tissues in unstressed conditions. ATP has been reported to accumulate at the leaf surface of *Arabidopsis* seedlings at a concentration of 60 pMol/cm^2 (Thomas *et al.,* 2000). A concentration as high as 40 μM has been reported at wounding sites in *Arabidopsis* leaves (Song *et al.,* 2006). Extracellular ATP concentrations of 20 nM have been measured in the surrounding medium from a single *Arabidopsis* seedling, ~10 nM in actively growing regions and ~1 nM in non-growing regions of seedlings (Weerasinghe *et al.,* 2009). Clark and co-workers (Clark *et al.,* 2010a) have reported eATP concentrations of 300 nM in the media surrounding cotton fibres. In tobacco, guttation fluid collected from the leaf surface when plants are maintained at high humidity concentrations had an eATP concentration of 200 nM (Chivasa *et al.,* 2010). The concentrations reported must be carefully considered because there are several technical limitations that could produce underestimated or overestimated eATP concentrations. eATP concentrations in the bulk medium of *in vitro* tissues, such as cell cultures or cotton fibres, are dependent on the density of the cells in the medium as well as the degree of mechanical stress they are under, since mechanical stress results in ATP release (Jeter *et al.,* 2004). Apoplastic fluid collected from leaf tissue undergoing guttation is likely to be heavily diluted with water originating from the vascular system. Collection of apoplastic fluid without resorting to guttation is problematic because any damage to cells would result in contamination with intracellular ATP, resulting in an overestimation of eATP concentrations. If the real concentrations of eATP in plants are close to the currently reported values, then they would be similar to eATP values reported in animal tissues (Lazarowski *et al.,* 2003).

Further evidence for this comes from studies on extracellular apyrases, enzymes that specifically degrade eATP. *Arabidopsis* apyrase 1 and 2 have Michaelis constant (K_m) values of 26 and 30 μM respectively (Steinebrunner *et al.,* 2000). These values are similar to animal apyrases, suggesting eATP concentrations in plants could be similar to animals on the assumption that eATP is largely controlled by apyrases, but this is still unclear. In order to maintain eATP concentrations at normal physiological levels, plants must employ regulatory mechanisms to prevent significant fluctuations over time.

1.6.5 Mechanisms for regulation of eATP levels

ATP released into the ECM eventually has to be recycled back into the cell to avoid significant losses of stored energy, in the form of ATP itself, and phosphate. Even though ATP is constantly released in growing cells, eATP concentrations are kept at stable levels. This is due to the activity of extracellular NTPDases (nucleoside triphosphate diphosphohydrolases). Several types exist, such as acid and alkaline phosphatases, but members of the apyrase family are the best studied in plants. Ecto-apyrases are catalytically active in the ECM (Plesner 1995) and are membrane-bound proteins that regulate eATP levels by sequentially hydrolyzing the phosphate groups of ATP and ADP producing AMP and inorganic phosphate (Komoszynski *et al.,* 1996). Apyrases have been investigated mostly in legume species and most are membrane bound due to a transmembrane domain in their N-terminus, although they can also be soluble (Handa and Guidotti 1996). The *Arabidopsis* genome contains seven members of this family, but only *AtAPY1* and *AtAPY2* have been shown to act extracellularly on eATP (Steinebrunner *et al.,* 2000; Jeter and Roux 2006). Transgenic *Arabidopsis* over expressing the pea apyrase *psNTP9* have increased biomass when supplemented with ATP in the medium, demonstrating the role of apyrases in recycling the phosphate groups of eATP (Thomas *et al.,* 1999). In potato, a cell wall-bound apyrase has been characterized and found to work in combination with extracellular phosphatases and a cell wall-bound adenosine nucleosidase in a complete salvage mechanism of eATP (Riewe *et al.,* 2008b). In potato, ATP is broken down into adenine, ribose and inorganic phosphate that are recycled back into the cell by specific membrane transporters (Riewe *et al.,* 2008b). The turn-over speed of eATP is not known and is likely to differ from tissue to tissue. However, the half-life of eATP in the bulk medium of *Arabidopsis* seedling has been estimated to be 180 minutes, with a hydrolysis rate of 2.8 fmol/min (Weerasinghe *et al.,* 2009), although the authors point out that the hydrolysis is likely to be greatly underestimated.

It is not clear how plants avoid significant loss of eATP into the surrounding environment, especially in roots where there is no physical barriers between the plant ECM and the surrounding soil. Using *in vitro* systems such as cell suspension cultures, eATP levels in the bulk medium are kept at fairly low concentrations. It should be noted that eATP levels in the bulk medium result from diffusion of eATP and the levels of eATP at the cell surface (pericellular ATP) are likely to be much higher. In mammalian cells, the plasma membrane-associated adenylate kinase together with radiolabelled [^{3}H]AMP, was used as a sensor for pericellular ATP concentrations *in vivo* (Yegutkin *et al.,* 2006). The study found that levels of eATP at the plasma membrane are up to 1000-fold higher than in the bulk medium and remain constant over time. If such a scenario happens in plants, it would indicate the presence of an apyrase-resistant ATP pool that would not contribute to the bulk medium ATP concentration. However, it is not known if high pericellular ATP concentrations are present in plants. The ubiquitous presence of eATP in plants suggests a mechanism for its detection if eATP is to have a physiological role.

1.6.6 Possible mechanisms underlying eATP perception in plants

Unlike in animals, not much is known about how eATP is perceived in plants. One of the major questions in the field is: what is the eATP receptor(s)? There are two main possibilities for explaining how eATP is detected. Firstly, eATP is being used to modulate the kinome and phosphatome network of plant ECM via extracellular kinases and phosphatases, and secondly, it is directly binding to soluble or plasma-membrane bound receptor protein(s) in the plant ECM similarly to animal purinoreceptors. There are reports in support of both possibilities but the identity of the receptor(s) in both scenarios remains elusive.

Numerous phosphorylated proteins have been detected in the cell wall of *Arabidopsis* cell cultures (Chivasa *et al.,* 2002; Ndimba *et al.,* 2003) and of maize cultures (Chivasa *et al.,* 2005b), indicating that eATP could be used to phosphorylate extracellular proteins, presumably by the action of kinases. Some ECM proteins can be dephosphorylated following *Fusarium* elicitor treatment (Chivasa *et al.,* 2005b), illustrating active *in vivo* regulation of the ECM phosphoproteome. A phosphorylation-dependent post-translational modification (PTM) of an ATP receptor protein could be part of the mechanism of eATP sensing. However, the target protein(s) and ecto-kinases in this hypothesis have yet to be identified. In addition to ECM-bound proteins, eATP has been shown to bind to soluble ECM proteins (Chivasa *et al.,* 2007). A protein fraction obtained from the culture filtrate of

cell cultures was incubated with ^{32}P-labelled azido-ATP that binds specifically to ATP binding domains. Illumination with UV light irreversibly cross-links the ATP to its binding protein and these can then be detected through the radiolabel phosphate. These findings clearly show that proteins in the ECM reversibly bind ATP. No plasma membrane-bound ATP binding proteins that bind ATP at the extracellular surface have yet been identified, but bioinformatics has provided preliminary evidence for possible receptor-like kinase transmembrane proteins located at the plasma membrane (Chivasa *et al.,* 2007).

There is considerably more evidence for eATP sensing via purinoreceptors-like proteins in plants. This was first suggested from pharmacological studies on the effects of eATP on calcium influx which showed that addition of extracellular purines (ATP and ADP) and their non-hydrolysable analogues increases cytosolic free calcium ($[Ca^{2+}]_{cyt}$) (Demidchik *et al.,* 2003). This effect can be blocked by calcium channel blockers as well as the general animal P2 receptor antagonists pyridoxalphosphate- 6-azophenyl-2',4'-disulfonic acid (PPADS) and suramin on *Arabidopsis* roots (Demidchik *et al.,* 2003). The antagonistic effects of suramin and PPADS on eATP-mediated signalling have also been shown in other *Arabidopsis* tissues and plant species (Wu *et al.,* 2008a; Clark *et al.,* 2010b; Tonon *et al.,* 2010). Additionally, other animal P2 antagonists reactive blue, Evans blue and TNP-ATP also block the effects of eATP-mediated increase in $[Ca^{2+}]_{cyt}$ (Wu *et al.,* 2008a; Clark *et al.,* 2010b; Tanaka *et al.,* 2010), providing evidence for purinoreceptor activity in plants.

There is specific evidence that both P2X-like and P2Y-like receptors are present in plants. Evidence in support of P2X-like receptors arises from studies showing that ATP and ADP do not produce the same effects. For example, exogenously applied ATP is twice as efficient at increasing $[Ca^{2+}]_{cyt}$ than ADP in *Arabidopsis* roots (Demidchik *et al.,* 2003), only ATP addition can prevent cell death in *Arabidopsis* cell cultures (Chivasa *et al.,* 2005a), only ATP induces significant accumulation of nitric oxide (NO) (Foresi *et al.,* 2007) and phosphatidic acid (PA) (Sueldo *et al.,* 2010). Other results suggest the activity of P2Y-like metabotropic receptors in plants (Figure 1.1). Uridine triphosphate (UTP), a specific ligand of some P2Y receptors in animals, is capable of increasing $[Ca^{2+}]_{cyt}$ similarly to ATP, although at very high concentrations (Demidchik *et al.,* 2003). Other studies have shown that ATP and ADP can produced the same effects on the cell. For example, ATP and ADP were equally effective at depolarizing *Arabidopsis* root hairs (Lew and Dearnaley 2000) and triggering ROS accumulation (Song *et al.,* 2006). Studies using non-hydrolysable ATP (ATPγS) and ADP (ADPβS) analogues demonstrated that these

analogues were equally effective in increasing $[Ca^{2+}]_{cyt}$ in *Arabidopsis* seedlings (Jeter *et al.,* 2004), and modulating root growth (Clark *et al.,* 2010b). Adenosine monophosphate (AMP) and AMPαS on the other hand, consistently produced no effect in all studies performed, indicating that the 2 terminal phosphates in ATP and ADP are critical for the signalling role of ATP and ADP.

Tanaka and co-worker (Tanaka *et al.,* 2010) have recently suggested the presence of multiple receptors with different affinities for different nucleotides, both purines and pyrimidines, similarly to animal P2Y metabotropic receptors. Besides P2-like receptors, extracellular annexins have also been proposed as eATP sensors due to their ATP binding properties and the ability to transport calcium across membranes *in vitro* but this has not been experimentally tested yet (Shang *et al.,* 2009).

Regardless of the true mechanism of eATP perception, there is now strong evidence that this occurs at the plasma membrane (Demidchik *et al.,* 2009). Protoplasts derived from root epidermis cells expressing the calcium reporter aequorin were shown to respond to external ATP by increasing in $[Ca^{2+}]_{cyt}$. This response was blocked by P2 antagonists, suggesting plasma-membrane located P2-like receptors. The authors were careful to mention that the involvement of the plasma membrane was only shown for root epidermis cells and that this should not be generalized for all cell types, since the activity of ECM proteins might be required in other tissues. So far, this is the strongest experimental evidence for purinoreceptor homologues in plants.

Although there has been intense bioinformatic searches for plant homologues of purinoreceptors in plants since the publication of the *Arabidopsis* genome (AGSC 2000), these have not yet been successful. Bioinformatic searches based on sequence similarity to animal purinoreceptors sequences have not yielded good candidates (Kim *et al.,* 2006a; Moriyama *et al.,* 2006; Gookin *et al.,* 2008). Searches based on the sequence of the intracellular P2X receptor identified the unicellular algae *Ostreococcus tauri,* which only shares ~28% identity with all human P2X receptors, have also been unsuccessful (Fountain *et al.,* 2008). This is intriguing because the presence of purinoreceptors in distant groups of organisms suggests they appeared early on in evolution (Burnstock 2009). However, they could be heavily modified in plants, which could explain why bioinformatic searches based on sequences from other organisms have not produced a credible candidate so far.

Some research suggests plants might have used eATP as a signalling molecule for a long time because they share common mechanistic features with algae (Clark and Roux 2009). The macroalga *Dasycladus vermicularis* can release ATP when damaged and this ATP can initiate ROS production (Torres *et al.,* 2008) similarly to plants (Song *et al.,* 2006). The unicellular alga *Ostreococcus lucimarinus*, that belongs to a group of algae close to the evolutionary origin of photosynthetic plants (Derelle *et al.,* 2006), has one putative apyrase gene in its genome that phylogenetic analysis showed to cluster with *Arabidopsis* extracellular apyrases that have a role in regulating eATP levels (Steinebrunner *et al.,* 2000), possibly suggesting a common origin (Clark *et al.,* 2009). Little is known about the physiological processes which are regulated by eATP in plants and what is known is a patchwork of isolated reports, many of them performed on different plant species and tissues.

1.6.7 Physiological processes under eATP control

It is now widely accepted that ATP is released into the plant ECM and that it modulates specific physiological processes essential for plant growth and development. There is now evidence linking eATP signalling to plant growth control in roots, pollen and other plant tissues, plant-pathogen interactions and defence responses and regulation of plant cell viability.

1.6.7.1 Root gravitropism

One of the first physiological effects shown to be modulated by eATP was root gravitropism (Tang *et al.,* 2003), a response that enables roots to grow straight down into the soil. Seedlings grown on agar medium supplemented with 2 mM ATP or higher showed significant primary root curling and increased lateral root induction. Importantly, the effects were specific to ATP since inosine triphosphate (ITP), AMP or inorganic phosphate were incapable of eliciting the same phenotype. Seedlings grown on plain agar transferred into agar containing ATP and bent 90 degrees were unable to re-orientate their root tip to grow straight down. The effects of ATP were linked to accumulation of auxin at the root tip by inhibiting shootward auxin transport (Tang *et al.,* 2003). Although the concentrations of eATP used (≥ 2 mM) are probably not physiologically relevant, they provided initial evidence for a signalling role for eATP in obstacle avoidance in roots.

1.6.7.2 Thigmotropism

Thigmotropism is the orientation of growth in response to mechanical contact. This response usually requires unequal growth within the same organ. When roots grow into the soil, they constantly encounter obstacles they must circumvent. Previous research showed that mechanical stress stimulates ATP release (Jeter *et al.,* 2004) and that tips of growing roots hairs actively secrete ATP (Kim *et al.,* 2006b). Using the ATP reporter system (Kim *et al.,* 2006b), ATP release at a root tip was found to be asymmetrical when roots comes into contact with an obstacle (Weerasinghe *et al.,* 2009). When a root was touched on one side, ATP is released through the root tip, but this released is prolonged on the opposite side from which it was touched. This side was the one that the root eventually bent to enable growth around the obstacle, probably as a consequence of asymmetrical auxin transport. During continuous touch stimulation, there is a refractory period for ATP release of 9.3 minutes, probably to prevent excessive ATP from being released after signalling had been initiated. The G-protein double KO mutant *agb1-2,gpa1-4*, that does not express the Gα and Gβ subunits, was found to have impaired asymmetrical ATP release and refractory period (Weerasinghe *et al.,* 2009). This indicates that thigmotropism requires the activity of a functional G-protein complex but the mechanism by which G-proteins intersect with eATP signalling is unclear.

1.6.7.3 Plant growth

Several studies have implicated eATP perception as an essential component in the control of plant growth. The best studied tissues so far are pollen tubes and root hairs, both good models of tip-growth. Studies on *Arabidopsis* KO plants for the extracellular apyrases *APY1* and *APY2* provided the first evidence for the role of eATP in modulating pollen tube growth (Steinebrunner *et al.,* 2003). Single KO lines for either apyrase displayed no significant phenotype, but double KO plants produced sterile pollen and no double KO seed could be produced. This effect appears to be related to increased eATP levels in the pollen ECM in the absence of these apyrases, since abolishment of wildtype pollen germination was achieved by germinating pollen in agar supplemented with ≥2 mM ATP (Steinebrunner *et al.,* 2003). In a later study, double KO *apy1/apy2* plants were generated using a complementation strategy involving a dexamethasone-inducible promoter to enable seed production of double KO plants (Wu *et al.,* 2007). These plants were dwarf, had reduced root and hypocotyls length and were sterile. Further characterization of stable

apyrase double KO lines overexpressing apyrase under the control of a pollen specific promoter, revealed several developmental defects including lack of functional root and shoot meristems and cell pattern and shape abnormalities in the cotyledons (Wolf *et al.,* 2007). These findings might indicate a more ubiquitous role of eATP in plant growth and development. Overexpression of *APY1* in *Arabidopsis* results in faster hypocotyl growth rates whereas inhibition of apyrase activity in wild type plants, either by using a specific apyrase inhibitor or an apyrase antibody, incurred in reduced pollen germination while simultaneously increasing eATP levels (Wu *et al.,* 2007). The effects of ATP on pollen are mediated by NO signalling because NO signalling agonists promoted the effects of ATPγS on pollen tube germination and elongation (Reichler *et al.,* 2009). Treatment of nitrate reductase double mutant *nai1nai2* with inhibitory concentrations of ATPγS resulted in no significant change in pollen germination rates, indicating that a significant source of NO production induced by ATPγS is mediated by nitrate reductases (Reichler *et al.,* 2009). Extracellular ATP is also important in controlling root hair growth. The first indication that extracellular nucleotides might affect growth came from studies in *Arabidopsis* root hairs, where application of exogenous ADP caused increase elongation rates (Lew *et al.,* 2000). *In vivo* visualization of eATP showed that ATP is actively secreted at the tips of growing *Medicago* root hairs (Kim *et al.,* 2006b). The treatment of root tips with apyrase severely inhibited their growth due to depletion of eATP levels, directly implicating eATP in growth regulation (Kim *et al.,* 2006b).

The effects of eATP on plant growth are not limited to specialized growth in tip-growing tissues such as pollen tubes and root hairs. Initial research showed that *Arabidopsis* seedlings overexpressing the pea apyrase *psNTP9* supplemented with 0.3 mM concentrations of ATP displayed enhanced growth rates (Thomas *et al.,* 1999). However, this was due to increased phosphate uptake, since the same transgenic seedlings supplemented with inorganic phosphate also displayed increased growth rates. General growth retardation has been observed in *Arabidopsis* apyrase double KO mutants (Wolf *et al.,* 2007) and in transgenic potato plants silenced for the apyrase family genes using an RNA interference silencing approach (Riewe *et al.,* 2008a). When apyrase genes were only silenced in the potato tuber, this resulted in increased number of tubers with higher starch content but with lower average weight, probably due to increased transcription of cell wall and starch related genes (Riewe *et al.,* 2008a). In cotton fibres derived from cultured ovules, increased eATP levels appear to modulated fibre growth (Clark *et al.,* 2010a).

Treatment of fibres with low concentrations (30 μM) of ATPγS increased fibre growth but higher concentrations (150 μM) inhibited growth. Inhibition of the cotton ectoapyrases *GhAPY1* and *GhAPY2*, proteins highly similar to *Arabidopsis APY1* and *APY2*, either by using apyrase inhibitors or apyrase antibodies, also inhibited fibre growth due to elevated eATP concentrations (Clark *et al.,* 2010a). In etiolated *Arabidopsis* seedlings, the inhibitory effects of reducing agents on elongation rates are reversed by ATP treatment (Tonon *et al.,* 2010). In an attempt to take onboard all the literature on the subject, it was proposed that the effects of ATP on growth follow a bell-shaped curved (Roux and Steinebrunner 2007). In this model, depletion of eATP levels causes growth retardation and sterility (Kim *et al.,* 2006b; Wu *et al.,* 2007) and even death (Chivasa *et al.,* 2005a). Similarly, when high levels of eATP are present, achieved by ATP addition, blocking of apyrase activity or by treating plants with non-hydrolysable ATP analogues, growth retardation is also observed (Steinebrunner *et al.,* 2003; Wolf *et al.,* 2007; Wu *et al.,* 2007; Reichler *et al.,* 2009; Clark *et al.,* 2010a; Clark *et al.,* 2010b). There are some studies that suggest a bell-shaped curve for the effects of ATP, such as the production of undecylprodigiosin in *Streptomyces coelicolor* (Li *et al.,* 2008), and ADPβS on root hair growth (Clark *et al.,* 2010b). However, the effects of high ATP concentrations on growth remain poorly understood. In some of these studies, high levels of ATP were mimicked by using the non-hydrolysable ATP analogue ATPγS instead of ATP. The application of high levels (1 mM) of another analogue adenosine 5'-[(β,γ)-methyleno] triphosphate (AMP-PCP), kills plant cells instead of just inhibiting growth (Chivasa *et al.,* 2005a; Chivasa *et al.,* 2010). Whereas it is true that ATP analogues correctly mimic high levels of ATP in situations where ATP binding is required, these analogues also block events requiring ATP hydrolysis, which would not be inhibited by high levels of ATP. Extrapolation of the effects of high ATP levels on growth based on experimentation using ATP analogues should be considered with care. The results of manipulating extracellular apyrase activity should also be carefully considered. Although it is true that blocking apyrase activity, either by using specific inhibitors or antibodies, causes increased levels of eATP *in vivo* (Wu *et al.,* 2007; Clark *et al.,* 2010a) the possibility that apyrases might have other biological roles apart from their function in hydrolyzing eATP should also be considered. This is supported by the extreme dwarf phenotype of apyrase double KO mutants, which suggest multiple developmental roles for apyrases (Wolf *et al.,* 2007). The effects of ATP on growth are almost certainly different between different plant tissues. For example, the stimulating effects of ATPγS on growth are mediated by NO and can be blocked by 1 μM

of the NO scavenger carboxy-PTIO (cPTIO). Plant growth is unaffected by cPTIO in root hairs (Clark *et al.,* 2010b) but is inhibited in elongating hypocotyls (Tonon *et al.,* 2010), suggesting different regulatory mechanisms between the tissues.

1.6.7.4 Plant-microbe interactions

The connection between eATP signalling and the interactions of plants with microbes should come as no surprise. The environment surrounding a plant is a mixture of beneficial and pathogenic microbes that the plant must interact with during its life cycle. This is especially relevant in the roots, where no thick physical barrier separates the plant ECM from the surrounding soil environment. Therefore, eATP levels can be altered by the dynamic interaction between the plant and its surrounding microbes and it is only natural that eATP could have evolved into an important signalling component between plants and microbes. It is now clear that eATP is important in regulating defence responses to plant pathogens and in symbiosis interactions in legumes.

Plants have evolved defence responses that are activated upon recognition of specific molecules produced by pathogens termed pathogen-associated molecular patterns (PAMPs) which could be proteins, carbohydrates or toxins of various natures (Jones and Dangl 2006). Initial evidence of a possible connection between eATP and plant pathogens originates from studies showing that PAMPs can trigger ATP release. This phenomenon has been observed in *Medicago* roots treated with chitin (Kim *et al.,* 2006b), *Salvia miltiorrhiza* hairy roots cultures treated with yeast extract (Wu *et al.,* 2008a) and wheat seedlings following treatment with the mycotoxin beauvericin (Srobarova *et al.,* 2009). It was initially thought that the ATP released following PAMP recognition could be acting as an extracellular signalling cue that positively regulates pathogen defence responses (Song *et al.,* 2006). This hypothesis was based on observations that eATP can rapidly induce ROS accumulation, an essential component of defence responses to pathogens (Torres *et al.,* 2006), and transcriptionally activate genes that encode for enzymes critical for the synthesis of defence-related hormones salicylic acid (SA), jasmonic acid and ethylene (Song *et al.,* 2006). A later study elegantly showed that eATP actually acts as a negative regulator of plant defence (Chivasa *et al.,* 2009a). Prolonged exposure to high levels of ATP attenuated SA- and tobacco mosaic virus-induced expression of pathogenesis-related (PR) proteins, classical markers for activation of defence responses (Feys and Parker 2000). ATP does this by antagonizing basal SA accumulation. Correlatively, prolonged

treatment with AMP-PCP, a non-hydrolysable ATP analogue, was sufficient to induce PR expression. Moreover, plants treated with ATP were more susceptible to *Pseudomonas syringae* and tobacco mosaic virus disease whereas plants treated with AMP-PCP showed enhanced resistance (Chivasa *et al.,* 2009a).

There is growing evidence that eATP might play a role in signalling events in the symbiotic relationship between rhizobia and legume plant hosts. Indirect evidence for this role comes from studies of ecto-apyrases on nodulation. An ECM localized lectin expressed in root nodules of the legume *Dolichos biflorus* was characterized as having apyrase activity, hydrolyzing both ATP and ADP (Etzler *et al.,* 1999). Antisera raised against this lectin significantly inhibited root nodulation by rhizobia, indicating that either its Nod-binding or its apyrase activity is critical for the nodulation process. In soybean, the GS52 ectoapyrase is induced within hours following inoculation with the symbiont *Bradyrhizobium japonicum* and apyrase specific antisera can inhibit nodulation (Day *et al.,* 2000). Overexpression of soybean GS52 in the legume *Lotus japonicus* resulted in higher levels of nodulation (McAlvin and Stacey 2005) and RNAi silencing of GS52 resulted in reduced levels of nodulation (Govindarajulu *et al.,* 2009). These observations suggest that eATP levels inversely correlate with the degree of infection of symbiotic bacteria, if eATP concentrations are primarily regulated by apyrases in legume plants. This would be in agreement with the role of eATP as a negative regulator defence responses (Chivasa *et al.,* 2009a) in the sense that nodulation events, although beneficial to the plant due to increased nitrogen uptake, are conducted by bacteria that express PAMPs and activate defence responses designed to restrict their growth. Therefore, increased apyrase activity in root nodules can lower eATP levels locally and enable the beneficial bacteria to grow.

From the examples described, it is clear that eATP is recognized by plants and plays a role in several physiological processes. From research in the animal field, it would be expected that eATP mediates these processes by initiating some sort of downstream signalling events. Very little is known about the role of second messenger signalling in eATP signalling, although several different signalling molecules have been implicated.

1.6.8 The signalling role of eATP in plants

There is now considerable evidence for a signalling role of eATP in plants. Extracellular ATP can trigger a wide variety of second messenger signalling molecules. Up to date these

include intracellular calcium ($[Ca^{2+}]_{cyt}$), reactive oxygen species (ROS), such as superoxide (O_2^-), hydrogen peroxide (H_2O_2) and nitric oxide (NO), cyclic guanosine monophosphate (cGMP), and phosphatidic acid (PA). The first evidence that extracellular ATP could be a signalling molecule came from studies in *Arabidopsis* roots showing that several nucleotides, including ATP, trigger membrane depolarization (Lew *et al.,* 2000). This data suggested eATP was capable of triggering ion fluxes across the membrane, but the authors found no changes in $[Ca^{2+}]_{cyt}$. Later studies unquestionably show that $[Ca^{2+}]_{cyt}$ is modulated by eATP concentrations.

1.6.8.1 eATP triggers calcium signalling

Free calcium is an extensively studied second messenger that mediates the regulation of a wide range of cellular processes in all living organisms (Clapham 2007). Because of its ubiquitous nature, early research for a possible signalling role of eATP focused on measuring calcium levels. The first evidence that eATP could trigger $[Ca^{2+}]_{cyt}$ came from studies in *Arabidopsis* plants overexpressing the aequorin calcium reporter protein in the cytosol (Demidchik *et al.,* 2003). ATP concentrations as low as 300 nM were capable of producing measurable increases in $[Ca^{2+}]_{cyt}$. This increase was shown to require calcium channels because the ATP response could be abolished by adding the non-specific calcium channel blocker gadolinium (Gd^{3+}). A later study using the same *Arabidopsis* aequorin expressing plants showed that the non-hydrolysable analogues ATPγS and ADPβS triggered an increase in $[Ca^{2+}]_{cyt}$ in the roots (Jeter *et al.,* 2004). Using the calcium chelator 1,2-bis(o-aminophenoxy)ethane- N,N,N9,N9-tetraacetic acid (BAPTA), the authors were able to block calcium influx triggered by ATP treatment, suggesting that the calcium being mobilized originated from the ECM. This data, in addition to the fact that AMPαS is unable to trigger the increases in $[Ca^{2+}]_{cyt,}$ provided further clues as to a plasma membrane localization of the channel(s) being activated by both ATP and ADP. Increases in $[Ca^{2+}]_{cyt}$ has been shown in *Salvia miltiorrhiza* hairy root cultures in response to ATP and this can also be inhibited by using calcium channel blockers and calcium chelators (Wu *et al.,* 2008a). These studies demonstrated the effects of eATP on calcium signalling at the whole organism or tissue level.

Recently, eATP has been shown to elicit an increase in $[Ca^{2+}]_{cyt,}$ specifically in root epidermis cells devoid of cell wall (Demidchik *et al.,* 2009). This is the first report of the effects of eATP at a specific cell level. The authors also showed that eATP-mediated

hyperpolarization of the plasma membrane requires Ca^{2+} conductance via an unknown Ca^{2+} permeable channel that is a prime candidate for an ATP receptor. Although previous research was indicated that the calcium influx triggered by eATP originates from the ECM, this study suggests that at least some intracellular calcium release is also stimulated by eATP. This was confirmed in a later study, where ATP elicited two distinct calcium peaks: an early one initiated 10 seconds after ATP addition, and a later one initiated 60 seconds after ATP addition (Tanaka *et al.,* 2010). The dynamics of calcium influx elicited by eATP are complex. Adjacent root cells respond differently to ATP addition, suggesting differences in cell specific calcium channels (Tanaka *et al.,* 2010).

1.6.8.2 eATP triggers ROS signalling

ROS are well studied second messengers elicited by a variety of stimuli (Apel and Hirt 2004). eATP was initially found to induce the accumulation of superoxide in *Arabidopsis* leaves infiltrated with high levels of ATP (Song *et al.,* 2006). Both ATP and ADP were capable of triggering this response and it was shown to be dependent on NADPH oxidase activity. ATP concentrations as low as 50 μM significantly induced superoxide accumulation and such concentrations were found to occur in nature during wounding responses. Interestingly, superoxide accumulation is dependent on eATP-triggered calcium influx because calcium channel blockers and purinoreceptors antagonist successfully abolished superoxide accumulation (Song *et al.,* 2006). This showed that two separate signalling molecules work together in eATP-mediated signalling. ROS production triggered by ATP or the non-hydrolysable ATP analogue βγmeATP has been co-localised to the tips of growing root hairs in *Medicago* using the fluorescent ROS dye CM-H_2DCFDA (Kim *et al.,* 2006b). Specific eATP-induced ROS accumulation and increase in pH medium has been documented in *Salvia miltiorrhiza* hairy root cultures and this response is dependent on calcium signalling (Wu *et al.,* 2008a). Demidchik and co-workers (Demidchik *et al.,* 2009) found eATP-induced ROS production in *Arabidopsis* root epidermis cells was caused by stimulation of the plasma membrane *Arabidopsis* respiratory burst oxidase homolog C (*AtRBOHC*). This gene encodes for a NADPH oxidase and the *rhd2* mutant, a loss-of-function mutant for *AtRBOHC*, failed to accumulate similar levels of ROS in response to eATP. Moreover, they showed that increased calcium conductance following ATP treatment was downstream of ROS production, revealing a complex interaction between calcium and ROS (Demidchik *et al.,* 2009).

Several studies have looked specifically at NO accumulation in response to eATP. This was first discovered in tomato cell cultures (Foresi *et al.,* 2007). Using the NO-specific fluorescent probe diaminofluorescein-FM diacetate, the authors measured increased NO accumulation that followed increasing eATP concentrations. The NO scavenger cPTIO, nitric oxide synthase and nitrate reductase inhibitors blocked eATP-induced NO accumulation, as well as purinoreceptor antagonists. Specific eATP-induced NO accumulation has also been documented in *Salvia miltiorrhiza* hairy root cultures and this response also requires calcium signalling since it was blocked by the calcium antagonists EGTA and verapamil (Wu and Wu 2008b). NO accumulation has also been reported in dark grown *Arabidopsis* hypocotyls (Tonon *et al.,* 2010) and in growing root hairs (Terrile *et al.,* 2010). Experimental results using the *nia1nia2* mutant, a double mutant for nitrate reductase genes which has diminished NO production, provide preliminary evidence for the role of nitrate reductase as the primary producer of NO in response to ATP (Reichler *et al.,* 2009).

1.6.8.3 eATP triggers cGMP and PA signalling

Two isolated reports have implicated the ubiquitous second messenger signalling molecules cGMP and PA in the eATP signalling cascade. Experiments performed on germinating pollen found that high levels of eATP and its non-hydrolysable analogue ATPγS inhibited pollen germination (Reichler *et al.,* 2009). Downstream production of cGMP in response to NO accumulation was the cause of the effects of ATPγS on pollen germination because inhibition of cGMP production using specific inhibitors abolished the inhibitory effects of high concentration of ATPγS, showing that ATP stimulates cGMP signalling downstream of NO accumulation (Reichler *et al.,* 2009).

A study in tomato suspension cell cultures has shown that eATP induced the production of the signalling lipid PA and that it is dependent on the classical PA synthesis enzymes phospholipase C, phospholipase D and diacylglycerol kinase (Sueldo *et al.,* 2010). Interestingly, ATP-induced PA production was not abolished by the calcium channel inhibitor La^{3+}, showing that PA production is independent of eATP-triggered calcium signalling. Experiments using inhibitors of phospholipase C and diacylglycerol kinase, enzymes involved in PA synthesis, showed that eATP-mediated NO production requires PA signalling (Sueldo *et al.,* 2010). These results suggest that PA is one of the earliest signalling molecules recruited by eATP.

1.6.8.4 eATP triggered gene expression and protein abundance changes

Signalling cascades can result in gene expression changes and several plant studies have shown that eATP-mediated signalling modulates changes in gene expression. Some studies looked at the effects of increasing eATP concentrations, either by adding excessive amounts of ATP or by using a non-hydrolysable analogue to mimic sustained high concentrations of eATP. Several genes have now been shown to change following ATP treatment in plants. These include stress responsive genes such as mitogen-activated protein kinase family members (Jeter *et al.,* 2004; Demidchik *et al.,* 2009) and ethylene responsive genes (Jeter *et al.,* 2004; Kim *et al.,* 2009), phytohormone related synthesis genes *PAL1*, *LOX2*, and *ACS6* (Song *et al.,* 2006), genes involved in ROS production such as *AtrbohD* (Song *et al.,* 2006) and genes of unknown function (Chivasa *et al.,* 2009b). Proteomic studies in tobacco revealed a component of the proteome is modulated by long-term exposure to high ATP levels (Chivasa *et al.,* 2010). Studies performed at Durham University have shown that some components of eATP-mediated signalling require ATP hydrolysis. Abolishment of eATP signalling by depleting eATP levels *in vivo* using a glucose-hexokinase trap in cell cultures caused several protein abundance changes (Chivasa *et al.,* 2005a) and application of AMP-PCP also results in protein abundance changes (Chivasa *et al.,* 2010). These studies show that basal eATP levels *per se* mediate signalling that regulates protein abundance.

All the reported signalling events controlled by eATP cannot currently be connected with a particular physiological process. There are two reasons for this. Firstly, eATP is capable of initiating all the signalling events simultaneously, making it complicated to link a physiological role with one particular second messenger molecule. Only when specific downstream elements of the signalling cascade are identified can the relative contribution of each signalling molecule be investigated using KO mutants. Secondly, different observations have been performed in different plants species and even on different tissues in the same species. For example, the specific requirement of plasma-membrane proteins for initiating calcium signalling following ATP treatment has only been demonstrated in protoplast derived from *Arabidopsis* mature root epidermis cells (Demidchik *et al.,* 2009) and PA production has only been reported in the artificial system of tomato-derived suspension cell cultures (Sueldo *et al.,* 2010). The specific signalling components initiated by eATP might be different depending on the tissue and what is crucial for one particular tissue might not be so in another.

Overall, eATP is now accepted as a molecule with a signalling role, capable of initiating downstream intracellular signalling by recruiting well known signalling molecules, calcium, superoxide, nitric oxide, cGMP and PA. This signalling ultimately results in gene expression and protein abundance changes that mediate the physiological processes known to be regulated by eATP. A schematic diagram of the current state of knowledge about the ATP field in plants is summarized in Figure 1.2. The figure does not include some speculative hypothesis that have been put forward regarding the less well understood aspects of the field, such as the possible role of annexins in channelling the signalling initiated by eATP into the cell (Shang *et al.,* 2009).

1.6.9 Programmed cell death and eATP

Recently, eATP was found to play a critical role in the control of programmed cell death (PCD) (Chivasa *et al.,* 2005a). PCD in plants is a widespread phenomenon triggered by different biotic and abiotic stimuli. Unlike necrosis, PCD is an active form of cellular suicide that is tightly regulated at the genetic level only being activated when required (Lam 2004). During growth and development, cell death occurs in many processes such as vascular tissue differentiation (Fukuda 1997), senescence (Lim *et al.,* 2007) and as a result of pathogen attack, where it is known as Hypersensitive Response (HR) cell death (Jones *et al.,* 2006). Some abiotic stresses that are capable of initiating PCD are heat stress (McCabe *et al.,* 1997), cold stress (Koukalova *et al.,* 1997), ultraviolet radiation (Danon and Gallois 1998) and ozone treatment (Rao and Davis 2001). However, PCD is not fully understood in plants.

The study of PCD in plants has been hampered by the absence of clear core cell death regulators such as BCL-2, APAF1 and caspase families present in animals (Jacobson *et al.,* 1997). However, some features of plant PCD share mechanistic similarities with animal apoptosis, suggesting that these cell death effectors might have been conserved between

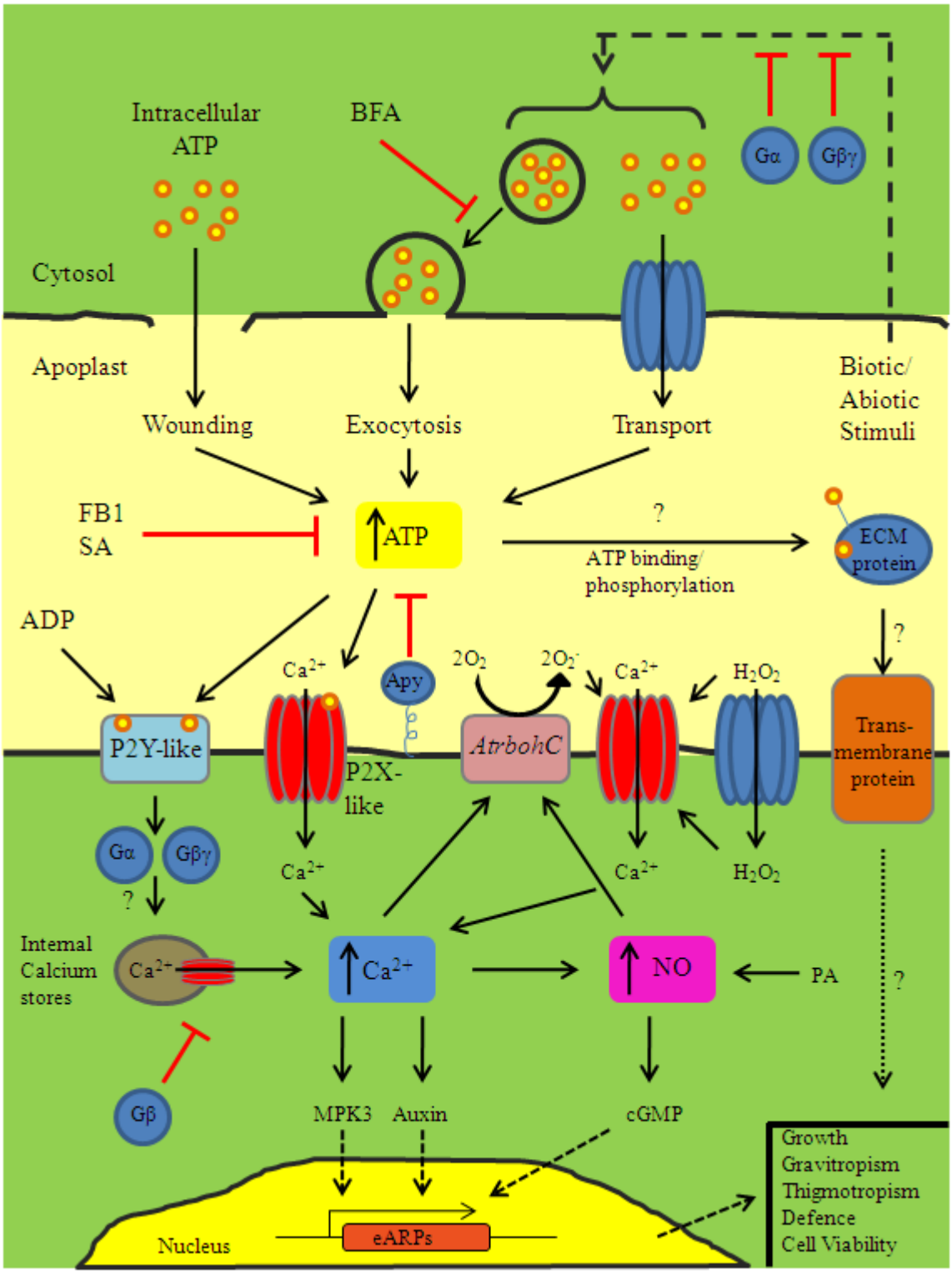

Figure 1.2 Schematic diagram showing the current knowledge on eATP signalling in plants. ATP is release to the apoplast by exocytosis or through membrane channels and ABC transporters by a variety of external stimuli (touch, osmoticum, pathogen elicitors) or as a result of membrane disruption (wounding). eATP levels are regulated by ecto-nucleotidases such as apyrase (Apy) and can be depleted by salicylic acid (SA) or

(Figure 1.2 continued) Fumonisin B1 (FB1). eATP might be perceived at the cell surface by membrane proteins similar to purinoreceptors that are also activated by ADP or by soluble ECM proteins that bind ATP and/or are phosphorylated by it (ECM kinome and phosphatome signalling). Increased eATP triggers an increase in cytosolic calcium levels $[Ca^{2+}]_{cyt}$. This in turn triggers increased production of NO or ROS via activation of plasmamembrane NADPH oxidase (*AtrbohC*), which then causes further increase in $[Ca^{2+}]_{cyt}$ via calcium influx. eATP triggers phosphatidic acid (PA) accumulation that also increases NO production, leading to production of a further second messenger cGMP. The multitude of secondary messengers (Ca^{2+}, NO, ROS, cGMP, PA) modulates several physiological processes, probably via gene expression changes in genes coding for extracellular eATP regulated proteins (eARPs). Heterotrimeric G-proteins seem to have a role in desensitizing stimulus-induced ATP release (Gα, Gβγ) and calcium release from internal stores (Gβ). The interaction of eATP with auxin signalling appears to play a critical role in root growth.

animals and plants throughout evolution (Ausubel 2005). Caspases play a pivotal role in animal apoptosis by specifically cleaving target substrates and orchestrating the proteolytic degradation of the proteome. Treatments of plant cells with caspase inhibitors blocks PCD, suggesting functional homologues to animal caspases (D'Silva *et al.,* 1998). Although plant orthologues of animal caspases have not been identified after sequencing of the *Arabidopsis* genome, a closely related group called metacaspases has been suggested as possible regulators of PCD (Watanabe and Lam 2004), since these metacaspases are specifically required for successful progression of PCD (Suarez *et al.,* 2004). A more recent report identified a metacaspase that regulates developmental PCD by a selective cleavage of target substrate, suggesting metacaspases could indeed function via a similar mechanism to animal caspases (Sundstrom *et al.,* 2009). In animals, several core cell death factors such as cytochrome *c* (Liu *et al.,* 1996), endonuclease G (Li *et al.,* 2001) and apoptosis-inducing factor (Susin *et al.,* 1999) are located inside the mitochondria and only participate in apoptosis when translocated to the cytosol. Although cytochrome *c* leakage into the cytosol has been associated with some forms of plant PCD, it does not appear to directly activate PCD per se (Reape and McCabe 2010). However, the breakdown of plant mitochondria integrity correlates with cell death induction (Curtis and Wolpert 2002; Tiwari *et al.,* 2002), probably due to the release of unknown plant-specific cell death factors.

Recent experiments performed in *Arabidopsis* cell suspension cultures and whole plants showed that removal of ATP from the plant ECM using artificial enzyme depletion systems resulted in cell death (Chivasa *et al.,* 2005a). This cell death was not the consequence of energy depletion resulting from the fast hydrolysis of eATP by these systems because the same cell death could be mimicked when plants were treated with AMP-PCP (Chivasa *et al.,* 2005a). Since AMP-PCP treatment does not deplete eATP concentrations, cell death was clearly the result of inhibition of eATP-mediated signalling originating from the ECM. The cell death effects of AMP-PCP are light dependent, suggesting a critical requirement of light in this type of cell death (Chivasa *et al.,* 2010). Moreover, the observation that PCD could also be initiated by eATP depletion in other plant species, namely tobacco (*Nicotiana tabacum*), bean (*Phaseolus vulgaris*) and maize cell cultures (Chivasa *et al.,* 2005a), suggests a ubiquitous role of eATP in the control of PCD, possibly with a role in pathogen-induced HR.

HR cell death is a form of defensive response that contributes to the prevention of pathogen spread into uninfected plant tissue. It is triggered by PAMPs such as flagellin (Gomez-Gomez and Boller 2002; Zipfel *et al.,* 2004) and bacterial elongation factor Tu (Kunze *et al.,* 2004), or by gene-for-gene interactions between plant resistance (*R*) genes and pathogen avirulence genes (Jones *et al.,* 2006). Host HR cell death can also be caused by pathogen-derived phytotoxic molecules that function as key virulence determinants. Fumonisin B1 (FB1), one such mycotoxin secreted by fungi members of the *Fusarium* genera. Similarly to other PAMPs, FB1 elicits classical defence responses, like production of ROS and expression of PR genes (Stone *et al.,* 2000), and is able to initiate PCD in both plants and animals (Visconti *et al.,* 1994; Gilchrist 1997).

In animals, FB1 ingestion can cause fatal diseases such as porcine pulmonary edema and equine leukoencephalomalacia (Stockmann-Juvala and Savolainen 2008). The enzyme ceramide synthase, a crucial enzyme in sphingolipids biosynthesis, is a major target of FB1, possibly due to the structural similarity of FB1 to the long-chain base backbones of sphingolipids (Wang *et al.,* 1991). Inhibition of ceramide synthase activity results in the accumulation of toxic amounts of its precursor sphingoid bases sphingosine and sphinganine, which could account for FB1's toxic effects (Wang *et al.,* 1992). Curiously, the toxic effects of FB1 are not exclusively the result of ceramide synthase inhibition indicating FB1 has other unknown targets critical for cell death inception (Seefelder *et al.,* 2003).

1.6.10 Fumonisin B1-eATP connection in plants

In plants, very little is known about how FB1 causes cell death. Unlike in animals, in *Arabidopsis* the cell permeable C2-ceramide is unable to block FB1-induced cell death, suggesting that it is not caused solely by ceramide depletion (Stone *et al.,* 2000). Only a few genes specifically involved in FB1-induced PCD have been identified in plants. A forward genetic screen identified several FB1 resistant mutants (Asai *et al.,* 2000). One of these mutants, *fbr6* was later characterized and found to have a mutation in the gene *AtSPL14*, a plant-specific SBP-domain putative transcription factor (Stone *et al.,* 2005). These *fbr6* mutants displayed altered plant architecture and were not resistant to FB1 in the adult stage, suggesting the resistant phenotype observed in the forward genetic screen is due to tissue specific-expression of *AtSPL14* in germinating seedlings (Stone *et al.,* 2005). This mutant showed no difference to wild type Columbia plants in its susceptibility to avirulent *Pseudomonas. syringae* pv. maculicola, but other mutants have shown a resistant

phenotype to virulent *P. syringae* (Stone *et al.,* 2000), suggesting FB1-mediated signalling eventually diverges into separate defence and cell death branches. The *Arabidopsis* vacuolar processing enzyme (*vpe*)-null mutant, lacking all *Arabidopsis* VPE genes, is resistant to FB1 (Kuroyanagi *et al.,* 2005). This resistant phenotype is related to VPE activity being a requirement for the collapse of the tonoplast during FB1-induced cell death. VPE proteins exhibit caspase-1 activity and treatments with VPE-specific or caspase-1 inhibitors prevented FB1-induced lesions, indicating that caspase activity is required during FB1-induced cell death (Kuroyanagi *et al.,* 2005). Another study identified the long-chain base 1 subunit of a serine palmitoyltransferase to be required for PCD initiated by FB1 (Shi *et al.,* 2007). This gene is required for ROS production mediated by the free sphingoid bases, demonstrating that sphingolipid-mediated signalling precedes ROS production and is a critical component in FB1-induced cell death. Identification of further genes critical for FB1-induced cell death in plants will enable a better understanding of the mechanistic details of this particular toxin.

Recently, it was discovered that FB1 activates cell death by gradually reducing eATP levels (Chivasa *et al.,* 2005a). As FB1 is a naturally occurring toxin secreted by a plant pathogen that initiates PCD in nature, this connection provides a physiological basis for the control of PCD by eATP as was shown using artificial ATP depletion systems in the same study (Chivasa *et al.,* 2005a). The specific requirement for the eATP depletion step during FB1-induced cell death was made clear from experiments in cell cultures, where FB1-treated cultures could be prevented from irreversibly undergoing PCD by the addition of ATP to the medium enabling the cells to recover. This effect was found to be time dependent, being only observed if ATP was added no later than 40 hours after FB1 exposure in their assay conditions (Chivasa *et al.,* 2005a). Addition of ATP 48 hours or later after FB1 treatment could not block cell death in *Arabidopsis* cell cultures, suggesting that critical signalling events take place between 40 and 48 hours after FB1 exposure. The identities of the genes downstream of eATP that are activated during this period are unknown but their identification is paramount for achieving the global goal of elucidating the mechanism of eATP signalling in plant physiology.

1.7 Objectives of the project

The overall objective of this project is to employ state-of-the-art proteomics and transcriptomics technologies to identify critical proteins and genes that account for the toxic effects of FB1 on *Arabidopsis thaliana* as well as the specific effects of eATP on this particular type of cell death and on plant physiology in general. The details of specific aims are as follows:

1. Utilize proteomics and reverse genetics to identify candidate cell death regulators that are differentially regulated by ATP during FB1-induced cell death. An experimental approach based on previous research performed at Durham University will be employed using cell cultures treated with FB1 only (committed to dying) and ATP+FB1 (rescued from dying). Protein fractions from these cultures will be analysed by 2D-DiGE proteomics and candidate genes identified tested for a role in FB1-induced cell death using KO mutants.

2. Identification of new genes and proteins regulated by eATP signalling by analysis of the proteomic response of *Arabidopsis* cell cultures to ATP treatment and by re-examination of a previously acquired DNA chip experiment performed in the Slabas group. The effects of ATP treatment on the proteome of unstressed cell cultures will be analysed by 2D-DiGE proteomics and the possible physiological significance of these findings interpreted using bioinformatic tools. Predictions obtained from analysis of the DNA chip data will be confirmed by conventional molecular biology methods and also analysed by bioinformatic tools.

3. Utilize proteomics and reverse genetics to identify candidate cell death regulators that mediate the specific effects of FB1 on *Arabidopsis* cell death that are unrelated to its ability to deplete eATP prior to cell death.

Chapter 2 Materials and Methods

2.1 Chemicals

Unless stated otherwise, all chemicals were molecular biology grade and purchased from, Sigma-Aldrich Company Ltd., (Gillingham, UK), Fisher Scientific UK Ltd (Loughborough , UK) and Gibco BRL (Life Technologies, Paisley, UK). Reagents were used and stored according to the manufacturer's instructions unless otherwise stated. Milli-Q (MQ) ultrapure water (Milli-Q Plus, Millipore, Billerica, MA, USA) was used routinely to prepare solutions, media and dilute chemicals.

2.2 Plant material

2.2.1 *Arabidopsis* suspension cell culture medium

The culture medium used was made up of 3% (w/v) tissue culture tested sucrose, 4.43 g/L of Murashige and Skoog basal salts with minimum organics (MSMO), 0.5 mg/L 1-naphthaleneacetic acid and 0.5 mg/L of kinetin. The pH was adjusted to 5.7 with KOH and the medium autoclaved at 120ºC for 20 minutes in 250 ml flasks sealed with 4 layers of aluminium foil. The flasks were stored at room temperature until needed.

2.2.2 *Arabidopsis* cell suspension culture maintenance

Arabidopsis thaliana var *Landsberg erecta* cell suspension cultures (May and Leaver 1993) were grown in a 100 ml medium volume inside a 250 ml sterile flask. Flasks were kept under constant shaking (60 RPM) in a growth room at constant 22ºC under a 16 hour photoperiod of 100 $\mu mol.s^{-1}.m^{-2}$. Cultures were maintained by routine subculturing every seven days in a clean laminar flow cabinet previously sterilized with 70% (v/v) ethanol before each use. 10 ml of culture were subcultured using a sterile burette to a new flask containing 90 ml of fresh medium. Cell cultures were used for experiments in mid-exponential growth phase (3 days post-subculturing).

2.2.3 *Arabidopsis* plant growth conditions

Soil used for growing plants, both wildtype Columbia-0 accession and T-DNA insertional lines, was sterilised by autoclaving in order to remove pests that could damage the plants. Soil grown-plants were incubated in a growth chamber with a 16 hour photoperiod (100-120 $\mu mol.s^{-1}.m^{-2}$) maintained at 22°C during the light phase and 15°C during the dark phase. Plants were used for experiments 4-5 weeks after sowing before they started to bolt.

2.2.4 Hydroponics medium

For hydroponically grown plants, a medium consisting of 1% (w/v) tissue culture tested sucrose and 2.2 g/L of MSMO was used. The pH was adjusted to 5.7 with KOH and 5 ml of medium autoclaved in 25 ml flasks similarly to *Arabidopsis* cell culture medium.

2.2.5 *Arabidopsis* seed sterilization

Arabidopsis seeds for hydroponics were sterilized in a sterile flow cabinet. Seeds were immersed in 70% (v/v) ethanol for 30 seconds followed by a 30 minutes incubation in 10% (v/v) Domestus bleach containing 5% (v/v) Tween 20. Seeds were then rinsed twice with sterile MQ water and resuspended in sterile MQ water, where they can be stored at 4ºC for up to 3 weeks.

2.3 Cell suspension culture treatments

All cultures were adjusted to a cell density of 5% (w/v) prior to treatment to ensure reproducibility of the results. All treatments were performed in a sterile flow cabinet. Samples for proteomic analysis were prepared from 100 ml cultures and samples for sqRT-PCR analysis and MTT assays were prepared in 5 ml cultures.

2.3.1 Preparation of stock solutions

Stock solutions of 1 mM FB1 were prepared in 70% methanol and filter-sterilised before use. FB1 stocks could be stored at -20ºC for several months. Stocks of 100 mM ATP (sodium salt) were prepared in MQ water and adjusted to pH 6.5 with KOH. ATP stocks were prepared fresh every time because ATP quickly degrades in water and is not stable at -20ºC. Adenosine 5'-[(β,γ)-methyleno] triphosphate (AMP-PCP) 100 mM stock solutions were prepared in MQ water and pH adjusted to 6.5 with KOH. AMP-PCP stocks could be stored at -20ºC for several months. Sucrose and UDP-glucose stock solutions were also prepared fresh. All solutions were filter sterilized with a 0.2 µm size exclusion filter (Anachem Ltd., Luton, UK) before use.

2.3.2 Treatment conditions in ATP feeding experiments

ATP samples were treated with a final concentration of 1 mM ATP while mock samples were treated with the same volume of sterile MQ water. The cells were harvested by filtering in 2 layers of Miracloth (Merk, Nottingham, UK) and frozen in liquid nitrogen.

2.3.3 Treatment conditions in ATP reversal experiments

FB1 samples were treated with 1 μM FB1 at the beginning of the experiment, while mock treatments were performed with an equivalent dilution of 70% (v/v) methanol. FB1+ATP samples were similarly treated with FB1, but ATP was added to a final concentration of 1 mM 40 hours later, while mock and FB1 only treatments were treated with the same volume of sterile MQ water. The cells were harvested 48 hours after the start of the experiment by filtering in 2 layers of Miracloth (Merk, Nottingham, UK) and were frozen in liquid nitrogen.

2.4 Cell death assays

2.4.1 MTT assay as a measure of mitochondrial activity

The 3-(4,5-Dimethylthiazol-2-yl)-2,5-diphenyltetrazolium bromide (MTT) assay is a standard colorimetric assay for measuring the activity of reductase enzymes that reduce yellow MTT to the purple coloured formazan. This mostly happens in mitochondria and as such it is in large a measure of mitochondrial activity and can be viewed as a viability measurement. 100 μL of cell cultures were transferred to an eppendorf using a cut tip and incubated with an equal volume of 5 mg/ml MTT in water for 1 hour at room temperature. The supernatant was removed by careful pipetting from the bottom of the tube and 1 ml of DMSO was mixed vigorously with the cells to ensure complete lysis and release of the purple formazan. Cell debris was pelleted at 16.000*g* for 10 minutes using a bench top centrifuge and the resulting supernatant transferred to a plastic cuvette. The absorbance at 470 nm of each sample was recorded using an Ultrospec 1100 pro spectrophotometer (GE Healthcare, Amersham, UK). Three technical replicates were performed for each sample for statistical purposes.

2.4.2 Leaf infiltration assay

5-10 μM FB1, 150 mM sucrose and mock solutions were infiltrated into the apoplast of attached leaves from the abaxial surface using a 1 ml syringe without a needle. Symptom development was visually monitored every 24 hours and photographed when appropriate using a PowerShot A640 10 Megapixel digital camera (Canon Ltd., Surrey, UK). Infiltrated leaves were marked with coloured markers on the petiole for identification of treatments applied.

2.4.3 Conductivity assay using FB1

Discs of 8 mm diameter were cored from leaves of 4-week-old plants and floated on 2.5-10 μM FB1 solutions in small petri-dishes. This was repeated 3-5 times depending on the

experiment. Each replicate had 10 leaf discs each originating from one of 10-replicate plants. The discs were incubated in the dark for 48 hours to allow uptake of FB1 prior to the onset of cell death. After the dark incubation, the discs were placed at 22ºC under a 16 hour photoperiod regime (100-120 $\mu mol.s^{-1}.m^{-2}$) and the conductivity of the underlying solution measured at 24 hour intervals using a Jenway conductivity meter (Jenway Ltd., Felsted, UK).

2.4.4 Conductivity assay using *Pseudomonas syringae* pv. tomato DC3000 (*AvrRpm1*)

All experiments using plant pathogens were conducted in a dedicated level 2 containment lab. Bacterial glycerol stocks of *Pseudomonas syringae* pv. tomato DC3000 expressing the *avrRpm1* avirulence gene were kindly donated by Dr. Luís Mur, Aberystwyth University, UK. Stocks stored at -80ºC were spread on a fresh King's B agar plates containing 20 mg/ml kanamycin and grown overnight at 28ºC. Fresh colonies were streaked onto a fresh plate and grown overnight at 28ºC. The new colonies were then collected from the surface of the agar using an inoculation loop and resuspended in water and the optical density of the mixture was adjusted to 0.3 at OD_{600},using an Ultrospec 1100 pro spectrophotometer (GE Healthcare, Amersham, UK), that corresponds to $1x10^8$ CFU's per millilitre for this pathogen. A solution containing $1x10^7$ CFU's was infiltrated into *Arabidopsis* leaves from the abaxial surface using a syringe without a needle. Discs of 8 mm diameter were cored from the infiltrated leaves immediately after infiltration and floated in MQ water in 5 replicate petri-dishes. Each replicate had 10 leaf discs each originating from one of 10-replicate plants. The discs were placed under constant light (100-120 $\mu mol.s^{-1}.cm^{-2}$) and the conductivity of the underlying solution measured at 1 hour intervals using a Jenway conductivity meter (Jenway Ltd., Felsted, UK).

2.4.5 Evans Blue staining

Arabidopsis seedlings were grown in hydroponic medium for 5 days in the same conditions as cell suspension cultures. They were then treated with AMP-PCP for 5 days. Seedlings were then fixed in 3 ml of lactophenol [9% (w/v) phenol, 9% (v/v) glycerol, 9% (v/v) lactic acid, 73% (v/v) ethanol] overnight at 37ºC in a bijou bottle. They were then incubated in fresh lactophenol saturated with Evans Blue dye at 37ºC until all the tissue absorbed the dye. Stained seedlings were then distained in chloral hydrate (250% w/v) in MQ water at 37ºC until background staining was minimal. Seedlings were observed using an Olympus SZH10 Research Stereo dissecting microscope (Olympus Ltd., Southend-on-

Sea, UK) and photos taken using a Fast1394 QIcam (QImaging, Surrey, BC, Canada). For mature leaf tissue, leaves were infiltrated with 10 μM FB1 and 8 mm leaf disks cored from the infiltrated tissue and stained similarly to the seedlings.

2.5 Molecular biology

All molecular biology techniques were performed on a bench space cleaned with 70% ethanol using clean sterile plasticware or glassware. Disposable gloves were used routinely to avoid contamination during manipulations. Commercial kits were used when available.

2.5.1 RNA isolation

Plant total RNA for cDNA synthesis was obtained using an RNeasy Plant Mini Kit (Qiagen, Crawley, UK) according to the manufacturer's instructions for plant tissue. Plant material, either suspension cell cultures or mature leaves, was frozen in liquid nitrogen before being ground to a fine powder using a chilled porcelain pestle and mortar. The pestle and mortars were baked at 180ºC overnight to remove contaminating RNA and RNAses. A maximum of 100 mg of the powder was used per extraction. During the extraction protocol, the optional in-column DNAse (Qiagen, Crawley, UK) treatment was performed to eliminate any DNA carryover in the sample. RNA was eluted from the column in the final step in two 30 μL volumes of autoclaved MQ water.

2.5.2 RNA quantification and integrity check

Typically, 100 mg of grounded tissue yielded 30-50 μg of total RNA eluted in MQ water. Fresh RNA preparations were quantified using a NanoDrop ND-1000 spectrophotometer (NanoDrop technologies, Inc). The NanoDrop automatically calculates total RNA yield by measuring the absorbance values at 260 nm and 280 nm (Abs_{260} and Abs_{280}) and calculating the ratio between these values. Abs_{260} measures total nucleic acid and Abs_{280} measure the degree of contamination by proteins in the sample. RNA samples with ratios of $Abs_{260}/Abs_{280} \geq 1.5$ were considered of good enough quality for downstream applications. RNA quality was confirmed by running 1 μg of the sample on an agarose gel. Total RNA samples were stored at -80ºC until required for reverse transcription.

2.5.3 RNA separation on agarose gel

RNA samples were routinely separated via electrophoresis on a 1.2% (w/v) high purity agarose (Bioline, London, UK) gel made up with 3-(N-morpholino)propanesulfonic acid

(MOPS) buffer [4.18% (w/v) MOPS, 20 mM sodium acetate, 10 mM EDTA, pH 7 adjusted with 2 M NaOH]. 1 µg of total RNA was mixed with 5 µL of RNA loading buffer (50% (v/v) formamide, 17.5% formaldehyde, and 100 µg Ethidium Bromide (EtBr) in 1:2 dilution of MOPS buffer) for 15 minutes at 55ºC to allow the EtBr to bind to the RNA. The samples were separated using a dedicated gel tank, washed with 2% SDS overnight, at constant 100 V for 20 minutes to allow proper separation of RNA bands. 28S and 18S ribosomal RNA bands were visualized on the gel using a UV transilluminator and used as a quality control for RNA degradation. Gels were photographed with a UVP Bioimaging systems 55+2 camera and images printed using a Mitsubishi P93 thermal printer (Mitsubishi) on high density paper. RNA samples that showed no significant degradation on gel (Figure 2.1) were used for reverse transcription.

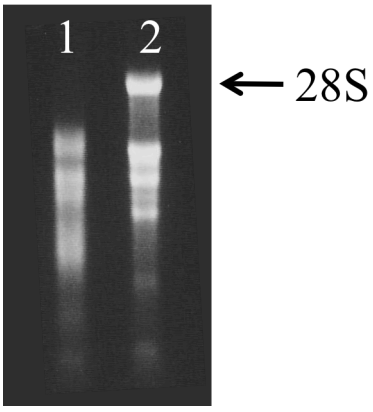

Figure 2.1 The integrity of RNA samples visualized by gel electrophoresis. 1- RNA sample that shows significant degradation where the 28S ribosomal RNA band is not visible. 2- Intact RNA sample.

2.5.4 First strand cDNA synthesis by reverse-transcription (RT)

cDNA synthesis was performed using the SuperScript III RT kit (Invitrogen Ltd., Paisley, UK) according to the manufacturers recommendations. For each sample, 3 µg of total plant RNA were mixed with 0.5 µg of oligo $dT_{(15)}$ (Promega Ltd., Madison, WI, USA) and 0.2 µM of each dNTP (Bioline, London, UK) to a final volume of 13.5 µL with MQ water. The mix was incubated in a water bath for 5 minutes at 65ºC to allow the $dT_{(15)}$ oligos to bind to the poly-A tails of the messenger RNA and to destroy RNA secondary structure. The samples were then quenched on ice for 1 minute to prevent secondary structure from reforming and spun down to remove condensation droplets before adding 5 µL of 5X First strand buffer (250 mM Tris-HCl, 375 mM KCl, 15 mM $MgCl_2$, pH 8.3 at room

temperature), 2 mM DTT, 200 units of SuperScript III and 20 units of RNasin (Promega Ltd., Madison, WI, USA) to a final volume of 20 µL. The samples were gently mixed with a pipette and incubate in a 50ºC water bath for 90 minutes. The SuperScript III enzyme was denatured by heating the sample to 70ºC for 15 minutes and the reaction was terminated. The mix was diluted 1:4 with autoclaved MQ water to create working dilution suitable for polymerase chain reactions. Diluted mixes were stored at -20ºC for long term storage.

2.5.5 Polymerase Chain Reaction (PCR)

PCR reaction mixtures were routinely prepared on ice using 200 µL thin walled flat cap PCR tubes using a BioTaq DNA Polymerase kit (Bioline, London, UK). The final volume was made up to 50 µL with MQ water. Each reaction consisted of 2 µL of cDNA template in Taq polymerase buffer [16 mM $(NH_4)_2SO_4$, 67 mM Tris-HCl (pH 8.8 at 25ºC), 0.01% stabilizer] containing 1U of BioTaq, 1.5 mM $MgCl_2$, 0.2 µM of each primer and 0.2 mM of each dNTP. A master mix containing all common reagents was prepared when multiple PCR reactions were setup. Reactions were carried out on a G-Storm Thermal Cycler GS1 (GRI, Essex). As a standard protocol, samples were heated at 94ºC for one minute before cycling commenced to disrupt any unspecific binding that might have formed earlier. A heated lid at 111ºC was used to prevent condensation of the mixture during cycling. Each cycle typically consisted of 40 seconds denaturation at 94ºC followed by annealing, at 56-62ºC, for 40 seconds and elongation at 72ºC for 1 minute. A final elongation step at 72ºC was carried out for 5 minutes and reactions left on hold at 4ºC until analysed by gel electrophoresis.

2.5.6 DNA agarose gel electrophoresis

DNA samples were routinely analysed by agarose gel electrophoresis. High purity agarose (Bioline, London, UK) was dissolved in TAE buffer (40 mM Tris-acetate, 1 mM EDTA) to a final concentration of 0.8-1.5% (w/v) by boiling in a microwave oven. The agarose percentage used depended on the size of the expected fragments and guidelines for these are given in (Sambrook *et al.,* 1989). Warm agarose was mixed with the intercalating dye ethidium bromide to the final concentration of 0.5 µg/ml. The agarose was poured directly into the clean casting apparatus and sample wells formed by insertion of a comb in the warm agarose taking care to avoid air bubbles. Once solidified, the comb was removed and the gel was stored at 4ºC until needed. The gel was submerged in an electrophoresis tank

containing TAE buffer prior to loading samples. A total of 10 µl of PCR product was mixed with 1.5 µl of Orange G DNA loading buffer [3% (v/v) glycerol 0.2% (w/v) Orange G] before loading into the agarose gel. Electrophoresis was performed at a constant voltage of 100 V until the Orange G dye that moves ahead of the DNA fragments reached the end of the agarose gel. The DNA molecular weight marker φ-X174 (New England Biolabs, Ipswich, MA, USA), containing DNA fragments of 1353, 1078, 872, 603, 310, 281, 271, 234, 194, 118 and 72 bp long was routinely used for sample band size estimation. The DNA molecular marker HyperLadder I (Bioline, London, UK) containing 14 regularly spaced marker bands, ranging from 200 to 10,000 bp was also used on occasions. Resolved DNA bands were visualized under UV light (UVB, λ=300 nm) using a UV transilluminator.

2.5.7 Genotyping of T-DNA insertional mutant lines

For genotyping of individual *Arabidopsis* SALK homozygous KO plants and segregation analysis of heterozygous lines the Phire Plant Direct PCR kit (Finnzymes, Espoo, Finland) was used according to the manufacturer's instructions. Briefly, a 5 mm leaf disk was manually grounded with a pipette tip in 100 µL of the kit buffer. The resulting solution was directly added to PCR mix containing every component except the DNA template. The PCR was then performed using the DNA polymerase supplied in the kit.

2.5.8 Primer design strategy

Primers for PCR reactions were designed using the Primer-BLAST sequence analysis web software available from the National Centre for Biotechnology Information (NCBI; http://www.ncbi.nlm.nih.gov/tools/primer-blast/). This software uses a combination of Primer3 primer design software (Rozen and Skaletsky 2000) and BLAST in order to identify specific primers in the template sequence that don't amplify unintended sequences in the genome or transcriptome of the organism being used. Only primer pairs amplifying the intended product were selected. The input sequence was the full length genomic DNA sequence or full length mRNA sequence of the gene of interest. The default parameters were used when designing primers for gDNA and cDNA amplification except for the following changes for cDNA primers intended to ensure specificity to cDNA template over possible gDNA contaminants:

- reference database: *Arabidopsis thaliana* Refseq RNA

- GC clamp: 2 bp
- primer must span and exon-exon junction

If no suitable exon-exon junction primer set was available then the default setting was used.

Primers were synthesized by Sigma Genosys Service. Upon delivery, primers were resuspended in sterile distilled water to a concentration of 100 µmol /ml and stored at -20ºC. Primers used in this work are listed in Table 2.1

Table 2.1 Oligonucleotides used in this study. The F and R in the beginning of each name denote a forward and reverse primer, respectively.

Oligo Name	DNA Sequence 5' to 3'
L1	GTATACATGCCTGTCCTAGTGG
R1	CAATTCAATTGACGGGTTCG
L2	CAAGGTAATGTAACGAATCATGG
R2	CTTCATAAACTTGCTTTGCTGTGC
LBa1	TGGTTCACGTAGTGGGCCATCG
F-ACT2	GGATCGGTGGTTCCATTCTTGC
R-ACT2	AGAGTTTGTCACACACAAGTGCA
F-UGP1	GTGGCTACTTTCTTGAGCCG
R-UGP1	TAAACTTGCTTTGCTGTGCC
F-At3g15450.1	CAGAAAGCTTTTGCTCACCC
F-At4g37610.1	TTCTAATGTCATCGGAATGGC
F-At3g28210.1	GCAAATTGGTGTTTTGTTTGG
F-At4g01360.1	GAAGTAAGCGGTAACATTTCGG
F-At3g22910.1	TAAAATGGCGGTTACTTCCG
F-At5g13200.1	TGGCACAATCTGAAGACAGG
F-At3g01830.1	TACAATCGAAAGATGCGTCG
F-At2g40000.1	TCGGTGTAAGTACACGCTCG
F-At1g61290.1	TTCCTCCTAACAGGCAGAGG
F-At5g40000.1	TGCTTACAGCAACATCCAGC
R-At3g15450.1	CCACAGAACAACCTTTGACG
R-At4g37610.1	ATTACACGCTTGAAATCCGC
R-At3g28210.1	CTCTTCCACACCCTTTCTGG
R-At4g01360.1	TCACAAAGAGACTGCATGGC
R-At3g22910.1	GCCAATGTCAATGTCACAGC
R-At5g13200.1	GGACGATCGCTACAAAAAGC
R-At3g01830.1	TTGGGAAATCATAACCTCGC
R-At2g40000.1	CTGTCTTCCTCGCGTAAAGC
R-At1g61290.1	GTGAAATATCTGCGCTCTACGG

R-At5g40000.1	TCTGGCCATAAGATTTTCCG
F-ATPaseB	AGCTGACTGTTGCCCGTGCC
R-ATPaseB	TCACAATGCCTCAGCAGACAACC
F-ATPB2	TCCACACACCCACTCATGGCG
R-ATPB2	TTGGAGCACCAGTGTTGAGAACC
F-PDIL	TGTTGCCGAGAGCCTTGACG
R-PDIL	CGTCCTTTGCGGCCGTTTCC
F-SEN1	TTAAAATTCCTACGTCAGTACCAG
R-SEN1	TCTCTGTCCAAGCGACGTATCC
F-ACD2	TGTGTCACCCACGCGGAAGC
R-ACD2	ACACCGCTCCAACCAAACCTC
F-SAG12	GACCAATCCAAAAGCAACTTCTAT
R-SAG12	TTTAGACATCAATCCCACACAAAC
F-DND1	ACACACAAATCTTGCGGCTTT
R-DND1	ACACTGCCTGAGGGACAGGG
F-PR1	TCGTCTTTGTAGCTCTTGTAGGTG
R-PR1	TAGATTCTCGTAATCTCAGCTCT
F-PR3	CGGTGGTACTCCTCCTGGACCCACCGGC
R-PR3	CGGCGGCACGGTCGGCGTCTGAAGGCTG

2.7 Protein analysis

2.7.1 Protein isolation methods

2.7.1.1 French press protein extraction of cell cultures

All protein extractions steps were performed at 4°C to minimize protein degradation. Treated cells were filtered in 2 layers of Miracloth (Merk, Nottingham, UK) and resuspended in 20 ml of cold (4°C) Tris/EDTA buffer (10 mM Tris base, 1 mM EDTA, pH 8.0 adjusted with HCl concentrated) and homogenised using a 4°C water bath cooled French Press (Constant systems Ltd., Warwick, UK) by passing the sample 2 times under 24,200 PSIs of pressure. Homogenate was centrifuged at 20,000 *g* for 30 minutes at 4°C to remove cell debris. The supernatant was centrifuged at 100,000 *g* for 1 hour at 4°C to separate the microsomal fraction (green pellet) from the Total Soluble Protein (TSP) fraction (supernatant).

2.7.1.2 Total Soluble Protein fraction (TSP) isolation

The supernatant (TSP) was precipitated in 80% acetone overnight at -20°C. The resulting protein pellet was washed twice with 80% acetone and once in 100% acetone. The final pellet was resuspended in lysis buffer (LB; 9 M urea, 2 M thiourea, 4% w/v CHAPS, 30

mM Tris-HCl, pH 8.8) by mixing in an orbital shaker (180 RPM) overnight. Protein samples were quantified by the modified Bradford method and stored at -20°C for long term storage.

2.7.1.3 Microsomal protein fraction isolation

The microsomal fraction pellet was washed 3 times in Tris/EDTA buffer (10 mM Tris base, 1 mM EDTA, pH 8.0 adjusted with HCl concentrated) in order to remove soluble proteins. This was achieved by manually disrupted the pellet in 20 ml of Tris/EDTA buffer inside the centrifugation tube using a pipette and re-pelleted by centrifuging at 100,000 *g* for 1 hour at 4°C. After the final wash, the microsomal pellet was solubilised in LB by mixing in an orbital shaker (180 RPM) overnight. Protein samples were quantified by the modified Bradford method and stored at -20°C for long term storage.

2.7.2 Protein quantification by the modified Bradford assay

A modification to the standard Bradford assay, developed by Ramagli (Ramagli *et al.,* 1985) to allow the use of this assay on samples containing carrier ampholytes and thiol-containing compounds that would interfere with the standard assay, was used. The calibration curve was made by making Bovine Serum Albumin (BSA) dilutions in LB ranging from 1-10 µg. To each sample, the required volume of BSA in LB was mixed with 10 µl of 0.1 N HCl and the volume made up to 100 µl with MQ water, taking care that the same volume of LB used for the highest BSA concentrations was also present in the lower concentrations. All protein samples were pelleted on a benchtop centrifuge before 2 µl of each sample was measured in triplicate. Calibration and sample solutions were mixed with 900 µl of Protein Assay Dye Reagent concentrate (Bio-Rad Laboratories Ltd, Hemel Hempstead, UK) 1:4 diluted with MQ water. Proper mixing was insured by vortexing the cuvette. After 5 minutes of incubation at room temperature, the absorbance at 595 nm was recorded using an Ultrospec 1100 pro spectrophotometer (GE Healthcare, Amersham, UK). Protein concentration was calculated using Microsoft Excel by plotting the absorbance values in a scatter graph where the Y-axis represents the absorbance measured and the X-axis the protein concentration being estimated (Figure 2.2). The calibration line should have R^2 over 0.985 to be suitable for proteomic studies (Bio-Rad 2D-DiGE manual). A new calibration curve was made for every set of samples to be quantified to take into account day-day variations of the reagents, temperature, etc.

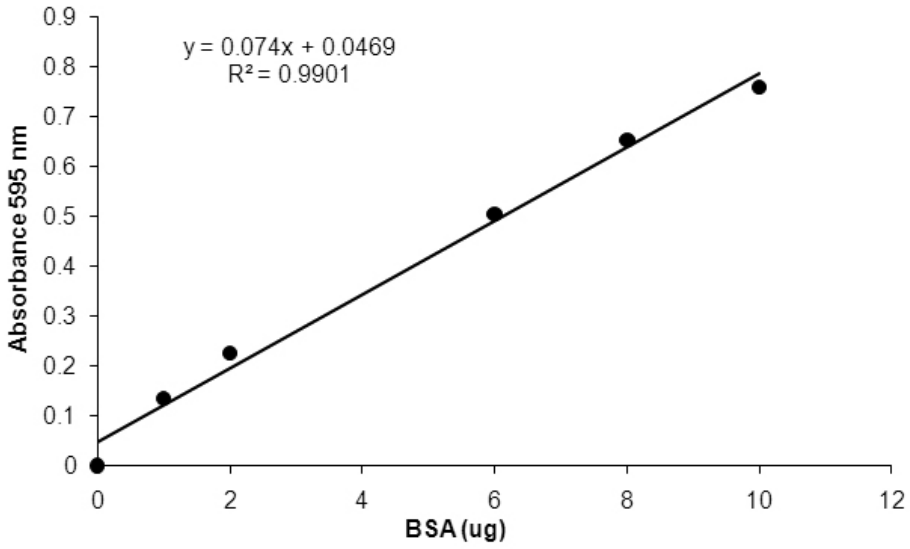

Figure 2.2 Typical Bradford calibration curve using BSA.

2.7.3 Protein samples care

All protein samples were clarified of insoluble material by spinning the sample at 16,000*g* for 5 minutes before being used for any downstream protein analysis. Some samples accumulated insoluble material over time while stored at -20ºC so this procedure was mandatory.

2.7.4 One-dimensional SDS-PAGE gels

Separation of proteins based on their molecular weight was performed by sodium dodecyl sulphate polyacrylamide gel electrophoresis (SDS-PAGE) as outlined by Laemmli (Laemmli 1970).

2.7.4.1 Gel casting

1D SDS-PAGE analysis of protein samples was performed using a Bio-Rad's Mini Protean II vertical gel apparatus (Bio-Rad Laboratories Ltd.). Glass plates were cleaned with 70% (v/v) ethanol prior to use to remove contaminating protein or residual acrylamide. Gels were 0.75 mm thick and consisted of a stacking gel on top of a resolving gel. The stacking gel ensures the proteins enter the resolving gel at the same time while the resolving gel separates the proteins based on their molecular weight. Resolving gel contained 12% (w/v) acrylamide (acrylamide:bis-acrylamide 37.5:1) (Bio-Rad Laboratories Ltd.), 375 mM Tris-

HCl pH 8.8, 0.1% (w/v) SDS, 0.05% (w/v) APS (Bio-Rad Laboratories Ltd.), and 0.02% (v/v) TEMED (Bio-Rad Laboratories Ltd.). Immediately after mixing all reagents, the resolving gel was poured into the glass plates taking care not to trap air bubbles. Since oxygen inhibits acrylamide polymerization the gels were covered with water saturated butan-1-ol and allowed to polymerize. After polymerization, the butan-1-ol was washed away and the stacking gel [5% (w/v) acrylamide, 125 mM Tris-HCl pH 6.8, 0.05% (w/v) APS and 0.04% (v/v) TEMED] was poured on top of the resolving gel. A 0.75 mm comb was inserted into the stacking gel before it polymerized to create the wells. A minimum thickness of stacking gel between the bottom of the wells and the beginning of the resolving gel was 5 mm. The comb was carefully removed after polymerization and the resulting wells were rinsed with MQ water to remove debris.

2.7.4.2 Protein sample preparation and gel loading

The SDS-PAGE gels were placed in an electrophoresis tank with SDS running buffer [25 mM Tris-HCl, 190 mM glycine, 0.1% (w/v) SDS]. Protein samples in LB were mixed with the adequate volume of 5X loading buffer [10% (w/v) SDS, 5% (w/v) DTT (Melford Laboratories Ltd., Ipswich, UK), 0.05% (w/v) bromophenol blue, 0.312 M Tris-HCl pH 6.8, 50% (v/v) glycerol] resulting in 1X loading buffer concentration mix in a volume of up to 25 µL. The mixture was then boiled for 5 minutes to ensure complete breakage of disulfide bonds. The samples were loaded into separate wells using an extra thin tip. An SDS7 marker set was used in each gel for protein band size estimation purposes (Table 2.2). The first and last lanes of a gel were avoided if possible as they can result in smiling artefacts towards the edge of the gel resulting in poor band resolution.

2.7.4.3 1D gel electrophoresis

Electrophoresis was carried out at room temperature initially at 100 V for 15 minutes, to allow the proteins to enter the resolving gel, followed by 120 V until the bromophenol blue dye front reached the bottom of the gel. Gels were then stained with coomassie brilliant blue R-250 or SYPRO Total Protein Stain (Genomic Solutions Ltd, Huntingdon, UK) for protein visualization or used directly for western blotting.

Table 2.2 Composition of SDS7 molecular weight marker.

Protein	Molecular weight (KDa)
BSA	66
Ovalbumin	45
glyceraldehyde–3–phosphate dehydrogenase	36
Bovine carbonic anydrase	29
Trypsinogen	24
Bean trypsin inhibitor	20
α-Lactoalbumin	14.2

2.7.5 Mini-format two-dimensional electrophoresis SDS-PAGE gels

2.7.5.1 Protein loading by in-gel rehydration

The in-gel rehydration procedure was used for mini-format 2DE (Rabilloud *et al.,* 1994). The 7 cm IPG strips were rehydrated overnight in a clean strip tray using a 125 µL solution containing 50-100 µg of protein mixture in rehydration solution [1% (m/v) fresh DTT, 1% (v/v) of relevant IPG ampholite buffer (GE Healthcare, Amersham, UK) and 0.002% (w/v) bromophenol blue in LB]. The solution was pipetted onto the bottom of the tray and spread evenly. The strip was carefully placed gel-side down on top of the solution taking care not to create air bubbles between the solution and the gel. The strip was then covered with 3 ml of paraffin oil to prevent evaporation of the sample and crystallization of the urea. A maximum of 12 strips could be rehydrated simultaneously.

2.7.5.2 First dimension focusing

Strips were removed from the rehydration tray and rinsed with MQ water to remove excess paraffin and unabsorbed sample and were carefully dried by touching the plastic side of the strip to a Whatman paper. They were then placed gel-side up with acidic ends towards the anode and basic ends towards the cathode on the grooves of the plastic strip holder on a MultiPhor II Electrophoresis Unit. Temperature was kept constant at 20°C by using a circulating water bath (Grant Instruments, Cambridgeshire, UK). An electrode wick (GE Healthcare, Amersham, UK) was placed between the strip and the electrodes in order to absorb salts and other contaminants that could cause streaking during focusing. Electrode wicks were cut to the required length in order to span all the strips being focused and were slightly dampened in MQ water before being placed on top of the strips. After electrodes were place at each end of the strips, strips were submerged in paraffin oil to prevent

sample evaporation and urea crystallization. The IEF was performed under constant 5 W and a current of 50 µA per strip using the following step-and-hold protocol:

Step/variable	Voltage	Volts.hour^{-1}
1	100V	5Vh
2	3500V	2800Vh
3	3500V	3700Vh

Total of 6500 volts.hour^{-1} was achieved per run and a current of 50 µA per strip was used. The run time depended on the type of sample being focused. A typical run would last 2-2.5 hours.

2.7.5.3 IPG strip equilibration

The main purpose of the equilibration step is to re-supply SDS to the proteins necessary for SDS-PAGE and to break any disulphide bonds that could result in unwanted protein-protein complexes. After IEF, strips were rinsed with MQ water to remove paraffin oil and equilibrated in a plastic equilibration tray. Strips were equilibrated in 5 ml of equilibration buffer [6 M urea, 30% (v/v) glycerol, 2% (w/v) SDS, 50 mM Tris-HCl pH 8.8, 0.002% (w/v) bromophenol blue] containing 1% (w/v) DTT for 15 minutes at room temperature under constant slow shacking. The strips were further equilibrated in equilibration buffer containing 4.8% (w/v) iodoacetamide for a further 15 minutes. Equilibration buffer made up without DTT or iodoacetamide was stored at -20ºC. DTT and iodoacetamide were always added fresh to the equilibration buffer before each equilibration.

2.7.5.4 Second dimension gel electrophoresis (2DE)

Second dimension electrophoresis was performed similarly to 1D SDS-PAGE described previously, with the only difference being the absence of a stacking gel on top of the resolving gel. After gel casting, the top of the resolving gel was rinsed with MQ water and the equilibrated strips placed on top of the gel. To avoid getting air bubbles trapped between the strip and the gel, the strip was placed on top of the gel while immersed in water. After full contact between the two was achieved, the water was removed with Whatman paper taking care not to dislodge the strip. 1 µL of the SDS7 molecular weight marker was carefully dispensed onto 0.25 cm^2 Whatman paper square and allowed to air-dry. The paper squares containing the marker were then placed on the anodic side of the strip on the edge of the gel. The strip was overlaid with warm 0.5% (w/v) agarose

containing 0.002% (w/v) bromophenol blue and electrophoresis carried out initially at 80 V for 15 minutes, to allow the proteins to enter the resolving gel, followed by 100 V until the dye front reached the bottom of the gel.

2.7.6 Mini gel long term storage

Coomassie stained gels were preserved in a desiccated state by drying between two water-soaked cellophane membranes using the EasyBreeze Gel Drying system (Hoefer Scientific Instruments, San Francisco, CA, USA). Air bubbles were carefully removed from in-between the cellophane membranes before drying because they would result in cracks after drying.

2.7.7 Large format 2D SDS-PAGE

2.7.7.1 Large format gels

Large format gels were cast in 26 x 20 x 1 cm low fluorescence glass cassettes, using the a2DE Optimizer (nextgensciences Ltd, Alconbury, UK). Prior to gel casting, glass plates were scrubbed and then soaked for 1 hour in 1% (v/v) Decon (Decon Laboratories Limited, Sussex, UK), rinsed with MQ water, soaked in 1% HCl (v/v) for 1 hour and then thoroughly rinsed with MQ water. Clean plates were then allowed to air dry protected from dust. When dried, the plates were assembled into cassettes and place inside the nextgenautocast tank (nextgensciences Ltd, Alconbury, UK), each separated from each other by a thin plastic spacer. The a2DE Optimizer supervisor software (version 1.4.0.27313) was used for computer assisted automated gel casting. A custom program was created for casting gradient gels using a commercial kit supplied by the same company. After automatic gel casting, the gels were overlaid with 1 ml of isopropanol and left to polymerize until the following day. The acrylamide gradient generated on the gels was linear from 10% to 15% with a rapid increase in concentration close to the end of the gel (hook). The gradient scheme is illustrated on Figure 2.3.

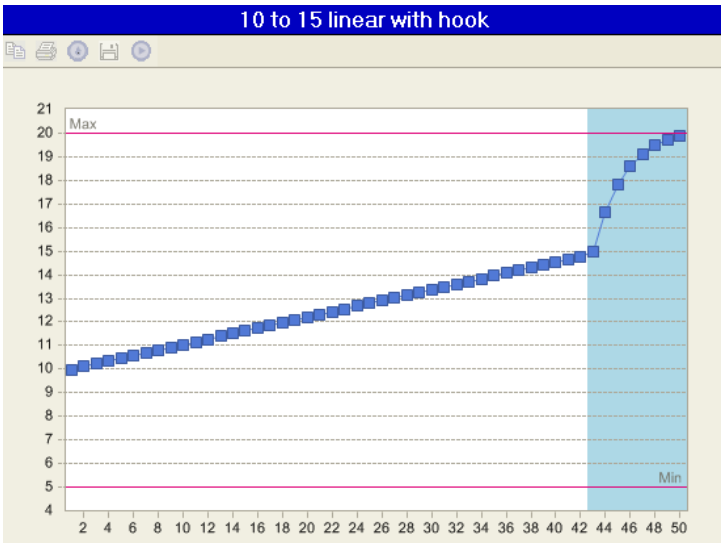

Figure 2.3 Schematic depicting the acrylamide percentage profile used in casting large format gradient gels. The acrylamide gradient chosen was linear from 10-15% and increased rapidly in the bottom of the gel. The gel is comprised of 50 acrylamide bands, increasing in concentration from the first (10%, top of the gel) to the last (20%, bottom of gel).

2.7.7.2 Large format backed gels

Backed gels are immobilized to the non-spacer glass plates and were cast for protein spot picking purposes. After the plates were cleaned and dried, 3 ml of fresh Bind-Silane solution [0.01% (v/v) PlusOne Bind-Silane (GE Healthcare, Amersham, UK), 80% (v/v) ethanol, 0.2% (v/v) acetic acid glacial] were evenly applied to a non-spacer glass plate using a lint-free KimTech Pure Wiper and left to air dry for 1 hour protected from dust. The plates were then assembled into cassettes with the spacer plates for gel casting as described above.

2.7.7.3 Protein loading by anodic cup

Rehydration of 24 cm pH 4-7 IPG strips (GE Healthcare, Amersham, UK) was performed similarly to the mini-2D SDS-PAGE gels. A total volume of 450 µl rehydration solution [1% (m/v) fresh DTT, 1% (v/v) of relevant IPG ampholite buffer and 0.002% (w/v) bromophenol blue in LB] was used to rehydrate the strips for 12-24 hours. Rehydrated strips were then transferred gel side up to clean individual ceramic Ettan IPGphor strip holders (GE Healthcare, Amersham, UK), gel-side up, with the acidic end at the anode. Electrode wicks soaked with MQ water were blotted with filter paper to remove excess

water and placed on top of both ends of each strip and electrodes placed firmly on top of each electrode wick. Sample loading cups were positioned as close as possible to the acidic end of each strip and checked for leaks by loading paraffin oil on the cup prior to loading. Strips were then completely covered in paraffin oil to prevent dehydration. Protein samples were centrifuged at 16,000 *g* for 5 minutes prior to loading to remove insoluble material. A total volume of 70 µl containing the protein sample in rehydration solution was loaded by pipetting under the paraffin oil. Rehydration solution is denser than paraffin oil and remains underneath the oil until it is taken up by the IPG strip.

2.7.7.4 Large format first dimension isoelectric focusing

Rehydrated IPG strips with the protein samples loaded in the cup were focused in an Ettan IPGphor unit using fixed a setting of 50 µA per strip at constant 20°C. IPG strips were focused to 70,000 $V.hr^{-1}$ in order to achieve optimal focusing. A longer $V.hr^{-1}$ count could result in overfocusing and poor spot separation. The 5 step program used is detailed in Table 2.3

Table 2.3 IEF parameters used for focusing 24 cm IPG strips on an Ettan IPGphor unit.

Step	**Voltage (V)**	**Step type**	**Time (hr:min)**	**Volt.hr^{-1} achieved**
S1	500	Gradient	00:10	83
S2	1000	Gradient	1:20	1333
S3	4000	Gradient	1:40	6666
S4	6500	Step-n-hold	10:00	65000
S5[1]	1000	Step-n-hold	60:00[a]	ignored

[a] This time is in excess and is designed to keep the strip under current, preventing protein diffusion, until the user stops it after an overnight run.

The gradient steps allow salts to gradually enter the electrode wicks and proteins to enter the strip from the cup. The maximum voltage Ettan IPGphor could achieve was 6500 V.

2.7.7.5 IPG strip equilibration

Immediately after IEF completion, strips were removed from the strip holders and carefully rinsed with MQ water to remove excess paraffin oil. Next, they were placed inside large cylindrical equilibration tubes for equilibration. Strips were equilibrated in 5 ml of equilibration buffer [6 M urea, 30% (v/v) glycerol, 2% (w/v) SDS, 50 mM Tris-HCl pH 8.8, 0.002% (w/v) bromophenol blue] containing 1% (w/v) DTT for 15 minutes at

room temperature. The strips were further equilibrated in equilibration buffer containing 4.8% (w/v) iodoacetamide for a further 15 minutes.

2.7.7.6 Second dimension large format SDS-PAGE

Large format 2D gradient gels were rinsed with MQ water and the equilibrated IPG strips were laid onto the resolving gel similarly to mini format 2DE. IPG strips were then overlaid with a warm agarose sealing solution [0.5% (w/v) agarose, 0.002% (w/v) bromophenol blue]. Second dimension electrophoresis was performed using the Ettan DALT*twelve* vertical electrophoresis system (GE Healthcare, Amersham, UK) that could run a total of 12 gels in parallel. Run settings were 5 W per gel for 30 minutes followed by 17 W per gel until the bromophenol blue dye front reached the bottom of the gels. Each run required 7.5 litres of 1X SDS running buffer in the lower reservoir and 2.5 litres of 2X concentrated SDS running buffer in the upper reservoir of the tank. Buffer mixing during electrophoresis was achieved by the built-in pump and temperature was maintained at a constant 25°C by an inbuilt temperature control system. A typical run lasted 5 hours.

2.7.8 In-gel protein staining

2.7.8.1 Coomassie brilliant blue R-250

Gels were stained with Coomassie brilliant blue R-250 using a sequential staining method consisting of 3 coomassie staining solutions that stain and fix the proteins in SDS-PAGE gels simultaneously (Table 2.4). The method was used for improved sensitivity due to its gradual removal of background staining. Each stain solution was warmed in a microwave oven for 30 seconds in a plastic container and gel submerged in the solution for at least 1 hour under gentle shacking. Stained gels could be left in distain until scanned and stored in desiccate state.

Table 2.4: Concentrations of reagents in the coomassie stain series. Percentages shown are v/v.

Reagents/Solutions	**Coomassie 1**	**Coomassie 2**	**Coomassie 3**	**Distain**
Coomassie stock (1.25% w/v)	2%	0.25%	0.25%	N.A.
Propan-2-ol	25%	10%	N.A.	N.A.
Glacial acetic acid	10%	10%	10%	10%
Glycerol	N.A.	N.A.	N.A.	10%

2.7.8.2 SYPRO Ruby total protein stain

SYPRO Ruby total protein stain (Genomic Solutions Ltd, Huntingdon, UK) was used for fluorescently staining proteins in analytical and picks gels. Gels were fixed with fixing solution [methanol 40% (v/v), acetic acid glacial 10% (v/v)] twice for 1 hour under gentle shaking in clean glass containers. SYPRO stain was filtered before use using two layers of Whatman qualitative filter paper using a vacuum pump prior to use to remove particles that can result in gel speckling. After fixing, gels were incubated overnight in SYPRO stain in the dark. Destaining was achieved by two 1 hour incubations in distaining buffer [methanol 10% (v/v), acetic acid glacial 6% (v/v)] before scanning. SYPRO solution was recycled after staining for further use. SYPRO stained gels were visualized under UV light (UVB, λ=300 nm) using a UV transiluminator or using a Typhoon imager. The fluorescence remains visible for at least 2 years after staining.

2.7.9 Gel imaging

2.7.9.1 Imaging using the ImageMaster scanner

Coomassie stained gels were imaged using an Image Master flat bed scanner (GE Healthcare, Amersham, UK), in transparency mode and images stored as TIFF files. Gels were placed directly on the scanner in order to avoid trapped air bubbles.

2.7.9.2 Imaging using the Typhoon 9400 variable mode imager

SYPRO stained and DiGE protein gels were scanned with the Typhoon 9400 Variable Mode Imager (Amersham Biosciences). Before scanning, the instrument was turned on for 15 minutes to warm up and the scanner surface (platen) cleaned with fresh 10% (v/v) hydrogen peroxide using lint-free KimTech Pure Wiper at the beginning of each scanning session. Between scanning two gels, the platen was cleaned again with 70% (v/v) ethanol. DiGE analytical gels were imaged inside their respective glass cassettes immediately after 2DE finished in fluorescent mode, normal sensitivity at the + 3 mm focal plane and using the appropriate combination of laser/filter for each of the three CyDyes (Table 2.5). They were held in place by Ettan Dalt gel holders during each scan. Each gel was prescanned once for each CyDye at a low resolution (pixel size 500 μM) to adjust PMT settings so that the most abundant protein spot had a signal intensity close to 70,000 AU, in a maximum linear dynamic range of 100,000 AU. This PMT value was used in the final scan at high resolution (pixel size 100 μM). 1D gels were imaged directly on the platen. SYPRO gels

were scanned in fluorescence mode, normal sensitivity, on the platen focal plane using the Cy3 laser/filter settings. The images acquired were saved as .gel files, and converted into TIFF files using IQTools software (GE Healthcare, Amersham, UK) for import into other image manipulation software.

Table 2.5 Emission filters and laser combinations used during the scanning of DiGE gels using the Typhoon 9400. BP denotes band pass.

Dye	**Emission filter (nm)**	**Laser (nm)**
Cy2	520 BP	Blue (488)
Cy3	580 BP	Green (532)
Cy5	670 BP	Red (633)

2.7.10 2-Dimentional Difference in Gel Electrophoresis (DiGE)

To ensure successful CyDye labelling of both TSP and Microsomal samples, a cleanup step was performed on the samples to remove contaminants that might interfered with the labelling process.

2.7.10.1 TSP Sample preparation

The 2D Clean-Up Kit (GE Healthcare, Amersham, UK) was used according to the manufacturer's instructions on TSP proteins for removal of compounds that could interfere with downstream analytical processes. Protein pellets were resuspended in DiGE labelling buffer [9 M urea, 2 M thiourea, 4% (w/v) CHAPS, 30 mM Tris-HCl pH 8.8] and the pH of all protein samples adjusted to 8-8.5 using 1 M NaOH. The pH was measured by pippeting 1 µl of the sample onto pH indicator strips. The samples were requantified using the modified Bradford assay to determine the new protein concentration after cleanup.

2.7.10.2 Microsomal Sample preparation

1.5 M Tris-HCl (pH 8.8) was added to microsomal samples in LB to the final concentration of 30 mM Tris-HCl before being precipitated in 80% (v/v) acetone for 30 minutes at room temperature with regular vortexing. Protein pellets were obtained by centrifugation at 13,000 *g* for 10 minutes and the supernatant discarded. Protein pellets were resuspended in DiGE labelling buffer and the pH adjusted to 8-8.5 similarly to the

TSP sampled. The samples were requantified using the modified Bradford assay to determine the new protein concentration and protein loss.

2.7.10.3 Preparation of CyDyes

CyDye DiGE fluor minimal dyes (GE Healthcare, Amersham, UK) were reconstituted from their supplied dry form using unopened high quality dimethylformamide (DMF) anhydrous (≥ 99.8% pure). It is essential to use unopened DMF because the reactive groups of the dyes are very water-sensitive. Unopened CyDye vials were removed from the -20ºC freezer and allowed to equilibrate at room temperature for at least 5 minutes prior to opening. The contents of each vial were centrifuged at 13,000 *g* for 5 minutes prior to opening and resuspended in 10 µl of DMF to obtain the primary stock solution (1 nmol/µl) which is stable at -20ºC for at least 4 weeks. The working stock was obtained by further diluting the primary stock to 400 pmol/µl in DMF.

2.7.10.4 Protein CyDye labelling

All labelling reactions with CyDyes were done using the recommended ratio of 400 pmol dye/50 µg protein. A total of 50 µg of each sample was labelled in a final volume of 30 µl. A pooled standard was obtained by mixing 50 µg of all the samples in the experiment and labelled with Cy2 using the same dye-to-protein ration. The labelling reaction was carried out in 500 µl eppendorfs at 4ºC, in the dark, inside an ice bath. Reaction was started with the addition of 1 µl of working stock dye, vortexed and was left incubating in the ice bath in the dark for exactly 30 minutes. The reaction was stopped by adding of 1 µl of 10 mM lysine that quenches un-reacted dye, after which the tubes were left for a further 10 minutes on ice. Tubes containing labelled protein were stored at -20ºC. The final protein concentration in each sample was 1.66 µg/µl, in a final volume of 30 µl. Each protein sample was labelled with both Cy3 and Cy5 in two parallel labelling reactions in a dye swap experiment to eliminate potential preferential dye labelling artefacts. Labelled protein was stable indefinitely when stored at -20ºC in the dark.

2.7.10.5 DiGE sample mixing and large format 2DE of DiGE analytical gels

Sample mixture consisted of 12.5 µg of the Cy3-, Cy5- and Cy2-labelled protein samples, making up a total loading of 37.5 µg of protein per gel. The mixture was made up to 70 µl with blue LB [9 M urea, 2 M thiourea, 4% (w/v) CHAPS, 0.05% (w/v) bromophenol blue]

containing 1% (w/v) DTT and 2% (v/v) pH 4-7 carrier ampholites (GE Healthcare, Amersham, UK) as shown in Table 2.6. The mixture was separated using large format 2DE using anodic cup loading and the analytical gels imaged using the Typhoon variable mode imager as described earlier.

Table 2.6 Loading volumes for a 24 cm pH 4-7 IPG strip for analytical 2D-DiGE.

Component	Volume
Cy3 sample	7.5 µL
Cy5 sample	7.5 µL
Cy2 sample	7.5 µL
50% (w/v) DTT	1.4 µL
IPG buffer 4-7	1.4 µL
Blue LB	44.7 µL
Final volume	70 µL

2.7.10.6 Image analysis of DiGE gels using DeCyder software

DiGE gel datasets were cropped using IQTools software (GE Healthcare, Amersham, UK) to remove unnecessary data prior to analysis. The DeCyder Differential Analysis Software suite (version 6.5.11, GE Healthcare, Amersham, UK) was used to perform spot detection, inter-gel matching, normalisation and volume calculations across all gels. The batch process module was used to automatically perform all these calculations simultaneously across all the gel images in the experiment. The number of spots was estimated at 5000 for the TSP and microsomal samples. The gel with the highest number of features was automatically selected as the master gel. The matching quality of the batch process analysis was verified manually in the biological variation analysis (BVA) module and mistakes in inter-gel matching between spots were manually corrected (Figure 2.4). Where a spot was not detected but was clearly visible the spot boundary was copied from the master gel image to the respective gel image. Spots of interest between treatments were selected based on their *p*-value using the independent Student's *t*-test for independent samples and fold change ratio. For the ATP only treatment experiment, spots with a very significant ($p \leq 0.01$) minimum fold change of 2 were considered as

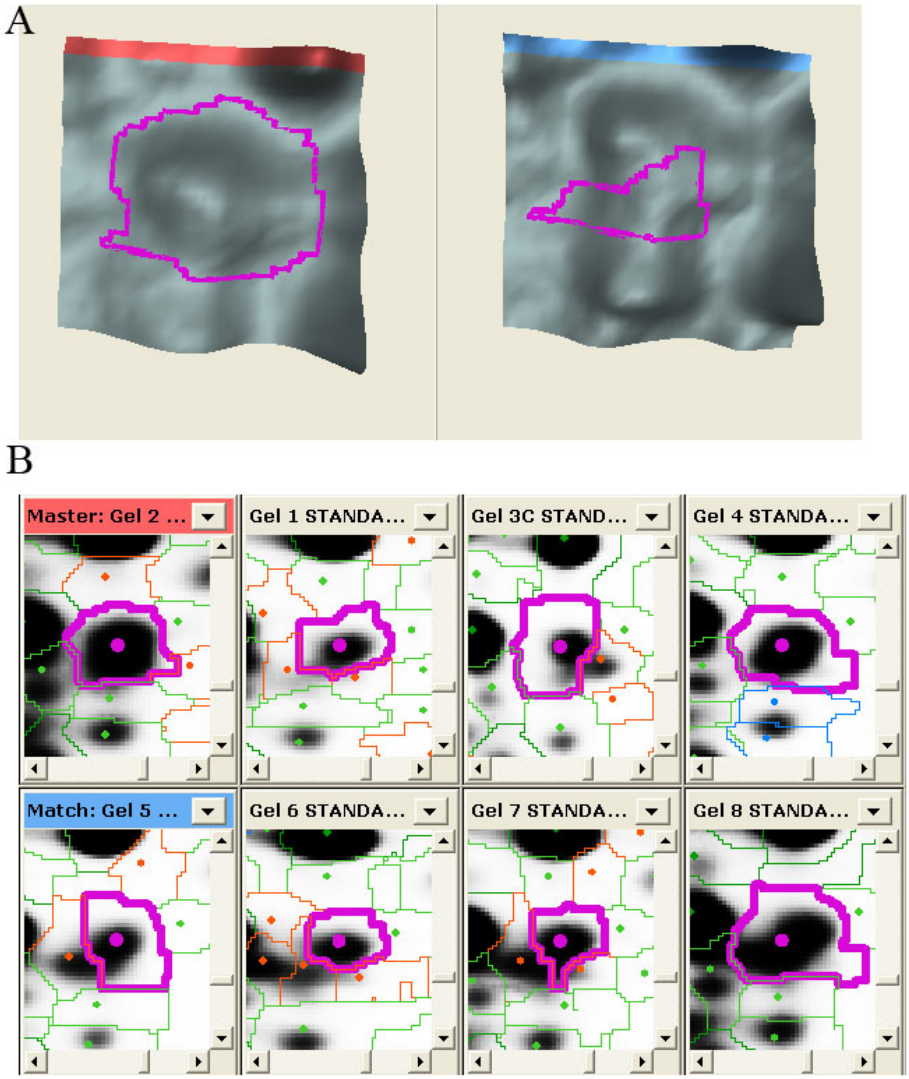

Figure 2.4 An example of matching problems in 2D-DiGE. (A) 3D view of a spot from the BVA module in DeCyder. The purple line delineates the boundary of the spot. By comparing the same spot in the master gel to another gel, it is hard to decide on what the real profile is for one particular spot. (B) Comparing the same spot across 8 gels simultaneously makes it possible to decide on the best spot matching. Here it was decided the correct matching is a single spot as the one seen in the master gel, because 5 out of 8 images showed 1 spot instead of 2 (Gel 2, 1, 4, 6 and 8).

changing with ATP. In the FB1 only treatment, spots with a significant ($p \leq 0.05$) minimum fold change of 1.2 in the TSP sample or 1.5 fold in the microsomal sample were considered as changing with FB1. Of these, spots with a significant ($p \leq 0.05$) minimum fold change of 1.2 between FB1 and ATP+FB1 treatment were considered as changing with ATP in the ATP+FB1 treatment. These spots were termed as responding to ATP availability (reversed

spots). It was not necessary for a spot to be detected across all gels to be considered a spot of interest. Spots of interest were selected for identification by mass spectrometry by MALDI-ToF or MS/MS following proteolytic cleavage with trypsin.

2.7.11 Identification of proteins by mass spectrometry

Large-format backed pick gels, loaded with 400 μg of total protein, were performed as described for analytical gels specifically for picking proteins for identification by mass spectrometry. Protein spots selected for picking were identified in the pick gel by matching it with the analytical master gel in DeCyder.

2.7.11.1 Manual excision of protein spots

An image of the pick gel highlighting the spots selected for picking was generated in DeCyder and used for referencing during picking. Spots from SYPRO stained pick gels were carefully excised using One Touch Plus spot picking pipettes (The Gel Company), combined with filtered disposable tips, into separate wells of a 96-well microtitre plate (Genomic Solutions Ltd, Huntingdon, UK). Picking was performed on a UV transiluminator with gloves and head mask to minimize keratin contamination of gel plugs. Gels were rinsed frequently with distain solution to wash away contaminants and prevent gel dehydration due to the heat generated by the UV transilluminator.

2.7.11.2 Robotic excision of protein spots

Robotic excision of spots was carried out using a ProPic spot picking robot (Genomic Solutions Ltd, Huntingdon, UK) in combination with Phoretix Evolution image analysis software (Nonlinear Dynamics, Newcastle upon Tyne, UK) and DeCyder software. A SYPRO stained pick gel was imaged using the CCD camera inbuilt in the ProPic robot with UV transilluminator and the image was imported into Phoretix software. Spots selected for picking were highlighted in the master gel image in DeCyder and manually marked in the pick gel image in Phoretix. The resulting picking list coordinates were then imported to the ProPic robot. Spots were then automatically excised into separate wells of a 96-well microtitre plate. The gel was periodically rehydrated with water to prevent distortion of the spot profile.

2.7.11.3 Trypsin in-gel digestion of proteins

96-well microtitre plates containing gel plugs were transferred to a ProGest Workstation (Genomic Solutions Ltd, Huntingdon, UK) for automated tryptic digestion and peptide extraction according to the ProGest overnight trypsin digestion protocol. Gel plugs were equilibrated in 50 µl of 50 mM ammonium bicarbonate and subsequently reductively alkylated with 10 mM DTT and 100 mM iodoacetamide, followed by destaining and desiccation with acetonitrile. Gel plugs were rehydrated with 50 mM ammonium bicarbonate containing 6.6% (w/v) trypsin (Promega Ltd., Madison, WI, USA) and digested overnight. Peptides were extracted from the gel using 50% (v/v) acetonitrile and 0.1% (v/v) TFA into a final volume of 50 µl and lyophilised in a vacuum concentrator. Peptides were re-suspended in 10 µl of 0.1% formic acid and sonicated in an ultra-sonic water bath at room temperature for 1 minute for maximum re-suspension of peptides prior to spotting on a MALDI target plate.

2.7.11.4 MALDI ToF protein identification

MALDI ToF protein identification was carried out using a Voyager DE-STR Biospectrometry workstation (Applied Biosystems, Warrington, Cheshire, UK). A total of 0.5 µl of each digest was spotted together with 0.5 µl of a saturated solution of α-cyano-4-hydroxycinnamic acid matrix directly onto a MALDI target plate manually or using an Applied Biosystems symbiot robot (Boston, MA, USA) and allowed to air dry for 1 hour. Individual spots were then washed with 5 µl ice-cold 0.1% (v/v) TFA to remove non-peptide impurities. Instrument calibration was carried out for each sample using PE sequazyme calibration mixture I (containing des-Arg-bradykinin, angiotensin I, glu-fibrinopeptide B, and neurotensin). Spectra were acquired from 480 laser shots using system parameters optimised for the mass range of 800-3500 *m/z*. After each spot's spectra were acquired, automated peak detection, peak de-isotoping and noise reduction was carried out using Applied Biosystems Proteomic Solutions 1 software to generate peak mass tables. Trypsin autolysis peaks (842.500 and 2211.100 *m/z*) were used as internal calibrates and excluded from database searches. The PMF for each spot was used to search the non-redundant NCBInr database version 20070713 (5269953 sequences; 1825351362 residues) using the Mascot search engine (Perkins *et al.,* 1999) version 2.2 (Matrix Science, Boston, UK). The following search parameters were used: peptide mass tolerance:

± 50 ppm, maximum number of missed cleavages: 1, fixed modifications: carbamidomethylation of cysteine residues, variable modifications: oxidation of methionine residues. Searching was restricted to *Viridiplantae* (green plants), where the Mascot software probability-based MOWSE score cut-off for a significant ($p \leq 0.05$) positive protein identification was 71. Where more than one database entry was obtained from a single spot, the spots were highlighted as a mixture since it was impossible to know which of the proteins in the mixture were differentially regulated.

2.7.11.5 MALDI-ToF-MS/MS protein identification

MALDI-ToF-MS/MS protein identification was performed using a 4800 Proteomic Analyser (Applied Biosystems, Foster City, USA). All samples were subjected to a combination of ToF-MS and MS/MS analysis, for increased confidence in the identification, with automated data acquisition and processing controlled by the Applied Biosystems 4000 series Explorer software (version 3.5). The following settings were used: reflector mode, mass range of 700–4000 *m/z*, 1000 total laser shots per spectrum, and a laser intensity of 3300 V. The acquired ToF-MS spectra were noise-corrected, peak de-isotoped, and internally calibrated with the trypsin autolysis peaks of 842.500 and 2211.100 *m/z*. For MS/MS analysis, the software selected up to 10 of the most abundant precursor ions for fragmentation using a 1 kV CID fragmentation method collecting 4000 laser shots per spectrum with a laser intensity of 3800 V over the whole mass range. The peak lists of ion masses for each spectra were generated by the Applied Biosystems GPS explorer software (version 3.6) using the calibrated and de-isotoped MS and MS/MS spectra for each sample. The combined lists of MS and MS/MS data were used for database searches with Mascot version 2.2 (Matrix Science, Boston, USA), against NCBInr 9655479 sequences (released 1st September 2009). For database interrogation the following search parameters were used: digestion enzyme used: trypsin, maximum number of missed cleavages: 1, variable modifications of carboxymethyl cysteine, and oxidised methionine, precursor mass tolerance of ± 50 ppm and fragment ion tolerance of 0.2 Da. Searching was restricted to *Viridiplantae* (green plants). Protein identification was considered positive when the combined protein score, incorporating the MS/MS-derived individual ion scores where available and the PMF-associated score, was more than 95% confident ($p \leq 0.05$). The cut-off threshold for this score in Mascot with the searched

parameters used was 71. Where more than one database entry was obtained from a single spot, the spots were highlighted as a mixture since it was impossible to know which of the proteins in the mixture were differentially regulated.

2.8 Bioinformatic analysis

For Database for Annotation, Visualization and Integrated Discovery (DAVID) analysis, a list containing the Arabidopsis Gene Identifier (AGI) number of all relevant genes was compiled. This list was uploaded on to the DAVID web-based tool (http://david.abcc.ncifcrf.gov/) and analysis performed online using the provided default settings. Medium stringency setting was used due to the small number of genes in each list. For functional clustering analysis, the default annotations selected were:

1. Functional Categories (COG_ONTOLOGY, SP_PIR_KEYWORDS and UP_SEQ_FEATURE)
2. Gene Ontology (GOTERM_BP_FAT, GOTERM_CC_FAT and GOTERM_MF_FAT)
3. Pathways (KEGG_PATHWAY)
4. Protein domains (INTERPRO, PIR_SUPERFAMILY and SMART)

For metabolic pathways analysis, only KEGG_PATHWAY annotations were selected.

Chapter 3 Identification of eATP-regulated cell death proteins using proteomics and reverse genetics

3.1 Introduction

It has been established that eATP plays a central regulatory role in plant cell death processes (Chivasa *et al.,* 2005a). An understanding of the signalling components controlled by eATP in cell death regulation, both receptors and downstream signalling components, will provide insight into the mechanistic details of how eATP signals in plant physiological processes, particularly PCD. Extracellular ATP-mediated signalling negatively regulates cell death, as its removal by application of ATP-degrading enzymes, such as apyrase, to the apoplast or the competitive exclusion of eATP from target binding sites using non-hydrolysable ATP analogues activates plant cell death (Chivasa *et al.,* 2005a). The components of this pathway are still not known. Fumonisin B1 (FB1) manipulates this eATP-regulated signalling to deliberately trigger PCD in plants. FB1 is a mycotoxin secreted by fungi in the genus *Fusarium moniliforme* and initiates PCD in both animal and plant cells (Gilchrist 1997), but the underlying proteome changes are still poorly understood. In *Arabidopsis thaliana* (*Arabidopsis*), FB1-dependent PCD induction is preceded by the inactivation of eATP-mediated signalling via a gradual collapse in the levels of eATP (Chivasa *et al.,* 2005a). This depletion in eATP levels is essential for cell death to progress, as addition of exogenous ATP up to 40 hours after FB1 addition is sufficient to prevent cells from irreversibly initiating PCD. Although cell death can be prevented in this way, this process is dependent on the time of ATP addition (Figure 3.1A). In a cell culture experimental system, Addition of ATP up to 40 hours after FB1 can still rescue cells from committing to cell death, but if ATP is added beyond 48 hours after FB1 treatment cells can no longer be prevented from undergoing PCD [Figure 3.1A, (Chivasa *et al.,* 2005a)].

Because eATP-mediated signalling is likely to affect the protein abundance of cell death regulators (Figure 3.1A), an experimental approach was designed to identify proteins with altered abundance in response to FB1-mediated eATP depletion whose response to FB1 is attenuated by ATP addition. This provides the basis for a specific filter – the ATP filter (Figure 3.2A) – designed to identify putative cell death regulators directly controlled by eATP signalling. It is expected that this approach will aid in achieving the global objective of elucidating the mechanism of eATP signalling in plant cell death regulation.

The aim of this chapter is to identify novel eATP-regulated cell death proteins using an *Arabidopsis* suspension cell culture system. It is proposed to achieve this goal by using the

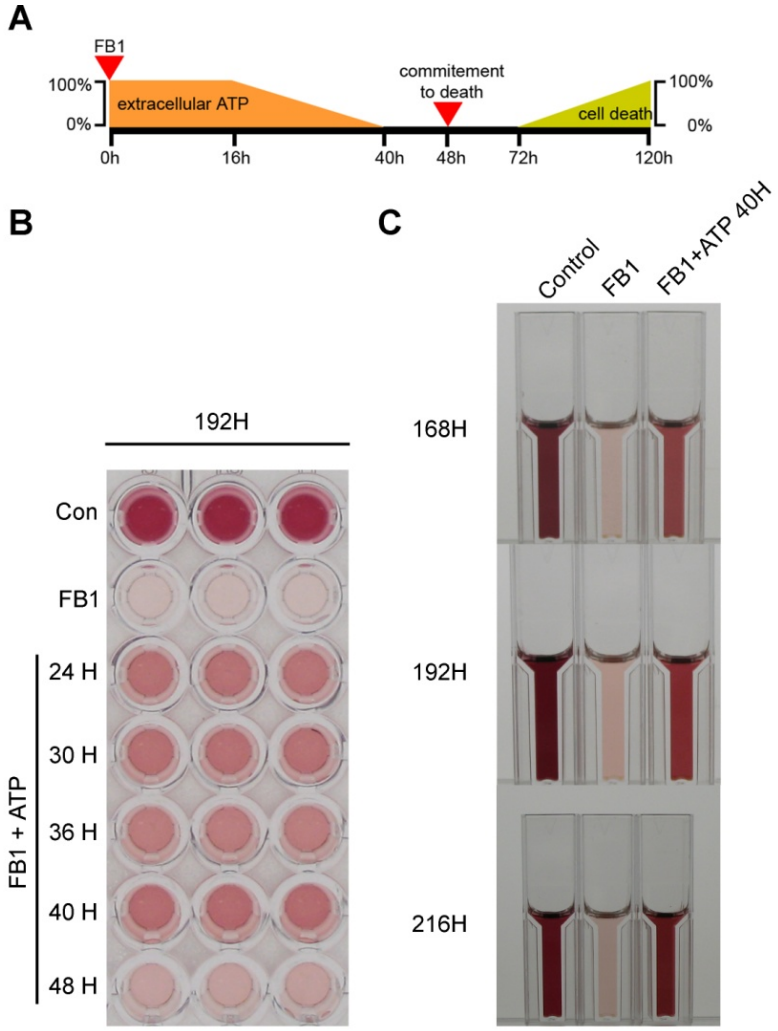

Figure 3.1 The effects of exogenous ATP addition on FB1-induced cell death in *Arabidopsis* cell suspension cultures. (A) Schematic representation of FB1-induced changes on eATP levels and cell viability overtime. Cell cultures irreversibly commit to death at ~48 h after FB1 addition and cell death starts at ~72 h. Exogenous ATP added up to 40 h blocks FB1-induced cell death. Schematic is not drawn to scale. (B) MTT assay cell viability results 192 hours after FB1 addition. ATP was added at different timepoints after FB1 addition, shown by the numbers on the left of the panel. Purple colour indicates viability of cells, as indicated in the controls in the first 2 rows. Highest extent of recovery was observed when ATP was added 40 hours after FB1. (C) MTT assay of cell cultures where ATP was added 40 hours after FB1 over 3 consecutive timepoints. Recovery is practically complete 216 hours after the start of the experiment.

ATP filter in 2D-DiGE analysis of protein abundance to identify proteins which are differentially regulated by FB1 and also showed a differential, but opposite, regulation pattern upon ATP treatment in the concurrent treatment. Such a response would indicate a direct regulation by eATP signalling rather than FB1 specific signalling. This will be achieved by comparing the proteomes of untreated controls with FB1-treated only and with a combination of FB1 and ATP before the predicted cell death commitment step (Figure 3.1A). This approach will be applied to two protein fractions: a total soluble protein fraction (TSP) that provides a global view of the proteome, and a microsomal membrane fraction enriched for membrane-bound proteins. By using the ATP filter, it is predicted that a subset of proteins that play a role in eATP-mediated PCD can be identified.

The use of the ATP filter will provide a list of proteins differentially regulated by eATP availability. This, however, is not enough evidence in support of a putative role in PCD. Confirmation of such a role is necessary. Therefore, validation of a putative PCD function of these proteins will be investigated by characterizing the cell death response of T-DNA homozygous KO lines for the selected gene where available. Thus, this approach will enable the identification of novel genes that are components of the eATP-mediated signalling pathway as well as PCD effectors that are regulated by eATP signalling. Additionally, it is also expected to provide insight into the proteome changes induced by FB1 that precede cell death commitment in *Arabidopsis*. The lists of proteins differentially regulated by FB1 obtained in this chapter will be invaluable for later studies aimed at understanding the specific mechanisms of FB1-induced cell death in plants.

In this chapter, I demonstrate the potential of the ATP filter in identifying novel cell death targets. The ATPase β–subunit was identified as a differentially regulated protein by eATP levels and its role in PCD regulation validated using 3 independent T-DNA KO lines.

3.2 Results

3.2.1 FB1-induced PCD is blocked by ATP addition

It has been shown that ATP can block FB1-induced PCD if added concurrently up to 40 hours after FB1 (Chivasa *et al.,* 2005a). Since this whole chapter is based on the effective reversal of FB1-induced cell death by ATP addition, it was decided to reproduce the same experiments in order to be absolutely confident that this system could be reproducibly

replicated before generating protein samples for 2D-DiGE analysis. This was necessary because if the ATP treatment failed to rescue FB1-induced cell death under my conditions, the results would be compromised. An ATP addition timecourse on FB1 treated cultures was performed in order to confirm what is reported in the literature and investigate if different ATP addition timepoints have any effect on the extent of recovery of the cultures.

The metabolic state of cell cultures was assessed by measuring the mitochondrial activity of 1 ml of culture using the MTT assay. Mitochondrial activity provides a good estimate of the general metabolic status of cultures treated with FB1 and can be used to measure the extent of cell death of a culture (Chivasa *et al.,* 2005a). FB1-treated cultures were treated with 1 mM ATP at 24, 30, 36, 40 and 48 hours after FB1 addition and the relative metabolic status of the cultures was measured every 24 hours thereafter using the MTT assay. An FB1 only culture was used as a positive control. In this control, the gradual decrease in purple colour indicates a complete shutdown of mitochondrial activity as a consequence of cell death. It was observed that 144 hours after FB1 addition, ATP treatment successfully prevented cell death in all the timepoints tested except for when ATP was added 48 hour after FB1 (data not shown), confirming that ATP rescue of cultures is limited to a 40 hour time window after FB1 treatment (Chivasa *et al.,* 2005a). However, no significant differences in the recovery rate between them were evident at this timepoint. Therefore, these cultures were allowed to grow further and MTT readings taken until a clear difference was visible between them. As it turned out, 192 hours after FB1 treatment, the culture where ATP was added 40 hours after FB1 displayed a significant stronger purple colour than the cultures where ATP was added 24, 30 and 36 hours after FB1 (Figure 3.1B). From these results, it is clear that the culture treated with ATP at 40 hours had recovered faster than the others. Indeed, the extent of recovery in this culture was such that it displayed a similar mitochondrial activity rate to untreated controls 216 hours after FB1 treatment (Figure 3.1C). This shows that ATP addition is most efficient in blocking the FB1-induced cell death the closer it is added to the commitment timepoint (Figure 3.1A). This could indicate a drop in eATP levels bellow a critical threshold immediately after 40 hours and that this drop is more efficiently blocked by exogenous ATP addition just before 40 hours after FB1 treatment. Hence, this timepoint was chosen for ATP addition when generating the protein samples for the ATP filter. Additionally, it was decided to harvest all cell cultures for protein analysis 48 hours after FB1 treatment. The advantages of this timepoint are twofold. Firstly, at this stage the FB1-induced

changes in protein abundance have already committed the cell cultures to dying but cell death itself has not started. Cell death starts around 72 hours after FB1 addition [Figure 3.1A (Chivasa *et al.,* 2005a)]. Secondly, uncontrolled protein degradation likely to result in changes in protein abundance unrelated to PCD induction has not yet begun. This would be a consequence of loss of cellular integrity. In a study employing large scale analysis of protein abundance, it is important to avoid this as it would result in the identification of several artefactual protein abundance changes that would make the interpretation of the results very difficult.

3.2.2 FB1-induced gene expression is reversed by ATP addition

The re-establishment of eATP-mediated signalling in FB1 treated cultures blocks PCD and this fact entails that at least a subset of cell death regulators is differentially regulated by eATP signalling (Figure 3.2A), but this has not been tested yet on known cell death regulators. A preliminary experiment was performed to confirm the ATP filter approach can detect molecular targets involved in PCD before performing a large scale proteomics study. The senescence-associated gene 1 (*SEN1*, AT4G35770), a gene that is induced during senescence-associated cell death (Oh *et al.,* 1996), was used for this purpose. Since senescence is a form of PCD, it is expected that some of its signalling/effectors will overlap with FB1-induced PCD. In the absence of a specific antibody for *SEN1* protein, the abundance of the coding mRNA was investigated in cell cultures using sqRT-PCR. *SEN1* was found to be highly upregulated with FB1 after 40 hours at the mRNA level, and this increase was significantly attenuated by eATP addition within two hours (Figure 3.2B and 3.2C). This shows that eATP can effectively reverse FB1-induced changes at the transcript level in a known cell death-associated gene in accordance with its ability to block FB1 cell death. It is likely that changes at the transcript level will be mirrored by changes at the protein abundance level. These results provide supporting evidence for using the ATP filter in a study employing 2D-DiGE comparative analysis of protein abundance to identify eATP-regulated proteins that mediate cell death control.

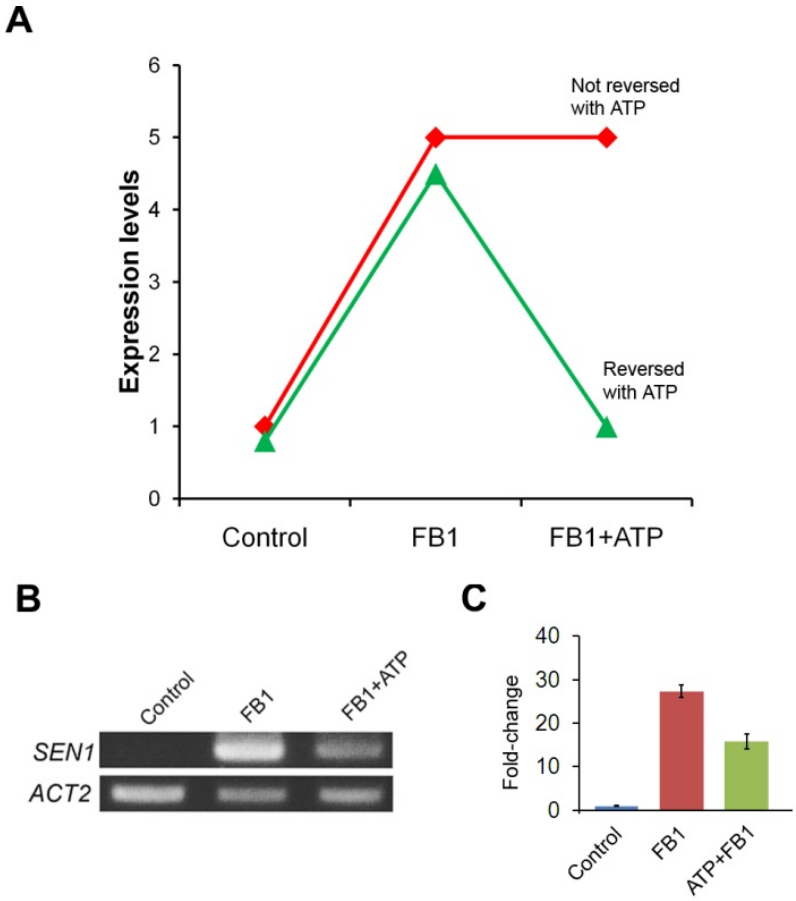

Figure 3.2 Principle of the ATP filter at the gene expression level. (A) Schematic representation of the ATP filter in action. Both red and green lines change in abundance with FB1 treatment, but only the green line returns to control levels after ATP treatment, indicating that it is regulated by eATP signalling. Protein spots with this profile in response to FB1 only and ATP+FB1 are referred to as "reversed with ATP". (B) Induction by FB1 of a cell death marker, *SEN1*, is attenuated by exogenous ATP. Samples for RT-PCR were harvested at 42 h, 2 hours after ATP addition. Actin-2 (*ACT2*) was used as a constitutive reference control. (C) Densitometric analysis of *SEN1* PCR bands from (B) expressed as fold-change relative to the control sample. Data and error bars are means ± SE (n = 3).

3.2.3 2D-DiGE protein gel analysis and protein identification results

3.2.3.1 Principle of 2D-DiGE

2D-DiGE is a good improvement of 2DE (Unlu *et al.,* 1997). It allows the labelling of protein samples with three spectrally resolvable CyDyes of very similar molecular masses (Cy2: 550.6, Cy3: 582.7, Cy5: 580.7). This enables multiplexing gels, where up to 3 protein samples labelled with different CyDyes are mixed in the same 2D gel co-migrate, greatly reducing inter-gel matching difficulties. The use of an internal standard, a protein mixture consisting of equal amounts of all samples in the experiment labelled with Cy2, enables automated spot volume normalization, matching and quantitation using DeCyder software. By reducing user input, user-derived artefacts are also reduced. Protein samples are minimally labelled with CyDyes at the recommended ratio of 400 pmol/ 50 μg of protein, where only 1-2% of lysine residues are labelled. However, the sensitivity of the platform enables accurate quantitation of very low (1 ng) amounts of labelled-protein while maintaining a linear dynamic range of 4 orders of magnitude and the capability of detecting protein abundance changes as low as 10% (Tonge *et al.,* 2001). Before protein labelling with CyDyes, protein samples must pass a strict quality control procedure designed to ensure samples are accurately quantified, resolve correctly on a 2D gel and are equally labelled with CyDyes. Because DiGE can confidently detect changes in protein abundance as low as 10%, it is imperative to ensure protein abundance changes measured are a result of the treatments employed and not an artefact of protein sample handling.

3.2.3.2 Protein sample generation and quality control checks

A 4 independent biological replicate experiment was performed for increased statistical significance. A mother culture was initially grown to mid exponential phase before subculturing into 12 new flasks. These "sister" cultures were then used to generate the protein samples for 2D-DiGE analysis. Cell cultures in mid exponential stage were exposed to FB1 for 40 hours. Half the cultures were then mock treated and the other half treated with 1 mM ATP. Treated cells were harvested for protein extraction at the 48 hour timepoint. Cells were disrupted in a French Press cell disruption system (Constant systems Ltd., Warwick, UK) at 4ºC. This system compromises the integrity of the plasma membrane and all subcellular compartments, releasing soluble proteins. After mechanical disruption of cell cultures using the French Press, the TSP fraction was separated from the microsomal membranes by ultra centrifugation and precipitated in 80% acetone and

solubilised in lysis buffer (LB) as described in the materials and methods chapter. The microsomal protein fraction is enriched for disrupted membranes and LB was used to directly solubilise the protein in this fraction.

After sample generation and protein extraction, protein samples in LB were quantified by the modified Bradford assay. Heating of the protein samples in LB buffer to aid solubilisation was avoided because this can lead to carbamylation of primary amines in the proteins resulting in spot trains and reduced labelling with CyDyes. It is imperative that protein quantification is as accurate as possible since an inaccurate estimation of protein concentration would result in labelling unequal amounts of protein, compromising downstream analysis of protein abundance. For checking protein quantification accuracy and reproducibility of the profiles between biological replicates, 10 µg of each sample were loaded on a 1D gel and resolved by 1D SDS-PAGE. The gels containing samples from TSP and microsomal replicas 1 and 2 are shown in Figure 3.3.

In order to obtain the best resolution on a 2D gel images for the samples in this study, the isoelectric range of IPG strips was optimized using the TSP sample in mini-2D gels. A broad range strip of a linear pI range 3 to 10 was initially used to locate the bulk of the proteins in a 2D profile (Figure 3.4A). The TSP sample contained few proteins with isoelectric points between 3-4 and 8-10. The majority of protein spots were concentrated between pI 4 and 8. Using an IPG strip with linear pI range 4 to 7 greatly increased spot resolution in that pI range (Figure 3.4B). It was decided to use this pI range for subsequent 2D analysis in the absence of a commercial IPG strip 4-8.

3.2.3.3 Sample preparation and analytical gel generation for 2D-DiGE

Once correct quantification was verified on a gel and the pI range of 2D gels selected, the samples were ready for labelling with CyDyes. After cleaning up the samples using a 2D Clean-Up Kit (Amersham) designed to remove contaminants such as salts that can hinder labelling and interfere with first dimension focusing of the samples, the protein samples were labelled with the 3 available CyDyes. Equal amounts of all samples were labelled with Cy3 and Cy5 in a full dye-swap experiment to preclude dye specific effects (Karp *et al.,* 2005).

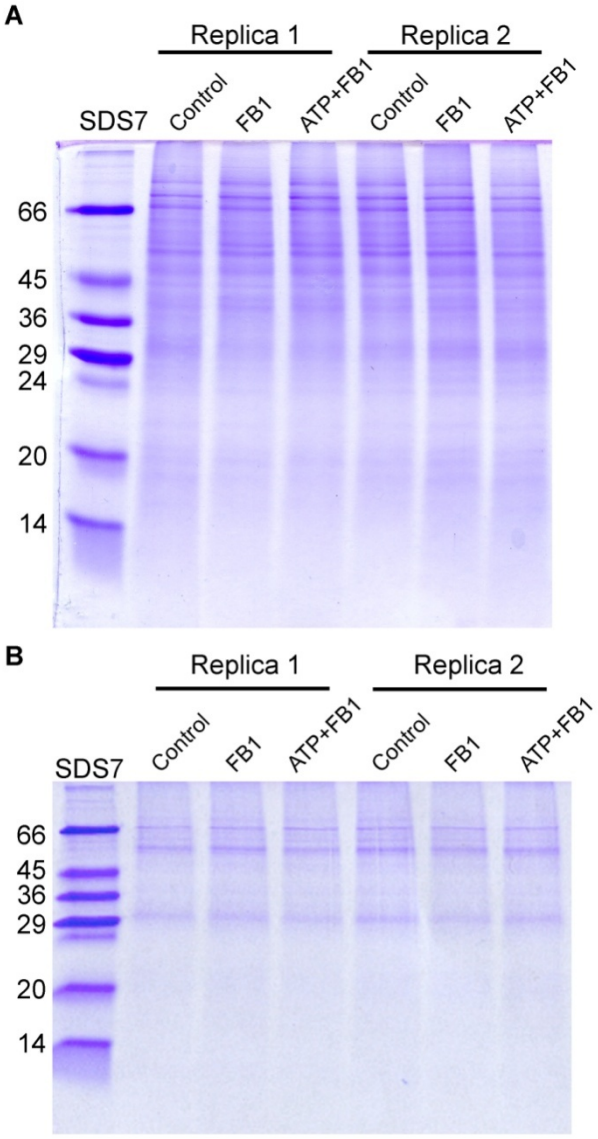

Figure 3.3 Independent biological replicate reproducibility and validation of quantification. (A) TSP and (B) microsomal samples from replicates 1 and 2 are shown. Sample reproducibility between independent biological replicates and protein quantification accuracy by the modified Bradford assay was evaluated by resolving 10 µg of each sample on a 1D gel stained with Coomassie brilliant blue. SDS7 MW values (KDa) are indicated on the left.

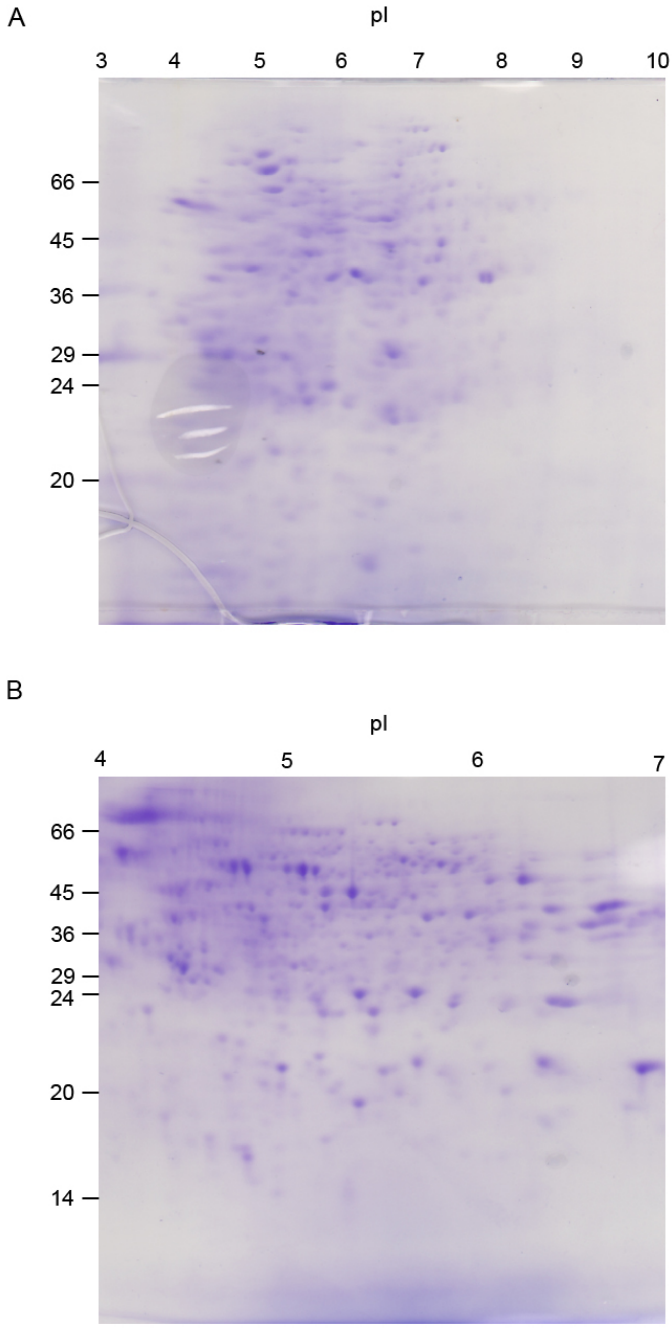

Figure 3.4 Optimization of pI range for 2DE of TSP protein samples. A total of 100 µg of TSP sample was resolved by mini 2DE using IPG strips 3-10 (A) and 4-7 (B) and stained with Coomassie brilliant blue R-250. The bulk of proteins spots in the pI 3-10 2D profile were concentrated between pI 4 and 8. A pI 4-7 strip successfully enhanced the separation of spots in the busiest area of the 2D profile and was selected for subsequent 2DE analysis. SDS7 MW values (KDa) are indicated on the left and pI subdivisions on the top of the gels.

The internal standard was labelled with Cy2. All labelling reactions were performed in an ice bath in the dark. To verify that labelling was equal across all samples for each dye, a 5 µg aliquot of each sample was resolved on a 1D gel and the gel scanned using the Typhoon 9400. The labelling was confirmed equal across the samples and the signal intensity sufficient for detection using the Typhoon (Figure 3.5).

It was essential to obtain the best possible analytical gels for DiGE analysis. To this end, samples were focused using the cup loading method instead of in-gel rehydration used for mini 2DE because it is known that it produces less streaking, although sample precipitation in the cup can happen resulting in a vertical smear in the cup position (Rabilloud *et al.,* 1994; Sanchez *et al.,* 1997). Proteins start entering the gel under current and migrate to their respective isoelectric point on the immobilized pH gradient strip. This results in better focusing because proteins move in the same direction after leaving the cup preventing the crossing of paths between proteins migrating in opposite directions as happens when using the in-gel rehydration method. The 4 independent replicas were focused in a total of 12 IPG strips (24 cm, pH 4-7 linear), each loaded with a Cy2 internal standard and a Cy3- and Cy5-treatment randomly arranged. All large format 2D gels were resolved simultaneously to eliminate batch to batch variation in the 2D profile that could arise from different run times. Gels were scanned while still inside the glass plates immediately after 2DE to prevent protein diffusion in the polyacrylamide matrix. During gel scanning, it was proposed to scan each CyDye at the highest PMT setting in order to better detect protein signals close to background noise. Care was taken to avoid spot saturation. Spot saturation can happen in the signal intensity is higher than the maximum dynamic range of the Typhoon variable mode imager (100.000 AU) resulting in underestimation of the spot volume. Gels were prescanned for each CyDye at a low resolution in order to determine the specific PMT value for each sample. If spot saturation was observed after the final scan, all 3 samples in the gel were rescanned with a lower PMT value for the saturated dye. After scanning, the Cy3 and Cy5 images can be merged using false colour, giving the user a quick and global view of protein abundance changes before quantitative analysis is performed (Figure 3.6).

As expected, the resulting 2D profiles revealed big differences between the TSP and microsomal membrane protein profiles, with the TSP fraction containing many more protein spots than the microsomal fraction (Figure 3.7A and 3.7B). Analysis of the two separate fractions enables

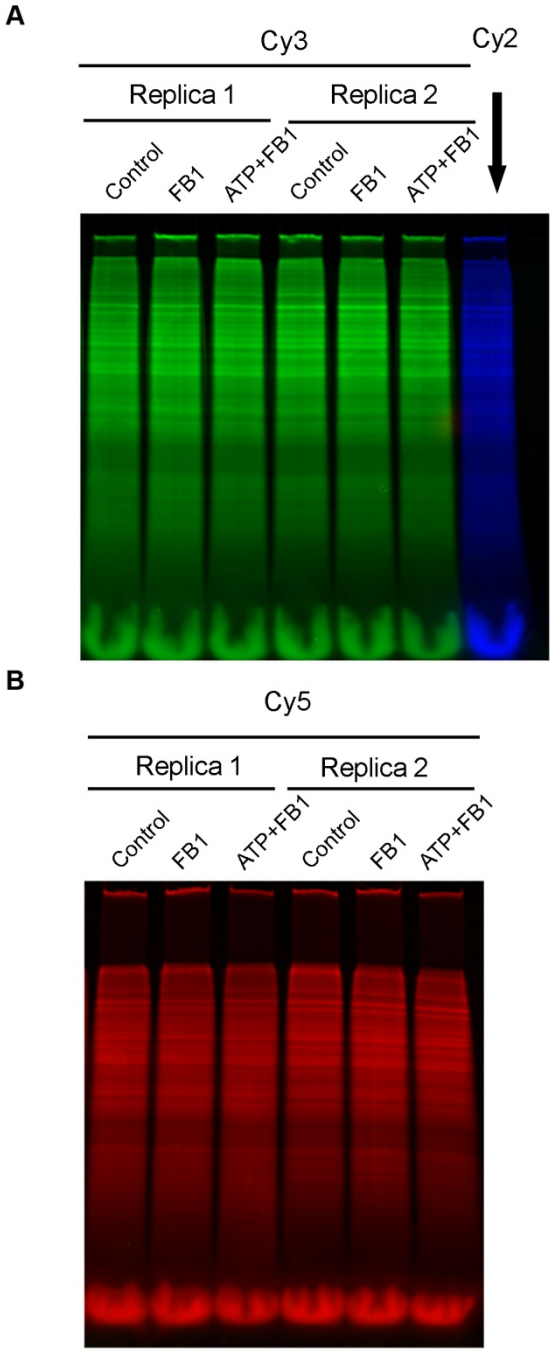

Figure 3.5 Evaluating CyDye labelling efficiency between samples. The labelling efficiency for each of the CyDyes and evaluation of equal labelling of each sample with Cy3 and Cy5 was confirmed by resolving 5 µg of each sample on a 1D gel. After SDS-PAGE, the gels were scanned using the Typhoon variable mode imager. Samples from TSP replicates 1 and 2 are shown. (A) Merged image of Cy3 and Cy2 samples separated on the same 1D gel. (B) Cy5 labelled samples.

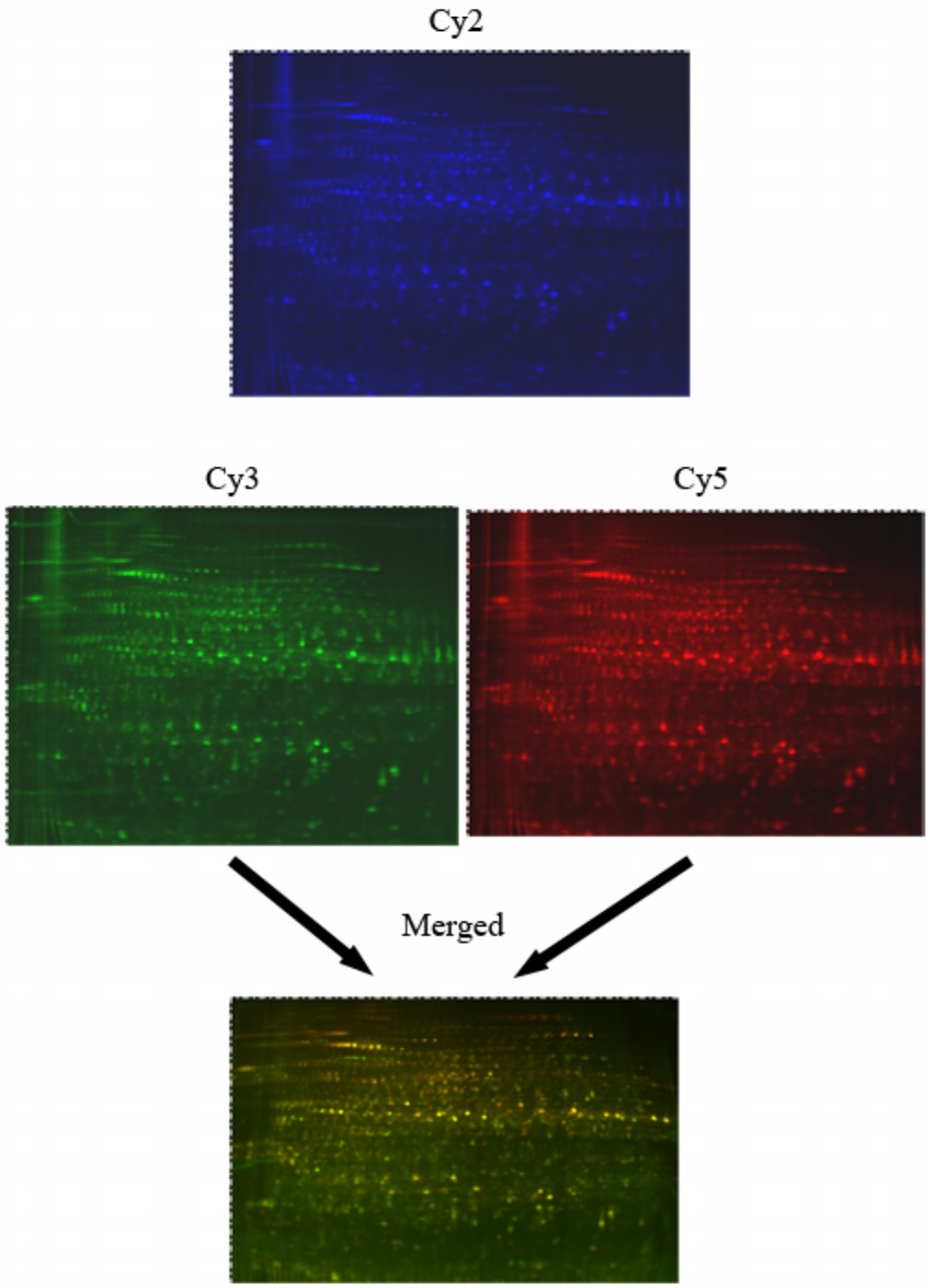

Figure 3.6 2D-DiGE protein profiles of TSP protein samples. The 3 images were obtained from the same gel loaded with Cy2-, Cy3- and Cy5-labelled protein samples. Qualitative changes in protein abundance of individual protein spots can be quickly observed when Cy3-control and Cy5-FB1 treatment images are merged. Yellow spots indicate no change in abundance, green spots indicate a downregulation with FB1 and red spots indicate an upregulation with FB1.

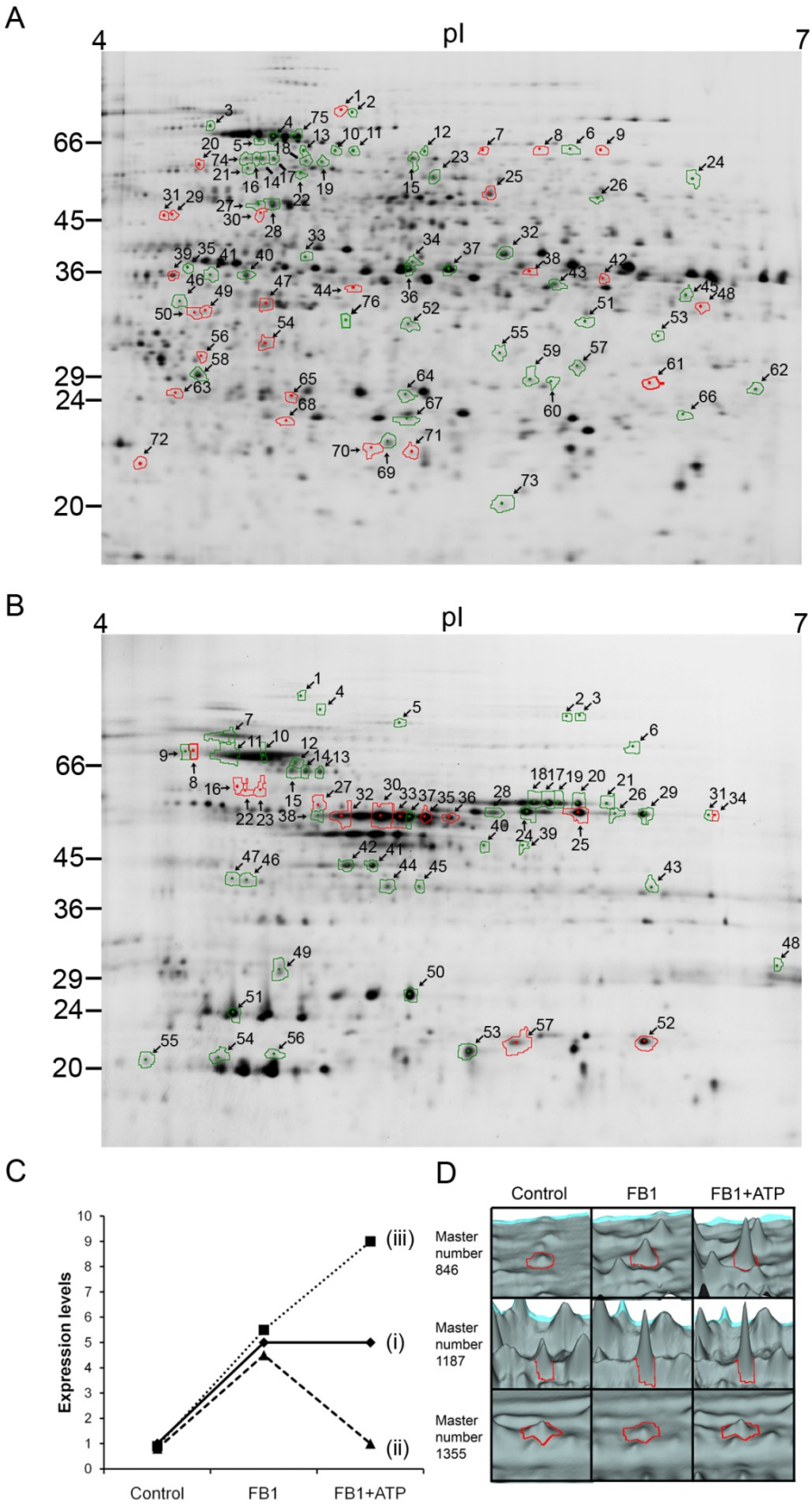

Figure 3.7 2D DIGE analysis of *Arabidopsis* proteins and their response profiles.

Figure 3.7-continued: (A) TSP and (B) microsomal membrane protein fractions were analysed by 2D-DiGE and protein spots differentially regulated by FB1 only (green boundary) or to both FB1 and exogenous ATP (red boundaries) were identified by MALDI-TOF MS. Spots were re-numbered from their master number for clarity purposes. (C) Protein response profiles encountered in this study. Some proteins responded only to FB1 (profile i), and others to both FB1 and ATP (profiles ii and iii). Reciprocals of these profiles are also considered to belong to the same response group. (D) 3D visualization of representative spots belonging to the response profiles shown in (C). Spot boundary is highlighted by a red line.

the coverage of a wider range of proteins than would be achievable if only one of the protein fractions was targeted for analysis. Due to the inherent limitations of gel-based approaches, it is obvious that only a small fraction of the membrane-associated proteins are represented in this study, since highly hydrophobic proteins containing trans-membrane domains cannot easily enter 2D gels. However, this inadvertently helped to simplify the microsomal protein profile by reducing the number of proteins. This fraction will be enriched for membrane-associated proteins that are soluble in LB, such as peripheral proteins and soluble subunits of membrane bound protein complexes. Therefore, low abundance proteins that might otherwise be masked by high abundance protein in the TSP will be visible in this fraction.

3.2.3.4 Analysis of differential protein abundance changes using 2D-DiGE

Quantitative analysis was performed using DeCyder software package. This software is designed specifically for 2D-DiGE and consists of two main modules: the difference in-gel analysis (DIA) module and the biological variation analysis (BVA) module. The DIA module detects spot boundaries and quantifies the volume of each individual spot above background levels. The BVA module performs gel matching between different gels by matching the internal standard image from each individual gel in the experiment. The BVA module also performs statistical interpretation of spot volumes, making it possible to identify statistically significant changes between different treatments on 4 independent

biological replicates of each treatment and 2 technical replicates (dye-swap) of each sample resulting in a total of 12 analytical gel images per treatment in each protein fraction. Over 5000 features, both authentic protein spots and artefacts, were automatically detected on the master gels images for each gel using the DIA module. Biological and technical replicas were grouped in their respective groups (Control, FB1 and ATP+FB1) before statistical analysis. Statistical analysis in the BVA module was performed in two stages. Firstly, spots significantly changing with FB1 treatment were identified. The average standardised spot volumes of the control and FB1 treatments were compared using Student's *t*-test and the fold change in protein abundance calculated by generating the ratio [FB1/control] for up-regulated spots or [control/FB1] for down-regulated spots. These will include spots that respond to both FB1-induced eATP depletion and to FB1 specific effects. Secondly, the effects of ATP addition on previously identified FB1 responsive spots will be analysed in order to select the spots that respond directly to eATP availability, the ATP filter. To quantify the effects of ATP, average spot volumes of the FB1 and FB1+ATP treatments were compared using the Student's *t*-test and the ratio [(FB1+ATP)/FB1] or [FB1/(FB1+ATP)] was generated for up-regulated or down-regulated spots, respectively. The ratio of down-regulated spots is indicated by a minus sign in both tables. It is after these two sets of analysis that spots that pass the ATP filter are identified and it is in this group that putative eATP-regulated cell death proteins are expected to be present.

The majority of protein spots in both the TSP and microsomal protein fractions did not respond to FB1 treatment and the ones that did usually responded by a small amount (Tables 3.1 and 3.2). The highest significant change in the TSP fraction was 1.87 fold (spot master number 2405, Table 3.1) whereas in the microsomal faction it was 5.18 fold (spot master number 471, Table 3.2). Because of the small changes observed, it was initially decided to use a minimum fold change ratio of 20% (twice the minimum detection limit of 2D-DiGE) for the TSP and microsomal fraction as a threshold value for a biologically significant change. However, later it became evident that a 20% cut off value for the microsomal fraction produced an overwhelming large number of spots significantly changing with FB1 (408 spots). Such a large number of candidates would result in a very large list of mutants to be screened for a role in PCD. Therefore, it was decided to raise the minimum fold change ratio to 50% in the microsomal fraction in order to concentrate my efforts on the spots exhibiting the biggest changes (Table 3.2). The abundance of 145

protein spots in the TSP fraction was significantly ($p \leq 0.05$) altered in response to FB1 treatment by at least 20% (Table 3.1). Of these 145 spots, 86 were positively identified accounting for an identification rate of 59.3% of all FB1 responsive spots and a successful identification rate of 73.5% for spots selected for picking (Table 3.3). Of the remaining 59, 28 were not selected for picking due to poor pick gel separation or low staining using SYPRO and the remaining 31 could not be positively identified - the majority being low abundance spots, from which inadequate sample was present in the preparative gel to enable confident identification. A total of 10 spots were identified as protein mixtures of 2 or more proteins (Table 1A in Appendix A). Spots with protein mixtures were excluded from further analysis since it was not possible to confidently determine which of the proteins was changing in abundance in response to the treatments without further experimentation. A possible way to resolve this issue would be to re-run the same samples using a narrower pI range to separate the spot mixtures on the gel, but the prohibitive costs of further 2D-DiGE experiments prevented this. All the identified spots in the TSP fraction that returned a single confident identification are shown in Table 3.1.

In the microsomal membrane fraction, a total of 83 protein spots significantly ($p \leq 0.05$) responded to FB1 by at least a 50% change in abundance (Table 3.2). Only 57 of these were positively identified as a single protein and two were protein mixtures resulting in a an identification rate of 73.5% of all FB1 responsive spots and a successful identification rate of 77.6% for spots selected for picking (Table 3.3). The identification of the rest was similarly hindered by low abundance issues or impossibility of confident picking a spot from a pick gel. The total number of positively identified protein spots in both the TSP and microsomal membrane fractions, excluding the protein mixtures, was 133, but this only represented 75 unique proteins (Table 3.1 and Table 3.2). The redundancy revealed by the inequality between the number of protein spots and unique proteins arises from the existence of post-translationally modified forms of the same protein and an overlap of 13 proteins that were identified in both protein fractions. Full spot expression and protein identification data of both protein fractions is presented in Tables 1A and 2A in Appendix A.

Table 3.1 TSP proteins differentially expressed in response to FB1 and FB1+ATP.[a]Arabidopsis Genome Initiative (AGI) gene identifier. [b]MOWSE, for a significant (p<0.05) positive protein identification, cut-off threshold was 71. [c]Number of peptides matched to the protein sequence. [d]Ratio represents fold-change of FB1 relative to the control treatment. [e]Ratio represents fold-change of FB1+ATP relative to FB1 i.e., comparison of the FB1+ATP average with the FB1 average to check if ATP addition significantly altered protein response to FB1 alone. Statistically significant ratios that exhibit a minimum 20% fold change are highlighted in grey. [f]Probability value was replaced by nss when the difference between the treatments being compared was not statistically significant (i.e. p-value >0.05).

							FB1/Control		FB1+ATP/FB1	
Gel spot no.	Master number	Gene locus[a]	Annotation	MOWSE score[b]	sequence coverage (%)	peptides[c]	Fold change[d]	p-value	Fold change[e]	p-value[f]
Molecular chaperones										
69	2987	AT1G53540	17.6 kDa class I small heat shock protein	90	38	10	1.3	0.0045	-1.04	nss
74	4003	AT3G09440	heat shock cognate 70 kDa protein 3	97	32	21	1.25	0.031	-1.22	nss
4	943	AT3G12580	heat shock protein 70 (HSP70)	146	36	24	1.22	0.036	1.22	nss
18	1124	AT3G12580		129	33	22	1.42	5.60E-05	-1.02	nss
19	1127	AT3G12580		80	19	13	1.52	3.00E-05	1.04	nss
22	1205	AT3G12580		112	26	22	1.78	8.30E-05	-1.19	nss
75	4066	AT3G12580		249	56	37	1.27	0.0072	1.16	0.011
29	1514	AT4G24190	heat shock 90.7 like protein	104	30	11	1.34	0.00066	-1.38	0.00082
31	1518	AT4G24190		95	22	15	1.23	0.0083	-1.38	0.00042
21	1170	AT4G37910	mitochondrial heat shock protein 70-1	177	38	25	-1.26	0.0095	-1.19	nss
3	874	AT5G02500	heat shock cognate protein 70-1	85	31	15	1.21	0.0022	1.05	nss
14	1090	AT5G02500		89	28	20	1.24	0.013	-1.13	nss
16	1102	AT5G02500		126	40	18	1.26	0.015	-1.13	nss
17	1103	AT5G02500		123	33	20	1.36	0.0033	-1.1	nss
57	2553	AT5G02500		83	18	15	-1.57	0.0018	-1.2	nss
10	1047	AT5G09590	heat shock protein 70 (Hsc70-5)	250	49	35	1.24	0.0071	-1.15	0.011

Gel spot no.	Master number	Gene locus[a]	Annotation	MOWSE score[b]	sequence coverage (%)	peptides[c]	FB1/Control Fold change[d]	FB1/Control *p*-value	FB1+ATP/FB1 Fold change[e]	FB1+ATP/FB1 *p*-value[f]
30	1515	AT5G52640	heat shock protein AtHSP90.1	76	15	11	1.38	5.80E-06	-1.26	0.014
39	1944	AT5G52640		123	27	19	1.2	0.028	-1.7	0.0043
Glycolytic enzymes										
8	1044	AT1G23190	putative phosphoglucomutase	169	37	21	-1.75	0.00021	1.73	0.021
7	1043	AT1G70730	putative phosphoglucomutase	181	44	23	-1.41	0.025	1.38	0.042
50	2215	AT1G79550	phosphoglycerate kinase (PGK)	124	62	19	-1.38	0.0036	-1.41	0.0027
51	2256	AT2G36460	putative fructose-bisphosphate aldolase	85	45	9	-1.44	0.00094	-1.08	nss
42	1975	AT3G04120	GAPDH (C subunit)	104	45	16	-1.24	0.019	1.68	0.0008
43	2012	AT3G04120	GAPDH (C subunit)	141	43	15	-1.22	9.10E-07	-1.06	nss
15	1097	AT3G08590	putative phosphoglycerate mutase	142	52	19	-1.22	0.023	1.33	nss
38	1930	AT3G52930	putative fructose-bisphosphate aldolase	95	42	10	-1.21	0.025	1.35	0.006
52	2275	AT3G52930	putative fructose-bisphosphate aldolase	146	57	14	-1.22	0.014	-1.17	0.045
65	2728	AT3G52930	putative fructose-bisphosphate aldolase	86	48	11	1.25	0.01	-1.58	0.0024
Antioxidant enzymes										
71	3056	AT1G02930	glutathione transferase	114	38	11	1.53	0.00029	-1.58	0.009
67	2881	AT1G19570	dehydroascorbate reductase	109	66	10	-1.25	0.00016	-1.05	nss
20	1153	AT1G77510	protein disulfide isomerase-like (PDIL)	148	51	19	-1.26	0.015	1.23	0.025
6	1039	AT3G52880	monodehydroascorbate reductase	100	33	11	-1.53	1.20E-05	1.23	nss
49	2200	AT5G03630	monodehydroascorbate reductase	116	45	18	-1.49	2.80E-05	-1.26	0.015
53	2345	AT5G16970	2-alkenal reductase (EC 1.3.1.74)	96	48	14	1.26	0.0013	-1.13	nss
72	3118	AT5G42980	thioredoxin	99	72	11	-1.49	0.00065	-1.38	0.025
Cytoskeleton-related proteins										
27	1436	AT1G04820	alpha tubulin isoform	135	45	16	-1.28	0.023	1.33	nss
38	1437	AT1G04820		178	47	15	-1.27	0.042	1.3	nss
35	1904	AT3G60830	actin-related protein	84	33	9	-1.5	0.0056	-1.12	nss

Gel spot no.	Master number	Gene locus[a]	Annotation	MOWSE score[b]	sequence coverage (%)	peptides[c]	FB1/Control Fold change[d]	FB1/Control *p*-value	FB1+ATP/FB1 Fold change[e]	FB1+ATP/FB1 *p*-value[f]
64	2718	AT5G09810	actin 7	80	45	15	1.29	0.00041	1.1	nss
73	3280	AT5G59880	actin depolymerizing factor 3	111	75	12	-1.21	0.0019	1.08	nss
Protein degradation										
63	2703	AT1G64520	regulatory particle non-ATPase 12a	116	51	15	1.2	0.027	-1.45	0.0087
59	2630	AT2G27020	20S proteasome subunit PAG1	117	39	14	1.21	0.0056	-1.13	nss
2	786	AT2G30110	ubiquitin-activating enzyme (E1)	91	17	16	-1.33	0.019	1.29	nss
62	2688	AT3G22110	alpha-3 subunit of 20s proteasome	89	47	11	-1.36	1.50E-06	1.18	nss
66	2854	AT3G60820	20S proteasome beta subunit PBF1	156	60	15	1.38	0.00064	-1.02	nss
Aminoacid metabolism										
36	1905	AT3G17820	glutamine synthetase	108	29	13	1.32	0.00015	1.2	nss
37	1906	AT3G17820		219	76	27	1.47	9.60E-06	1.16	nss
47	2157	AT3G53580	diaminopimelate epimerase	153	57	21	-1.22	0.00078	-1.26	0.00062
23	1233	AT3G58610	ketol-acid reductoisomerase	189	30	18	-1.29	0.017	1.31	nss
24	1240	AT5G17920	cobalamin-independent methionine synthase	90	17	11	1.27	0.014	-1.13	nss
13	1054	AT5G53460	NADH-dependent glutamate synthase	130	41	16	1.52	0.00099	-1.14	nss
Miscellaneous/unclassified										
44	2050	AT1G03475	coproporphyrinogen III oxidase	140	46	18	-1.29	0.022	1.32	0.0056
40	1946	AT1G62380	ACC oxidase	85	43	12	-1.59	0.0027	1.19	nss
32	1805	AT1G77120	alcohol dehydrogenase	81	24	9	-1.45	0.007	1.56	nss
1	759	AT1G79690	Nudix hydrolase homolog 3 (atnudt3)	74	39	12	-1.37	0.0085	1.52	0.046
9	1045	AT2G17980	ATSLY1 protein transporter	102	36	21	-1.5	0.0019	1.29	0.042
60	2640	AT2G21250	putative mannose 6-phosphate reductase	77	37	11	-1.48	0.00024	1.02	nss
46	2140	AT2G44060	late embryogenesis abundant family protein	137	61	21	1.28	0.00013	-1.13	0.024
76	2253	AT3G03250	UGP1 (UDP-glucose pyrophosphorylase 1)	71	30	12	1.29	0.014	-1.3	nss
12	1052	AT3G09840	cell division cycle protein	92	29	16	1.26	0.011	1.09	nss

Gel spot no.	Master number	Gene locus[a]	Annotation	MOWSE score[b]	sequence coverage (%)	peptides[c]	FB1/Control		FB1+ATP/FB1	
							Fold change[d]	*p*-value	Fold change[e]	*p*-value[f]
41	1951	AT3G14990	thiazole monophosphate biosynthesis protein	95	45	19	-1.58	4.00E-05	1.15	nss
48	2173	AT3G18130	similarity to mammalian RACKs	111	46	14	-1.51	0.016	1.88	0.011
34	1853	AT3G29360	putative UDP-glucose 6-dehydrogenase	162	58	28	1.27	1.70E-05	-1.05	nss
68	2888	AT3G56090	ferritin 3 AtFER3	123	52	17	1.26	0.013	-1.5	0.005
11	1049	AT3G60750	putative transketolase	92	20	12	1.35	0.0037	-1.08	nss
26	1395	AT4G13430	Isopropyl malate isomerase large subunit 1	98	35	16	-1.24	0.015	1.31	nss
25	1355	AT4G13940	S-adenosyl-L-homocysteine hydrolase	125	46	21	1.35	0.027	1.65	0.009
56	2477	AT4G13940		82	38	10	1.29	0.0006	-1.2	0.011
58	2597	AT4G13940		137	57	17	1.22	0.0051	-1.26	nss
54	2405	AT4G34050	putative caffeoyl-CoA 3-O-methyltransferase	136	61	21	1.87	1.90E-06	-1.33	0.0018
5	976	AT5G03340	putative cell division cycle protein 48	80	26	16	1.18	0.0048	1.05	nss
45	2110	AT5G08670	ATP synthase beta-subunit	90	49	20	1.27	0.0057	-1.06	nss
33	1817	AT5G08690		138	42	21	1.27	3.40E-05	-1.14	0.023
61	2658	AT5G15650	Reversibly Glycosylated Polypeptide-2	123	26	10	1.38	0.014	-1.51	0.023
70	3036	AT5G38480	general regulatory factor 3	108	34	12	1.25	0.0092	-1.3	0.015
55	2465	ATMG01190	ATPase subunit 1	282	52	27	-1.21	0.0003	-1.19	0.0033

Table 3.2 Microsomal proteins differentially expressed in response to FB1 and FB1+ATP. [a]Arabidopsis Genome Initiative (AGI) gene identifier. [b]MOWSE, for a significant (p<0.05) positive protein identification, cut-off threshold was 71. [c]Number of peptides matched to the protein sequence. [d]Ratio represents fold-change of FB1 relative to the control treatment. [e]Ratio represents fold-change of FB1+ATP relative to FB1 i.e., comparison of the FB1+ATP average with the FB1 average to check if ATP addition significantly altered protein response to FB1 alone. Statistically significant ratios that exhibit a minimum 20% fold change are highlighted in grey. [f]Probability value was replaced by nss when the difference between the treatments being compared was not statistically significant (i.e. p-value >0.05).

							FB1/Control		FB1+ATP/FB1	
Gel spot no.	Master number	Gene locus[a]	Annotation	MOWSE score[b]	sequence coverage (%)	peptides[c]	Fold change[d]	p-value	Fold change[e]	p-value[f]
Molecular chaperones										
1	269	AT1G79930	high molecular weight heat shock protein	128	36	27	1.93	2.40E-07	-1.09	nss
12	612	AT3G12580	heat shock protein 70 (HSP70)	218	48	26	2.13	3.60E-07	-1.17	nss
8	574	AT4G24280	chloroplast heat shock protein 70-1	74	21	15	2.19	4.50E-09	-1.2	0.0097
9	581	AT4G24280		137	31	21	2.09	5.10E-07	-1.18	0.014
54	1799	AT4G25200	AtHSP23.6-mito	84	52	10	-2.29	1.40E-06	-1.03	nss
15	649	AT4G37910	mitochondrial heat shock protein 70-1	102	44	28	-1.54	0.00023	1.21	nss
16	742	AT4G37910		98	34	20	2.04	9.90E-05	-1.31	0.025
22	760	AT4G37910		106	47	29	3.14	1.10E-05	-1.65	0.0096
23	761	AT4G37910		101	26	16	4.34	8.30E-08	-1.6	0.0032
10	594	AT5G02500	heat shock cognate protein 70-1	214	56	29	1.79	9.30E-07	-1.1	nss
11	605	AT5G02500		187	48	27	2.13	2.30E-08	-1.08	nss
5	371	AT5G15450	chloroplast-targeted Hsp101 homologue	90	32	31	-1.59	0.0035	1.14	nss
46	1182	AT5G52640	heat shock protein AtHSP90.1	98	23	16	2.85	4.50E-05	-1.41	nss
47	1189	AT5G56010	heat shock protein 90 (HSP90)	85	27	14	2.87	3.80E-05	-1.43	nss
7	485	AT5G56030	heat shock protein 90 (HSP90)	218	39	36	1.78	1.10E-06	1	nss

Gel spot no.	Master number	Gene locus[a]	Annotation	MOWSE score[b]	sequence coverage (%)	peptides[c]	FB1/Control Fold change[d]	FB1/Control *p*-value	FB1+ATP/FB1 Fold change[e]	FB1+ATP/FB1 *p*-value[f]
ATP synthesis machinery										
13	637	AT1G78900	subunit A of the vacuolar ATP synthase	156	47	25	-1.8	7.00E-05	1.19	nss
14	640	AT1G78900		192	39	22	-1.63	0.00019	1.19	nss
50	1604	AT2G21870	unknown protein mitochondrial	137	65	19	-2.03	2.10E-05	1.23	nss
56	1813	AT3G52300	ATP synthase D chain	212	83	20	-2.32	3.60E-06	-1.12	nss
53	1767	AT5G08670	mitochondrial ATP synthase beta-subunit	124	59	22	-1.7	3.20E-06	1.12	nss
30	832	AT5G08690		225	63	28	-1.88	4.10E-07	1.24	0.016
32	839	AT5G08690		248	63	28	-2.17	5.30E-08	1.23	0.014
33	840	AT5G08690		250	62	28	-1.86	8.20E-07	1.32	0.025
35	844	AT5G08690		251	64	25	-1.72	3.00E-05	1.34	0.029
36	846	AT5G08690		249	60	25	-1.74	0.00029	1.38	0.018
37	849	AT5G08690		217	58	27	-2.04	5.90E-06	1.28	nss
38	857	AT5G08690		112	33	14	-1.78	1.80E-06	1.13	0.022
39	964	AT5G08690		206	55	27	3.07	1.60E-07	1.16	nss
52	1753	AT5G13450	ATP synthase delta chain	185	63	18	-1.83	3.50E-06	1.23	0.034
57	2337	AT5G13450		133	53	14	-1.68	8.60E-06	1.23	0.027
27	802	ATCG00120	ATPase CF1 alpha subunit	216	37	20	-1.7	0.00019	1.29	0.034
24	788	ATMG01190	ATPase subunit 1	207	41	20	-2.01	5.50E-06	1.3	0.041
25	793	ATMG01190		213	51	27	-1.96	2.20E-06	1.28	nss
26	799	ATMG01190		235	60	29	-2.81	4.00E-06	1.29	nss
28	803	ATMG01190		164	35	16	-2.31	4.40E-08	1.17	nss
29	812	ATMG01190		207	51	24	-1.93	2.00E-05	1.26	nss
31	837	ATMG01190		197	36	18	-1.69	0.00059	1.21	nss
34	841	ATMG01190		79	23	10	-1.69	0.00083	1.22	0.026
Miscellaneous/unclassified										
2	326	AT1G56070	translation elongation factor 2-like protein	88	38	28	2.28	2.20E-05	1.04	nss
3	327	AT1G56070		125	46	30	2.24	6.40E-09	1.09	nss

Gel spot no.	Master number	Gene locus[a]	Annotation	MOWSE score[b]	sequence coverage (%)	peptides[c]	FB1/Control		FB1+ATP/FB1	
							Fold change[d]	*p*-value	Fold change[e]	*p*-value[f]
44	1163	AT1G79550	cytosolic phosphoglycerate kinase (PGK)	118	55	18	2.62	1.40E-08	-1.04	nss
45	1176	AT1G79550		132	44	15	3.29	1.20E-10	-1.01	nss
17	743	AT3G02090	metalloendopeptidase (MPPBETA)	137	37	15	-1.92	9.40E-05	1.21	nss
18	746	AT3G02090		209	59	26	-1.94	1.40E-05	1.19	nss
19	747	AT3G02090		184	57	22	-1.9	0.00015	1.23	nss
20	749	AT3G02090		224	59	25	-1.8	0.00024	1.26	nss
21	752	AT3G02090		87	17	9	-1.61	0.00067	1.2	nss
4	335	AT3G09840	cell division cycle protein	91	14	14	3.35	9.40E-09	-1.09	nss
55	1810	AT3G16640	translationally controlled tumor protein	93	54	10	2.73	2.20E-10	1.03	nss
49	1531	AT3G23400	plastid-lipid associated protein	142	53	14	-1.63	1.90E-06	-1.01	nss
51	1653	AT3G23400		106	38	9	-1.58	1.90E-06	1.07	nss
43	1154	AT3G52930	putative fructose-bisphosphate aldolase	121	48	13	1.58	5.50E-06	-1.09	nss
40	976	AT4G01850	S-adenosylmethionine synthetase 2	92	47	17	2.66	1.30E-09	1.12	nss
41	1079	AT5G09810	Actin 7	203	62	23	2.3	4.50E-08	-1.03	nss
42	1085	AT5G09810		187	59	22	2.3	5.90E-08	-1.07	nss
6	471	AT5G17920	cobalamin-independent methionine synthase	88	37	21	5.18	9.10E-10	1.11	nss
48	1496	AT5G40770	prohibitin 3	121	38	11	-1.74	9.80E-05	1.1	nss

In order to simplify the interpretation of all the relevant data from Tables 1A and 1B, a summary table for each protein fraction was constructed (Table 3.3). This table groups the results of the 2D-DiGE analysis and the results of the protein identification experiments for both protein fractions. The total number of spots differentially regulated by FB1 is broken down into upregulated and downregulated spots. Approximately equal numbers are present in both classes, showing FB1 does not preferentially induce the upregulation or downregulation of the proteome. The number of spots selected for picking, spots identified and the identification results (single identification and mixtures) for each fraction is shown. The success of the identification of protein spots was determined by the percentage of successfully identified spots based on the total number of picked spots and percentage values are shown. The same results are also shown for reversed spots only.

The ATP filter revealed the subset of FB1-responsive proteins which is regulated by the level of eATP. The response of 39 TSP (Table 3.1) and 16 microsomal protein spots (Table 3.2) to FB1 was blocked or attenuated by exogenous ATP addition (Figure 3.7C, profile ii). This represented 26.9% and 19.3% of the total FB1-responsive proteins in the TSP and microsomal fraction, respectively, indicating a higher degree of eATP responsiveness in the TSP fraction. These reversed proteins are the proteins most likely to mediate the physiological effects of eATP, and so extra effort was undertaken to identify all of them. This included running pick gels with a higher protein load and loading pick gels with the same amount of CyDye-labelled protein sample as the analytical gels in order to more accurately match the pick gel profile with the DiGE analytical gels Almost all spots in this category were confidently picked for identification with a successful identification rate of 75% and 93.8% for the TSP and microsomal fractions respectively (Table 3.3). A total of 41 spots in this category were identified corresponding to 23 unique proteins, 17 from the TSP and 6 from the microsomal fraction (Table 3.3). Spot identification redundancy was particularly evident in the microsomal fraction, where 14 identified spots belonged to only 6 unique proteins (Table 3.2). However, the majority of the FB1-responsive spots [73.1% and 80.7% in the TSP and microsomal fraction respectively (Table 3.3)] remained unaffected by exogenous ATP (Figure 3.7C, profile i), indicating that FB1 has other targets and physiological effects that are independent of its ability to trigger eATP depletion. A minority of the spots [5 spots (gel spot numbers 25, 47, 49, 50, 72); Table 3.1] had their response to FB1 enhanced by the addition of exogenous ATP (Figure 3.7C, profile iii). This result suggests that FB1 and eATP activate common, but as yet uncharacterised,

TSP spot classes		
FB1 responsive spot statistics	**Value**	**% total**
Spots responding to FB1 (>20%)	145	100.0
Spots upregulated with FB1	78	53.8
Spots downregulated with FB1	67	46.2
spots reversed with ATP	39	26.9
Enhanced spots	8	5.5
Spots selected for picking	117	80.7
Spots identified	86	59.3
Single identifications	76	52.4
Mixtures	10	6.9
Unique proteins identified	59	40.7
Identification success rate	86	73.5
Reversed spot statistics	**Value**	**% total**
spots reversed with ATP	39	100.0
Reversed selected for picking	36	92.3
Reversed picked and identified	27	69.2
Single identifications	21	53.8
Reversed Mixtures	6	22.2
Reversed Unique proteins	18	66.7
Reversed Identification success rate	27	75.0

Microsomal spot classes		
FB1 responsive spot statistics	**Value**	**% total**
Spots responding to FB1 (>50%)	83	100.0
Spots upregulated with FB1	35	42.2
Spots downregulated with FB1	48	57.8
spots reversed with ATP	16	19.3
Enhanced spots	0	0.0
Spots selected for picking	76	91.6
Spots identified	59	71.1
Single identifications	57	68.7
Mixtures	2	2.4
Unique proteins identified	29	34.9
Identification success rate	59	77.6
Reversed spot statistics	**Value**	**% total**
spots reversed with ATP	16	100.0
Reversed selected for picking	15	93.8
Reversed picked and identified	14	87.5
Single identifications	14	100.0
Reversed Mixtures	0	0.0
Reversed Unique proteins	6	42.9
Reversed Identification success rate	14	93.3

Table 3.3 Summary of the 2D-DiGE protein analysis and mass spectrometry protein identification on the TSP and microsomal protein fractions from Tables 1A and 1B in Appendix A. Percentage of total (% total) values refer to either the total number of differentially regulated spots with FB1 or total number of reversed spots in each protein fraction. The identification success rate was calculated based on the total number of picked spots.

signalling events where a combination of the two compounds has a synergistic effect on the protein's abundance. Representative 3D drawings of real spots in each category of Figure 3.7C are shown in Figure 3.7D, where the relative abundance of each spot is represented by its spot volume using the 3D view feature provided by the BVA module of DeCyder software.

3.2.4 Classification and discussion of differentially expressed proteins

3.2.4.1 The proteomic changes mediating the switch to FB1-induced cell death

Although the main purpose of this chapter is the identification of putative cell death regulatory proteins using the ATP filter, it also presents a great opportunity to investigate the FB1-induced proteome changes in *Arabidopsis* around the time of cell death commitment (Figure 3.1A). This was achieved by identifying FB1-responsive proteins regardless of their response to ATP treatment, but their response to ATP could provide more insight into their regulation mechanism. Proteins that do not respond to ATP will comprise the ATP-independent component in the FB1 response (Figure 3.7C, profile i), whereas proteins that do respond to ATP would constitute the ATP-dependent component of the FB1 response (Figure 3.7C, profile ii). Not only will their identification provide insight into which are the main metabolic pathways directly modulated by FB1 treatment prior to the inception of cell death, their response to ATP will provide insight into the mechanism of how eATP signalling blocks PCD in specific metabolic pathways.

3.2.4.2 Molecular chaperones

Molecular chaperones are essential under normal growth condition for correct protein folding and degradation. They form part of the general response mechanisms of cells to biotic and abiotic stresses, working tightly with other pathways, such as protein folding (Miernyk 1999), to maintain cell homeostasis. Increased expression of chaperone genes during stress is usually associated with maintaining normal protein conformation, thereby mitigating the adverse effects of stress on protein function (Wang *et al.,* 2004). Since FB1 activation of PCD is preceded by alterations in cellular metabolism, it is not surprising that chaperone proteins are recruited to control the accompanying increased in protein traffic through protein synthesis, translocation and degradation pathways. FB1 treatment upregulated molecular chaperones present in several different cell compartments including

the cytosol (eg. heat shock cognate protein 70-1), endoplasmic reticulum (eg. heat shock 90.7 like protein) and mitochondria (eg: mitochondrial heat shock protein 70-1). Proteins differentially expressed in this category are involved in plant-pathogen interactions, RNA degradation, endocytosis and spliceosome control. Not only does FB1 activate cell death signalling, it also initiates pathogen defence responses that include synthesis of PR proteins (Stone *et al.,* 2000), most of which transit through the endoplasmic reticulum and increase the demand for chaperones in this organelle, such as the heat shock 90.7 like protein identified in this study. Similar chaperone increases can occur in *Arabidopsis* responding to PCD-eliciting pathogens (Noel *et al.,* 2007) or exogenous plant hormones (Wang *et al.,* 2005). Interestingly, extracellular eATP treatment resulted in a downregulation of the molecular chaperones identified, showing that the increase in molecular chaperones is triggered by a specific PCD signal, the lowering of eATP concentration by FB1.

3.2.4.3 ATP synthesis machinery

Analysis of the microsomal fraction has revealed that a primary target for FB1 is cellular ATP synthesis. Remarkably, all proteins in this category were repressed by FB1 (Table 3.2) except for one ATP synthase β-subunit spot in the microsomal fraction (Table 3.2, spot 39). A total of eight unique proteins were identified in the microsomal fraction as being directly involved in ATP synthesis in the plant mitochondria via oxidative phosphorylation. The ATP synthase subunit 1 and the mitochondrial ATP synthase β-subunit were identified in multiple distinct spots indicating the presence of several PTM isoforms. These results show that the mitochondrial F_0/F_1-ATP synthase complex, the main producer of intracellular ATP, is significantly downregulated by FB1. This complex has two main parts: a catalytic F_1 sub-complex and the transmembrane proton-transporting F_0 sub-complex located in the mitochondrial inner membrane. The subunits α, β, and δ of the F_1 complex and subunit-D of the F_0 complex were all identified. The identification of subunit-D, a subunit of the ATP synthase rotor that is embedded in the membrane, demonstrates the extraction capability of LB in solubilisation of membrane-associated proteins. Though not determined experimentally in this study, the repression of ATP synthase proteins by FB1 is likely to disrupt oxidative phosphorylation and lead to a significant reduction in cellular ATP levels. Consistent with this hypothesis of reduced ATP levels are the documented effects of harpin, another pathogen-derived cell death-activating elicitor, that disrupts oxidative phosphorylation by triggering cytochrome *c* release (Krause and Durner 2004) and inhibits mitochondrial ATP production before the

establishment of cell death (Xie and Chen 2000; Krause *et al.,* 2004). Reduction in cellular ATP could also account for the growth retardation effects of FB1 on *Arabidopsis* as metabolism is slowed down (Chivasa *et al.,* 2005a). Remarkably, ATP addition reversed protein abundance of almost all proteins in this category (Table 3.2). Ten spots corresponding to ATPase subunit 1, mitochondrial ATP synthase β-subunit, ATP synthase delta chain and ATPase CF1 alpha subunit were all significantly reversed with ATP addition. This provides evidence that eATP signalling is able to initiate a feedback loop that controls gene expression of ATP synthesis proteins, possibly to sustain eATP levels above a certain critical threshold in stressed cells. AT5G08690 and AT5G08670 are located very close to each other being separated by AT5G08680, a gene that also codes for an ATPase-β subunit protein. The 3 genes form a gene cluster of functionally related genes that are probably paralogues that originated from tandem gene duplication. The higher number and intensity of protein spots identified as coding for AT5G08690 (Table 3.2; Figure 3.7B) shows that out of the 3 genes coding for ATPase-β subunit protein, AT5G08690 is preferentially used in the ATP synthase complex. Gene regulation by functionally related genes by operons is a common feature of prokaryote genomes (Rocha 2008). Although operon-like clusters of functionally related genes have been reported in plant, particularly in genes involved in secondary metabolite synthesis (Osbourn 2010), the remaining ATP synthesis proteins are not located in cluster with the ATPase-β subunit genes showing that eATP signalling does not regulate the ATP synthase complex subunits by an operon-like mechanism. As described previously, FB1-induced PCD can be prevented with addition of ATP up to a certain timepoint (Figure 3.1), after which it becomes irreversible. This data suggests that part of this commitment step could be due to prolonged reduction in energy levels brought about by a sustained decrease in ATP synthesis as a direct consequence of diminished eATP signalling. A direct control of ATP synthesis by eATP signalling has also been observed in tobacco plants treated with AMP-PCP (Chivasa *et al.,* 2010). The competitive exclusion of ATP by AMP-PCP and subsequent blocking of signalling requiring ATP hydrolysis resulted in a significant downregulation of ATP synthase proteins, providing further evidence of the control of ATP synthesis by eATP signalling.

3.2.4.4 Glycolytic enzymes

The glycolysis pathway proved to be a major target for active FB1 suppression as is reflected by the 7 unique proteins identified belonging to the pathway (Table 3.1). The

reduction in these proteins constricts carbohydrate flux through the pathway, a strategy that could be utilized by the cell in order to divert protein building blocks towards other processes required for the response to FB1, such as PR protein synthesis and calose deposition in the cell wall (Stone *et al.,* 2000). In addition to the downregulation of ATP synthesis related proteins (Table 3.2), the slowing down of central metabolic pathways could be a means by which FB1 starves the cells of energy in preparation for PCD. In rescuing the cells from death, eATP did not attenuate the response of all the glycolytic proteins to FB1, and even enhanced the suppression of one of them, the phosphoglycerate kinase (Table 3.1). This possibly indicates the need for eATP signalling to reset the global metabolic processes in a controlled sequence before the switch back to normal metabolism can be achieved. Reasons for the targeting of glycolytic enzymes by FB1 and eATP are complicated by the fact that some of the enzymes in this pathway have known secondary functions in PCD. For example, hexokinase, which catalyses the first step of glycolysis, is a critical regulator of PCD in plants (Kim *et al.,* 2006a) and animals (Downward 2003; Majewski *et al.,* 2004). Glyceraldehyde-3-phosphate dehydrogenase (GAPDH), that mediates the fifth step in glycolysis, can translocate to the nucleus of neuronal cells (Saunders *et al.,* 1999) where it activates apoptosis (Ishitani and Chuang 1996; Saunders *et al.,* 1999). In view of this, a possible role in FB1-induced cell death for the glycolytic proteins identified warrants further investigation.

3.2.4.5 Antioxidant enzymes/ROS metabolism enzymes

Amongst the proteins differentially expressed following FB1 treatment were several enzymes involved in protecting cells from oxidative damage originating from ROS, grouped under antioxidant enzymes (Table 3.1). The glutathione transferase and 2-alkenal reductase proteins are important in plant detoxification of lipid peroxide-derived cytotoxic metabolites (Marrs 1996; Mano *et al.,* 2005). Monodehydroascorbate reductase and dehydroascorbate reductase function in the antioxidant glutathione-ascorbate cycle (Noctor and Foyer 1998) while thioredoxin forms part of the thioredoxin antioxidant system (Holmgren 1989). Thioredoxin is also induced by *flg22* (Benschop *et al.,* 2007), a typical elicitor of PAMP triggered immunity (Zipfel *et al.,* 2004). This could be indicative that FB1 elicits defence responses (Stone *et al.,* 2000) utilizing a similar downstream signalling pathway as *flg22*. With the exception of glutathione transferase and 2-alkenal reductase that showed an increase, all the other enzymes were downregulated by FB1 (Table 3.1). An overall reduction of these enzymes may contribute to the observed accumulation of ROS in

Arabidopsis plants exposed to FB1 (Stone *et al.,* 2000) and also account for FB1-induced oxidative damage (Stockmann-Juvala *et al.,* 2004). ROS can function as signalling molecules (Apel *et al.,* 2004) or triggers of cell death by attacking membrane lipids to give rise to phytotoxic lipid peroxides (Montillet *et al.,* 2005). Shutdown of some anti-oxidative enzymes and upregulation of others by FB1 (Table 3.1) could indicate a highly regulated mechanism by which the cell exploits the signalling capabilities of ROS during FB1 stress, while simultaneously controlling their ability to trigger membrane damage and cell death. The blocking of the FB1 effects on these proteins by eATP (Table 3.1) implicates them as important elements downstream of eATP signalling in cell death control, possibly via regulation of signalling ROS levels.

3.2.4.6 Protein degradation

Three subunits of the 20S proteasome complex, one subunit of the 26S proteasome complex and an ubiquitin-activating enzyme were identified as differentially expressed following FB1 treatment, suggesting an important role for protein degradation in FB1-induced cell death. This is not surprising as changes in protein abundance in response to FB1 and ATP treatments require synthesis of new proteins and degradation of unnecessary proteins. This is further supported by the identification of the ubiquitin-activating enzyme E1 involved in attaching ubiquitin to proteins destined for degradation. Other proteins in this pathway have been shown to be essential for FB1-induced cell death. The RING1 E3 ligase (AT5G10380) is highly induced by FB1 and overexpression and repression of this protein results in a hypersensitivity and hyposensitivity to FB1, respectively (Lin *et al.,* 2008). An interesting observation is that eATP did not significantly attenuate the FB1 effects on 4 of the 5 proteins in this category (Table 3.1), suggesting eATP-mediated signalling also requires the activity of protein degradation complexes, possibly for degradation of pro-death proteins induced and/or required by FB1.

3.2.4.7 Other categories

Several cytoskeleton proteins were identified in this study, including actin 7 (AT5G09810) and alpha tubulin (AT1G04820), establishing the cytoskeleton as an important target of FB1. The cytoskeleton plays multiple functions during PCD in eukaryotes (Franklin-Tong and Gourlay 2008). Disruption of its structure by treating plants with actin depolymerising drugs, such as cytochalasin D, results in suppression of pathogen-induced PCD and increases pathogen infection rates (Skalamera and Heath 1998). Recently, it has been

suggested that a change in mitochondrial morphology, a common feature observed in different PCD inducing stresses and possibly a result of interference with the cytoskeleton, plays a role in activating PCD (Scott and Logan 2008). ATP did not significantly attenuate the FB1 effects in any cytoskeleton-related protein (Table 3.1) establishing the cytoskeleton as a subcellular structure that is modulated by FB1 independently of its ability to trigger eATP depletion. The significance of this regulation remains obscure.

Overall, the results from the 2D-DiGE analysis of TSP and microsomal protein fractions show that FB1 treatment disrupts several different major metabolic pathways prior to PCD establishment. ATP treatment also modulated some of these pathways, indicating that they were regulated by FB1-mediated eATP depletion. The possible significance of these protein abundance changes in light of FB1-induced cell death was briefly discussed.

3.3 Strategy for validation of putative eATP-regulated cell death genes by reverse genetics

The proteomic study above provides a set of putative cell death regulators associated with eATP regulation of PCD (Tables 3.1 and 3.2). Verification of this putative function requires the use of reverse genetics to determine if knockout mutants for the genes in question have an altered cell phenotype following FB1 treatment. Validation of a phenotype is best performed on complete loss-of-function mutants for the target gene that have been confirmed as real KO mutants for that gene. However, it was decided to perform the cell death characterization of putative homozygous KO lines before performing the KO status characterization only on mutant lines that showed a strong altered cell death phenotype. This strategy provides two main advantages over an initial check of KO status of all available KO lines when dealing with large numbers of them. Firstly, it skips the work of checking the KO status of mutants in genes with no cell death function. Secondly, it enables screening of mutant lines that are not complete KO's but still show a significant cell death phenotype, such as knockdown or overexpressing mutants, due to an insertion of the T-DNA in the promoter region (Krysan *et al.,* 1999). In this last example, an initial check on the line's KO status might have identified some lines as incomplete knockouts and therefore preventing the testing for an altered cell death phenotype in a possible cell death regulator. Because of these reasons, confirmation of KO status of the SALK lines

was only performed on each individual line if the lines showed a significant cell death phenotype after cell death characterization.

Post-translational modifications can modulate protein activity and there are many different types of PTM's with different effects already described (Haynes *et al.,* 1998; Pennington and Dunn 2001). 2D proteomics provides an excellent platform for detecting PTM forms of the same protein, as these usually are distinguishable from each other due to different pI and/or MW. Indeed, some proteins such as putative fructose-biphosphate aldolase, were identified as multiple spots in the TSP fraction (Table 3.1, gel spots numbers 30, 52 and 65), where not all of them were reversed following ATP treatment. Since different PTM forms of the same protein can have radically different functions, it was decided to include in the analysis for an altered cell death phenotype proteins identified in multiple spots if at least one of them was reversed following ATP treatment. From the total of 39 reversed spots in the TSP and 16 reversed spots in the microsomal fraction, a total of 24 unique proteins were identified as a result of applying the ATP filter (Table 3.3).

Agrobacterium tumefasciens-mediated transformation of *Arabidopsis* with a T-DNA fragment is an established process used to integrate DNA into plant genomes and is a widely used tool to generate T-DNA insertion collections invaluable for functional genomics employing reverse genetics (Alonso and Ecker 2006). The *Arabidopsis* SALK collection (Alonso *et al.,* 2003) was used to search for putative T-DNA homozygous KO lines for all the genes in this category. This collection was favoured over other T-DNA insertion-based collections such as GABI-Kat (Rosso *et al.,* 2003) and SAIL (Mengiste *et al.,* 1997), since these were originally designed for activation tagging using the 35S and 1' promoters, respectively. Activation tagging is designed to increase the expression of a gene if the T-DNA insert is inserted in frame into the promoter region of a gene. However, such mutants are not as good as a loss-of-function mutant for performing experimentation aimed at validation of a putative role in PCD of the targeted gene. Although the SALK collection provides a fast and easy means to obtain homozygous KO lines for genes of interest, it is not a very clean collection due to the mechanism of *Agrobacterium*-mediated T-DNA transformation. In its seminal paper (Krysan *et al.,* 1999) the authors elaborated the possible outcomes of T-DNA insertions into the genome and these have since then been confirmed. For example, insertions in the promoter region could result in reduced or increased expression of the target gene (Krysan *et al.,* 1999), T-DNA insertions could mediate a translocation/duplication event of a T-DNA left boarder-containing DNA

sequence into another locus in the genome (Tax and Vernon 2001) and T-DNA insertions into introns could be spliced out at different rates, resulting in an allelic series of mutants with varying amounts of decreasing expression levels of the target gene (Ulker *et al.,* 2008). One of the ways to prevent incorrect interpretation of T-DNA mutant data is to test multiple independent mutant lines for the same gene (Krysan *et al.,* 1999). Reproducibility of the phenotype increases the chances that the observed phenotype is a true consequence of the loss of function of the target gene, and not a result of other T-DNA insertion events in the same line or other T-DNA derived effects discussed above. Therefore, all the KO lines available for each gene of interest were ordered. The SALK collection is constantly increasing in the number of T-DNA lines it harbours and so was periodically checked for the availability KO lines for all the reversed genes that had no available line when it was first searched in 2008. Of the 24 unique reversed proteins, a total of 12 were annotated as having at least one homozygous KO line in the SALK collection. These, as well as a second independent KO line that was available for 4 of the genes, were ordered from the Nottingham *Arabidopsis* Stock Centre (NASC) as they became available over the course of this study (Table 3.4). A grand total of 18 T-DNA KO lines were ordered. The predicted insertion site of the T-DNA in each line is also shown in Table 3.4, as this could help interpret the results of the cell death assays. The remaining 12 unique reversed genes only had heterozygous lines available at the time of searching (Table 3.5) and were not considered for further analysis, since the amount of work required to obtain homozygous lines by genetic segregation would be too much time consuming as well as not posing any guarantees for a positive result. As of September 2010, some of these genes have homozygous KO lines available (Table 3.5).

3.3.1 Cell death assays

A differential cell death phenotype between mutant lines and wildtype plants would clearly defined novel cell death regulatory proteins under eATP control. The response of the homozygous KO mutants of the putative cell death genes to FB1 treatment was examined using qualitative and quantitative cell death assays. Several cell death assays were considered for screening KO mutants. The conductivity assay was selected as the main assay due to its quantitative nature over other qualitative cell death assays, such as leaf infiltration with an FB1 solution. This assay can confidently identify small, but significant, changes in cell death progression over short periods of time. In this assay, leaf disks of 4-5

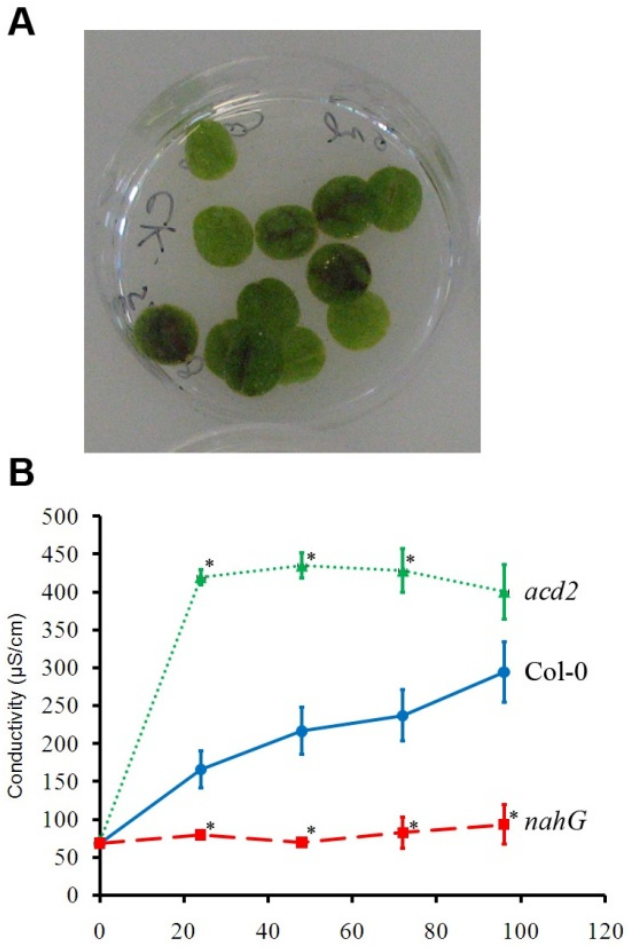

Figure 3.8 The conductivity assay used for identifying KO mutants with altered cell death phenotype to FB1. (A) A picture of 10 leaf disks floating on FB1 solution inside a transparent small petri dish. (B) Cell death profiles of the positive control *acd2* and negative control *nahG* plants. Leaf disks were floated on 10 µM FB1 solution and the conductivity of the solution was measured every 24 h after a 48 h dark incubation. Values and error bars represent means ± SE (n = 3). An asterisk denotes data points that show a significantly different means than Col-0 ($p \leq 0.01$). Notice *acd2* completely dies within the first 24 hours and *nahG* plants remains unchanged over the timecourse. X-axis represents hours after exposure to light.

week old plants are floated on an FB1 solution with their abaxial side facing down immediately after corking from an intact leaf (Figure 3.8A). FB1 is then taken up via the damaged edge of the leaf disk and through the stomata, initiating cell death that is detectable as early as 48 hours after floating the disks. As cells lose their membrane integrity due to PCD progression, intracellular ions are gradually released into the solution, increasing its conductivity. This assay detects cell death by measuring the conductivity of the FB1 solution over time. In order to increase statistical significance of the results, a total of 10 independent plants of similar age and size were used when testing each KO line, with each plant providing one leaf disk from the same leaf for 1 of each 3 replicates petri dishes (Figure 3.8A). Therefore, each replicate petri dish replicates plant tissue from 10 independent plants. The conductivity of the underlying solution was monitored every 24 hours until complete cell death of all the leaf tissue had occurred. This usually happened 9 days after FB1 exposure. Immediately after leaf disk corking, the disks were placed in the dark for the first 48 hours to facilitate maximum FB1 uptake through stomata, and were then placed in the light. The increase in conductivity in the first 48 hours was due to ion leakage from the damaged outer rim of the leaf disks, as FB1 requires light to induce PCD (Stone *et al.,* 2000). The assay was validated using the *accelerated cell death 2* (*acd2*) mutant (Greenberg *et al.,* 1994) and salicylate hydroxylase gene (*nahG*)-expressing plants (Lawton *et al.,* 1995) that are hypersensitive and resistant to FB1, respectively (Asai *et al.,* 2000). These plants displayed significantly higher and lower conductivity readings than wildtype Col-0 in the conductivity assay, respectively (Figure 3.8B), demonstrating the utility of this assay to detect mutant lines dying significantly faster or slower than wildtype *Arabidopsis*.

There are some limitations to using this assay. Because of the timecourse nature of this assay, a mutant line can display a significant cell death phenotype that can be only restricted to some specific timepoints, unlike the *acd2* and *nahG* controls that show a strong and consistent phenotype on all timepoints (Figure 3.8B). To discard KO lines for genes that showed a very small effect on FB1-induced cell death, mutant lines were only considered as having an altered cell death phenotype if they showed a significant ($p \leq 0.05$) change to Col-0 in at least 3 consecutive 24 hour timepoints. All 17 independent lines were tested using this assay (Table 3.4). The assay identified a total of 5 independent lines that showed a significant sustained decrease in FB1-induced cell death and 2 lines that showed very marginal resistance to FB1 (Table 3.4).

Annotation	Gene locus[a]	SALK number[b]	NASC number[c]	T-DNA insertion location[d]	Protein spots reversed with ATP	altered FB1 phenotype
glutathione transferase	AT1G02930	SALK_026398	N658155	intron	Yes	no
putative phosphoglucomutase	AT1G70730	SALK_139468	N665064	exon	Yes	no
protein disulfide isomerase-like (PDIL)	AT1G77510	SALK_111424	N661089	5' UTR	Yes	Yes
GAPDH (C subunit)	AT3G04120	SALK_044604	N662293	5' UTR	Yes (1 out of 2 spots)	no
similarity to mammalian RACKs	AT3G18130	SALK_001973	N661284	5' UTR	Yes	no
similarity to mammalian RACKs	AT3G18130	SALK_017913	N661664	5' UTR	Yes	Yes
putative fructose-bisphosphate aldolase	AT3G52930	SALK_124383	N663895	exon	Yes (2 out of 4 spots)	no
S-adenosyl-L-homocysteine hydrolase	AT4G13940	SALK_023915	N657174	exon	Yes (1 out of 3 spots)	no
heat shock 90.7 like protein	AT4G24190	SALK_048558	N661329	exon	Yes	no
heat shock 90.7 like protein	AT4G24190	SALK_004733	N662393	intron	Yes	no
putative caffeoyl-CoA 3-O-methyltransferase	AT4G34050	SALK_055103	N662518	5' UTR	Yes	Marginal
putative caffeoyl-CoA 3-O-methyltransferase	AT4G34050	SALK_151507	N664340	exon	Yes	Marginal
mitochondrial heat shock protein 70-1	AT4G37910	SALK_128982	N656969	Promoter	Yes (3 out of 5 spots)	no
ATP synthase beta-subunit	AT5G08690	SALK_024990	N658574	exon	Yes	Yes
ATP synthase beta-subunit	AT5G08690	SALK_135351	N653503	exon	Yes	Yes
ATP synthase beta-subunit	AT5G08690	SALK_005252*	N505252*	exon	Yes	Yes
Reversibly Glycosylated Polypeptide-2	AT5G15650	SALK_132152	N656992	intron	Yes	no

Table 3.4 Validation of putative eATP-regulated cell death genes using the conductivity assay. Reversed and enhanced genes were tested for an altered cell death phenotype with FB1 using *Arabidopsis* T-DNA KO homozygous lines available from SALK collection. NASC number indicates the corresponding homozygous NASC line available. Column 5 indicates the number of spots identified as the respective gene that were reversed with ATP from Tables 1 and 2. A "Yes" indicates all spots were reversed. An asterisk denotes the heterozygous ATP synthase beta-subunit KO line that was used to generate a third homozygous KO line by segregation analysis of 48 independent heterozygous plants. UTR- untranslated region of the mRNA. [a]Arabidopsis Genome Initiative (AGI) gene identifier [b]SALK number of homozygous T-DNA insertion lines mapped to the specific gene locus [c]line number for homozygous lines available at NASC [d]Predicted T-DNA insertion site in each SALK line

Annotation	Gene locus[a]	SALK number[b]	T-DNA insertion location[c]	Spots reversed with ATP
heat shock protein AtHSP90.1	AT5G52640	SALK_007614	exon	Yes
heat shock protein AtHSP90.1	AT5G52640	SALK_127450	5' UTR	Yes
putative phosphoglucomutase	AT1G23190	SALK_036631	exon	Yes
putative phosphoglucomutase	AT1G23190	SALK_034720	exon	Yes
regulatory particle non-ATPase 12a	AT1G64520	SALK_134934*	5' UTR	Yes
Nudix hydrolase homolog 3 (*atnudt3*)	AT1G79690	SALK_009963*	intron	Yes
Nudix hydrolase homolog 3 (*atnudt3*)	AT1G79690	SALK_041331*	3' UTR	Yes
ATSLY1 protein transporter	AT2G17980	SALK_106708	3' UTR	Yes
ATSLY1 protein transporter	AT2G17980	SALK_106706	exon	Yes
coproporphyrinogen III oxidase	AT1G03475	SALK_025589	exon	Yes
coproporphyrinogen III oxidase	AT1G03475	SALK_139746	5' UTR	Yes
ferritin 3 AtFER3	AT3G56090	SALK_076833	exon	Yes
ferritin 3 AtFER3	AT3G56090	SALK_076881	exon	Yes
general regulatory factor 3	AT5G38480	SALK_001646	3' UTR	Yes
general regulatory factor 3	AT5G38480	SALK_012320	Promoter	Yes
chloroplast heat shock protein 70-1	AT4G24280	SALK_140810	intron	Yes (1 out of 2)
ATPase subunit 1	ATMG01190	SALK_134219	exon	Yes (2 out of 7)
ATPase subunit 1	ATMG01190	SALK_044454	exon	Yes (2 out of 7)
ATP synthase delta chain	AT5G13450	SALK_010674	exon	Yes
ATP synthase delta chain	AT5G13450	SALK_042172	5' UTR	Yes
ATPase CF1 alpha subunit	ATCG00120	SALK_101141	exon	Yes

Table 3.5 Putative eATP-regulated cell death genes not tested using the conductivity assay. Heterozygous T-DNA lines available in the SALK collection. An asterisk indicated homozygous KO lines that became available in the end of this study. [a]Arabidopsis Genome Initiative (AGI) gene identifier [b]SALK number of heterozygous T-DNA insertion lines mapped to the specific gene locus [c]Predicted T-DNA insertion site in each SALK line.

The ATP synthase β-subunit (AT5G08690) showed the strongest altered cell death phenotype in all putative homozygous KO lines tested and it will be discussed later in more detail. Another gene (AT4G34050) showed only a marginal phenotype in both of its KO lines (Table 3.4). Although one line was significant in three consecutive timepoints (Figure 3.9A), the magnitude of the phenotype of both lines was not significant enough to warrant further experimentation. Another gene (AT3G18130) showed a significant phenotype in only one of the two lines tested predicted to homozygous KO for the gene (Table 3.4, Figure 3.9B). This lack of reproducibility between the two reported homozygous KO lines is not clear, but could be related to the location of the reported T-DNA insert in each line being in the 5' end UTR of the coding mRNA sequence, close to the promoter sequence. Regardless of the true reason for this discrepancy, extra homozygous KO lines for this gene were not available and so no further experimentation was performed on this gene. The results for the protein disulphide isomerase-like (AT1G77510) KO line (SALK_111424), which was the last line screened to produce a cell death phenotype, are reported in the end of this chapter. Most of the work in this chapter was focused on characterizing the ATP synthase β-subunit KO gene that had three independent KO lines showing a phenotype with FB1 in the conductivity assay (Table 3.4), since this provided strong evidence that the observed phenotype is being caused by a disruption in the targeted genes. Further experiments performed on the KO lines for the ATP synthase β-subunit, henceforth called ATPaseβ, are describe. In order to establish if ATPaseβ is an eATP-regulated cell death gene, it was necessary to confirm the KO status of the mutant lines tested by conductivity (SALK_024990, SALK_135351 and SALK_005252).

3.3.2 Altered cell death phenotype of ATPaseβ KO mutants

The initial cell death kinetics characterization was performed on SALK_024990 and SALK_135351 using the conductivity assay (Figure 3.10A). As soon as the third independent KO had been obtained by segregation analysis of a heterozygous line (SALK_005252), its cell death kinetics was also determined. In order to compare with previously obtained conductivity data, SALK_135351 was used together with SALK_005252 as a positive control for the extent of cell death (Figure 3.10C). The rate and extent of cell death was significantly diminished in all three lines relative to Col-0

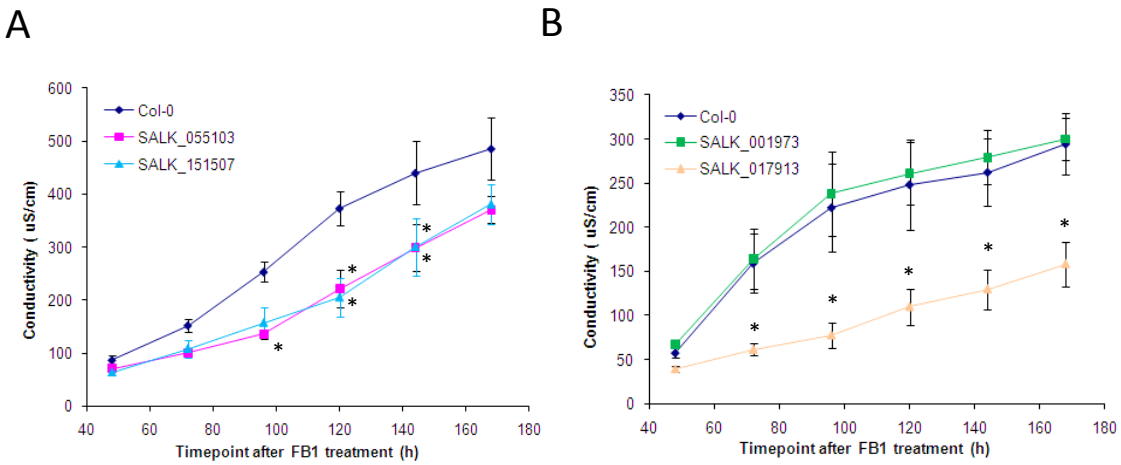

Figure 3.9 Cell death profiles of putative KO lines for AT4G34050 (A) and AT3G18130 (B). The different Col-0 cell death kinetics reflects different experiments. Leaf discs were treated with FB1 and incubated in the dark for 48 hours. The conductivity of FB1 solutions on which discs were floating was measured every 24 h after exposure to light (48 hours after FB1 treatment). Values and error bars represent means ± SE (n = 3). An asterisk indicates data points at which the mutants show a significantly ($p \leq 0.05$) lower conductivity that the Col-0.

controls, showing that they are resistant to FB1-induced cell death (Figure 3.10 A,C). The extent of cell death was also clearly visible in treated leaf tissue. Cell death symptom development was suppressed in SALK_024990 when FB1 was infiltrated into leaves attached to growing plants, whereas Col-0 leaves similarly infiltrated with FB1 developed extensive lesions (Figure 3.10B). Moreover, corresponding leaf disks from the conductivity assay of lines SALK_005252 and SALK_135351 showed little to no cell death when photographed 96 hours after FB1 exposure, at a time when Col-0 leaf disks were deprived of any chlorophyll (Figure 3.10D). These are in agreement with increased ion leakage derived from Col-0 leaf disks for the same timepoint (Figure 3.10C). Overall, these results clearly show that ATPaseβ is a novel cell death regulator. More importantly, they validate the experimental approach outlined in the beginning of this chapter, where the ATP filter applied to the analysis of protein abundance was predicted to be capable of identifying new cell death genes regulated by eATP signalling.

3.3.2.1 Confirmation of KO status of the ATPaseβ mutant lines by genotyping and RT-PCR

In order to firmly established ATPaseβ as a novel cell death regulator, it was now necessary to confirm the KO status of the lines tested as previously outlined in the reverse genetics strategy. This usually involves genotyping of the lines, i.e. confirmation that the lines are homozygous for the mutant allele by PCR and, most importantly, confirmation that no coding mRNA is being transcribed as detected by sqRT-PCR. KO lines with predicted T-DNA insertions in the exon are usually the best ones, since these will either produce a very large mRNA species, that includes part or the entire T-DNA insert, or fail altogether to produce stable mRNA of the targeted gene. In both cases a functional copy of the protein should be absent, making these lines a true loss-of-function KO.

The two independent putative homozygous KO lines for ATPaseβ, SALK_024990 and SALK_135351, have T-DNA inserted into predicted exonal regions of the gene (Table 3.4, Figure 3.11A). The initial PCR primer pair obtained, designed using PrimerBlast, consisted of the F-ATPaseB and R-ATPaseB primers and was designed to amplify a 349bp gene specific product close to the end of the mRNA (Figure 3.11A). Initial sqRT-PCR results showed SALK_024990 to be a complete KO, but surprisingly SALK_135351 appeared not to be a complete KO, since it amplified the gene specific product similarly to Col-0 (Figure 3.11B).

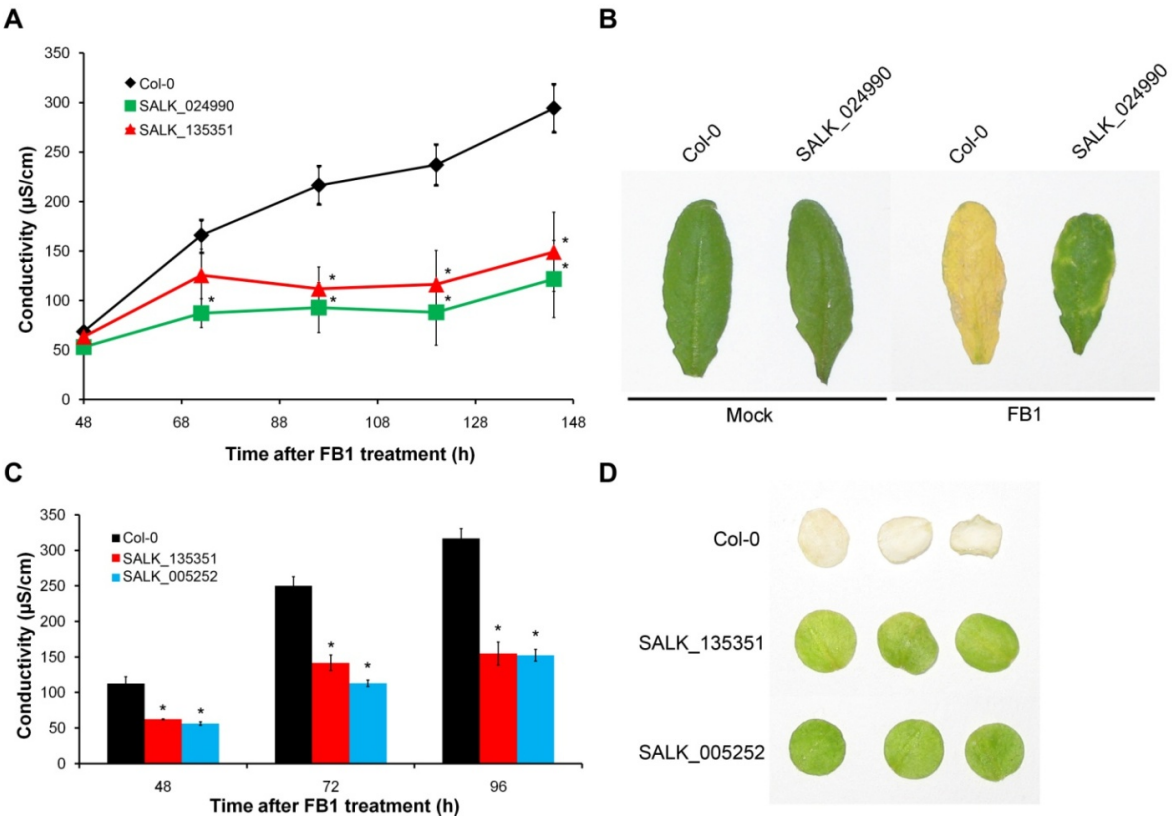

Figure 3.10 ATP synthase β-subunit (AT5G08690) gene KO mutant plants are resistant to FB1. (A) Cell death profiles of leaf disc tissues. Leaf discs were treated with FB1 and incubated in the dark for 48 hours. The conductivity of FB1 solutions on which discs were floating was measured every 24 h after exposure to light. Values and error bars represent means ± SE (n = 3). An asterisk indicates data points at which the mutants show a significantly ($p \leq 0.05$) lower conductivity that the Col-0. (B) Appearance of leaves 4 days after infiltration with FB1. Mock controls were infiltrated with carrier only solution. (C) Leaf disc cell death assay with SALK_135351 and SALK_005252 as described in (A). (D) Leaf discs treated as described in (C) and photographed 96 h after FB1 treatment.

This was not in agreement the conductivity results, since both lines showed a similar cell death phenotype. This discrepancy was investigated in light of the different predicted T-DNA insertion sites in the SALK_024990 and SALK_135351. The insert site of SALK_024990 is located inside the gene specific sequence targeted by the F-ATPaseB and R-ATPaseB primers used, preventing its proper amplification due to the presence of a very large T-DNA insert (Figure 3.11A). On the other hand, the insert site of SALK_135351 is located in the first exon of the gene, upstream of the gene specific sequenced being amplified (Figure 3.11A). It was rationalised that the amplification of the gene specific product in the SALK_135351 could be due to transcription read-through originating in the T-DNA itself. This can result from the strong constitutive cauliflower mosaic virus 35S promoter combined with a weak nopaline synthase gene terminator sequence present close to the left boarder of the T-DNA construct [Figure 3.12; (Baulcombe *et al.,* 1986)]. If this was indeed the case, the use of another primer pair that flanked the predicted SALK_135351 insertion site should fail to amplify the gene specific product in that line, similarly to the SALK_024990 using the F-ATPaseB and R-ATPaseB primers. A new primer set was designed with these characteristics (F-ATPB2 and R-ATPB2) and used to confidently confirm the homozygous KO status of the SALK_135351 by sqRT-PCR (Figure 3.11B). Surprisingly, when these same primers were used on the SALK_024990 line the 485bp gene specific product was amplified (Figure 3.11B), suggesting it is not a true KO. Again, this product could be the result of transcription initiated in the T-DNA, in this case originating from the *NOS* promoter located next to the right boarder [Figure 3.12; (Ulker *et al.,* 2008)]. To eliminate any possibility of T-DNA associated transcription influencing the KO status confirmation, it was then decided to amplify the full length ATPaseβ cDNA in both KO lines, using the F-ATPB2 and R-ATPaseB primers, since this sequence flanks both predicted insertion sites (Figure 3.11A). Using this primer combination it was possible to show in one PCR that both lines are complete KO for the ATPaseβ gene, as both failed to amplify the expected 1,795 bp coding cDNA, whereas in Col-0 this product was successfully amplified (Figure 3.11B). Overall, these results show that SALK_024990 and SALK_135351 are homozygous KO lines for the ATPaseβ in accordance with their resistant phenotype to FB1 treatment. They also show it is essential to use primers flanking the predicted T-DNA insertion sites in order to confidently confirm a true KO status by sqRT-PCR.

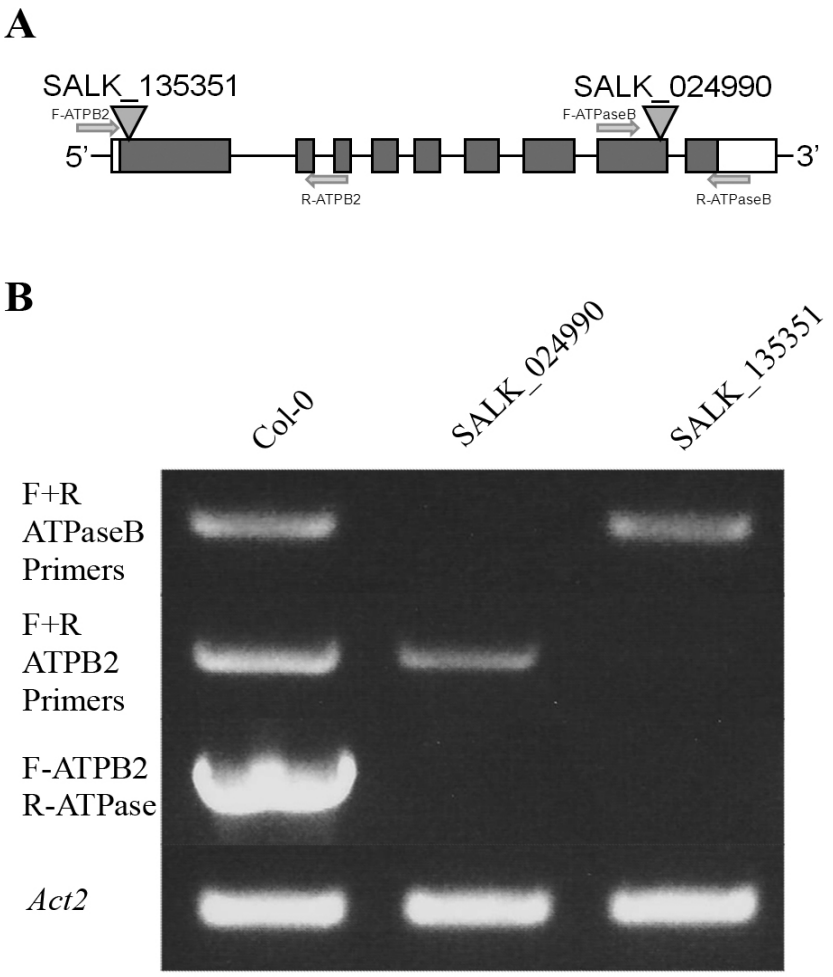

Figure 3.11 Strategy for confirmation of ATPaseβ KO lines by RT-PCR. (A) Schematic diagram showing T-DNA insertion sites in two independent ATPaseβ KO mutants (SALK_024990 and SALK_135351). Inverted triangles indicate insertion sites, white boxes and grey boxes represent untranslated regions and exons, respectively. Arrows with numbers indicate specific primer annealing locations. (B) Amplification of a full length gene transcript by RT-PCR is essential for confident characterization of KO status of T-DNA lines with predicted insert sites in the coding sequence. Amplification of a gene-specific sequence not spanning a predicted insert site resulted in the amplification of the expected PCR product (550 bp in SALK_024990 and 485 bp in SALK_135351). Actin-2 (*Act2*) was used as a constitutive reference control.

Figure 3.12 Schematic diagram showing the structure of the vector pROK2 used to generate the T-DNA lines in the SALK collection. The construct contains a cauliflower mosaic virus 35S promoter followed by a nopaline synthase gene (NOS) terminator close to the left boarder and a NOS promoter driving expression of the selectable marker *nptII*, (neomycin phosphotransferase II) gene conferring resistance to kanamycin. LB denotes left boarder and RB right boarder of the construct [Adapted from (Ulker *et al.,* 2008)].

Confirmation of the KO status of SALK_024990 and SALK_135351 implicated the ATPaseβ as a novel cell death regulator. Increasing the number of mutant alleles for the gene increases the confidence that an observed phenotype is due to the disrupted gene (Krysan *et al.,* 1999). Therefore, a third independent homozygous KO line for the ATPaseβ gene was obtained during the course of this study for a publication resulting from this work (Chivasa *et al.,* 2011).

The heterozygous SALK_005252 line, with a predicted insert site in the second last exon of the ATPaseβ gene (Figure 3.13A), was chosen to generate a third homozygous line by segregation analysis. A total of 48 individual plants were individually genotyped by PCR using the Phire plant PCR kit and homozygous ones allowed to set seed for later analysis. Subsequently, genotyping analysis was performed on all three lines to confirm their insertion sites. This provided further data to the previous acquired RT-PCR data on the KO status of SALK_024990 and SALK_135351 (Figure 3.11B). The same primers previously used for RT-PCR were used here to amplify the genomic full length ATPaseβ gene (2741bp long). Initially, unspecific PCR products were obtained using F-ATPB2 and R-ATPaseB on Col-0 genomic DNA (data not shown). Raising the annealing temperature from 56ºC to 64ºC eliminated the unspecific products and this annealing temperature was used for subsequent PCRs on genomic DNA. Col-0 successfully amplified the expected product whereas all the three KO lines fail to do so, indicating the presence of an insert in both alleles of the gene (Figure 3.13B). To confirm the insertion of a T-DNA insert, a PCR using the appropriate gene specific and T-DNA left boarder primer (LBa1) combination was performed on each individual SALK line. According to T-DNA express (http://signal.salk.edu/cgi-bin/tdnaexpress), a web-base tool hosted by the SALK institute that describes the exact location and orientation of all T-DNA lines in the SALK collection, the left boarder of the T-DNA insert in all three lines is closer to the 3' end of the gene. This means that the successful amplification of a T-DNA-ATPaseβ gene specific hybrid product in the mutant lines requires a combination of LBa1 primer, annealing to the anti-sense strand and a reverse gene specific primer, annealing to the sense strand of the gene. For SALK_024990 and SALK_005252, the primer combination used was LBa1 and R-ATPaseB (Figure 3.13B) that amplified a ~990bp and ~770bp PCR product, respectively. For the SALK_135351 the LBa1 and R-ATPB2 primers were used (Figure 3.13B) and a ~750bp PCR product was amplified in the SALK_135351 line. Therefore, all three lines amplified their respective products as expected, showing they were genetically

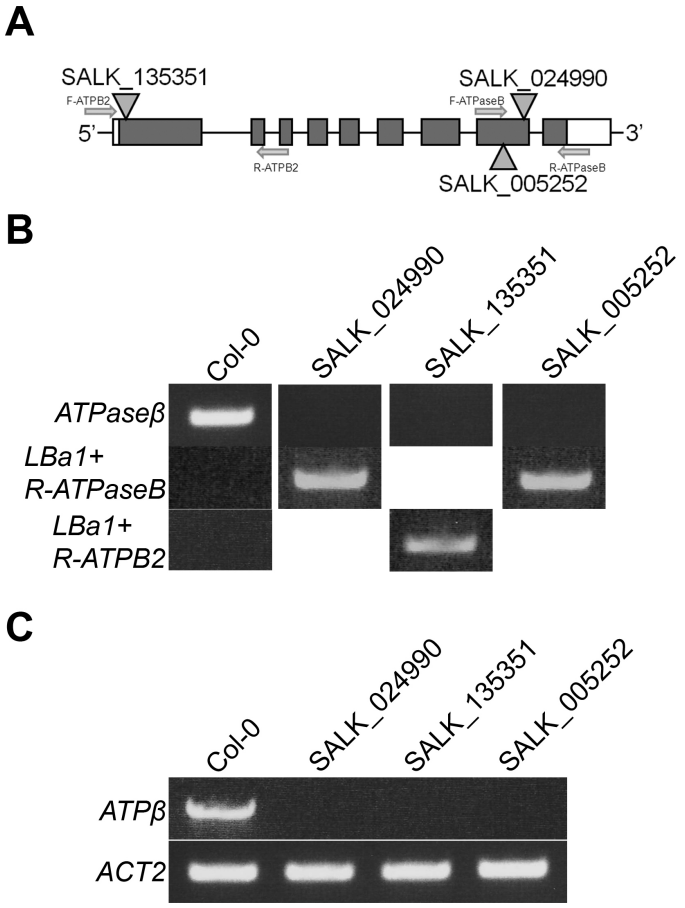

Figure 3.13 Genotyping of all three ATPaseβ KO lines and confirmation of KO status by sqRT-PCR. (A) Schematic diagram of ATPaseβ gene, insertion sites and primer locations using similar representation as Figure 3.11A. (B) Genotyping PCR's using the appropriate combination of T-DNA and gene specific primers for each line. Col-0 amplified the full genomic DNA product (2741 bp) that failed to amplify in any of the KO lines. A left boarder-gene specific product was amplified in SALK_024990, SALK_135351 and SALK_005252. Band sizes were 990 bp, 750 bp and 770 bp respectively. (C) sqRT-PCR amplification of full-length ATPaseβ in RNA samples derived from Col-0 plants and the three independent T-DNA insertion mutants. Actin-2 (*ACT2*) was used as a constitutive reference control.

homozygous for the T-DNA insert site (Figure 3.13B). The full length ATPaseβ cDNA was not amplified by sqRT-PCR in all three lines, confirming them to be complete KO lines for the ATPaseβ gene (Figure 3.13C). These results confirm that the altered cell death phenotype of the putative ATPaseβ homozygous KO lines is indeed the result of a disruption in the ATPaseβ gene. It conclusively shows that the experimental approach outlined in the beginning of this chapter, where the ATP filter applied to analysis of protein abundance was predicted to be capable of identifying new cell death genes regulated by eATP signalling, can work and produced new knowledge in the eATP field. Further insight could be gained on what is happening to the ATPaseβ protein following FB1 treatment. Therefore, it was decided to look in more detail at the FB1- and ATP- induced proteomic changes associated with this protein to better understand the mechanism behind ATPaseβ resistance to FB1.

3.3.2.2 Analysis of ATPaseβ protein spots

In order to gain further insight into the mechanism of how ATPaseβ promotes PCD using the 2D-DiGE proteomic data generated in this chapter, the effects of eATP signalling on the distribution and abundance of individual ATPaseβ spots was investigated in more detail. ATPaseβ is a dominant microsomal fraction eATP-regulated protein found as a charge train of ~55KDa consisting of 8 spots (spot 30, 32, 33, and 35-38; Figure 3.7B; Table 3.2) and as a lower MW spot (spot 39) of ~49KDa. Surprisingly, it was also present in the TSP fraction (spot 33) as a ~38KDa spot (Figure 3.7A; Table 3.1). The charge train spots were all downregulated by FB1 treatment whereas the low MW spots were both upregulated by FB1 treatment. This could reflect a specific effect of FB1 on the mature protein.

The primary sequence of ATPaseβ contains 566 amino acid residues and, according to MitoProt II prediction algorithm (Claros and Vincens 1996), the first 38 residues on the N-terminus constitute a cleavable mitochondrial-targeting signal peptide, in line with its function in mitochondrial oxidative phosphorylation. As a consequence, the mature protein sequence with 528 amino acid residues has a predicted MW of 54,5 KDa, which is very close to the experimentally determined MW of ~55 KDa observed for all the charge train spots (Figure 3.3B). All the seven spots in the charge train were significantly downregulated in response to FB1 but spot 33 and 39 were up-regulated (Tables 3.1 and 3.2). The significance of the appearance of these lower molecular weight species of ATPaseβ or their possible role in cell death is unclear, but they could originate from

proteolytic processing of the mature protein. The distribution of peptides identified by MALDI-ToF from both lower MW spots was carefully examined to test this hypothesis. When examining the peptide coverage of spot 33, if all the amino acids upstream of the most extreme N-terminal peptide identified (IMNVLGEPIDER; Figure 3.14A) and downstream of the most extreme C-terminal peptide identified (ENINSFQGLLDGK; Figure 3.14A) were cleaved off from the mature protein sequence, the predicted size of the truncated sequence becomes 38.7 KDa, which nearly matches the experimentally determined size of the ~38 KDa TSP low molecular weight spot (spot 33, Figure 3.3A). Similarly, the ~49 KDa microsomal spot based on the identified peptides (Figure 3.14B) yields a putative product whose predicted size of 47.6 KDa also closely matches its experimentally observed low molecular weight on 2D gels (spot 39, Figure 3.3B). Further analysis of the 38 KDa TSP spot by MS/MS confirmed the presence of peptides originating specifically from the central portion of the protein, with the most extreme N-terminal sequenced peptide matching the most extreme N-terminal predicted by MALDI-ToF (Figure 3.14C). These findings provide additional data supporting proteolytic processing of ATPaseβ in the N-terminal for spot 33. Thus, the FB1-induced increase in abundance of the low molecular weight spots, which is accompanied by a decrease in the ~55 KDa charge train, could be a consequence of proteolytic cleavage of the mature protein. The protein could be proteolytically processed in response to FB1 with ATP treatment protecting it from degradation. Indeed, ATP treatment significantly reversed the effects of FB1 on the protein abundance of spots 30, 32, 33, 35 and 36 of the charge train (Table 3.2). The presence of spot 33 in the TSP fraction could indicate the processed protein was already present in a soluble form due to detachment from the ATP synthase complex. However, the overall contribution to cell death regulation of the lower MW and intact ATPaseβ proteins is unknown. Future studies could look at overexpression of the truncated protein in the ATPaseβ KO background. I now decided to look at the possible role of ATPaseβ protein in gene expression.

3.3.2.3 Basal expression of cell death-associated genes in ATPaseβ KO lines

One of the ways a protein might modulate cell death response is by regulation of gene expression. This can be by direct regulation of gene transcription or by interfering with signalling mediated by cell death associated genes. Indeed, other primary metabolism proteins, such as GAPDH (Saunders *et al.,* 1999), have been shown to have secondary roles in gene expression regulation in addition to their primary function. Therefore, further

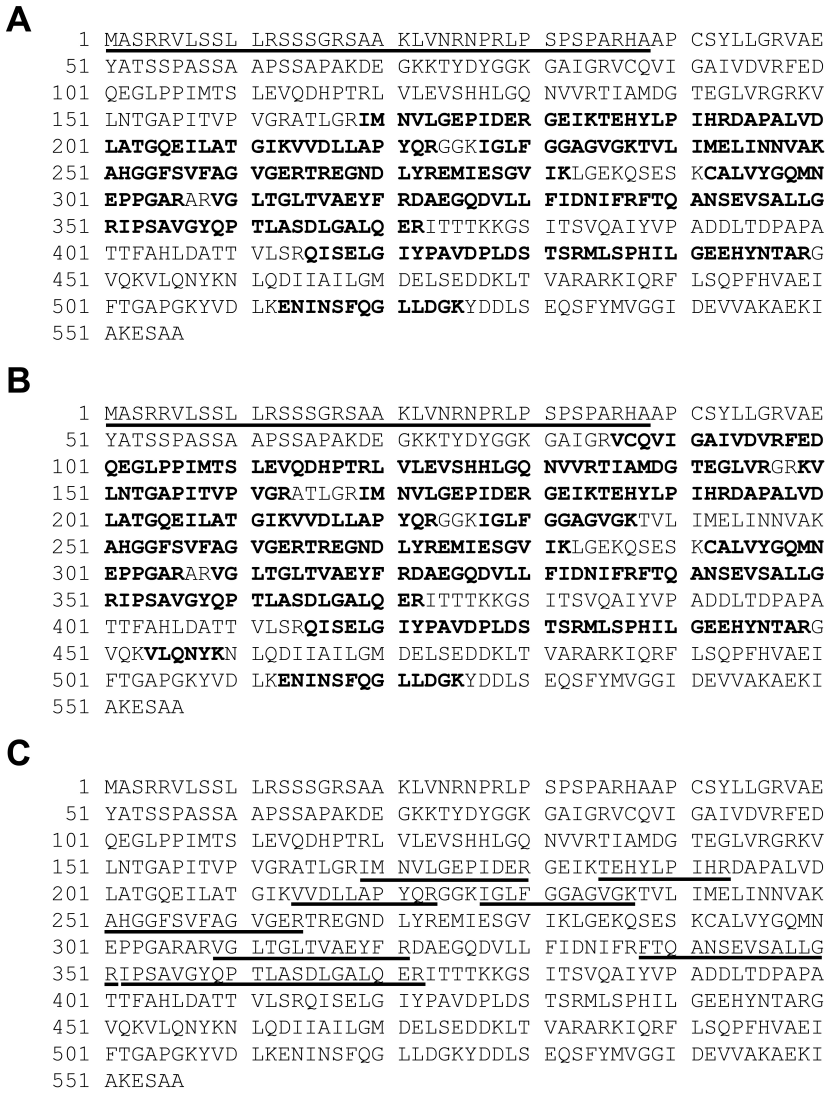

Figure 3.14 MALDI-ToF PMF and MS/MS identification of ATPaseβ protein. MALDI-ToF PMF sequence coverage of ATPaseβ spot 33 (A) and 39 (B), in the TSP and Microsomal protein fractions respectively. Identified peptides are bold and the subcellular localization sequence in the N-terminal is underlined. (C) Spot 33 was further analysed by MS/MS, where a total of 8 peptides were directly sequenced. The sequenced peptides are underlined in the sequence of the full protein.

insight could be gained on the potential position of ATPaseβ in a cell death signalling cascade or gene regulatory events by comparing the gene expression of known cell death regulators in the ATPaseβ mutant background relative to Col-0. The *ACD2* and *DND1* genes encode for a chlorophyll catabolite reductase and cyclic nucleotide gated channel 2, respectively. KO mutants for these genes show altered cell death phenotypes, with the *acd2* showing spontaneous lesion formation (Mach *et al.,* 2001) and *dnd1* unable to initiate PCD elicited by avirulent pathogens (Clough *et al.,* 2000). These two genes mediate cell death by interfering with ROS and calcium signalling, respectively. The *MLO10* is a gene that belongs to a 15 member family of plasma membrane located proteins in *Arabidopsis* that are homologues of the mildew resistance locus o (MLO) protein. These proteins play a role in defence responses to oomycete pathogens that cause powdery mildew disease (Consonni *et al.,* 2006). *SAG12* encodes for a cysteine protease that is only expressed during senescence with a characterised senescence-responsive *cis* element (Noh and Amasino 1999). The basal expression level of these 4 cell death-associated genes was examined between Col-0, SALK_024990 and SALK_135351. Basal expression levels showed no consistent significant response in the two KO lines relative to Col-0 (Figure 3.15). *ACD2* and *MLO10* showed no change in expression levels to Col-0. The *DND1* and *SAG12* genes were slightly downregulated and upregulated in the SALK_024990 line, respectively. However, this change is not connected with the absence of a functional ATPaseβ protein, because SALK_135351 line showed the same expression levels as Col-0. More likely, it could indicate a presence of multiple insertions in the SALK_024990 that could be regulating other pathways. These finding show that, at least for the cell death-associated genes tested, either ATPaseβ does not have a secondary function in gene regulation or might modulate genes downstream of these cell death-associated genes.

3.3.2.4 Possible mechanisms of ATPaseβ regulation of PCD

The function of ATPaseβ during FB1-induced cell death is not understood and it has not been previously described as a cell death regulator in plants. Nonetheless, three possible ways by which ATPaseβ could be performing this function are discussed bellow and schematically represented in Figure 3.16. First, it could directly interact with core cell death factors in a protein complex independently of it classical function in ATP production. This possibility would be a similar scenario as with cytochrome *c*, a mitochondrial protein involved in oxidative phosphorylation, which translocates to the cytosol, following a cell death-activating stimulus, and forms a complex with the

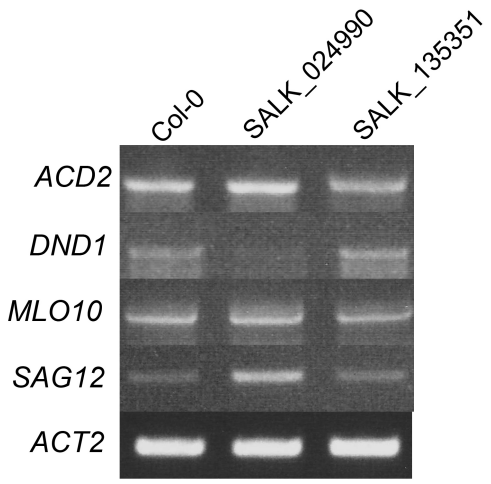

Figure 3.15 Basal expression levels of cell death-associated genes in Col-0, SALK_024990 and SALK_135351 in the absence of FB1 treatment. Actin-2 (*ACT2*) was used as a constitutive reference control.

Apoptotic protease activating factor 1 (Apaf-1) and caspase-9 to initiate apoptosis in animal cells (Li *et al.,* 1997). Second, ATPaseβ might be capable of influencing gene expression, thereby activating cell death genes. The WoLF PSORT eukaryotic localization prediction software (Horton *et al.,* 2006) predicts a mitochondrial localization for this protein as expected by its function in mitochondrial oxidative phosphorylation. Additionally, transcription associated characteristics, such as nuclear localization signal peptides or DNA binding motifs, are not predicted in ATPaseβ primary protein sequence (data not shown). However, there is precedence for proteins with an established metabolic function also being capable of regulating gene expression. Cytosolic proteins such as GAPDH (Saunders *et al.,* 1999) and enolase (Lee *et al.,* 2002) are now known to translocate to the nucleus to affect gene expression, though they are classical glycolytic enzymes. Finally, ATPaseβ within the F_1 complex could be a specific target for direct interaction by the FB1 toxin or another pro-death protein/signal, resulting in an inhibition of mitochondrial ATP production, as is suggested by the general downregulation of ATP synthase complex proteins with FB1 treatment (Table 3.2). Similarly, the basis for phytotoxicity of tentoxin, another fungal-derived toxin that causes PCD, is cellular depletion of ATP resulting from inhibition of chloroplastic photophosphorylation (Steele *et al.,* 1976). In this scenario, FB1 resistance in the ATPaseβ KO mutants could result from the absence of a binding site for FB1 in the mitochondrial F_1 complex, as in the absence of ATPaseβ, the other two other family members, AT5G08680 and AT5G08670 would replace it. The *Arabidopsis* ATPaseβ protein is part of a multigene family consisting of only 3 members, all sharing a 98% sequence similarity at the amino acid level, with differences only in the first 61 amino acids in the N-terminal. Therefore, this region of the protein is the ideal target for future studies to determine the basis for its novel cell death promotional function identified in this study, since the binding of FB1 could be specific to this region. As precedence, specific residues of the chloroplastic ATP synthase β-subunit have been shown to be critical for binding of the PCD-inducing tentoxin to the chloroplast F_1-ATP synthase (Avni *et al.,* 1992). The mutagenesis of one specific chloroplastic ATP synthase β-subunit gene codon from tentoxin resistant *Chlamydomonas reinhardtii* to match the corresponding codon of a tentoxin-sensitive *Nicotiana tabacum* species is sufficient to generate tentoxin-sensitive algae mutants (Avni *et al.,* 1992), demonstrating a very specific structural requirement for chloroplastic ATP synthase β-subunit function in cell death promotion. Similarly, a single amino acid substitution in the chloroplastic ATP synthase β-subunit is enough to switch tentoxin-resistant F_1-ATP synthase of *Bacillus* PS3

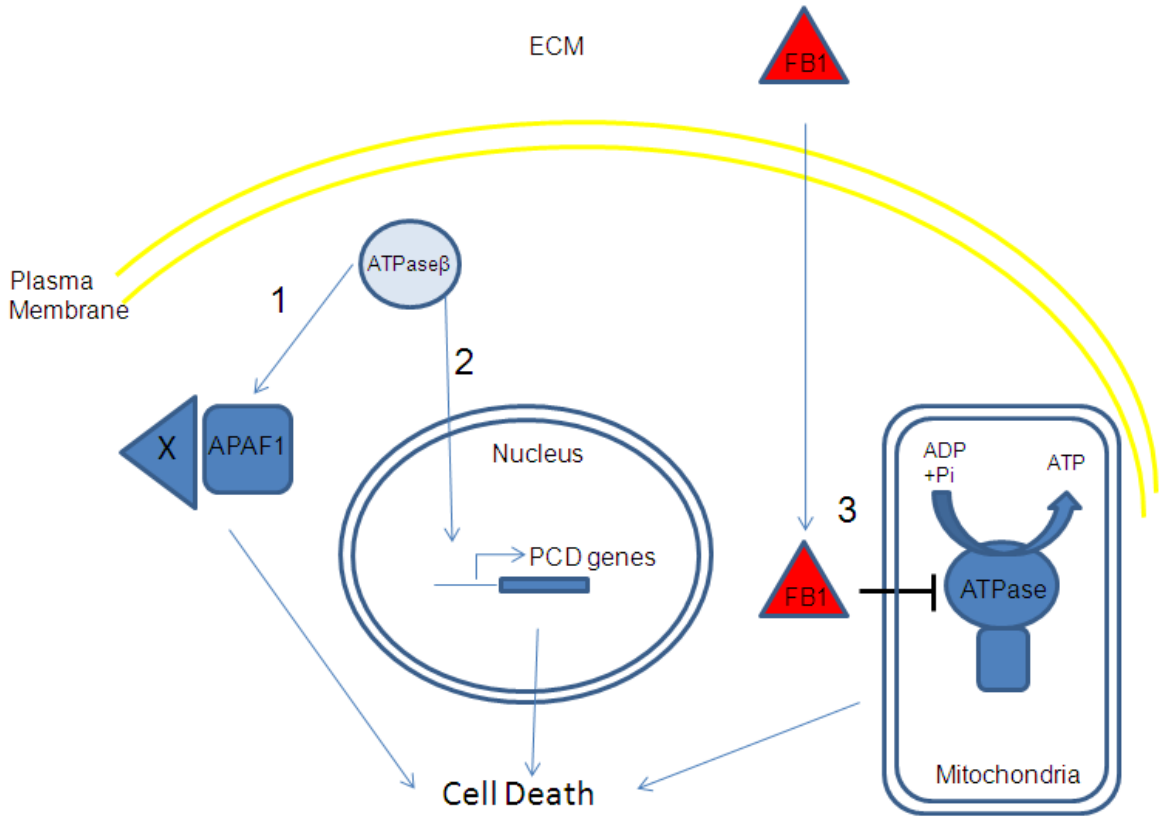

Figure 3.16 Possible mechanisms of the ATPaseβ protein in FB1-induced cell death. Numbers correspond to the three different hypothesis discussed in the text. In mechanism 1, ATPaseβ interacts with known (eg: Apaf-1) or unknown core cell death factors (X) to activate cell death. In mechanism 2, ATPaseβ regulates gene expression of cell death genes. In mechanism 3, ATPaseβ interacts with FB1 and this blocks ATP synthesis, resulting in cell death.

to a tentoxin-sensitive mutant (Groth *et al.,* 2002). These examples from the literature provide evidence that a similar situation could account for the non-redundant function of ATPaseβ protein in PCD, as is revealed by FB1 resistance in the KO mutant lines. The overall role of the ATPaseβ protein in FB1 cell death mechanism remains to the elucidated.

3.3.3 Protein disulfide-isomerase mutant

The protein disulfide isomerase-like (PDIL, AT1G77510) spot was downregulated with FB1 treatment and significantly upregulated following ATP treatment (Table 3.1), making this a putative cell death regulator that fits the ATP filter criteria and was therefore selected for validation using reverse genetics (Table 3.4). The only KO line obtained from SALK (SALK_111424) showed a resistant phenotype to FB1 treatment using the ion leakage assay (Figure 3.17A) similarly to ATPaseβ KO mutants (Figure 3.10A), although the resistance was less pronounced. Subsequent characterization of the KO status of this line was performed by amplifying a gene specific product by sqRT-PCR (Figure 3.17C). The results show that SALK_111424 is a knock-down line establishing a connection between the observed cell death response and the PDIL gene. This downregulation could be due to the location of the T-DNA insert in the promoter region of the PDIL gene (Figure 3.17B), a situation that can cause incomplete silencing of a gene but still produce a phenotype (Krysan *et al.,* 1999). However, one line is not considered enough to link the observed phenotype to the targeted gene because of the small chance that multiple insertions in that line could be knocking out another gene that is the real cause for the observed phenotype. No other putative KO lines were available for this gene at the time, nor were there heterozygous lines with predicted T-DNA inserts in an exon where a homozygous KO line could have been generated by segregation. Therefore, no further experimentation was performed on this gene. Overall, the results provide preliminary evidence for a strong link between PDIL and FB1 resistance in the PDIL knockdown line SALK_111424, but this link could not be confidently confirmed via a second independent KO line.

3.4 Conclusions

The main aim of this chapter was to use a proteomics approach, combined with the use of an ATP filter, to identify potential novel cell death regulators. To this end an experimental approach combining a PCD-inducing toxin FB1 with ATP treatment was used to identify protein spots that show an opposite response to FB1-induced eATP depletion and reversal

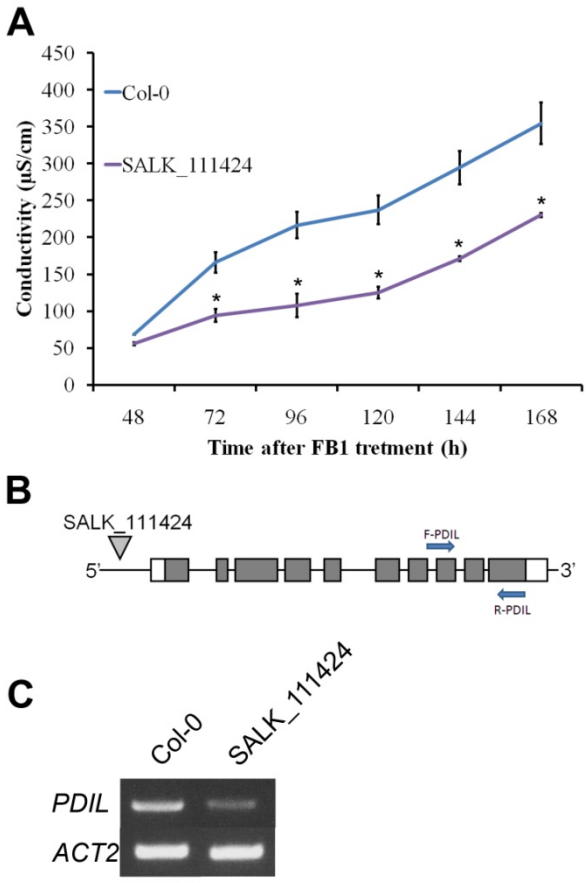

Figure 3.17 Protein Disulphide Isomerase-like (PDIL) KO lines cell death phenotype and KO status characterization. (A) Cell death profiles of leaf disc tissues. Values and error bars represent means ± SE (n = 3). An asterisk indicates a significance ($p \leq 0.05$) difference between the lines and Col-0. (B) Schematic diagram showing T-DNA insertion site in the PDI-like KO mutant SALK_111424. Schematic notations are the same as in Figure 3.13A. (C) sqRT-PCR amplification of a PDIL gene specific product in the predicted homozygous KO line using gene specific primers shown in (B). Actin-2 (*ACT2*) was used as a constitutive reference control.

via addition of ATP (Figure 3.2A). This approach was rigorous as it used 4 independent biological replicates as well as two technical replicates for each treatment. A rigorous statistical analysis was performed employing fold change and *t*-test significance values in order to identify the most significant and reproducible changes in spot abundance. Two separate protein fractions of *Arabidopsis* cell cultures were analysed by 2D-DiGE using the ATP filter to identify the subset of proteins which could be involved in regulating cell death. Gel analysis of both protein fractions returned a total of 55 reversed spots corresponding to 24 unique proteins (Table 3.1 and 3.2). This list of putative cell death targets provided a starting point for validation of a cell death role of the genes using a cell death assay. A total of 12 genes were tested for an altered cell death phenotype with FB1in homozygous KO lines using an ion leakage based cell death assay that enables an accurate and confident quantification of cell death progression.

One of the genes identified using the ATP filter, the ATP synthase β-subunit, displayed a strong resistant phenotype to FB1-induced cell death in three independent KO mutant lines. The resistance to FB1 was characterized by reduced lesion formation in attached leaf tissue and reduced ion leakage from floating leaf disks. Some difficulties were encountered during KO status confirmation and a practical solution is presented for use in future studies. It was attempted to gain further insight into the mechanism by which the ATP synthase β-subunit plays a role in FB1-induced cell death by analysis of gene expression of cell death related genes and possible mechanism were discussed. The identification of the first plant cell death regulator directly regulated by eATP signalling shows conclusively that the adopted experimental approach based on the ATP filter in this chapter can work.

Additionally, new insights into the proteomic changes induced by FB1 prior to cell death establishment were provided by the identification of 58 and 29 FB1 responsive spots in the TSP and microsomal fractions, respectively. The possible role of these FB1 responsive proteins in PCD and their regulation by eATP signalling is discussed. These results provide a list of targets for future studies on the mechanism of FB1, and possibly other fungal toxins, in plant cell death.

Finally, this chapter sets the stage for the identification of more genes with a putative role in cell death. A total of 12 genes identified using the ATP filter were not tested for a role in cell death due to no homozygous KO mutant being available at the time of this study. Once these mutants become available, their role in PCD can be tested using a cell death assay

such as the conductivity assay. The validated approach using the ATP filter can also be employed in future studies to other protein fractions such as plasma membrane and nuclear enriched fractions. Additionally, once all genes involved in FB1-mediated signalling are established from mutant studies, it should be possible to order them in a cell death signalling cascade, as well as establish their position to other core cell death regulators. The work in this chapter has been published in Molecular and Cellular Proteomics, 14 December, doi:10.1074/mcp.M110.003905 (Chivasa *et al.,* 2011) and a copy of that paper is present in Appendix B.

Chapter 4 Identification of genes and proteins which change in abundance in response to eATP using proteomic and bioinformatic approaches

4.1 Introduction

At the beginning of this project in October 2006, relatively few proteins and genes regulated by eATP had been identified. This was partly due to no study employing large-scale quantitative analysis of mRNA or protein abundance changes with ATP addition having been conducted. Studies focused on exploring the biological effects of increasing eATP concentrations on second messenger signalling uncovered some genes changing at the level of transcript abundance. These include the several MAP kinases (Jeter *et al.,* 2004), the NADPH reactive burst oxidase homologue *D* and *F* and enzymes involved in synthesis of salicylic acid (SA) such as *PAL1*, jasmonic acid (*LOX2*) and ethylene (*ACS6*) (Song *et al.,* 2006). A study conducted the previous year at University of Durham identified several proteins changing with depletion of eATP levels using a glucose hexokinase eATP depletion system (Chivasa *et al.,* 2005a). Proteins identified belonged primarily to the main metabolic hubs such as amino acid metabolism, carbon metabolism and energy biosynthesis. Although that study provided several putative targets regulated by eATP, it did not attempt to investigate the global effects of eATP depletion on the proteome. The study was designed to show that the cell death inducing treatment, brought about by eATP depletion, can result in protein abundance changes. The lack of information on eATP-responsive genes is also evident in The *Arabidopsis thaliana* (*Arabidopsis*) Information Resource (TAIR) database. Searches performed on this database it in October 2006 using the search keywords "eATP", "response to eATP" or "response to ATP" no genes were retrieved. In comparison to animal systems, very little is known about eATP-regulate genes and proteins in plants.

Since the eATP area is a relatively new one, particularly in respect to plants, I wished to identify proteins and genes associated with alterations in eATP levels in plants. Exogenous ATP regulation of its downstream components can happen at the gene expression level and at the post-transcriptional level. Therefore, the combined use of a proteomic and a transcriptomic approach is expected to provide a comprehensive picture of the full scope of genes and proteins regulated by eATP-mediated signalling.

The aim of this chapter is to identify genes and proteins regulated by alterations in eATP levels employing large-scale proteomic and transcriptomic approaches using an *Arabidopsis* suspension cell cultures system. For the proteomic approach, it was proposed

to achieve this by using large-scale quantitative analysis of eATP-induced protein abundance changes induced by ATP addition to cell cultures employing 2D-DiGE technology combined with mass spectrometry identification of target proteins. A preliminary study will be performed to determine the earliest timepoint after ATP addition where protein abundance changes resulting from eATP signalling can be detected.

In addition to this proteomic approach, it was decided to re-examine a DNA chip experiment, conducted by Dr. John Hamilton, Dr. Stephen Chivasa, Dr. Sean Coughlan and Prof. Toni Slabas, originally designed to identify eATP-regulated genes with a putative role in PCD. The basis of the experiment was to investigate the effects on gene expression of replenishing eATP levels in FB1-treated cultures around the time of commitment to death and identify putative PCD genes using the ATP filter (Chivasa *et al.,* 2005a). Due to the experimental design, the same datasets can be re-examined to potentially identify eATP only gene expression changes. A DNA chip can screen the whole genome at the gene expression level providing a more complete picture of the total number of genes regulated by eATP when compared to the limited number of proteins screened by 2D-DiGE.

The resulting lists of eATP-responsive targets from both proteomic and transcriptomic approaches will be analysed by bioinformatic tools in order to identify putative physiological processes under eATP control, increasing the understanding of the eATP field in plants. Additionally, the identification of eATP responsive genes opens up the possibility of utilizing some of these genes as molecular markers for eATP-mediated signalling. Such markers would constitute valuable tools for future studies in the eATP area in plants and might be used similarly as pathogenesis-related (PR) genes are in the study of plant defence responses to pathogens.

In this chapter, a total of 35 eATP responsive proteins and 100 eATP responsive genes are identified. Bioinformatic tools provide a comprehensive picture of pathways, organelles and physiological processes under eATP control and this will be discussed in light of the literature. Finally, 10 genes predicted by the DNA chip to be changing following ATP treatment were validated by semi-quantitative RT-PCR (sqRT-PCR), becoming molecular markers for eATP-mediated signalling. Two of these markers were shown to have ATP- and SA-dependent gene expression profiles consistent with genes predicted to be involved in regulating viability or defence (Chivasa *et al.,* 2009b), providing the first molecular evidence for the hypothesised way in which ATP and SA signalling pathways interact to

regulate plant defence (Chivasa *et al.,* 2009a) and plant viability (Chivasa *et al.,* 2005a). The molecular markers identified in this chapter will prove useful as a tool to probe the eATP signalling pathway, particularly in mutants with an altered cell death response.

4.2 Results

4.2.1 Selection of a timepoint for protein sample generation

In order to identify early eATP-regulated proteins by 2D-DiGE, a minimum duration of the ATP treatment of cell cultures was determined. Analysis of protein abundance changes provides a snapshot of the proteome at the time of protein collection and it is usually not feasible to perform the preliminary 2D-DiGE analysis on several timepoints before selecting the best one for full analysis. Protein abundance changes can occur as early as 10 minutes (Mega *et al.,* 2010) or as late as 7 days (Chivasa *et al.,* 2010) after treatment. For timepoint selection, a pilot study is usually performed, either looking at protein abundance changes of a few proteins, such as a marker proteins, or at the progression of a metabolic variable during a timecourse. In both cases the treatment timepoint is selected when a significant change in marker protein abundance or metabolic variable is detected. In this study it was necessary to identify a suitable timepoint after ATP treatment for harvesting of the cultures and analysis of protein samples. In order to identify eATP-induced protein abundance changes, it is best to analyse the earliest reasonable timepoint, where changes in the proteome are resulting from eATP-induced effects. Since eATP is gradually degraded by extracellular enzymes, later timepoints would gradually start to identify proteomic changes induced by eATP breakdown products, especially inorganic phosphate that would complicate the interpretation of the results.

It was initially purpose to generate an ATP addition timecourse in order to select the earliest timepoint where eATP-induced protein abundance changes in the TSP fraction are visible on a 1D SDS-PAGE gel and use this timepoint for subsequent 2D-DiGE sample generation. Culture samples were taken every two hours after ATP treatment in both control and ATP-treated cultures and resolved on 1D gels (Figure 4.1). 1D gels stained with Coomassie brilliant blue did not show significant changes between control and ATP treated cultures. This could be due to the weak resolving power of 1D gels for a complex sample such as TSP, where changes in low abundant proteins could be masked by high

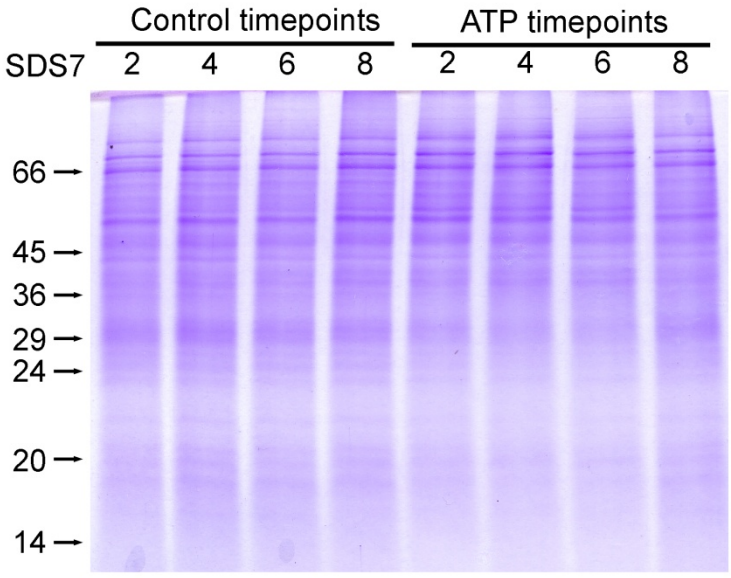

Figure 4.1 ATP treatment timecourse of TSP protein samples resolved by 1D SDS-PAGE. Numbers indicate the time in hours of culture harvesting after treatment. No changes are visible on a 1D gel. SDS7 MW values (KDa) are indicated on the left.

abundance proteins if their bands overlap. This can be overcome by the higher resolving power of 2D gels.

Instead of performing 2D analysis on all the samples generated in order to determine the earliest timepoint where protein abundance changes are visible, a preliminary experiment using the MTT assay was performed in order to identify a timepoint where early protein abundance changes induced by ATP could be occurring. The MTT assay measures mitochondrial activity in a cell culture. Changes between control and treated cultures measured by MTT indicate changes in mitochondrial activity and this is likely to be the result of protein abundance changes. Such potential changes can then be analysed by 2D gel analysis. Cell cultures adjusted to 5% (w/v) were treated with 1 mM ATP and controls were treated with an equal volume of water. MTT assay was performed on control and ATP-treated cultures every 2 hours for 12 hours (Figure 4.2). ATP addition did not produce a significant effect in mitochondrial activity in the first 6 hours. However, after 8 hours the control significantly increased in MTT signal (absorbance at 470 nm) whereas the ATP treatment remained unchanged for up to 12 hours (Figure 4.2). This shows that mitochondrial activity was repressed with ATP treatment and might reflect metabolic changes in ATP treated cells as they respond to increased eATP signalling. These results show that after 8 hours changes in metabolism have occurred in the ATP-treated cultures.

It was now necessary to show that 8 hours after ATP treatment early changes in protein abundance had actually taken place. The TSP protein sample was selected for analysis as it is the most complex protein sample from cell cultures. The TSP samples for the 8 hour timepoint were resolved using mini 2D SDS-PAGE of pI range 4-7. After careful observation of the Coomassie stained 2D gels, it was evident that ATP-treatment resulted in visible protein abundance changes (Figure 4.3). These results confirm that after 8 hours eATP-induced protein abundance changes have already occurred. Therefore, it was decided to use this timepoint for eATP-induced quantitative analysis of protein abundance changes in a full 2D-DiGE experiment.

4.2.2 Analysis of differential protein abundance changes using 2D-DiGE

For increased statistical significance of the results, a 2D-DiGE experiment consisting of 4 independent biological replicates was performed. A mother culture was initially grown for

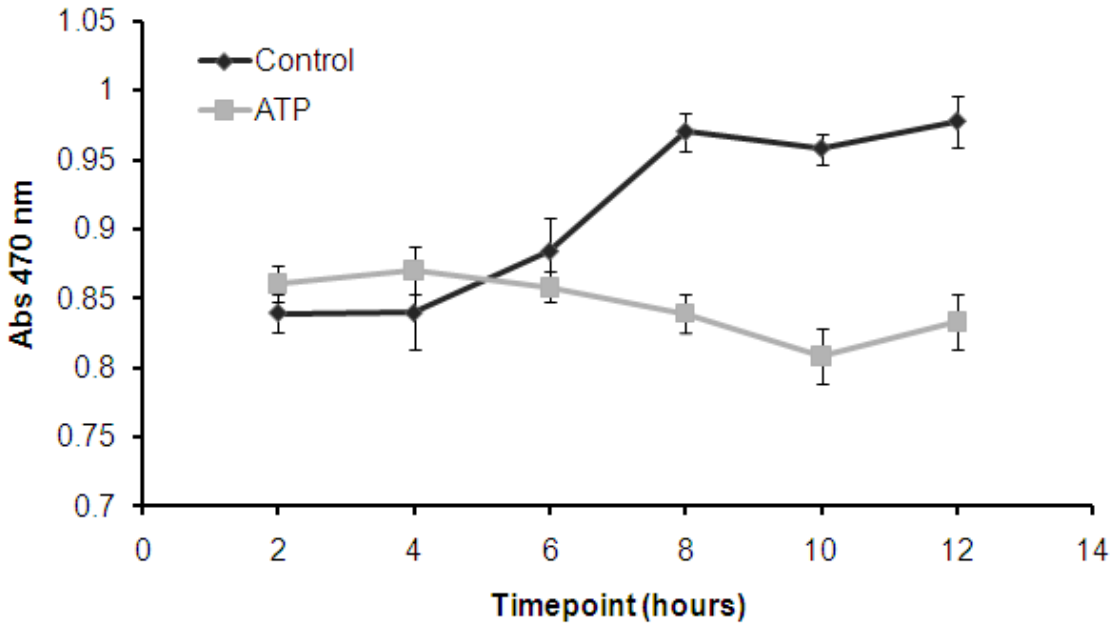

Figure 4.2 Quantification of ATP effects on cell culture mitochondrial activity using the MTT assay. Change in mitochondrial activity was measured every 2 hours in the first 12 hours post treatment. The increase in absorbance at 470 nm wavelength is a direct measurement of mitochondrial activity and can be considered a measurement of viability. An asterisk denotes a significant ($p \leq 0.01$) change between control and ATP treatment. Values and error bars represent means ± SE ($n = 9$).

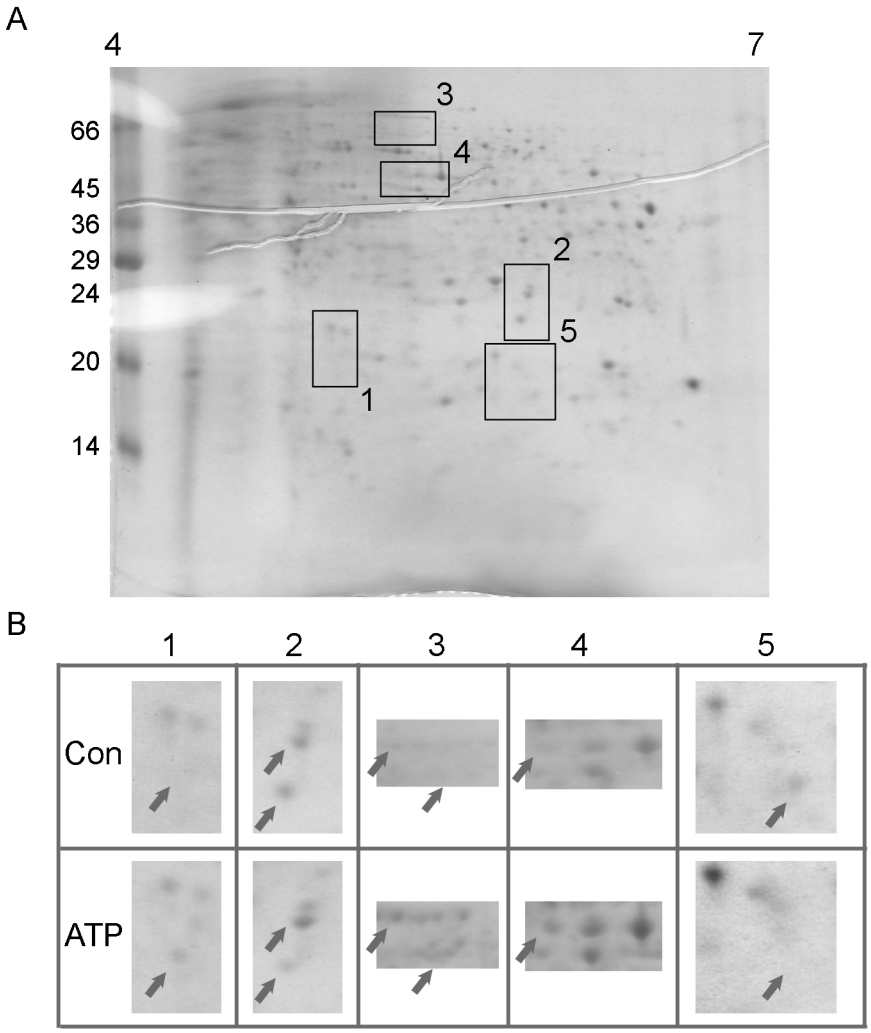

Figure 4.3 An 8 hour ATP treatment induces visible protein abundance changes in the TSP fraction on a mini 2D gel. (A) A typical 7 cm mini-2DE gel profile of TSP protein sample stained with Coomassie. SDS7 MW values (KDa) are indicated on the left. (B) Protein samples from control (Con) and 1 mM ATP-treated (ATP) cultures were resolved as in (A). Numbers indicate the box regions in (A) where spot abundance changes were visually observed between ATP-treated and control gels. Arrows indicate specific spots that show differential protein abundance in these boxes. Some protein spots were upregulated [numbers 1, 2 (upper arrow), 3 and 4] or downregulated [numbers 2 (lower arrow) and 5] in the ATP treated sample.

3 days before subculturing into 8 new flasks. These "sister" cultures were then used to generate the 4 independent biological replicates for the control and ATP treatment. TSP protein fractions were prepared from *Arabidopsis* cell cultures exposed to 1 mM ATP or equal volume of water for 8 hours. After mechanical disruption of cell cultures using the French press, the TSP fraction was separated from the microsomal fraction by ultra centrifugation and precipitated in 80% acetone as described in the material and methods. Protein processing, quantification, labelling with CyDyes in a full dye swap experiment and protein quality checks were performed in the same way as in chapter 3. First dimension focusing was performed on pI 4-7 24cm IPG strips and large-format 2DE in custom made gradient gels similarly to chapter 3. The 4 independent replicates were focused in a total of 8 IPG strips, each loaded with a Cy2 internal standard and a Cy3-control and Cy5-ATP and vice-versa. Second dimension electrophoresis was performed on all 8 large format 2D gels in the same run. During gel scanning, spot saturation that could jeopardize downstream DiGE analysis was avoided in the same way as chapter 3. Spot resolution was excellent across all replicate samples. The gradient gels used allowed the resolution of low molecular weight proteins spots just above the bromophenol blue dye front.

DeCyder software package was used for analysis of differential protein abundance changes in the same way as in chapter 3. All gel images of control samples and ATP-treated samples were grouped in distinct groups before statistical analysis of protein abundance changes was performed. In a preliminary analysis, gel features displaying a fold change greater than ± 1.2 (twice the minimal sensitivity of DeCyder) with a 95% statistical confidence level ($p \leq 0.05$) using an independent 2-tailed Student's *t*-test were designated as differentially expressed with ATP. This resulted in a staggering 1909 features out of a total of 4089 significantly changing (Table 4.1). Such a high percentage of changes provided preliminary evidence that ATP treatment was causing massive changes in the proteome within 8 hours. In order to simplify the analysis, it was decided to increase the minimum statistical significance value and minimum fold change until a smaller list encompassing only gel features displaying the biggest and most confident protein abundance changes was obtained. Eventually, a total of 184 features displayed a fold change greater than ± 2 and a 99% statistical confidence ($p \leq 0.01$) following ATP treatment (Table 4.1) and this was considered a reasonable number. In order for a gel feature to be considered a real spot, it has to have a roughly round shape and not be an

	Significance threshold	
Fold change	$p \leq 0.05$	$p \leq 0.01$
1.2	1909	1461
2	341	184

Table 4.1 Summary table showing the number of spots significantly changing with ATP using different significance thresholds and minimum fold changes. Total number of features detected by DeCyder was 4089.

obvious gel artefact, such as a speckle that can result from dust particles in the gel cassette during scanning. Therefore, all 184 features were manually checked and 107 were confirmed as real spots in the master gel. Of these 107, the automatic matching between replicates was manually checked in order confirm that the correct spot was being considered for analysis, ensuring accurate protein statistics. If spots were mismatched between gels, the correct spot boundary was copied to the mismatched gel image from the master gel image if possible. A total of 65 protein spots were upregulated with ATP and 42 were downregulated with ATP (Figure 4.4). Complete expression data of all the 107 spots, including those not identified, is presented in Table 1C in Appendix A.

4.2.3 Protein identification results

2D-DiGE analytical gels contain too little protein load (37,5 µg of total protein) to be used for identification of spots of interest. Because of this, preparative pick gels loaded with much higher protein loads (500 µg of total protein) were specifically generated for protein identification purposes using unlabelled protein samples. These gels were stained with SYPRO ruby stain for protein visualization, as it has been shown that this fluorescence stain results in comparable profiles with CyDye stains (Rowland 2006). Matching between the master gel and SYPRO-stained preparative gels was easily achieved using DeCyder. A total of 64 out of the 107 spots were selected for picking (Figure 4.5). The remaining 43 spots either could not be confidently visualized in the preparative gels or were clearly very low abundance spots. The higher protein load in preparative gels can result in two closely spaced spots merging into one spot. When this was the case, the spot could not be selected for identification due to the high possibility of incorrect protein identification result. Spots were picked from preparative gels either manually or by robotic excision and were submitted for protein identification, initially by MALDI-ToF using a Voyager DE-STR and later by a combination of MALDI-ToF and MS/MS using a 4800 MALDI-ToF-ToF Proteomic Analyser, purchased by the Slabas group during the course of this study. The MOWSE score threshold for a confident ID was 71 when searching in the *Viridiplantae* group. Searching was restricted to this group because the protein samples originated from *Arabidopsis* cell cultures, a fully sequenced model plant organism (AGSC 2000). Of the 64 spots selected for picking, 55 were confidently identified with 2 of these being a mixture and 9 spots returned with no confident identification result (Table 4.2).

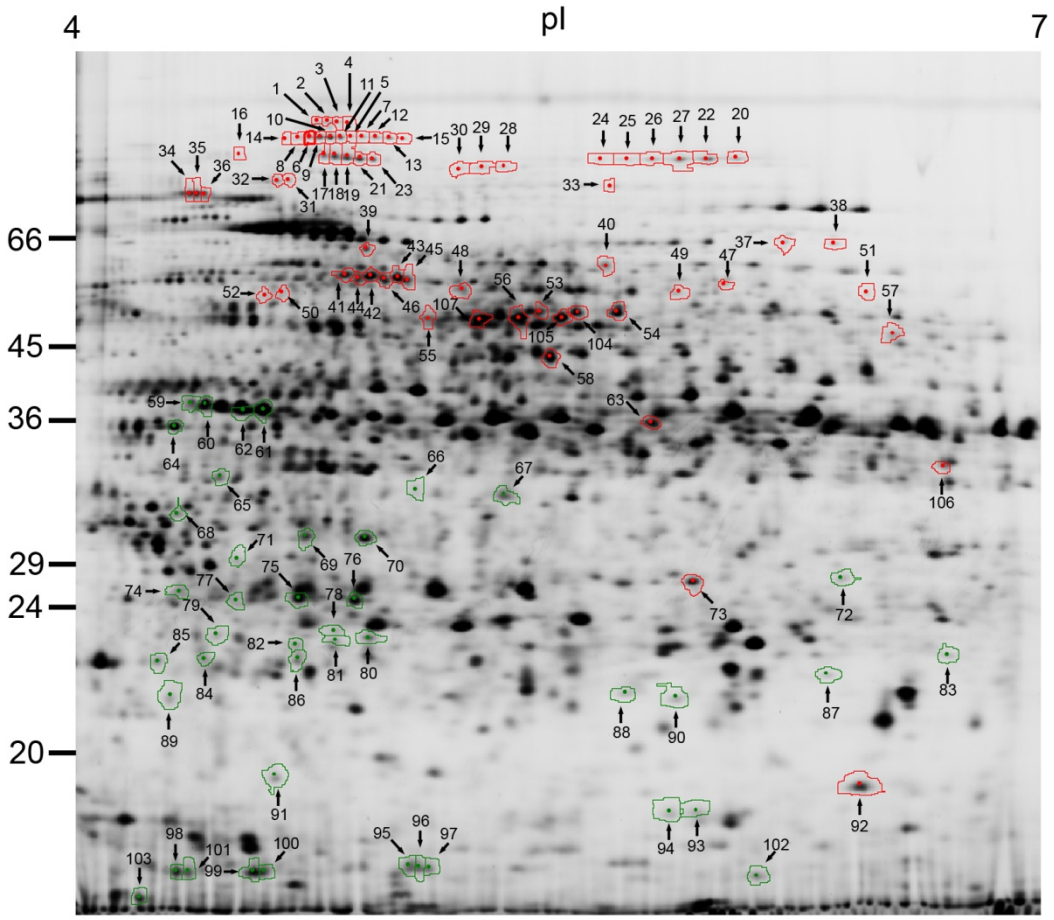

Figure 4.4 Protein spots of interest differentially regulated by ATP. 2D DiGE master gel image showing the position of protein spots identified by DeCyder analysis as significantly (p<0.01) changing to ATP treatment by a minimum of 2 fold change to the control (n = 8). Red boundaries indicate protein spots upregulated by ATP (65 spots) and green boundaries indicate protein spots downregulated by ATP (42 spots).

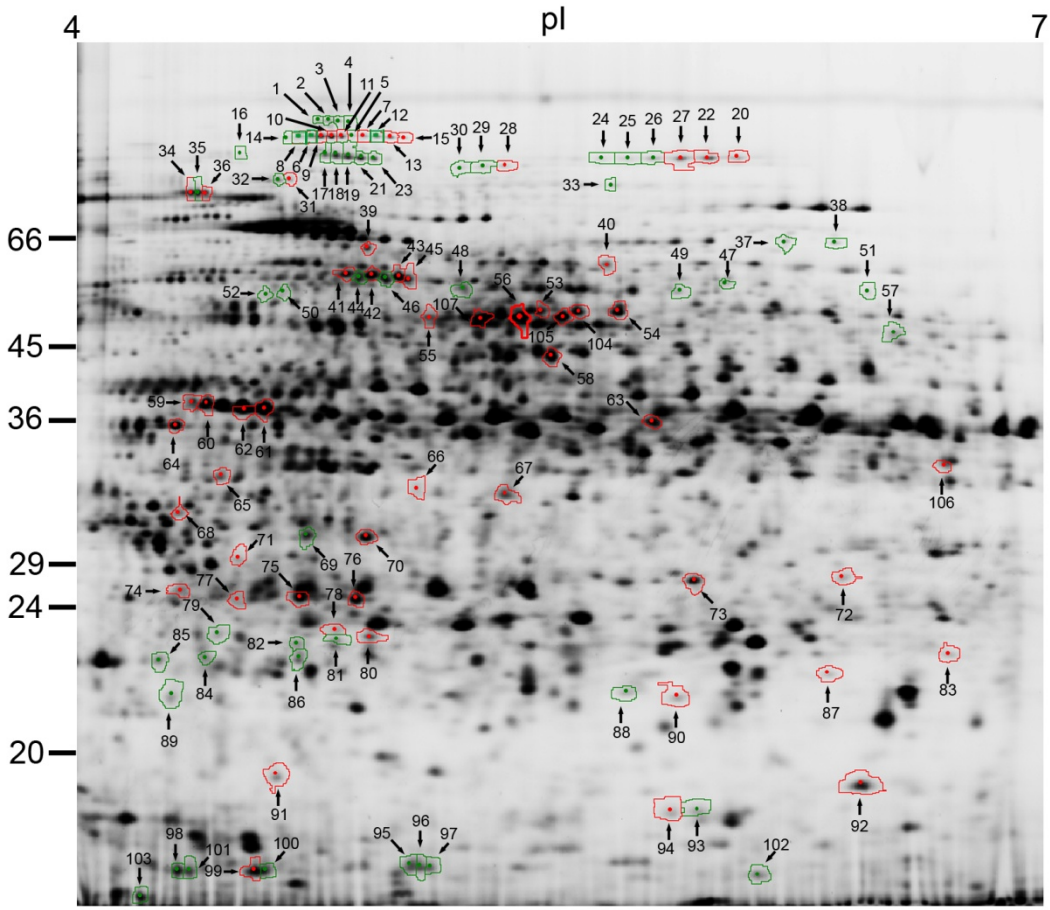

Figure 4.5 Protein spots successfully identified using MALDI-ToF or MS/MS. 2D DiGE master gel image showing the position of protein spots that were identified (red boundary, 55 spots) and protein spots for which no ID was obtained (green boundary, 52 spots) out of a total of 107 spots. Spot identification rate for successfully pick spots was 82%.

Table 4.2 Identified proteins differentially regulated with ATP treatment. Of the 64 spots selected for identification, 55 returned a positive ID, 2 of which were identified as a mixture, and 9 returned no confident ID. Ratio represents fold change of ATP treatment relative to the control. A (–) sign in the ratio column denotes an ATP-induced downregulation of the spot. [a]Arabidopsis Genome Initiative (AGI) gene identifier. [b]MOWSE, for a significant ($p \leq 0.05$) positive protein identification, cut-off threshold was 71. [c]Number of peptides matched to the protein sequence. [d]Ratio represents fold-change of ATP relative to the control treatment.

Gel spot no.	Master number	Gene locus[a]	Annotation	MOWSE score[b]	sequence coverage (%)	peptides[c]	Fold change[d]	*p*-value
71	2577	At1g11840&At2g36530	Mixture: LOS2 ; AtGLX1 (Glyoxylase 1 Homolog)	N.A.	N.A.	N.A.	-2.06	1.00E-06
68	2362	At1g35160	GF14 protein phi chain member of 14-3-3 protein family	133	42	14	-2.37	1.20E-05
20	576	At1g56070	encodes a translation elongation factor 2-like protein	270	36	35	2.32	0.00071
22	582	At1g56070		305	37	39	2.58	0.0003
27	590	At1g56070		329	36	37	2.6	0.00026
63	1933	At1g60730	aldo/keto reductase family protein	94	16	7	2.52	3.60E-05
28	624	At1g63770	peptidase M1 family protein	74	11	15	3.25	3.40E-05
74	2703	At1g64520	regulatory particle non-ATPase 12a (RPN12a)	116	51	15	-2.09	7.50E-07
39	1030	At1g78900	Encodes catalytic subunit A of the vacuolar AtP synthase	227	36	26	2.23	0.00046
9	511	At1g79920	putative heat-shock protein, ATP binding	278	30	33	4.04	2.00E-05
10	512	At1g79920		195	25	30	3.81	4.20E-05
11	513	At1g79920		286	29	31	3.47	8.60E-05
7	505	At1g79930	encodes high molecular weight heat shock protein 70	92	18	19	3.21	3.00E-05
13	517	At1g79930		199	28	32	3.48	2.30E-05
15	524	At1g79930		163	21	23	2.88	5.80E-06
31	681	At1g79930		157	24	29	2.2	0.0017
34	741	At2g04030	Encodes a chloroplast-targeted 90-kDa heat shock protein	338	42	37	2.54	0.00011
36	743	At2g04030		219	33	27	2.26	0.00032
60	1842	At2g04030		248	26	23	-2.22	4.10E-05
75	2736	At2g21170	Encodes a plastidic triose phosphate isomerase	467	44	15	-2.18	5.10E-07

Gel spot no.	Master number	Gene locus[a]	Annotation	MOWSE score[b]	sequence coverage (%)	peptides[c]	Fold change[d]	*p*-value
76	2747	At2g21170		190	36	12	-2.89	2.10E-06
45	1182	At2g33210	heat shock protein 60-2	102	26	18	2.27	0.0007
56	1384	At2g36530	Involved in light-dependent cold tolerance and encodes an enolase	572	62	31	2.22	9.40E-05
105	4008	At2g36530	enolase 2	523	58	29	2.06	0.00077
107	4062	At2g36530		360	57	25	2.08	1.50E-06
106	4040	At2g37760	aldo/keto reductase family protein	382	48	24	2.52	9.60E-06
99	3757	At3g04120	encodes cytosolic GAPDH (C subunit)	330	25	11	-2.65	5.90E-07
70	2468	At3g17820	encodes a cytosolic glutamine synthetase	212	22	15	-2.45	8.80E-07
41	1161	At3g23990	mitochondrial chaperonin HSP	313	40	29	2.26	3.90E-05
42	1163	At3g23990		372	44	33	2.36	3.10E-05
43	1166	At3g23990		364	37	31	2.13	0.00029
73	2672	At3g29200	L-ascorbate peroxidase	88	42	11	2.48	5.90E-06
67	2275	At3g52930	putative fructose-bisphosphate aldolase	146	57	14	-2.08	8.70E-05
77	2759	At3g52930&At5g20830	Mixture: fructose-bisphosphate aldolase; sucrose synthase	N.A.	N.A.	N.A.	-2.18	5.50E-06
78	2888	At3g56090	ferritin 3 AtFER3	123	52	17	-2.29	4.70E-05
91	3360	At3g60750	putative transketolase	343	12	13	-2.36	3.90E-06
92	3387	At4g09320	nucleoside diphosphate kinase type 1	233	55	15	2.25	6.60E-05
94	3486	At4g09320		102	43	8	-2.66	6.80E-05
54	1355	At4g13940	S-adenosyl-L-homocysteine hydrolase	125	46	21	2.68	1.20E-06
104	4006	At4g13940	Encodes a S-adenosyl-L-homocysteine hydrolase	229	29	23	2.65	2.20E-07
53	1347	At4g26900	encodes a glutamine amidotransferase and cyclase	147	35	26	2.53	2.90E-06
40	1114	At4g33070	pyruvate decarboxylase, putative	138	17	19	2.02	8.80E-08
65	2200	At5g03630	monodehydroascorbate reductase	116	45	18	-2.14	1.60E-06
55	1383	At5g08690	Encodes the mitochondrial ATP synthase beta-subunit	389	55	33	2.08	8.10E-06
72	2658	At5g15650	Reversibly glycosylated Polypeptide-2	123	26	10	-3.35	2.30E-05
87	3063	At5g19550	aspartate aminotransferase 2	142	20	13	-2.01	4.40E-05
90	3151	At5g19770	tubulin 3	73	12	6	-2.24	0.00021
58	1605	At5g20070	NUDIX HYDROLASE HOMOLOG 19	167	26	16	2.18	0.00027

Gel spot no.	Master number	Gene locus[a]	Annotation	MOWSE score[b]	sequence coverage (%)	peptides[c]	Fold change[d]	*p*-value
80	2921	At5g20720	Encodes a chloroplast co-chaperonin	141	37	13	-2.05	7.00E-06
83	2989	At5g20830	sucrose synthase (SUS1)	388	11	8	-2.06	8.40E-05
66	2253	At5g35360	acetyl-CoA carboxylase	179	23	16	-2.14	1.80E-05
59	1829	At5g52640	Encodes a cytosolic heat shock protein AtHSP90.1	212	20	23	-2.03	0.00012
64	1944	At5g52640		123	27	19	-2.48	6.60E-09
61	1860	At5g56010	A member of heat shock protein 90 gene family	688	42	35	-2.04	1.50E-08
62	1868	At5g56010		556	38	31	-2.07	4.90E-06
23	584		No significant hit				2.15	0.0012
29	634		No significant hit				2.97	2.30E-05
30	638		No significant hit				2.7	0.00019
32	687		No significant hit				2.02	1.10E-03
33	718		No significant hit				2.16	0.00025
46	1189		No significant hit				2.36	0.00012
79	2904		No significant hit				-2.31	1.00E-07
93	3479		No significant hit				-2.44	3.10E-06
98	3756		No significant hit				-2.37	7.40E-05

This corresponds to an overall identification success rate of 82%. The total number of identified protein spots, excluding the 2 mixtures, represented 35 unique proteins. Such redundancy revealed by the lower number of unique proteins compared to spots changing in abundance is explained by the existence of post-translationally modified (PTM) forms of the same protein. There are over 400 different characterized PTM's (Pennington *et al.,* 2001). PTM's can alter proteins in a variety of ways including regulating enzymatic activity, sub cellular localization and protein stability. They can alter the mass of the protein (Mann and Jensen 2003) and isoelectric point resulting in protein trains of the same proteins on a 2D gel, with spots displaying the same molecular mass but different isoelectric points. These changes in spot attributes were observed in this dataset.

Spots 7, 13 and 15 form a spot train (Figure 4.5) all returned the same protein identification result: a high molecular weight heat shock protein 70 (Table 4.2). This was also observed for spots 34 and 36, indicating that spot 35 would probably have returned the same identification result had it been successfully identified. The high molecular weight spot trains were upregulated by ATP treatment (Figure 4.4), suggesting ATP is altering protein abundance of the unmodified protein. A chloroplast-targeted 90 KDa heat shock protein was identified as 3 distinct spots (Table 4.2). It was identified in spots 34 and 36 that were upregulated with ATP and in spot 60 that was downregulated with ATP (Figure 4.4). Interestingly, spot 60 shows a lower MW (~39KDa) compared to the other two spots (>66KDa). This could reflect a proteolytic cleavage event of the mature protein, possibly suggesting ATP has a protective effect on protein degradation of this particular protein.

Six of the proteins identified here (AT3G04120, AT3G52930, AT1G63770, AT1G78900, AT3G17820 and AT5G19770) have previously been reported as differentially regulated with eATP depletion (Chivasa *et al.,* 2005a). For two of these proteins (AT3G04120 and AT3G52930), their abundance levels inversely correlated with eATP availability, since they were upregulated with eATP depletion in the 2005 study and downregulated following 1 mM ATP treatment in this study, confirming the specificity of the 8 hour ATP treatment for identifying eATP-regulated proteins. The remaining four proteins (AT1G63770, AT1G78900, AT3G17820 and AT5G19770) however, were responding in the same direction in both studies. The reasons for this observation are not clear, but could reflect differences between the two experimental approaches such as in the protein extraction protocol, where 10% (w/v) trichloroacetic acid was used during protein extraction, or in the controls employed, where glucose was used instead of water (Chivasa

et al., 2005a). Indeed glucose is well known to regulate gene expression (Moore *et al.,* 2003; Rolland *et al.,* 2006) which could explain the discrepancies observed.

4.2.4 Bioinformatics analysis of differentially expressed proteins

Having identified 35 eATP-regulated proteins, it was now necessary to interpret the data in light of the multiple functions these genes are reported to be involved in and how eATP signalling modulates their abundance *in vivo*. The interpretation of even relatively small datasets produced by proteomic studies can be a daunting task due to the very large amount of information available for each gene in the literature and on online databases. The interpretation of these datasets is challenging if done manually on a gene-by-gene basis, where non-trivial connections between the genes, or between subsets of genes, can be easily overlooked by the user. A comprehensive analysis requires the use of all available information about all the genes in an organized form and this is when the aid of bioinformatic tools is paramount. For this study, two bioinformatic tools were used to better comprehend the global effects of ATP treatment in plant cell physiology based on the 35 genes identified (Table 4.2). These were the literature mining tool Pubmatrix (Becker *et al.,* 2003) and the gene functional classification and annotation clustering tool Database for Annotation, Visualization and Integrated Discovery v6.7 [DAVID; http://david.abcc.ncifcrf.gov/ ; (Huang da *et al.,* 2007; Huang da *et al.,* 2009)]. The results obtained from these analyses will be of a purely predictive nature, as many of the annotations assigned to *Arabidopsis* genes are only supported by theoretical predictions based on primary gene and/or protein sequence instead of experimental evidence. However, the annotations of each gene are taken at face value as it is beyond the scope of this Ph.D. to verify them. Nonetheless, the conclusions obtained from this analysis are expected to provide clues on novel physiological roles of eATP signalling that can be pursued in future studies.

4.2.4.1 Pubmatrix analysis

As an initial analysis, I was interested in searching if the proteins reported in this study as differentially expressed with eATP had already been reported previously in the literature. The Pubmatrix tool searches the literature for pair-wise associations between two lists of text terms, such as a gene name and a biological function, in the abstracts of publications available in the National Centre for Biotechnology Information (NCBI) online literature

database. This enables fast detection of relevant papers and also gives a general view of how frequently documented the word associations are in the literature. A high number of associations reflect a well studied phenomenon, whereas no associations are indicative of a new association. Therefore, this tool provides a quick global overview about if any of the proteins identified as regulated by eATP have been previously established in plants or other organisms. To this end, the Pubmatrix web-based tool (http://pubmatrix.grc.nia.nih.gov/secure-bin/index.pl) was used for text mining the literature for reported connections between a list containing the descriptive names of the proteins identified in Table 4.2 and another list containing the modifier terms "extracellular ATP", "extracellular ATP plant" and "extracellular ATP Arabidopsis". The descriptive name of each gene was used instead of the AGI's so as to include research papers derived from model organisms other than *Arabidopsis*. The results of this analysis are reported in Table 4.3. It is clear that 11 of the proteins have previously been linked in some way with "extracellular ATP" in the literature. Some of them (eg. heat shock protein 90) have been connected in several publications. Manual checking of all the publications identified using Pubmatrix in Table 4.3 revealed that all of them were from animal, bacteria or fungi research and not a single publication was conducted on a plant species. This is further supported by the fact that no hit is obtained when using the terms "extracellular ATP Arabidopsis" or "extracellular ATP plant", as is evident by both columns with these terms showing only zeros (Table 4.3). Because Pubmatrix failed to identify any connections in the literature between the dataset and extracellular ATP in plants, this provides preliminary evidence supporting this study as the first to empirically show a connection between these proteins and eATP signalling in plants.

4.2.4.2 DAVID analysis

DAVID version 6.7 web-based tool provides a more powerful analysis platform since it systematically retrieves all functional annotations for each gene of sequenced model organisms, with the first version developed in 2000 (Ashburner *et al.,* 2000). The gene identifiers for all *Arabidopsis* predicted genes are provided by the TAIR database (www.arabidopsis.org). Associated with each gene identifier is an extensive collection of heterogeneous functional annotations in the DAVID knowledge base. These include Gene

	Modifier terms		
Gene description	**extracellular ATP**	**extracellular ATP plant**	**extracellular ATP *Arabidopsis***
heat shock protein 90	13	0	0
aldo/keto reductase	0	0	0
aspartate aminotransferase 2	0	0	0
chloroplast co-chaperonin	0	0	0
cytosolic glutamine synthetase	1	0	0
cytosolic heat shock protein	3	0	0
glutamine amidotransferase	0	0	0
plastidic triose phosphate isomerase	0	0	0
S-adenosyl-L-homocysteine hydrolase	1	0	0
translation elongation factor 2-like protein	0	0	0
catalytic subunit A of the vacuolar ATP synthase	1	0	0
cytosolic GAPDH	0	0	0
high molecular weight heat shock protein 70	0	0	0
mitochondrial ATP synthase beta-subunit	5	0	0
enolase 2	4	0	0
ferritin 3	0	0	0
GF14 protein	0	0	0
heat shock protein 60-2	1	0	0
heat shock protein AtHSP90.1	0	0	0
L-ascorbate peroxidase	0	0	0
mitochondrial chaperonin HSP	0	0	0
monodehydroascorbate reductase	0	0	0
nucleoside diphosphate kinase	31	0	0
nudix hydrolase homologue 19	0	0	0
peptidase M1	0	0	0
putative fructose-bisphosphate aldolase	0	0	0
putative heat-shock protein	1	0	0
putative transketolase	0	0	0
putative pyruvate decarboxylase	0	0	0
regulatory particle non-ATPase 12a	0	0	0
Reversibly glycosylated Polypeptide-2	0	0	0
S-adenosyl-L-homocysteine hydrolase	1	0	0
sucrose synthase	0	0	0
tubulin 3	0	0	0

Table 4.3 Pubmatrix analysis results for differentially expressed proteins identified. The 34x3 co-occurrence frequency matrix shows the number of co-occurrences between the gene description and modifier terms at the top of each column.

Ontology (GO), protein-protein interactions, literature connections, protein domains, metabolic pathways, sequence features and functional categories (Huang da *et al.,* 2007). Most of them were obtained by computational predictions based on primary gene and protein sequence, but also by direct experimental evidence. DAVID utilizes all the annotations for all the genes in the dataset and generates connections between them and localizes them to metabolic pathways (Huang da *et al.,* 2007). Besides listing the most represented annotations and their degree of overrepresentation in the dataset, DAVID also clusters genes that are functionally related based on several different annotations and quantifies the relative enrichment of each annotation in the dataset and associated statistical confidence. For example, a cluster could include genes that share a metabolic function in photosynthetic light reactions as well as being predicted to be localized to the chloroplast. The 35 unique proteins identified as being regulated by eATP signalling were analysed by functional annotation using the default settings detailed in the materials and methods chapter and the results are shown in Table 4.4. Several enrichment clusters were obtained but to simplify the analysis it was decided to consider only enrichment clusters with an enrichment value ≥ 2 as significantly enriched following ATP treatment. Six clusters were identified and these will be discussed individually below.

The most highly enriched cluster identified by DAVID showed a 15.5 fold enrichment and contained genes that are currently annotated as involved in the cells' response to inorganic substances, metal ions and specifically cadmium. This is a very broad stimulus range and could be related to the fact that the ATP used experiments is commercially available as a sodium salt and when administered to cultures could invoke a general response to inorganic substances. A total of 18 out of the 35 genes were annotated as responding to inorganic substances (Table 4.4). The response of these proteins to ATP did not follow a common differential regulation pattern. For example, of the 15 genes annotated as responding to cadmium (GO term identifier GO:0046686) in Table 4.4, 7 were upregulated and 8 were downregulated in response to ATP treatment (Table 4.2). This was a recurring scenario in all the clusters, suggesting that the cellular response to perturbations in eATP levels requires fine-tuning of the metabolic pathways affected.

Table 4.4 Functional annotation clustering of differentially expressed proteins using DAVID default settings and medium classification stringency (Huang et al, 2009). Cluster enrichment score represents the geometric mean of all the enrichment P-values for each annotation term associated with the gene members in the group. Only cluster with an enrichment value higher than 2 were considered significant. Category specifies which type of annotation is being used. Count is the total number of genes that share the same term and the % denotes the percentage of those genes in the list submitted. The *p*-value determines the significance of gene–term enrichment using a modified Fisher's exact test. Fold enrichment represents the degree of enrichment for that GO term in the sample relative to the whole genome.

Annotation Cluster 1	Enrichment Score: 15.58605804700606					
Category	Term	Count	%	*p*-Value	Genes	Fold Enrichment
GOTERM_BP_FAT	GO:0010035~response to inorganic substance	18	51.43	5.30E-17	AT3G52930, AT5G20830, AT2G04030, AT1G63770, AT3G60750, AT2G36530, AT1G79930, AT2G37760, AT4G09320, AT3G56090, AT3G23990, AT3G17820, AT5G52640, AT5G20720, AT5G15650, AT5G19770, AT5G03630, AT3G04120	15.0516129
GOTERM_BP_FAT	GO:0010038~response to metal ion	16	45.71	2.97E-16	AT3G52930, AT5G20830, AT1G63770, AT3G60750, AT2G36530, AT1G79930, AT2G37760, AT4G09320, AT3G56090, AT3G23990, AT3G17820, AT5G20720, AT5G15650, AT5G19770, AT5G03630, AT3G04120	18.8145161
GOTERM_BP_FAT	GO:0046686~response to cadmium ion	15	42.86	1.11E-15	AT3G52930, AT5G20830, AT1G63770, AT3G60750, AT2G36530, AT1G79930, AT2G37760, AT4G09320, AT3G23990, AT3G17820, AT5G20720, AT5G15650, AT5G19770, AT5G03630, AT3G04120	20.7132288

Annotation Cluster 2	Enrichment Score: 7.5353505371156615					
Category	Term	Count	%	*p*-Value	Genes	Fold Enrichment
GOTERM_BP_FAT	GO:0009628~response to abiotic stimulus	17	48.57	3.41E-10	AT5G56010, AT3G52930, AT5G20830, AT1G64520, AT1G78900, AT2G04030, AT3G60750, AT2G36530, AT1G79930, AT4G09320, AT3G23990, AT5G52640, AT5G20720, AT5G15650, AT1G56070, AT5G03630, AT3G04120	6.4129679

GOTERM_BP_FAT	GO:0006970~response to osmotic stress	10	28.57	9.55E-08	AT4G09320, AT3G52930, AT5G15650, AT5G20830, AT5G03630, AT1G78900, AT2G04030, AT3G04120, AT3G60750, AT2G36530	11.3170022
GOTERM_BP_FAT	GO:0009651~response to salt stress	9	25.71	7.61E-07	AT4G09320, AT3G52930, AT5G15650, AT5G03630, AT1G78900, AT2G04030, AT3G04120, AT3G60750, AT2G36530	11.0133753

Annotation Cluster 3 Enrichment Score: 5.448334801859085

Category	Term	Count	%	*p*-Value	Genes	Fold Enrichment
GOTERM_CC_FAT	GO:0031967~organelle envelope	14	40	1.55E-09	AT3G52930, AT2G21170, AT1G64520, AT2G04030, AT5G35360, AT1G78900, AT1G63770, AT3G60750, AT2G36530, AT3G56090, AT5G20720, AT5G08690, AT1G35160, AT3G04120	8.35271704
GOTERM_CC_FAT	GO:0031975~envelope	14	40	1.71E-09	AT3G52930, AT2G21170, AT1G64520, AT2G04030, AT5G35360, AT1G78900, AT1G63770, AT3G60750, AT2G36530, AT3G56090, AT5G20720, AT5G08690, AT1G35160, AT3G04120	8.28598428
GOTERM_CC_FAT	GO:0009941~chloroplast envelope	10	28.57	2.51E-07	AT3G56090, AT2G21170, AT5G20720, AT5G08690, AT1G64520, AT1G78900, AT2G04030, AT5G35360, AT1G63770, AT3G60750	10.1019062
GOTERM_CC_FAT	GO:0009526~plastid envelope	10	28.57	3.72E-07	AT3G56090, AT2G21170, AT5G20720, AT5G08690, AT1G64520, AT1G78900, AT2G04030, AT5G35360, AT1G63770, AT3G60750	9.64173256
GOTERM_CC_FAT	GO:0009507~chloroplast	20	57.14	2.98E-06	AT3G52930, AT2G21170, AT1G64520, AT1G78900, AT5G20070, AT2G04030, AT5G35360, AT1G63770, AT3G60750, AT2G36530, AT4G09320, AT3G56090, AT3G17820, AT5G20720, AT2G33210, AT5G08690, AT1G56070, AT4G26900, AT3G04120, AT3G29200	2.78498666
GOTERM_CC_FAT	GO:0009536~plastid	20	57.14	4.16E-06	AT3G52930, AT2G21170, AT1G64520, AT1G78900, AT5G20070, AT2G04030, AT5G35360, AT1G63770, AT3G60750, AT2G36530, AT4G09320, AT3G56090, AT3G17820, AT5G20720, AT2G33210, AT5G08690, AT1G56070, AT4G26900, AT3G04120, AT3G29200	2.72773164
GOTERM_CC_FAT	GO:0044434~chloroplast part	10	28.57	1.34E-04	AT3G56090, AT2G21170, AT5G20720, AT5G08690, AT1G64520, AT1G78900, AT2G04030, AT5G35360, AT1G63770, AT3G60750	4.65916007
GOTERM_CC_FAT	GO:0044435~plastid part	10	28.57	1.69E-04	AT3G56090, AT2G21170, AT5G20720, AT5G08690, AT1G64520, AT1G78900, AT2G04030, AT5G35360, AT1G63770, AT3G60750	4.51711251

GOTERM_CC_FAT	GO:0009570~chloroplast stroma	6	17.14	0.0019508	AT2G21170, AT5G20720, AT2G04030, AT5G35360, AT1G63770, AT3G60750	6.34976959
GOTERM_CC_FAT	GO:0009532~plastid stroma	6	17.14	0.0024381	AT2G21170, AT5G20720, AT2G04030, AT5G35360, AT1G63770, AT3G60750	6.03371771

Annotation Cluster 4 Enrichment Score: 4.557442451551364

Category	Term	Count	%	*p*-Value	Genes	Fold Enrichment
GOTERM_BP_FAT	GO:0009266~response to temperature stimulus	11	31.43	1.81E-09	AT5G56010, AT3G23990, AT5G52640, AT5G20720, AT5G20830, AT1G56070, AT1G64520, AT2G04030, AT3G04120, AT1G79930, AT2G36530	14.0311646
GOTERM_BP_FAT	GO:0009408~response to heat	7	20	2.46E-07	AT5G56010, AT3G23990, AT5G52640, AT1G64520, AT2G04030, AT3G04120, AT1G79930	24.8884938
SP_PIR_KEYWORDS	stress response	6	17.14	2.89E-06	AT5G56010, AT3G23990, AT5G52640, AT2G33210, AT2G04030, AT1G79930	25.8487013
GOTERM_BP_FAT	GO:0006457~protein folding	7	20	1.30E-05	AT5G56010, AT3G23990, AT5G52640, AT5G20720, AT2G33210, AT2G04030, AT1G79930	12.5929829
SP_PIR_KEYWORDS	Chaperone	5	14.29	2.64E-05	AT5G56010, AT3G23990, AT5G52640, AT5G20720, AT2G33210	28.0825397
INTERPRO	IPR019805:Heat shock protein Hsp90, conserved site	3	8.571	5.37E-05	AT5G56010, AT5G52640, AT2G04030	255.734694
INTERPRO	IPR001404:Heat shock protein Hsp90	3	8.571	5.37E-05	AT5G56010, AT5G52640, AT2G04030	255.734694
PIR_SUPERFAMILY	PIRSF002583:heat shock protein, HSP90/HTPG types	3	8.571	1.22E-04	AT5G56010, AT5G52640, AT2G04030	164.538462
PIR_SUPERFAMILY	PIRSF002583:Hsp90	3	8.571	1.71E-04	AT5G56010, AT5G52640, AT2G04030	141.032967
SMART	SM00387:HATPase_c	3	8.571	2.11E-04	AT5G56010, AT5G52640, AT2G04030	106.819444
INTERPRO	IPR003594:ATP-binding region, ATPase-like	3	8.571	0.0015654	AT5G56010, AT5G52640, AT2G04030	49.7261905
GOTERM_MF_FAT	GO:0051082~unfolded protein binding	3	8.571	0.023467	AT5G56010, AT5G52640, AT2G04030	12.2363636

Annotation Cluster 5	Enrichment Score: 3.3598179532600376					
Category	Term	Count	%	*p*-Value	Genes	Fold Enrichment
GOTERM_BP_FAT	GO:0006457~protein folding	7	20	1.30E-05	AT5G56010, AT3G23990, AT5G52640, AT5G20720, AT2G33210, AT2G04030, AT1G79930	12.5929829
SP_PIR_KEYWORDS	nucleotide-binding	12	34.29	1.79E-05	AT5G56010, AT4G09320, AT3G23990, AT3G17820, AT5G52640, AT2G33210, AT5G08690, AT1G56070, AT5G19770, AT1G78900, AT1G79920, AT1G79930	4.70219269
SP_PIR_KEYWORDS	atp-binding	10	28.57	2.31E-04	AT5G56010, AT4G09320, AT3G23990, AT3G17820, AT5G52640, AT2G33210, AT5G08690, AT1G78900, AT1G79920, AT1G79930	4.41858142
GOTERM_MF_FAT	GO:0017076~purine nucleotide binding	16	45.71	2.76E-04	AT5G56010, AT1G78900, AT2G04030, AT5G35360, AT1G79920, AT1G79930, AT4G09320, AT3G23990, AT3G17820, AT5G52640, AT5G20720, AT2G33210, AT5G08690, AT1G56070, AT5G19770, AT5G03630	2.57761819
GOTERM_MF_FAT	GO:0032553~ribonucleotide binding	15	42.86	5.50E-04	AT5G56010, AT1G78900, AT2G04030, AT5G35360, AT1G79920, AT1G79930, AT4G09320, AT3G23990, AT3G17820, AT5G52640, AT5G20720, AT2G33210, AT5G08690, AT5G19770, AT1G56070	2.56772224
GOTERM_MF_FAT	GO:0032555~purine ribonucleotide binding	15	42.86	5.50E-04	AT5G56010, AT1G78900, AT2G04030, AT5G35360, AT1G79920, AT1G79930, AT4G09320, AT3G23990, AT3G17820, AT5G52640, AT5G20720, AT2G33210, AT5G08690, AT5G19770, AT1G56070	2.56772224
GOTERM_MF_FAT	GO:0000166~nucleotide binding	17	48.57	5.91E-04	AT5G56010, AT1G78900, AT2G04030, AT5G35360, AT1G79920, AT1G79930, AT4G09320, AT3G23990, AT3G17820, AT5G52640, AT5G20720, AT2G33210, AT5G08690, AT1G56070, AT5G19770, AT5G03630, AT3G04120	2.28842884
GOTERM_MF_FAT	GO:0001883~purine nucleoside binding	14	40	0.0014016	AT5G56010, AT1G78900, AT2G04030, AT5G35360, AT1G79920, AT1G79930, AT4G09320, AT3G23990, AT3G17820, AT5G20720, AT5G52640, AT2G33210, AT5G08690, AT5G03630	2.48470464
GOTERM_MF_FAT	GO:0030554~adenyl nucleotide binding	14	40	0.0014016	AT5G56010, AT1G78900, AT2G04030, AT5G35360, AT1G79920, AT1G79930, AT4G09320, AT3G23990, AT3G17820, AT5G20720, AT5G52640, AT2G33210, AT5G08690, AT5G03630	2.48470464
GOTERM_MF_FAT	GO:0001882~nucleoside binding	14	40	0.0014444	AT5G56010, AT1G78900, AT2G04030, AT5G35360, AT1G79920, AT1G79930, AT4G09320, AT3G23990, AT3G17820, AT5G20720, AT5G52640, AT2G33210, AT5G08690, AT5G03630	2.47686646

GOTERM_MF_FAT	GO:0005524~ATP binding	13	37.14	0.0024027	AT5G56010, AT2G04030, AT5G35360, AT1G78900, AT1G79920, AT1G79930, AT4G09320, AT3G23990, AT3G17820, AT5G20720, AT5G52640, AT2G33210, AT5G08690	2.49259259
GOTERM_MF_FAT	GO:0032559~adenyl ribonucleotide binding	13	37.14	0.0026641	AT5G56010, AT2G04030, AT5G35360, AT1G78900, AT1G79920, AT1G79930, AT4G09320, AT3G23990, AT3G17820, AT5G20720, AT5G52640, AT2G33210, AT5G08690	2.46311937

Annotation Cluster 6 Enrichment Score: 2.895732102257125

Category	Term	Count	%	*p*-Value	Genes	Fold Enrichment
SP_PIR_KEYWORDS	transit peptide	9	25.71	2.56E-05	AT3G56090, AT3G23990, AT2G21170, AT5G20720, AT2G33210, AT5G08690, AT4G26900, AT5G20070, AT3G29200	6.97756354
SP_PIR_KEYWORDS	plastid	6	17.14	0.0025819	AT3G56090, AT2G21170, AT5G20720, AT4G26900, AT5G20070, AT3G29200	6.02565752
SP_PIR_KEYWORDS	chloroplast	6	17.14	0.0029713	AT3G56090, AT2G21170, AT5G20720, AT4G26900, AT5G20070, AT3G29200	5.83252747
UP_SEQ_FEATURE	transit peptide:Chloroplast	6	17.14	0.0133212	AT3G56090, AT2G21170, AT5G20720, AT4G26900, AT5G20070, AT3G29200	3.8833042

Cluster 2 grouped proteins that are involved in abiotic stress responses, such as AT1G79930 heat shock protein 70. Proteins in this group were largely the same as in cluster 1. Of the 18 genes in the largest category in cluster 1 (responsive to inorganic substance) and the 17 genes in the biggest category in cluster 2 (response to abiotic stimulus), a total of 13 genes were common in both categories. This shows that these two GO annotations are related to each other as they are usually co-occurring in the same gene. In this cluster, again no common response to ATP treatment was detected. For example, of the 9 annotated as responding to salt stress, 5 were upregulated and 4 were downregulated in response to ATP.

Perhaps the most interesting cluster is cluster 3, which groups proteins belonging to the chloroplast, chloroplast membrane (envelope) and chloroplast stroma (Table 4.4). The redundancy in GO terms is also evident in this cluster. Plastid and chloroplast are interchangeable as they have exactly the same genes in each category. The same holds true for organelle envelope and envelop. 40% of the 35 unique proteins identified were annotated as belonging to the chloroplast envelope, suggesting major plant-specific eATP-induced protein abundance changes in this organelle. Additionally, an elongation factor 2-like protein (AT1G56070) and a chloroplast-targeted 90 KDa heat shock protein (AT2G04030) were found to be significantly upregulated with ATP (Table 4.2). The upregulation of these proteins suggest a general increase in protein translation and an increase in chloroplast-targeted proteins that could be folded into their correct 3D structure in the chloroplast by the chloroplast-targeted molecular chaperone. These findings show that major changes happen in the chloroplast upon perturbations in eATP level. A previous study in tobacco provided evidence of eATP signalling in regulating the abundance of chloroplastic photosynthetic proteins (Chivasa *et al.,* 2010). In that study, the blocking of eATP signalling by AMP-PCP treatment resulted in significant downregulation of all photosynthetic proteins identified 7 days after treatment, whereas ATP treatment did not result in significant changes in these proteins' abundance. This indicated that photosynthetic proteins were regulated by the abolishment of eATP cleavage-mediated signalling. Now, data from this study shows that an increase in eATP concentrations in its own right can induced changes in protein abundance of chloroplastic proteins, although none of the identified proteins were involved in photosynthetic light reactions as in the tobacco study (Chivasa *et al.,* 2010).

Cluster 4 showed the highest enrichment value of any GO category in the dataset. A 255 fold enrichment for the INTERPRO domains IPR019805 and IPR001404 specific for Heat Shock Protein Hsp90 was identified. This was due to the identification of three proteins AT5G56010, AT5G52640 and AT2G04030 (Table 4.4). These proteins belong to the heat shock protein 90 (Hsp90) gene family, a ubiquitous family of proteins found in all eukaryotes. In *Arabidopsis*, this family has 7 predicted members (Krishna and Gloor 2001), with 3 of them detected in this study, accounting for the very high enrichment value obtained. Aside from their classical function as molecular chaperones in assisting proper protein folding, they also plays a role in concealing phenotypic variation under normal conditions (Queitsch *et al.,* 2002), abiotic stress responses (Millson *et al.,* 2005) and resistance to insect herbivores (Sangster *et al.,* 2007). The cytosolic Hsp90 proteins AT5G56010, AT5G52640 were significantly downregulated with ATP. The only upregulated protein in this group was AT2G04030, a chloroplastic localized Hsp90. Overexpression of this protein results in increased sensitivity to abiotic stresses such as salt and drought in *Arabidopsis*, but it is not clear how this happens (Song *et al.,* 2009). In this study, the increase in abundance of this protein might be explained in the context of increased demand for protein folding in the chloroplast, since AT2G04030 is one of the only two chloroplastic HSP90 in *Arabidopsis* (Cao *et al.,* 2003). Like in cluster 3, this data suggests that upon ATP treatment, the chloroplast has priority over the partition of newly synthesized proteins over other organelles, although the reason for this is unclear.

Cluster 5 showed significant 3.35 fold enrichment in proteins with nucleotide binding domains, specifically for purine and adenyl nucleotides and more specifically for ATP-binding. This shows that eATP signalling specifically targets ATP-binding proteins, although no obvious upregulation of downregulation trend is evident in this cluster. Several of these ATP-binding proteins are molecular chaperones involved in protein folding and abiotic stress responses (clusters 1 and 2). Their response to 1 mM ATP treatment is most probably the result of specific eATP-mediated signalling rather than to the mild osmotic stress caused by the amount of ATP added to the cell cultures. If this is indeed the case, then it would indicate abiotic stress and eATP-mediated signalling converge at some point in their signalling pathway. Although the same proteins are invoked in both cases, their specific function in either situation is likely to be different.

Cluster 6 shows enrichment for transit peptide-containing proteins, indicating an increase in protein trafficking of newly synthesised proteins in the cell. Interestingly, out of the 9

proteins annotated to posses such a keyword, 6 are either located in or directly connected to the chloroplast. This cluster provides further evidence in support of a strong connection between eATP signalling and the chloroplast, as was previously suggested in clusters 3 and 5.

Overall, DAVID analysis revealed new proteins regulated by early eATP-mediated signalling resulting from the specific increase of ATP levels in the ECM of *Arabidopsis* cell cultures. Proteins annotated as responsive to abiotic stresses, specifically inorganic substances and osmotic stresses, proteins belonging to the chloroplast and heat shock proteins were found to be highly enriched in the protein dataset of eATP-regulated proteins. The chloroplast was the major target organelle of the proteins identified, demonstrating a strong plant-specific component of eATP signalling. Finally, many of these proteins contained ATP binding domains, suggesting eATP signalling could affect metabolic functions controlled by ATP binding in intracellular target proteins. Since no metabolic pathway was significantly enriched in any of the clusters, it was decided to specifically look at the them using DAVID in order to establish if the 35 unique proteins identified show a specific role in metabolic pathway.

4.2.4.3 Metabolic pathways

Using default settings, DAVID did not significantly enrich for specific metabolic pathways eATP signalling might be modulating. However, when the settings were set to look at only metabolic pathways described in the Kyoto Encyclopaedia of Genes and Genomes [KEGG, (Kanehisa and Goto 2000)], the most interesting result was found for proteins annotated as being involved in carbon fixation in photosynthetic organisms (KEGG ID: ath00710). Four proteins shared this KEGG ID: AT3G52930, a putative fructose-bisphosphate aldolase; AT2G21170, a triose-phosphate isomerase (EC 5.3.1.1); AT5G19550, an aspartate aminotransferase and AT3G60750, a transketolase-like protein. All were significantly downregulated following ATP treatment (Table 4.2). This shows that eATP-mediated signalling has a specific effect in the first 8 hours after treatment in repressing proteins belonging to this pathway. This could reflect the metabolic re-adjustment that is evident 8 hours after ATP treatment (Figure 4.2). During this readjustment, the cells focus their energy on other pathways, such as response to inorganic substances, in detriment of photosynthetic carbon fixation. Unlike whole plant tissues, cell cultures can afford to do so from an energy point of view due to the abundance of sucrose in the culture medium.

Although a previous study in tobacco showed a clear role of eATP signalling in controlling protein expression of photosynthetic proteins involved in light reactions (Chivasa *et al.,* 2010), this study now shows that photosynthetic proteins involved in carbon fixation are also controlled by eATP signalling. When taken together, the combined results identify the chloroplast, and specifically photosynthesis, as an important target of eATP signalling.

4.2.5 Cell death phenotypes of eATP-induced proteins

The identification of these 35 novel proteins as responsive to ATP treatment opens up the possibility of further investigations into their physiological role in ATP signalling. For example, they could have a function in cell death regulation. In the previous chapter, the ATP filter approach was successful in identifying novel eATP-regulated cell death genes. In line with the theme of this thesis, I was curious to find out if the proteins identified in this chapter as eATP responsive would also yield a cell death regulator, even though the approach used was not as targeted as the ATP filter. To this end, the availability of SALK homozygous KO lines for the 35 ATP responsive genes was checked and available lines ordered for their cell death phenotype in response to FB1 to be investigated using the same ion leakage assay as in chapter 3. A total of 10 unique genes were found to have KO lines available (Table 4.5). It was noticed that there was an overlap of 5 genes between ATP responsive genes and genes that were reversed from chapter 3 that had already been tested for a phenotype (AT3G52930, AT4G13940, AT5G08690, AT3G04120 and AT5G15650). Except for the ATPaseβ, all these common genes showed no significant cell death phenotype. Of the remaining 5 genes tested that were identified specifically as eATP responsive (AT5G03630, AT1G79930, AT5G20830, AT5G20720 and AT3G17820) none of them showed any significant cell death phenotype (Table 4.5). These results suggest that this approach could have been successful in identifying cell death regulators, since it identified ATPaseβ as an ATP-responsive protein. However, none of the remaining 5 genes tested that were only identified as eATP responsive showed a significant cell death phenotype, suggesting this approach would return fewer positive candidates. Nonetheless, it is worth investigating the remaining eATP-responsive genes for a function in cell death, since ATPaseβ was in the list. The genes identified here provide another list of putative candidates for future studies in addition the list of reversed genes in chapter 3.

Gene description	Gene locus[a]	SALK number[b]	NASC number[c]	T-DNA insertion location[d]	altered phenotype FB1
putative fructose-bisphosphate aldolase	**AT3G52930**	**SALK_124383**	**N663895**	**exon**	**no**
S-adenosyl-L-homocysteine hydrolase	**AT4G13940**	**SALK_023915**	**N657174**	**exon**	**no**
monodehydroascorbate reductase	AT5G03630	SALK_135574	N664083	5' UTR	no
high molecular weight heat shock protein 70	AT1G79930	SALK_082815	N663129	exon	no
ATP synthase beta-subunit	**AT5G08690**	**SALK_024990**	**N658574**	**exon**	**Yes**
ATP synthase beta-subunit	**AT5G08690**	**SALK_135351**	**N653503**	**exon**	**Yes**
ATP synthase beta-subunit	**AT5G08690**	**SALK_005252**	**N505252**	**exon**	**Yes**
sucrose synthase (SUS1)	AT5G20830	SALK_044615	N670649	5' UTR	no
sucrose synthase (SUS1)	AT5G20830	SALK_014303	N660317	exon	no
GAPDH (C subunit)	**AT3G04120**	**SALK_044604**	**N662293**	**5' UTR**	**no**
Encodes a chloroplast co-chaperonin	AT5G20720	SALK_083054	N660988	5' UTR	no
Encodes a cytosolic glutamine synthetase	AT3G17820	SALK_148604	N669232	exon	no
Reversibly Glycosylated Polypeptide-2	**AT5G15650**	**SALK_132152**	**N656992**	**intron**	**no**

Table 4.5 Cell death phenotype characterization of eATP-responsive proteins. eATP-responsive proteins in bold were also identified as reversed proteins using the ATP filter in Chapter 3. [a]Arabidopsis Genome Initiative (AGI) gene identifier [b]SALK number of homozygous T-DNA insertion lines mapped to the specific gene locus [c]line number for homozygous lines available at NASC. [d]Predicted T-DNA insertion site in each SALK line.

4.3 Re-examination of a DNA chip experiment

4.3.1 Prediction of differentially expressed genes with ATP

When this project had started, a DNA chip experiment had already been performed with the aim of identifying novel cell death genes using an eATP filter in the same way as I did using proteomics in chapter 3. This experiment was devised based on the fact that FB1-treated cell cultures can be rescued from undergoing PCD by exogenous ATP addition (Chivasa *et al.,* 2005a).This was investigated by looking at the effects of 1 µM FB1 and 1 mM ATP + 1 µM FB1 treatments on the global gene expression profile of *Arabidopsis* and selecting putative cell death candidates for validation using reverse genetics. This DNA chip was the work of other people. Dr. John Hamilton, Dr. Stephen Chivasa and Prof. Antoni Slabas conceived the work, Dr. John Hamilton and Dr. Stephen Chivasa generated the RNA samples, Dr. Sean Coughlan (formerly of Agilent Technologies Inc., Little Falls Site, Wilmington, USA) probed the DNA microarrays and Dr. John Hamilton analysed the microarray data. The original analysis of this data performed by Dr. John Hamilton involved identifying putative cell death genes using the ATP filter approach. These genes showed significant gene expression changes brought about by eATP depletion, induced by FB1 treatment, and an opposite response to ATP replenishment in the ATP+FB1 treatment i.e. gene expression changes correlate directly or indirectly with eATP availability. A schematic diagram depicting the main steps of sample generation and processing in this experiment is shown in Figure 4.6.

As a consequence of the experimental design, the data can also be used for identifying genes that respond to ATP only and this is explained below. There are two separate sets of ratios for each gene: a fold change of FB1 only treatment to control and a fold change of FB1+ATP treatment to control at 4 different timepoints after ATP addition (Figure 4.6). By standardizing the FB1 fold change as specific baseline gene expression value for each gene 40 hours after FB1 treatment, then the (FB1+ATP)/FB1 ratio can be equated to the prediction of gene expression changes resulting from ATP treatment only for each gene. By performing the analysis in this way, it is possible to identify novel eATP-responding genes using the available DNA chip data. Should these genes proved highly responsive, they could be used as direct early markers of eATP signalling.

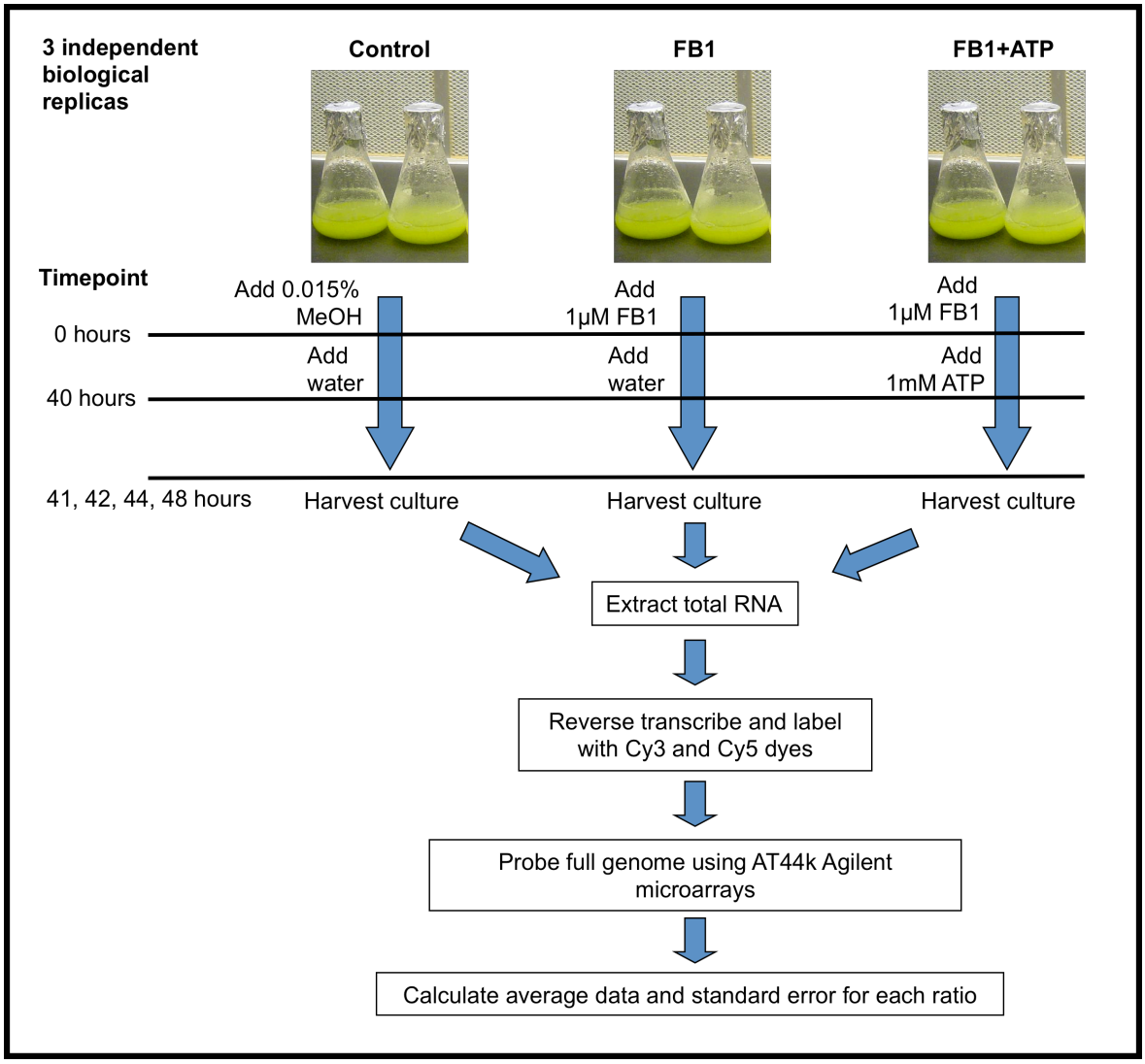

Figure 4.6 Schematic diagram outlining the strategy used for generating the DNA chip samples and data. Triplicate cell cultures were subjected to a 1 μM FB1 treatment or mock-treated with methanol carrier only. After 40h, 1 mM ATP was added to half of the FB1-treated samples to initiate ATP-induced changes in the transcriptome. Cells were harvested for RNA extraction at 1h, 2h, 4h and 8h after ATP addition. The average fold change and standard error between FB1 and control samples and FB1+ATP and control samples was performed using Microsoft Excel. MeOH: Methanol.

Moreover, this experimental design has an added advantage compared to the proteomics performed earlier in this chapter. The effects of eATP signalling should differ from one gene to another. It is possible that some genes only respond to basal levels of eATP and not to high ones, because basal eATP levels are already saturating the signalling pathway that regulates their expression. Such genes could only be identified as responsive to ATP if the basal levels of eATP are below normal in control cultures before ATP is added. The cultures taken as controls in my analysis of the DNA chip data were subject to 40 hours of FB1 treatment, where eATP depletion has already occurred (Chivasa *et al.,* 2005a). Because of this it is now possible for the ATP treatment to initiate gene expression changes in genes where basal levels of eATP are already saturating, as well as genes where these levels are not. As a consequence, more genes can potentially be detected via this experimental design as opposed to the classical experimental approach of comparing control vs. ATP only performed in the proteomics. However, due to the nature of the FB1 control, this new analysis strategy can only provide a prediction for the effects of ATP on gene expression because of possible eATP-independent FB1 effects on gene expression. Therefore, it becomes essential to verify the predictions of the DNA chip for the predicted eATP-only effects in unstressed cultures.

The availability of this data in the Slabas lab encouraged its use as a fast means to search the whole genome for novel genes involved in eATP-mediated signalling and novel physiological processes. It also provides complementary molecular data to the proteomics experiment, since data for all predicted *Arabidopsis* genes is available. Not only does it enable the study of putative candidates that would never be detected by 2D-DiGE, such as very low abundance or highly hydrophobic proteins, it also permits the identification of genes that don't respond to increase ATP availability above basal levels in the plant ECM.

Unlike the vast majority of proteins, significant changes in messenger RNA abundance can happen within minutes of a stimulus (Mizukami-Murata *et al.,* 2010). Since the experiment had 4 available timepoints to choose from (Figure 4.6), the earliest timepoint, 1 hour after ATP addition, was chosen to search for very early eATP-responsive genes. This timepoint was favoured over the remaining 3 later timepoints because, besides looking at the earliest events triggered by eATP, early responsive genes are likely to produce more specific molecular markers of eATP signalling than genes that only respond at later timepoints because of gradual eATP hydrolysis in the ECM. The high-density *Arabidopsis* 3 Oligo Microarrays G4142A (version date 06/01/2005) containing 44,290 features representing

over 28,500 genes (Agilent Technologies Inc., Americas) were used in this experiment. Due to the very high number of genes present in the chip (~28,500) it was decided to perform an analysis of the (ATP+FB1)/FB1 ratio looking only at transcript abundance changes of 99.9% confidence value ($p \leq 0.001$) for a significant change between FB1 and ATP+FB1. This resulted in a total of 6537 genes to be significantly changing following ATP treatment (data not shown). However, the vast majority of them were changing by a very small, albeit significant, percentage between FB1 and ATP+FB1. Therefore, it was then decided to only consider the top 100 genes with the highest (ATP+FB1)/FB1 ratio in order to simplify the analysis. These genes were all upregulated with ATP treatment and their respective ratios and statistical significance are reported in Table 4.6. In order to better understand of the biology behind these genes, a DAVID analysis was performed similarly to the proteomics dataset.

4.3.2 DAVID analysis

Functional annotation clustering of the 100 genes predicted to be changing with eATP was performed in exactly the same way as for the 35 genes identified as responding to ATP treatment and resulting clusters are showed in Table 4.7. Only 3 clusters were significantly enriched ≥ 2 fold and these are discussed below.

Cluster 1 showed the highest enrichment value of 3.2 and clustered 12 genes that respond to organic molecules. Six genes in particular (AT2G44840 ethylene binding protein, AT4G35480 zinc finger family protein, AT5G10380 zinc finger family protein, AT4G23550 WRKY family transcription factor, AT4G37610 TAZ zinc finger family protein, AT1G09650 F-box family protein) have been experimentally shown to respond specifically to chitin (Libault *et al.,* 2007), suggesting a role in defence responses to chitin-exhibiting pathogens. Due to the limitations of this experimental approach mentioned earlier, where FB1-treated cultures provide the baseline value for gene expression of each gene, the enrichment for genes with these characteristics could represent an artefact resulting from the FB1 treatment itself, as FB1 is a pathogen-derived organic molecule. However, later validation of the eATP prediction in unstressed cells shows that, at least for

Table 4.6 Putative eATP-regulated genes predicted by the DNA array experiment. After the data was acquired and processed, the 41 hour timepoint was re-examined in order to identify very early putative eATP-regulated genes. The FB1 signal was taken as a baseline signal for each gene and the FB1+ATP signal as a prediction of the eATP-only effect. Hence, genes are sorted by (ATP+FB1)/FB1 ratio (FA/F ratio in column 3). Only the top 100 out of 6537 genes significantly changing at a 99.9% confidence level ($p \leq 0.001$) are reported in this table. A 99.9% confidence level corresponds to a *t*-value over 2.57 or below -2.57 in a 2 tailed Student's *t*-value. A negative *t*-value indicates a gene upregulation following ATP addition.

Gene locus	Gene Description	FA/F ratio	*t*-value
At1g23160	auxin-responsive GH3 family protein similar to auxin-responsive GH3 product [Glycine max] GI:18591, auxin-responsive GH3 homologue [*Arabidopsis thaliana*] GI:11041726; contains Pfam profile PF03321: GH3 auxin-responsive promoter [At1g23160.1]	5.18	-3.6011
At1g67030	zinc finger (C2H2 type) family protein (ZFP6) identical to zinc finger protein, ZFP6 gi|790683|gb|AAA87302; contains Pfam domain, PF00096: Zinc finger, C2H2 type [At1g67030.1]	4.63	-2.9218
At2g37720	expressed protein [At2g37720.1]	4.62	-2.7092
At5g04950	nicotianamine synthase, putative similar to nicotianamine synthase [Lycopersicon esculentum][GI:4753801], nicotianamine synthase 2 [Hordeum vulgare][GI:4894912] [At5g04950.1]	4.4	-2.8504
At3g53260	phenylalanine ammonia-lyase 2 (PAL2) nearly identical to SP|P45724 [At3g53260.1]	4.31	-11.648
At1g61890	MATE efflux family protein similar to ripening regulated protein DDTFR18 [Lycopersicon esculentum] GI:12231296; contains Pfam profile PF01554: Uncharacterized membrane protein family [At1g61890.1]	4.21	-8.3648
At5g51900	cytochrome P450 family similar to cytochrome P450 86A1 (SP:P48422) [*Arabidopsis thaliana*] [At5g51900.1]	4.18	-2.7942
At5g22670	F-box family protein contains F-box domain Pfam:PF00646 [At5g22670.1]	4.1	-3.797
At2g24600	ankyrin repeat family protein contains ankyrin repeats, Pfam:PF00023 [At2g24600.1]	4.1	-5.0829
At2g38860	proteaseI (pfpI)-like protein (YLS5) contains Pfam profile PF01965: DJ-1/PfpI family; supporting cDNA gi|13122287|dbj|AB047808.1|; identical to proteaseI (pfpI)-like protein [*Arabidopsis thaliana*] GI:13122288, cDNA proteaseI (pfpI)-like protein...	4.09	-5.6647
At5g40000	AAA-type ATPase family protein BCS1 nuclear gene encoding mitochondrial protein - Homo sapiens, EMBL:AF026849 contains Pfam profile: ATPase family PF00004 [At5g40000.1]	4.09	-4.8629
At5g42830	transferase family protein similar to anthranilate N-hydroxycinnamoyl/benzoyltransferase, Dianthus caryophyllus [gi:2239091]; contains Pfam transferase family domain PF002458 [At5g42830.1]	4.09	-5.5154
At1g30730	FAD-binding domain-containing protein similar to SP|P30986 reticuline oxidase precursor (Berberine-bridge-forming enzyme) (BBE) (Tetrahydroprotoberberine synthase) [Eschscholzia californica]; contains PF01565 FAD binding domain [At1g30730.1]	4.07	-5.0076
At1g61290	syntaxin, putative (SYP124) similar to syntaxin-related protein Nt-syr1 GI:4206787 from [Nicotiana tabacum] [At1g61290.1]	4	-3.1933
At1g51680	4-coumarate--CoA ligase 1 / 4-coumaroyl-CoA synthase 1 (4CL1) identical to SP|Q42524 4-coumarate--CoA ligase 1 (EC 6.2.1.12) (4CL 1) (4-coumaroyl-CoA synthase 1) {*Arabidopsis thaliana*} [At1g51680.1]	3.97	-11.873
At1g58420	expressed protein [At1g58420.1]	3.94	-9.7595
At5g39580	peroxidase, putative identical to peroxidase ATP24a [*Arabidopsis thaliana*] gi|1890313|emb|CAA72484 [At5g39580.1]	3.92	-7.3899

Gene locus	Gene Description	FA/F ratio	*t*-value
At2g27660	DC1 domain-containing protein contains Pfam profile PF03107: DC1 domain [At2g27660.1]	3.92	-3.1728
At2g47550	pectinesterase family protein contains Pfam profile: PF01095 pectinesterase [At2g47550.1]	3.89	-5.8991
At1g02810	pectinesterase family protein contains Pfam profile: PF01095 pectinesterase [At1g02810.1]	3.82	-7.3125
At2g40000	expressed protein [At2g40000.1]	3.82	-6.6891
At2g16720	myb family transcription factor contains Pfam profile: PF00249 myb-like DNA-binding domain [At2g16720.1]	3.78	-4.9861
At1g70130	lectin protein kinase, putative similar to receptor lectin kinase 3 [*Arabidopsis thaliana*] gi|4100060|gb|AAD00733 [At1g70130.1]	3.77	-10.997
At2g01300	expressed protein [At2g01300.1]	3.75	-6.4393
At1g09650	F-box family protein contains Pfam PF00646: F-box domain; contains TIGRFAM TIGR01640 : F-box protein interaction domain [At1g09650.1]	3.72	-12.108
At1g71450	AP2 domain-containing transcription factor, putative similar to TINY GB:CAA64359; contains Pfam profile PF00847: AP2 domain [At1g71450.1]	3.71	-3.3688
At2g31345	expressed protein [At2g31345.1]	3.67	-2.8684
At1g61820	glycosyl hydrolase family 1 protein contains Pfam PF00232 : Glycosyl hydrolase family 1 domain; TIGRFAM TIGR01233: 6-phospho-beta-galactosidase; similar to beta-mannosidase enzyme (GI:17226270) [Lycopersicon esculentum] [At1g61820.1]	3.64	-14.105
At1g63450	exostosin family protein contains Pfam profile: PF03016 exostosin family [At1g63450.1]	3.63	-2.7673
At2g42560	late embryogenesis abundant domain-containing protein / LEA domain-containing protein low similarity to LEA protein [Glycine max] GI:1389897; contains Pfam profile PF02987: Late embryogenesis abundant protein [At2g42560.1]	3.63	-5.52
At5g22630	prephenate dehydratase family protein contains Pfam profile PF00800: prephenate dehydratase [At5g22630.1]	3.59	-3.9707
At4g02850	phenazine biosynthesis PhzC/PhzF family protein contains Pfam profile: PF02567 phenazine biosynthesis-like protein [At4g02850.1]	3.55	-3.8451
At4g39320	microtubule-associated protein-related contains weak similarity to microtubule-associated protein 1B (MAP 1B) (Swiss-Prot:P46821) [Homo sapiens] [At4g39320.1]	3.53	-5.5511
At2g23810	senescence-associated family protein similar to senescence-associated protein 5 [Hemerocallis hybrid cultivar] gi|3551954|gb|AAC34855 [At2g23810.1]	3.53	-7.6612
At3g10340	phenylalanine ammonia-lyase, putative similar to phenylalanine ammonia-lyase GB:S48726 [Petroselinum crispum] [At3g10340.1]	3.48	-4.4799
At5g64905	expressed protein [At5g64905.1]	3.47	-6.2634
At5g01100	expressed protein similar to axi 1 [Nicotiana tabacum] GI:559921; contains Pfam profile PF03138: Plant protein family [At5g01100.1]	3.46	-6.9896
At4g02330	pectinesterase family protein contains Pfam profile: PF01095 pectinesterase [At4g02330.1]	3.44	-5.1053
At1g51680	4-coumarate--CoA ligase 1 / 4-coumaroyl-CoA synthase 1 (4CL1) identical to SP|Q42524 4-coumarate--CoA ligase 1 (EC 6.2.1.12) (4CL 1) (4-coumaroyl-CoA synthase 1) {*Arabidopsis thaliana*} [At1g51680.2]	3.44	-3.9174
At3g11420	fringe-related protein similar to hypothetical protein GB:AAC23643 [*Arabidopsis thaliana*] + weak similarity to Fringe [Schistocerca gregaria](GI:6573138);Fringe encodes an extracellular protein that regulates Notch signalling. [At3g11420.1]	3.39	-5.4176
At2g45400	dihydroflavonol 4-reductase family / dihydrokaempferol 4-reductase family similar to dihydroflavonol 4-reductase (SP:P51102), vestitone reductase (Medicago sativa, GI:973249) [At2g45400.1]	3.39	-4.4649
At4g29780	expressed protein [At4g29780.1]	3.38	-6.1778
At4g27950	AP2 domain-containing transcription factor, putative DNA-binding protein Pti6, Lycopersicon esculentum, gb:U89257 [At4g27950.1]	3.36	-4.2287
At4g17660	protein kinase, putative similar to protein kinase [Lophopyrum elongatum] gi|13022177|gb|AAK11674 [At4g17660.1]	3.35	-4.216
At5g10380	zinc finger (C3HC4-type RING finger) family protein contains Pfam profile: PF00097 zinc finger, C3HC4 type (RING finger) [At5g10380.1]	3.34	-4.5602
At4g11170	disease resistance protein (TIR-NBS-LRR class), putative domain signature TIR-NBS-LRR exists, suggestive of a disease resistance protein. [At4g11170.1]	3.32	-5.2084
At4g20860	FAD-binding domain-containing protein similar to SP|P30986 reticuline oxidase precursor (Berberine-bridge-forming enzyme) (BBE) (Tetrahydroprotoberberine synthase) [Eschscholzia californica]; contains PF01565 FAD binding domain [At4g20860.1]	3.29	-7.7361

Gene locus	Gene Description	FA/F ratio	*t*-value
At1g56240	SKP1 interacting partner 3-related contains similarity to SKP1 interacting partner 3 GI:10716951 from [*Arabidopsis thaliana*] [At1g56240.1]	3.29	-4.7765
At2g37040	phenylalanine ammonia-lyase 1 (PAL1) nearly identical to SP|P35510 [At2g37040.1]	3.28	-5.5822
At3g26125	cytochrome P450, putative [At3g26125.1]	3.27	-2.826
At3g11650	harpin-induced family protein / HIN1 family protein / harpin-responsive family protein / NDR1/HIN1-like protein 2 identical to NDR1/HIN1-Like protein 2 (GP:9502174) [*Arabidopsis thaliana*]; similar to hin1 GB:CAA68848 [Nicotiana tabacum] [At3g11650.1]	3.27	-9.3634
At1g71697	choline kinase, putative similar to GmCK2p choline kinase gi|1438881|gb|AAC49375 [At1g71697.1]	3.26	-4.5152
At5g44360	FAD-binding domain-containing protein similar to SP|P30986 reticuline oxidase precursor (Berberine-bridge-forming enzyme) (BBE) (Tetrahydroprotoberberine synthase) [Eschscholzia californica]; contains PF01565 FAD binding domain [At5g44360.1]	3.25	-7.3574
At2g12400	expressed protein [At2g12400.1]	3.24	-4.669
At2g26390	serpin, putative / serine protease inhibitor, putative similar to phloem serpin-1 [Cucurbita maxima] GI:9937311; contains Pfam profile PF00079: Serpin (serine protease inhibitor) [At2g26390.1]	3.23	-6.127
At3g50940	AAA-type ATPase family protein contains Pfam profile: ATPase family PF00004 [At3g50940.1]	3.23	-5.7498
At2g22890	expressed protein ; expression supported by MPSS [At2g22890.1]	3.23	-5.543
At3g13650	disease resistance response protein-related/ dirigent protein-related similar to dirigent protein [Thuja plicata] gi|6694699|gb|AAF25360; similar to pathogenesis-related protein [Pisum sativum] gi|4585273|gb|AAD25355 [At3g13650.1]	3.22	-4.8823
At1g80820	cinnamoyl-CoA reductase, putative identical to CCR2 (GI:12407990), similar to cinnamoyl CoA reductase from Eucalyptus gunnii [GI:2058311] [At1g80820.1]	3.21	-3.5274
At1g69820	gamma-glutamyltranspeptidase family protein similar to SP|P19440 Gamma-glutamyltranspeptidase 1 precursor (EC 2.3.2.2) (Gamma-glutamyltransferase 1) (CD224 antigen) {Homo sapiens}; contains Pfam profilePF01019: Gamma-glutamyltranspeptidase [At1g69820.1]	3.21	-2.6699
At4g30280	xyloglucan:xyloglucosyl transferase, putative / xyloglucan endotransglycosylase, putative / endo-xyloglucan transferase, putative similar to xyloglucan endotransglycosylase TCH4 GI:886116 from [*Arabidopsis thaliana*] [At4g30280.1]	3.2	-7.2204
At2g28400	expressed protein contains Pfam profile PF04520: Protein of unknown function, DUF584 [At2g28400.1]	3.2	-3.3963
At4g30430	senescence-associated family protein similar to senescence-associated protein 5 [Hemerocallis hybrid cultivar] gi|3551954|gb|AAC34855 [At4g30430.1]	3.2	-6.5071
At5g11400	protein kinase-related contains eukaryotic protein kinase domain, INTERPRO:IPR000719 [At5g11400.1]	3.17	-3.0034
At5g36925	expressed protein [At5g36925.1]	3.16	-9.3164
At4g32920	glycine-rich protein [At4g32920.1]	3.16	-4.1681
At2g26380	disease resistance protein-related / LRR protein-related contains leucine rich-repeat domains Pfam:PF00560, INTERPRO:IPR001611; similar to Hcr2-2A [Lycopersicon pimpinellifolium] gi|3894389|gb|AAC78594 [At2g26380.1]	3.16	-9.4155
At5g37550	expressed protein [At5g37550.1]	3.16	-5.4838
At2g44790	uclacyanin II strong similarity to uclacyanin II GI:3399769 from [*Arabidopsis thaliana*]; contains Pfam profile PF02298: Plastocyanin-like domain; identical to cDNA uclacyanin II GI:3399768 [At2g44790.1]	3.15	-2.5865
At2g34930	disease resistance family protein contains leucine rich-repeat domains Pfam:PF00560, INTERPRO:IPR001611; similar to Cf-2.1 [Lycopersicon pimpinellifolium] gi|1184075|gb|AAC15779 [At2g34930.1]	3.15	-5.2404
At2g44840	ethylene-responsive element-binding protein, putative [At2g44840.1]	3.15	-6.9349
At4g09440	hypothetical protein contains Pfam PF04510 : Family of unknown function (DUF577); common family comprised of At4g09440, At1g66000, At1g66060 [At4g09440.1]	3.14	-2.8271
At5g05300	expressed protein similar to unknown protein (gb|AAF01528.1); expression supported by MPSS [At5g05300.1]	3.14	-5.8837
At4g39640	gamma-glutamyltranspeptidase family protein similar to SP|P19440 Gamma-glutamyltranspeptidase 1 precursor (EC 2.3.2.2) (Gamma-glutamyltransferase 1) (CD224 antigen) {Homo sapiens}; contains Pfam profilePF01019: Gamma-glutamyltranspeptidase [At4g39640.1]	3.14	-5.2724

Gene locus	Gene Description	FA/F ratio	*t*-value
At4g23550	WRKY family transcription factor contains Pfam profile: PF03106 WRKY DNA binding domain [At4g23550.1]	3.13	-7.9467
At4g30470	cinnamoyl-CoA reductase-related similar to cinnamoyl-CoA reductase from Pinus taeda [GI:17978649], Saccharum officinarum [GI:3341511] [At4g30470.1]	3.13	-9.7949
At4g39840	expressed protein [At4g39840.1]	3.13	-7.1455
At5g58120	disease resistance protein (TIR-NBS-LRR class), putative domain signature TIR-NBS-LRR exists, suggestive of a disease resistance protein. [At5g58120.1]	3.12	-2.7337
At4g20840	FAD-binding domain-containing protein similar to SP|P30986 reticuline oxidase precursor (Berberine-bridge-forming enzyme) (BBE) (Tetrahydroprotoberberine synthase) [Eschscholzia californica]; contains PF01565 FAD binding domain [At4g20840.1]	3.11	-5.1988
At3g57450	expressed protein [At3g57450.1]	3.11	-5.316
At3g16860	phytochelatin synthetase-related contains Pfam PF04833: Phytochelatin synthetase-like conserved region [At3g16860.1]	3.11	-6.1902
At2g06050	12-oxophytodienoate reductase (OPR3) / delayed dehiscence1 (DDE1) nearly identical to DELAYED DEHISCENCE1 [GI:7688991] and to OPR3 [GI:10242314]; contains Pfam profile PF00724:oxidoreductase, FAD/FMN-binding; identical to cDNA OPDA-reductase homolog...	3.11	-6.678
At5g48070	xyloglucan:xyloglucosyl transferase, putative / xyloglucan endotransglycosylase, putative / endo-xyloglucan transferase, putative similar to xyloglucan endotransglycosylase TCH4 GI:886116 from [*Arabidopsis thaliana*] [At5g48070.1]	3.11	-4.9399
At5g11650	hydrolase, alpha/beta fold family protein contains Pfam profile PF00561: hydrolase, alpha/beta fold family; low similarity to monoglyceride lipase from [Homo sapiens] GI:14594904, [Mus musculus] GI:2632162 [At5g11650.1]	3.1	-11.85
At2g44370	DC1 domain-containing protein highly similar to GP|2435515|AF024504 [At2g44370.1]	3.1	-5.923
At3g52400	syntaxin, putative (SYP122) similar to SP|Q9ZSD4 Syntaxin 121 (AtSYP121) (Syntaxin-related protein At-Syr1) {*Arabidopsis thaliana*} [At3g52400.1]	3.09	-5.1013
At4g35480	zinc finger (C3HC4-type RING finger) family protein contains Pfam domain PF00097: Zinc finger, C3HC4 type (RING finger) [At4g35480.1]	3.09	-6.8584
At4g02075	zinc finger (C3HC4-type RING finger) family protein contains InterPro Entry IPR001841 Zn-finger, RING [At4g02075.1]	3.08	-3.0877
At1g29680	expressed protein [At1g29680.1]	3.07	-3.3191
At1g54550	F-box family protein contains Pfam:PF00646 F-box domain; contains TIGRFAM TIGR01640 : F-box protein interaction domain [At1g54550.1]	3.07	-3.0175
At1g57990	purine permease-related low similarity to purine permease [*Arabidopsis thaliana*] GI:7620007; contains Pfam profile PF03151: Domain of unknown function, DUF250 [At1g57990.1]	3.07	-3.4076
At3g15370	expansin, putative (EXP12) similar to expansin GI:11191999 from [Lycopersicon esculentum]; alpha-expansin gene family, PMID:11641069 [At3g15370.1]	3.06	-5.2319
At2g40160	expressed protein [At2g40160.1]	3.06	-3.0923
At3g45960	expansin family protein (EXPL3) contains Pfam profile: PF01357 pollen allergen; expansin-like gene, PMID:11641069, www.bio.psu.edu/expansins [At3g45960.1]	3.05	-7.5377
At4g38420	multi-copper oxidase type I family protein similar to pollen-specific BP10 protein [SP|Q00624][Brassica napus]; contains Pfam profile: PF00394 Multicopper oxidase [At4g38420.1]	3.04	-7.963
At3g04640	glycine-rich protein predicted proteins, *Arabidopsis thaliana* [At3g04640.1]	3.04	-5.4542
At4g37610	TAZ zinc finger family protein / BTB/POZ domain-containing protein contains Pfam PF00651 : BTB/POZ domain; contains Pfam PF02135 : TAZ zinc finger; similar to Speckle-type POZ protein (SP:O43791) [Homo sapiens] [At4g37610.1]	3.04	-6.4286
At2g46210	delta-8 sphingolipid desaturase, putative similar to delta-8 sphingolipid desaturase GI:3819708 from [Brassica napus] [At2g46210.1]	3.04	-2.8991
At4g27720	expressed protein contains Pfam PF05631: Protein of unknown function (DUF791) [At4g27720.1]	3.03	-5.2539
At3g10930	expressed protein [At3g10930.1]	3.03	-4.8154

Table 4.7 Functional annotation clustering of differentially expressed proteins with eATP predicted by the DNA chip using DAVID default settings and medium classification stringency. Description of the terms in each column is the same as for Table 4.4

Annotation Cluster 1 Enrichment Score: 3.224422694978857

Category	Term	Count	%	*p*-Value	Genes	Fold Enrichment
GOTERM_BP_FAT	GO:0010200~response to chitin	6	6.06	9.55E-05	AT2G44840, AT4G35480, AT5G10380, AT4G23550, AT4G37610, AT1G09650	12.71774682
GOTERM_BP_FAT	GO:0009743~response to carbohydrate stimulus	6	6.06	7.63E-04	AT2G44840, AT4G35480, AT5G10380, AT4G23550, AT4G37610, AT1G09650	8.116350986
GOTERM_BP_FAT	GO:0010033~response to organic substance	12	12.1	0.0029115	AT2G44840, AT2G40000, AT4G27950, AT3G52400, AT1G23160, AT4G35480, AT5G10380, AT4G23550, AT1G71450, AT4G37610, AT1G09650, AT2G16720	2.746860283

Annotation Cluster 2 Enrichment Score: 2.895400175364539

Category	Term	Count	%	*p*-Value	Genes	Fold Enrichment
GOTERM_BP_FAT	GO:0006575~cellular amino acid derivative metabolic process	10	10.1	6.57E-07	AT5G04950, AT3G10340, AT4G39640, AT4G30470, AT2G37040, AT3G13650, AT3G53260, AT2G45400, AT1G51680, AT1G80820	9.614010989
GOTERM_BP_FAT	GO:0009698~phenylpropanoid metabolic process	8	8.08	2.17E-06	AT3G10340, AT4G30470, AT2G37040, AT3G13650, AT3G53260, AT2G45400, AT1G51680, AT1G80820	12.97312326
SP_PIR_KEYWORDS	Phenylpropanoid metabolism	4	4.04	5.58E-06	AT3G10340, AT2G37040, AT3G53260, AT1G51680	108.3183673
GOTERM_BP_FAT	GO:0006558~L-phenylalanine metabolic process	4	4.04	1.61E-05	AT3G10340, AT5G22630, AT2G37040, AT3G53260	76.91208791
GOTERM_BP_FAT	GO:0042398~cellular amino acid derivative biosynthetic process	7	7.07	7.03E-05	AT5G04950, AT4G30470, AT2G37040, AT3G13650, AT3G53260, AT2G45400, AT1G80820	9.713124504
UP_SEQ_FEATURE	cross-link:5-imidazolinone (Ala-Gly)	3	3.03	9.00E-05	AT3G10340, AT2G37040, AT3G53260	185.1041667
INTERPRO	IPR001106:Phenylalanine/histidine ammonia-lyase	3	3.03	9.77E-05	AT3G10340, AT2G37040, AT3G53260	182.1366279
INTERPRO	IPR005922:Phenylalanine ammonia-lyase	3	3.03	9.77E-05	AT3G10340, AT2G37040, AT3G53260	182.1366279

GOTERM_BP_FAT	GO:0009699~phenylpropanoid biosynthetic process	6	6.06	9.91E-05	AT4G30470, AT2G37040, AT3G13650, AT3G53260, AT2G45400, AT1G80820	12.61838942
GOTERM_BP_FAT	GO:0019438~aromatic compound biosynthetic process	7	7.07	1.24E-04	AT5G22630, AT4G30470, AT2G37040, AT3G13650, AT3G53260, AT2G45400, AT1G80820	8.764400716
GOTERM_MF_FAT	GO:0016841~ammonia-lyase activity	3	3.03	1.30E-04	AT3G10340, AT2G37040, AT3G53260	161.52
KEGG_PATHWAY	ath00940:Phenylpropanoid biosynthesis	5	5.05	1.86E-04	AT3G10340, AT2G37040, AT3G53260, AT1G51680, AT1G80820	13.13034188
GOTERM_BP_FAT	GO:0006559~L-phenylalanine catabolic process	3	3.03	1.93E-04	AT3G10340, AT2G37040, AT3G53260	134.5961538
PIR_SUPERFAMILY	PIRSF001436:histidine ammonia-lyase	3	3.03	2.24E-04	AT3G10340, AT2G37040, AT3G53260	118.8333333
GOTERM_BP_FAT	GO:0009074~aromatic amino acid family catabolic process	3	3.03	3.59E-04	AT3G10340, AT2G37040, AT3G53260	100.9471154
GOTERM_MF_FAT	GO:0016211~ammonia ligase activity	3	3.03	7.03E-04	AT3G10340, AT2G37040, AT3G53260	73.41818182
GOTERM_MF_FAT	GO:0016880~acid-ammonia (or amide) ligase activity	3	3.03	7.03E-04	AT3G10340, AT2G37040, AT3G53260	73.41818182
GOTERM_BP_FAT	GO:0019748~secondary metabolic process	8	8.08	8.04E-04	AT3G10340, AT4G30470, AT2G37040, AT3G13650, AT3G53260, AT2G45400, AT1G51680, AT1G80820	5.091107474
GOTERM_BP_FAT	GO:0009072~aromatic amino acid family metabolic process	4	4.04	0.0012829	AT3G10340, AT5G22630, AT2G37040, AT3G53260	18.25032595
KEGG_PATHWAY	ath00960:Tropane, piperidine and pyridine alkaloid biosynthesis	3	3.03	0.0013822	AT3G10340, AT2G37040, AT3G53260	45.51851852
GOTERM_BP_FAT	GO:0009611~response to wounding	5	5.05	0.0019892	AT1G71697, AT2G37040, AT2G06050, AT3G53260, AT1G51680	9.156200942
GOTERM_MF_FAT	GO:0016840~carbon-nitrogen lyase activity	3	3.03	0.0034229	AT3G10340, AT2G37040, AT3G53260	33.65
GOTERM_BP_FAT	GO:0019439~aromatic compound catabolic process	3	3.03	0.0046305	AT3G10340, AT2G37040, AT3G53260	28.84203297
KEGG_PATHWAY	ath01061:Biosynthesis of phenylpropanoids	5	5.05	0.0050279	AT3G10340, AT2G37040, AT3G53260, AT1G51680, AT1G80820	5.528565002
KEGG_PATHWAY	ath00910:Nitrogen metabolism	3	3.03	0.0074788	AT3G10340, AT2G37040, AT3G53260	19.50793651
GOTERM_BP_FAT	GO:0009063~cellular amino acid catabolic process	3	3.03	0.0111665	AT3G10340, AT2G37040, AT3G53260	18.35402098
GOTERM_BP_FAT	GO:0009310~amine catabolic process	3	3.03	0.0126719	AT3G10340, AT2G37040, AT3G53260	17.18248773
KEGG_PATHWAY	ath01064:Biosynthesis of alkaloids derived from ornithine, lysine and nicotinic acid	4	4.04	0.013159	AT3G10340, AT4G39640, AT2G37040, AT3G53260	6.580990629

KEGG_PATHWAY	ath01063:Biosynthesis of alkaloids derived from shikimate pathway	4	4.04	0.0149762	AT3G10340, AT2G37040, AT3G53260, AT1G51680	6.278416347
KEGG_PATHWAY	ath00360:Phenylalanine metabolism	3	3.03	0.0257909	AT3G10340, AT2G37040, AT3G53260	10.24166667
SP_PIR_KEYWORDS	lyase	4	4.04	0.0280362	AT3G10340, AT5G22630, AT2G37040, AT3G53260	6.051305438
INTERPRO	IPR001509:NAD-dependent epimerase/dehydratase	3	3.03	0.0322066	AT4G30470, AT2G45400, AT1G80820	10.5586451
GOTERM_BP_FAT	GO:0016054~organic acid catabolic process	3	3.03	0.0367201	AT3G10340, AT2G37040, AT3G53260	9.729842447
GOTERM_BP_FAT	GO:0046395~carboxylic acid catabolic process	3	3.03	0.0367201	AT3G10340, AT2G37040, AT3G53260	9.729842447
GOTERM_MF_FAT	GO:0016879~ligase activity, forming carbon-nitrogen bonds	5	5.05	0.0381552	AT3G10340, AT2G37040, AT3G53260, AT5G10380, AT2G22890	3.856733524
KEGG_PATHWAY	ath01070:Biosynthesis of plant hormones	4	4.04	0.0652721	AT3G10340, AT2G37040, AT2G06050, AT3G53260	3.593567251
INTERPRO	IPR016040:NAD(P)-binding domain	3	3.03	0.3501014	AT4G30470, AT2G45400, AT1G80820	2.404443933
SP_PIR_KEYWORDS	cytoplasm	4	4.04	0.4146142	AT3G10340, AT4G27950, AT2G37040, AT3G53260	1.69512312

Annotation Cluster 3 Enrichment Score: 2.703381409425689

Category	Term	Count	%	*p*-Value	Genes	Fold Enrichment
INTERPRO	IPR012951:Berberine/berberine-like	4	4.04	1.77E-04	AT4G20860, AT5G44360, AT4G20840, AT1G30730	35.97760551
GOTERM_MF_FAT	GO:0050662~coenzyme binding	8	8.08	3.77E-04	AT4G20860, AT5G44360, AT4G20840, AT4G30470, AT1G30730, AT2G06050, AT2G45400, AT1G80820	5.804851752
GOTERM_MF_FAT	GO:0048037~cofactor binding	9	9.09	5.86E-04	AT4G20860, AT5G44360, AT4G20840, AT4G39640, AT4G30470, AT1G30730, AT2G06050, AT2G45400, AT1G80820	4.614857143
INTERPRO	IPR006094:FAD linked oxidase, N-terminal	4	4.04	7.64E-04	AT4G20860, AT5G44360, AT4G20840, AT1G30730	22.07716702
INTERPRO	IPR016166:FAD-binding, type 2	4	4.04	0.0011107	AT4G20860, AT5G44360, AT4G20840, AT1G30730	19.42790698
GOTERM_MF_FAT	GO:0009055~electron carrier activity	8	8.08	0.0094099	AT4G20860, AT5G44360, AT4G20840, AT1G30730, AT2G44790, AT3G26125, AT5G39580, AT5G51900	3.282926829
GOTERM_MF_FAT	GO:0050660~FAD binding	4	4.04	0.0219162	AT4G20860, AT5G44360, AT4G20840, AT1G30730	6.565853659
COG_ONTOLOGY	Energy production and conversion	3	3.03	0.0344932	AT4G20860, AT5G44360, AT4G20840	9.153571429

the AT4G37610 TAZ zinc finger family protein, the eATP-induced upregulation is a true biological response. The AT5G10380 zinc finger family protein is required for FB1-induced cell death as *Arabidopsis* overexpressing plants are hypersensitive and knockdown lines are resistant to the toxin, respectively (Lin *et al.,* 2008). Its upregulation with eATP in FB1 elicited cells appears counter-intuitive and highlights how little it is known about eATP signalling cascades involved in PCD regulation. The upregulation of several genes with predicted transcription factor activity suggests multiple gene expression mechanisms that are directly regulated by eATP signalling. It also provides preliminary evidence that these genes could be critical in mediating defence responses controlled by eATP (Chivasa *et al.,* 2009a), although this possibility requires further research.

Cluster 2 shows a very clear role of eATP signalling in cellular amino acid derived metabolism, more specifically in L-phenylalanine metabolism was enriched 76.9 fold. A 182 fold enrichment, the highest in the dataset, was found in this cluster for proteins containing the InterPro domain IPR005922, specific to phenylalanine ammonia-lyase (PAL) activity. Three of the four PAL enzymes predicted in the *Arabidopsis* genome were identified as being upregulated in response to eATP: AT3G10340 (PAL4), AT2G37040 (PAL1) and AT3G53260 (PAL2). Only PAL3 (AT5G04230) was not identified in the top 100 genes (Table 4.6) or in the 6537 eATP responding genes (data not shown). PAL enzymes perform the first step of the plant phenylpropanoid pathway synthesizing *trans*-cinnamic acid from phenylalanine. This pathway produces many plant secondary metabolites such as lignins, and flavanoids (Ferrer *et al.,* 2008), and plays a role in plant growth and development (Huang *et al.,* 2010). SA, an important plant defence hormone (Gaffney *et al.,* 1993), is though to be partially synthesized from phenylalanine. Biochemical studies in the 1990's using isotope feeding suggested that SA can be synthesized from *trans*-cinnamic acid via benzoate (Lee *et al.,* 1995; Ribnicky *et al.,* 1998). Additionally, PAL activity is known to transiently increase prior to SA accumulation induced by plant pathogens (Smith-Becker *et al.,* 1998). Genetic studies using *SID2* mutants in *Arabidopsis* have shown that the bulk of SA (~95%) produced upon pathogen challenge is the result of isochorismate synthase 1 (*ics1*, AT1G74710) activity (Wildermuth *et al.,* 2001), although biosynthesis of SA in plants is still not fully understood due to the absence of enzymes with isochorismate pyruvate lyase activity (Chen *et al.,* 2009b) The *Arabidopsis* genome encodes for two isochorismate synthase genes, *ics1* and *ics2* (AT1G18870), but neither were identified in the 6537 eATP

responding genes (data not shown), indicating they are not regulated by eATP. This suggests that, at least for the *Arabidopsis* cell cultures eATP timepoint analysed in this chapter, eATP is not altering gene expression of these crucial enzymes in SA synthesis. It has recently been shown that SA is negatively regulated by eATP and reciprocally SA treatments lower basal eATP levels in tobacco (Chivasa *et al.,* 2009a). This relationship could indicate that eATP modulates SA levels by downregulating or inhibiting the enzymes responsible for SA synthesis, a connection that cannot be easily explained if PAL enzymes were the primary metabolic pathway for SA synthesis. Therefore, the significance of the observed upregulation of PAL1, PAL2 and PAL4 with eATP in relation to SA synthesis is not clear. A more simple explanation of this data is that it indicates increased synthesis of other phenylpropanoids such as 4-coumaric acid, a precursor of lignin, subrin and other cell wall phenolics that play a role in the defence responses to FB1. It has been reported previously that FB1 induced accumulation of calose in the cell wall (Stone *et al.,* 2000), with eATP treatment possibly bosting this response after blocking cell death signalling.

Cluster 3 was enriched for flavin adenine dinucleotide (FAD)-binding domains proteins involved in electron carrier activity and energy production. FAD-binding domain proteins are very abundant in eukaryotic genomes, accounting for 1% of all predicted proteins (Mattevi 2006). FAD-binding domain proteins are involved many redox pathways including electron transfer from succinate to complex II (succinate dehydrogenase, EC 1.3.5.1) in the mitochondrial electron transport chain (Garrett *et al.,* 2010). This enables the delivery of extra electrons to the quinone pool in the membrane and aids in the creation of the electrochemical proton gradient across the mitochondrial inner membrane required for ATP synthesis by oxidative phosphorylation. An increase in FAD-binding proteins following ATP treatment could indicate that eATP signalling is stimulating energy production in the mitochondria. This might result in an increase in ATP synthesis that could be followed by increased ATP secretion, a logical step in the mechanism of eATP rescue of FB1-elicited cells (Chivasa *et al.,* 2005a). One of the FAD-binding domain containing proteins (AT4G20840) is predicted to be located in the apoplast and plasma membrane, providing some evidence for eATP regulation of extracellular proteins.

Overall, these results show that eATP signalling is extremely fast and affects a significant number of genes. They also provide preliminary evidence for the transcription factors mediating eATP responses and indicate eATP signalling plays a significant role in the

response to organic molecules originating from plant pathogens. However, results originating from DNA chip experiments require separate confirmation via other techniques that measure actual transcript abundance changes, such as semi-quantitative RT-PCR (sqRT-PCR), and this issue is addressed below.

4.3.3 Semi quantitative RT-PCR analysis of putative eATP molecular markers

As mentioned in the introduction of this chapter, one of the objectives of this chapter is to identify genes that can be used as markers for eATP-induced signalling due to their specific response to ATP treatment. Ideally, these markers should be quickly induced following ATP treatment. The identification of many predicted eATP-responsive genes 1 hour following ATP addition using the DNA chip opens up the possibility of utilizing the biggest changers as molecular markers for eATP-mediated signalling, since none have been established so far in the literature. Therefore, I sought to confirm the prediction of the DNA chip by sqRT-PCR on the top 10 genes predicted to be changing. Of all the 6537 genes predicted to be regulated by eATP by the re-examination of the DNA chip, the top 10 that showed the biggest absolute increase in transcript abundance following ATP addition were selected for validation by sqRT-PCR (Table 4.8). These genes were selected for confirmation of the predicted eATP effect by sqRT-PCR because they show the biggest increase in signal intensity relative to their respective baseline level (FB1 only). The absolute increase in transcript abundance was calculated for each gene by the subtraction of FB1 (F) only ratio to the FB1+ATP treatment (FA) ratio for each gene and the top 10 are shown in Table 4.8. For validation of the predicted effects of eATP treatment on the gene espression of genes in Table 4.8, RNA samples were generated from cell cultures treated with 1 mM ATP, the same concentration used in the DNA chip experiment, and used to generate cDNA for sqRT-PCR analysis. Although the genes were responding to ATP addition within 1 hour in the DNA chip, this was not conclusive evidence that they would respond similarly when ATP was added in the absence of FB1 as was explained earlier. Therefore, it was decided to generate an ATP addition timecourse for the collection of RNA samples to identify a timepoint where these genes respond in the absence of FB1 stress. ATP-treated cultures were harvested at 0.5, 1, 2, 4 and 8 hours after ATP treatment and the expression profile of each gene was obtained (data not shown). sqRT-PCR results show that all the 10 selected genes were highly upregulated by ATP, as predicted by the

Gene locus	Description	Average F	Average FA	FA-F
AT3G15450	expressed protein similar to auxin down-regulated protein ARG10 [Vigna radiata] GI:2970051, wali7 (aluminum-induced protein) [Triticum aestivum] GI:451193 [At3g15450.1]	57.213527	86.521024	29.307
AT4G37610	TAZ zinc finger family protein / BTB/POZ domain-containing protein contains Pfam PF00651 : BTB/POZ domain; contains Pfam PF02135 : TAZ zinc finger; similar to Speckle-type POZ protein (SP:O43791) [Homo sapiens] [At4g37610.1]	12.577155	38.178589	25.601
AT2G40000	expressed protein [At2g40000.1]	5.2510614	20.046665	14.796
AT3G28210	zinc finger (AN1-like) family protein contains Pfam profile: PF01428 AN1-like zinc finger [At3g28210.1]	13.917310	27.068871	13.152
AT3G01830	calmodulin-related protein, putative similar to regulator of gene silencing calmodulin-related protein GI:12963415 from [Nicotiana tabacum]; Pfam HMM hit: EF hand [At3g01830.1]	9.8091335	22.152476	12.343
AT4G01360	expressed protein [At4g01360.1]	12.783736	24.385504	11.602
AT1G61290	syntaxin, putative (SYP124) similar to syntaxin-related protein Nt-syr1 GI:4206787 from [Nicotiana tabacum] [At1g61290.1]	3.6885301	14.769747	11.081
AT3G22910	calcium-transporting ATPase, plasma membrane-type, putative / Ca(2+)-ATPase, putative (ACA13) identical to SP|Q9LIK7 Potential calcium-transporting ATPase 13, plasma membrane-type (EC 3.6.3.8) (Ca(2+)-ATPase isoform 13) {*Arabidopsis thaliana*}	12.147253	23.181121	11.034
AT5G40000	AAA-type ATPase family protein BCS1 nuclear gene encoding mitochondrial protein - Homo sapiens, EMBL:AF026849 contains Pfam profile: ATPase family PF00004 [At5g40000.1]	3.2711180	13.371690	10.101
AT5G13200	GRAM domain-containing protein / ABA-responsive protein-related similar to ABA-responsive protein [Hordeum vulgare] GI:4103635; contains Pfam profile PF02893: GRAM domain [At5g13200.1]	13.071132	22.934565	9.8634

Table 4.8 Identification of the top 10 gene changes that could be regulated by eATP-mediated signalling as predicted by the re-examination of the DNA chip data. All the 6537 genes predicted to be regulated by eATP were re-sorted by decreasing order of their FA-F value which is the subtracting of their FB1 signal (Average F) to their ATP+FB1 signal (Average FA).

DNA chip, and this upregulation gradually decreasing over time. The gene upregulation was most pronounced 30 minutes after treatment, showing a fast response to ATP addition as was intended when the 1 hour after ATP addition timepoint of the DNA chip was selected. The gene expression changes induced by 30 minutes ATP treatment on these 10 genes are shown in Figure 4.7. These results clearly show that all the genes tested are highly responsive to eATP signalling as predicted by the DNA chip and, due to their fast response, are likely to be very close to the ATP receptor(s) in the signalling pathway. Moreover, they also indicate that the predictions obtained by the re-examination of the DNA chip are true, establishing the genes in Table 4.6 as genes under the control of eATP-mediated signalling. Although each gene needs to be confirmed independently, the results in Figure 4.7 suggest this is likely to be the case.

4.3.4 Applications of the novel eATP molecular markers

Having established these 10 genes as eATP-signalling molecular markers, it was decided to utilize them in cell death related research in three different ways. Firstly, they were used to test the hypothesis that SA- and eATP-signalling produce antagonistic transcript abundance changes in putative defence related genes and similar changes in viability related genes. Secondly, they were used to probe the status of eATP-mediated signalling and possible involvement in cell death in the KO lines for the eATP-regulated ATPaseβ cell death regulator. Thirdly, they provide a list of putative cell death genes and so were tested for a direct role in FB1-induced cell death using the conductivity assay.

4.3.4.1 Separation of putative defence and putative cell viability genes

Recently, it was established that eATP signalling is a negative regulator of defence responses due to its antagonistic effects on SA signalling (Chivasa *et al.,* 2009a), but no molecular evidence in support of this is available. A model explaining how SA- and eATP-mediated signalling is interconnected in controlling plant defence responses and cell viability was purposed and is shown in Figure 4.8. This model predicts that genes involved in maintaining viability ($eARPs^{via}$) are induced by both eATP signalling and SA signalling and that genes involved in defence responses ($eARPs^{def}$) are regulated antagonistically by eATP and SA signalling. This model was purposed based on the fact that eATP and SA antagonistically regulate PR gene expression, and that pathogens deplete eATP levels to

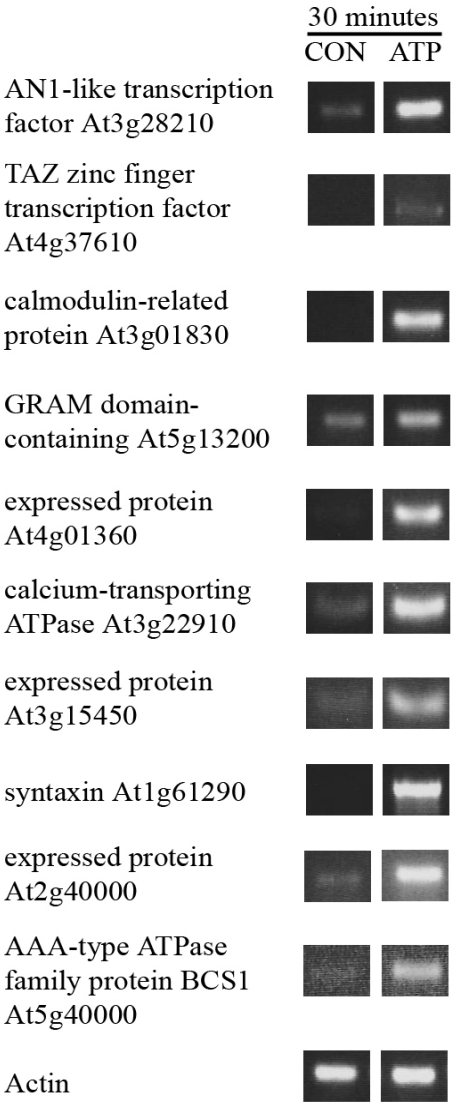

Figure 4.7 Confirmation of the predicted eATP-regulated genes by sqRT-PCR. Cell cultures were treated with 1 mM ATP (ATP) or equal volume of water (CON) and samples harvested for RNA analysis 30 minutes later. Actin-2 (Actin) was used as a constitutive reference control.

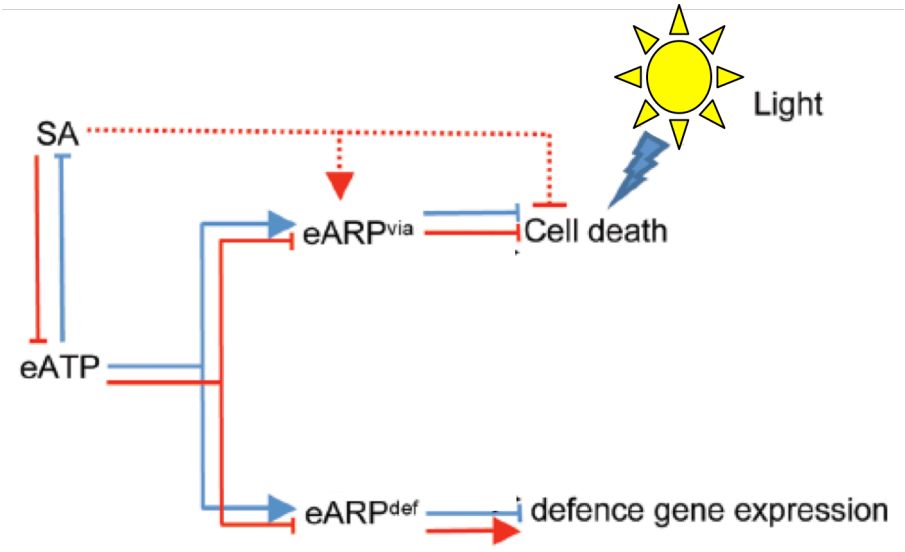

Figure 4.8 Model of how eATP- and SA-mediated signalling might interconnect. Under normal growth conditions, basal SA levels do not deplete eATP. Basal eATP negatively regulates cell death and defence gene expression through $eARP^{via}$ and $eARP^{def}$ activity, respectively (blue lines). The red lines represent signalling activated by increases in SA levels, caused by either exogenous application or elicitor/pathogen-induced biosynthesis. Inhibition of cell death by SA could involve eATP-independent signalling through $eARP^{via}$ activity or another independent pathway (represented by dotted red lines). Cell death occurs in the presence of high light, represented by the sun. Pointed arrows denote activation; blunt-ending lines denote downregulation. Adapted from (Chivasa *et al.,* 2009b).

promote disease, predicting the existence of eARPs^{def} genes (Chivasa *et al.,* 2009b). Even though exogenous SA treatments causes eATP depletion, SA in its own right does not initiate cell death, probably because SA activates a separate signalling cascade that protects against cell death. The protective effects of SA on cell death may be mediated by a positive regulation of eARP^{via} genes that are independently controlled by eATP signalling.

The identification of these novel eATP molecular markers (Figure 4.7), also called extracellular ATP regulated proteins (eARPs), provides an opportunity to test the predictions of this model by investigating how they respond to SA treatment. This was tested by treating cell cultures with 200 µM SA and measuring the gene expression changes of the eARP's via sqRT-PCR. Two of the eARP's were found to be responding as predicted by the model for eARPs^{def} and for eARPs^{via} genes (Figure 4.9). AT3G15450 was upregulated with ATP treatment and repressed following SA treatment making this gene an eARP^{def} with a putative role in defence responses. AT3G22910 was upregulated by both treatments, making this gene an eARP^{via} with a putative role in regulating viability (Figure 4.9A). Additionally, AT3G15450 was found to be downregulated following SA treatment and was completely repressed before PR1 and PR3 transcripts were upregulated (Figure 4.9B). This shows SA treatment dismantles eATP signalling that in turn blocks eARP^{def} gene expression before it initiates defence gene expression, indicated by PR1 and PR3 transcript accumulation. Although the putative function of AT3G15450 in plant defence remains unknown, it is here used as a proof of principle for showing that gene expression can be differentially regulated by ATP and SA treatments. Overall, these results show how the eARP's identified in this chapter can be used as tools for future research into the physiological roles of eATP in plants. These results were published in Plant Signalling and Behaviour (Chivasa *et al.,* 2009b) and a copy of that paper is presented in Appendix B.

4.3.4.2 eATP-mediated signalling in the ATPaseß KO lines

In the previous chapter, novel eATP-regulated proteins with a putative function in cell death were identified by an experimental approach combining ATP and FB1 treatments. The ATPaseβ was confirmed as a true cell death regulator by reverse genetics, but its mechanism remains unknown. Since ATPaseβ KO lines are resistant to FB1, it is possible that the absence of ATPaseβ could be affecting eATP perception and downstream signalling that modulates its cell death phenotype. The eARPs confirmed in Figure 4.7 were now used to investigate if eATP signalling is disrupted in the ATPaseβ KO

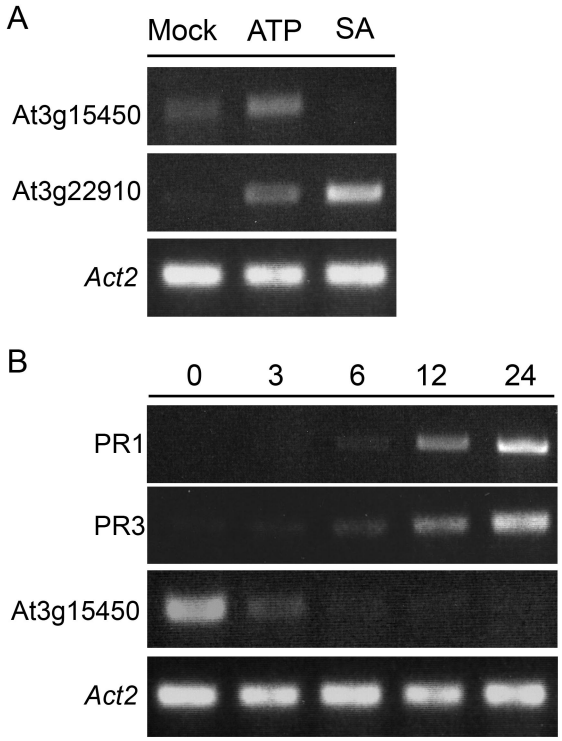

Figure 4.9 Gene expression of eATP molecular markers in response to SA and ATP treatments. (A) sqRT-PCR analysis of two eATP-responsive molecular markers with predicted functions in defence and cell viability respectively. Cell culture samples treated with 1 mM ATP or 200 μM SA for 30 minutes and 24 h, respectively. (B) sqRT-PCR analysis of AT3G15450, a putative eARP involved in defence, and two PR genes: PR1, an archetypal SA-inducible defence gene, and PR3 in response to SA treatment. *Arabidopsis* cell cultures were treated with 200 μM SA for the indicated time in hours. Actin-2 (*Act2*) was used as a constitutive reference control.

background. Changes in these genes' abundance would provide some evidence for altered eATP signalling and might provide some clues for the observed resistance of ATPaseβ KO lines to the eATP-depleting toxin FB1. With these considerations in mind, the basal expression levels of 5 eATP markers, including AT3G15450 with a putative role in defence and AT3G22910 with a putative role in viability (Figure 4.9A) was investigated in Col-0, SALK_024990 and SALK_135351 (Figure 4.10). The transcript abundance levels of 4 of the 5 tested genes showed no significant change between Col-0 and the KO lines (Figure 4.10). However, the plasma membrane-bound calcium-transporting ATPase (AT3G22910), the gene predicted to have a putative role in viability by its response to ATP and SA treatments (Figure 4.9A), showed a lower expression levels in both KO lines (Figure 4.10). This protein is involved in calcium transport across the plasma membrane, using ATP hydrolysis as an energy source, and has been reported to be differentially expressed with pathogen attack (Ascencio-Ibanez *et al.,* 2008), supporting its putative role in defence and HR cell death. Ligand-gate calcium channels, such as P2X purinoreceptors, mediate calcium signalling and usually are not required to change in abundance levels for their activity to be regulated, as regulating the amount of signalling transduced through them is the more common mechanism. A small downregulation in overall abundance of AT3G22910 could indicate significant changes in the ability of the cell to transduce calcium signalling in response to eATP (Jeter *et al.,* 2004; Song *et al.,* 2006; Tanaka *et al.,* 2010). Additionally, disruption of calcium-mediated signalling affects the resistance of tobacco to AMP-PCP induced cell death (Chivasa *et al.,* 2010), showing a direct connection between calcium signalling and eATP-mediated control of cell viability. Unfortunately, the state of calcium signalling cannot be inferred by a downregulation of one of its many plasma membrane channels, so further experiments done specifically to test this function in the KO mutants would be required to answer this question. Overall, these results show that eATP perception is not significantly affected in ATPaseβ KO lines, as this would produce an effect on all eARPs tested. However, the downregulation of AT3G22910 provides preliminary evidence for a role of this gene in FB1-induced cell death as well as for altered calcium signalling in ATPaseβ KO lines, providing possible avenues for future experiments using ATPaseβ KO lines. These markers can also be used to investigate differences in signalling downstream of eATP during FB1-induced cell death between Col-0 and ATPaseβ KO lines, providing another angle for investigating the mechanism of ATPaseβ KO resistance.

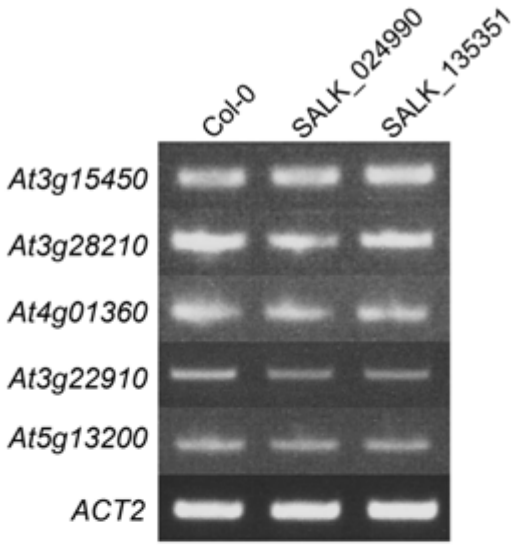

Figure 4.10 Gene expression of eATP molecular markers in Col-0 and ATPaseβ KO mutant lines. sqRT-PCR analysis of basal levels of 5 marker genes. Actin 2 (*ACT2*) was used as a constitutive reference control.

4.3.4.3 Cell death phenotypes of eATP molecular markers

In line with the goal of this thesis in identifying cell death genes regulated by eATP, I was curious in establishing if the eATP molecular markers identified in this chapter were also involved in cell death regulation using the conductivity-based cell death assay. Out of the 10 genes validated as markers (Figure 4.7), a total of 4 genes (AT1G61290, AT2G40000, AT3G15450 and AT4G01360) with one KO line available were obtained from the SALK collection and their cell death kinetics investigated using the conductivity assay (Table 4.9). However, none of the 4 lines tested showed any significant cell death phenotype following FB1 treatment indicating these genes don't have a role in cell death. One of the genes tested, AT3G15450, is proposed as an eATP-regulated gene involved in defence responses (Figure 4.9A) did not show an altered cell death phenotype. Unfortunately, no KO line was available for AT3G22910 plasma membrane-bound calcium-transporting ATPase, a gene with a putative function in cell viability (Figure 4.9A and Figure 4.10). An altered cell death phenotype in KO mutants for this gene would provide conclusive evidence that an experimental approach involving ATP and SA treatments could be used to identify novel cell death regulators similarly to the ATP filter. Nevertheless, this data further strengthens these genes as early eATP-mediated signalling markers, whose function still remains to be elucidated, that can be used in the eATP area.

Having identified genes that respond to alterations in eATP levels via a proteomic (Table 4.2) and a transcriptomic approach (Table 4.6) in this chapter, a pertinent question put forward was to examine the degree of overlap between these two lists.

4.4 Comparison between eATP-responsive genes and proteins from the DNA chip and proteomic datasets

It is known that changes in the transcriptome don't always result in changes in protein abundance (Gygi *et al.,* 1999; Hajduch *et al.,* 2010). In order to identify common genes between the two datasets, the two lists (Table 4.2 and Table 4.6) were cross-checked. No gene was found to be present in both datasets. Several possibilities could account for this finding. Firstly, it could be a result of the different lengths of time of the duration of the ATP treatment in the datasets. Secondly, it could be indicative of different transcriptional

Gene description	Gene locus[a]	SALK number[b]	NASC number[c]	T-DNA insertion location[d]	altered phenotype with FB1
syntaxin, putative (SYP124)	AT1G61290	SALK_111004	N667031	exon	no
expressed protein	AT2G40000	SALK_016065	N665365	exon	no
expressed protein	AT3G15450	SALK_037410	N660387	Promoter	no
expressed protein	AT4G01360	SALK_000131	N670978	3' UTR	no

Table 4.9 Cell death phenotype characterization of 4 eATP molecular markers. No line tested produced a significant phenotype. [a]Arabidopsis Genome Initiative (AGI) gene identifier [b]SALK number of homozygous T-DNA insertion lines mapped to the specific gene locus [c]line number for homozygous lines available at NASC. [d]Predicted T-DNA insertion site in each SALK line.

and translational controls of the eATP signalling response, where fast, but transient, increases in transcript abundance do not result in significant protein abundance changes. Thirdly, it could be the consequence of comparing results obtained from cell cultures where basal ATP signalling was undisturbed (proteomics) with cell cultures where basal eATP levels were significantly depleted with FB1 (DNA chip). Finally, it could be a consequence of the bias of 2D proteomics towards the identification of highly abundant proteins. This can happen in the spot detection step or in the protein identification step, where low abundance proteins have higher chances of not retrieving a confident hit. This last possibility is the most likely explanation, as the DNA chip dataset comprised of a significant amount of low abundance proteins such as transcription factors and protein kinases (Table 4.6) that are hard to detect in a TSP fraction by 2D-DiGE, a protein fraction dominated by highly abundant cytosolic proteins.

4.5 Conclusions

The mains objectives of this chapter were to identify new eATP-regulated genes and proteins that would help increase the understanding of eATP signalling at the molecular level, and to identify eATP-regulated genes to be used as molecular markers in the study of eATP signalling and its different physiological roles. For the identification of proteins regulated by an increase in eATP levels using a 2D-DiGE analysis of protein abundance in the TSP fraction, 4 independent biological replicates, as well as two technical replicates in a full dye swap experiment, were performed. A total of 35 unique proteins were identified as significantly changing with ATP treatment. ATP treatment was found to be differentially expressing proteins involved in a variety of metabolic functions. Using bioinformatic tools, molecular chaperones and chloroplast related proteins were observed as the most enriched classes of proteins in the dataset. Proteins in the photosynthetic carbon fixation pathway were all downregulated. These findings indicate major changes in the chloroplast happen upon perturbations in eATP-mediated signalling. The novelty of these findings was strengthened by the absence of literature or online databases annotations linking these genes with extracellular ATP in plants.

As a complementary study to the proteomics, the effects of ATP treatment on the whole genome were investigated by re-examination of a previously generated DNA chip experiment. eATP was found to be affecting many genes within 1 hour, in particular genes

that respond to chitin, genes involved in phenylpropanoid metabolism and genes involved in energy synthesis.

Importantly, the first early molecular markers for eATP signalling were validated by confirming the DNA chip predictions in cell cultures treated with ATP. These markers were subsequently used to test the hypothesis that eARPs involved in regulating viability respond differently to SA signalling than eARPs involved in defence (Chivasa *et al.,* 2009b). They also proved as useful tools in dissecting eATP signalling in the ATPaseβ KO mutants that are resistant to FB1. The lists of eATP-responsive genes and proteins generated in this chapter provide putative candidates involved in cell death regulation, as is shown by the identification of ATPaseβ, a confirmed cell death regulator, as an eATP-responsive protein. Part of the work in this chapter has been published in *Plant signalling and Behaviour*, (Chivasa *et al.,* 2009b) and a copy of that paper is presented in Appendix B.

Chapter 5 Identification of the UDP-glucose pyrophosphorylase as a novel cell death regulator in FB1-induced cell death

5.1 Introduction

Fumonisin B_1 causes cell death in plants. The mechanism by which it does so is not entirely understood, but involves a signalling component that is initiated by extracellular ATP depletion and can be blocked by the addition of exogenous ATP (Chivasa *et al.,* 2005a). As was shown in chapter 3, FB1 treatment resulted in changes in protein abundance that arise from its ability to trigger eATP depletion, because such changes could be reversed by the addition of exogenous ATP. The hypothesis put forward in chapter 3 that proteins with this response profile might be a critical component of FB1 cell death signalling was confirmed with the identification of the ATPaseβ cell death regulator.

In addition, FB1 also triggered changes in protein abundance that were not reversed by ATP treatment, implicating that this toxin has physiological effects that are unrelated to its ability to trigger eATP depletion. Proteins with this abundance profile constitute an eATP signalling-independent component of the FB1 response of *Arabidopsis thaliana* (*Arabidopsis*) cell cultures. It is not known if these proteins are involved in FB1-induced cell death (Figure 5.1). However, their putative role in FB1-induced cell death inception can be specifically tested by reverse genetics and this provides a targeted experimental approach for identification of cell death regulators independent eATP-mediated signalling in FB1-induced cell death.

The goal of this chapter is to identify cell death regulators of FB1-induced cell death that are specifically regulated by FB1 treatment at the protein abundance level. A list of these genes will be constructed based on the proteomic data already obtained from the 2D-DiGE experiment from chapter 3, where several proteins were found to be specifically regulated by FB1 independent of its ability to trigger eATP depletion. The list candidate genes will provide the basis for systematic screening of their homozygous KO mutants for an altered cell death phenotype with FB1 treatment using the conductivity assay.

In this chapter, the UDP-glucose pyrophosphorylase (*UGP1*) is identified as a novel plant cell death regulator whose expression is governed by FB1. The abolishment of its expression in *UGP1* KO lines results in a remarkable FB1-resistant phenotype. This phenotype was observed using the conductivity assay and FB1 leaf infiltration assays. This gene is not required for AMP-PCP triggered cell death, suggesting it operates independently of eATP signalling if AMP-PCP does indeed initiate cell death by the same mechanism as eATP depletion. Further characterization of the KO lines produced evidence

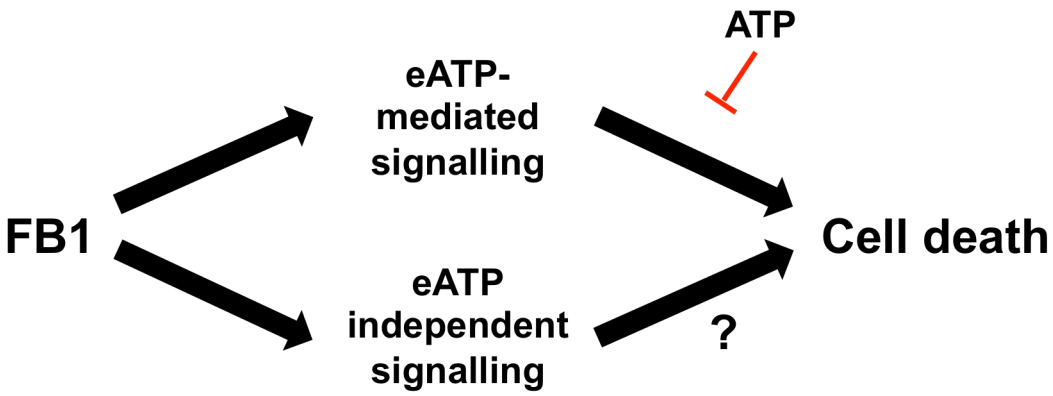

Figure 5.1 The different signalling events initiated by FB1. Signalling events triggered by complete elimination of eATP, or reduction of eATP concentrations below a certain threshold level, result in cell death. Cell death can be blocked by the addition of ATP to FB1 treated cultures, showing that eATP signalling is a critical component. Signalling events initiated by FB1 that are not regulated by eATP signalling might also mediate cell death in plants.

for altered eATP-mediated signalling perception and a possible role of *UGP1* in the pathogen-induced HR. Moreover, a serendipitous observation was made that increased sucrose levels accelerate FB1-induced cell death in cell cultures and whole leaves. This is a novel observation not previously reported in the literature. Since the *UGP1* transcript is specifically upregulated by sucrose-mediated signalling, it was investigate if this upregulation of *UGP1* was in any way connected with the observed sucrose effect on FB1-induced cell death. Remarkably, it was found that the upregulation of this one gene by sucrose is sufficient to explain the acceleration of FB1-induced cell death in plants. Although *UGP1* is the main producer of UDP-glucose in plants, cell cultures treated with a combination of UDP-glucose and FB1 did not display the accelerated cell death observed when *UGP1* is upregulated by sucrose, providing correlative evidence for a secondary cell death role of the UGP1 protein.

5.2 Results

5.2.1 FB1-regulated putative cell death genes

The experimental approach employed for selecting FB1-specific proteins, that are changing at the time of cell death commitment (48 hours after FB1 treatment) from the proteomic data from chapter 3, can be described as an "inverse ATP filter" approach: i.e. proteins that are differentially regulated by FB1 and not by ATP treatment in the FB1+ATP treated cell cultures. Such a response profile shows they are not regulated by eATP-mediated signalling and therefore make up the eATP-independent signalling component of the FB1 response that might play a role in cell death (Figure 5.1). The full lists of identified proteins obtained from the TSP and microsomal protein fractions from chapter 3 were filtered for FB1-specific proteins using the "inverse ATP filter". Proteins that were identified in more than one spot were considered as non-responsive to ATP only if all of their spots were not reversed following ATP treatment. This was necessary to avoid including proteins that have at least one PTM form which is responsive to ATP, as these were previously considered as reversed following ATP treatment and already tested for an altered cell death phenotype in chapter 3. The lists from the two protein fractions were combined and a total of 49 unique proteins were found to be specifically regulated by FB1 (Table 5.1). The SALK collection was then searched for homozygous KO lines for all these genes and a total of 25 independent homozygous lines corresponding to 18 unique

Gene locus	Protein name
AT1G04820	**alpha tubulin isoform**
AT1G19570	**dehydroascorbate reductase**
AT1G53540	17.6 kDa class I small heat shock protein
AT1G56070	translation elongation factor 2-like protein
AT1G62380	**ACC oxidase**
AT1G77120	alcohol dehydrogenase
AT1G78900	subunit A of the vacuolar ATP synthase
AT1G79550	cytosolic phosphoglycerate kinase (PGK)
AT1G79930	**high molecular weight heat shock protein**
AT2G21250	putative mannose 6-phosphate reductase
AT2G21870	unknown protein mitochondrial
AT2G27020	20S proteasome subunit PAG1
AT2G30110	ubiquitin-activating enzyme (E1)
AT2G36460	**putative fructose-bisphosphate aldolase**
AT2G44060	late embryogenesis abundant family protein
AT3G02090	metalloendopeptidase (MPPBETA)
AT3G03250	**UGP1 (UDP-glucose pyrophosphorylase 1)**
AT3G08590	putative phosphoglycerate mutase
AT3G09440	**heat shock cognate 70 kDa protein 3**
AT3G09840	cell division cycle protein
AT3G12580	**heat shock protein 70 (HSP70)**
AT3G14990	**thiazole monophosphate biosynthesis protein**
AT3G16640	translationally controlled tumor protein
AT3G17820	**glutamine synthetase**
AT3G22110	alpha-3 subunit of 20s proteasome
AT3G23400	plastid-lipid associated protein
AT3G29360	**putative UDP-glucose 6-dehydrogenase**
AT3G52300	**ATP synthase D chain**
AT3G52880	**monodehydroascorbate reductase**
AT3G58610	ketol-acid reductoisomerase
AT3G60750	putative transketolase
AT3G60820	20S proteasome beta subunit PBF1
AT3G60830	actin-related protein
AT4G01850	S-adenosylmethionine synthetase 2
AT4G13430	Isopropyl malate isomerase large subunit 1
AT4G25200	AtHSP23.6-mito
AT5G02500	heat shock cognate protein 70-1
AT5G03340	**putative cell division cycle protein 48**
AT5G08670	mitochondrial ATP synthase beta-subunit
AT5G09590	heat shock protein 70 (Hsc70-5)
AT5G09810	actin 7
AT5G15450	**chloroplast-targeted Hsp101 homologue**
AT5G16970	**2-alkenal reductase (EC 1.3.1.74)**
AT5G17920	cobalamin-independent methionine synthase
AT5G40770	prohibitin 3
AT5G53460	**NADH-dependent glutamate synthase**
AT5G56010	heat shock protein 90 (HSP90)
AT5G56030	heat shock protein 90 (HSP90)
AT5G59880	**actin depolymerizing factor 3**

Table 5.1 Proteins differentially regulated by FB1 only. This list was constructed based on the protein identification tables of the TSP and microsomal protein fractions from chapter 3. For proteins that were identified as multiple spots, only the ones where all spots showed no significant response to ATP treatment were considered as specifically regulated by FB1. Genes tested for a role in FB1-induced cell death by reverse genetics are highlighted in bold.

Gene description	Gene locus[a]	SALK number[b]	NASC number[c]	T-DNA insertion location[d]	Fraction identified[e]	altered FB1 phenotype
alpha tubulin isoform	AT1G04820	SALK_116587	N658379	5' UTR	TSP	no
alpha tubulin isoform	AT1G04820	SALK_080530	N660493	exon	TSP	no
dehydroascorbate reductase	AT1G19570	SALK_008446	N661410	intron	TSP	no
ACC oxidase	AT1G62380	SALK_027311	N665638	intron	TSP	no
high molecular weight heat shock protein	AT1G79930	SALK_082815	N663129	exon	Microsomal	no
putative fructose-bisphosphate aldolase	AT2G36460	SALK_014964	N659199	intron	TSP	no
putative fructose-bisphosphate aldolase	AT2G36460	SALK_015402	N661598	5' UTR	TSP	no
UGP1 (UDP-glucose pyrophosphorylase 1)	AT3G03250	SALK_020808	N658122	intron	TSP	Yes
UGP1 (UDP-glucose pyrophosphorylase 1)	AT3G03250	SALK_100183	N658355	exon	TSP	Yes
heat shock cognate 70 kDa protein 3	AT3G09440	SALK_013280	N667811	5' UTR	TSP	no
heat shock protein 70 (HSP70)	AT3G12580	SALK_088253	N655706	5' UTR	TSP+ Microsomal	no
heat shock protein 70 (HSP70)	AT3G12580	SALK_141521	N667499	Promotor	TSP+ Microsomal	no
thiazole monophosphate biosynthesis protei	AT3G14990	SALK_049637	N656477	5' UTR	TSP	no
glutamine synthetase	AT3G17820	SALK_148604	N669232	exon	TSP	no
putative UDP-glucose 6-dehydrogenase	AT3G29360	SALK_098492	N668721	Promotor	TSP	no
ATP synthase D chain	AT3G52300	SALK_060067	N657214	3' UTR	Microsomal	no
ATP synthase D chain	AT3G52300	SALK_102630	N658362	3' UTR	Microsomal	no
monodehydroascorbate reductase	AT3G52880	SALK_145224	N657464	exon	TSP	no
monodehydroascorbate reductase	AT3G52880	SALK_034893	N662081	exon	TSP	no
putative cell division cycle protein 48	AT5G03340	SALK_023524	N665544	exon	TSP	no
chloroplast-targeted Hsp101 homologue	AT5G15450	SALK_071985	N671512	5' UTR	Microsomal	no
chloroplast-targeted Hsp101 homologue	AT5G15450	SALK_128214	N672069	5' UTR	Microsomal	no
2-alkenal reductase (EC 1.3.1.74)	AT5G16970	SALK_005324	N667693	Promotor	TSP	no
NADH-dependent glutamate synthase	AT5G53460	SALK_115735	N667102	exon	TSP	no
actin depolymerizing factor 3	AT5G59880	SALK_139265	N664149	intron	TSP	no

Table 5.2 Testing of eATP-independent putative cell death genes using the conductivity assay. Genes identified as responding to FB1 only were tested for an altered cell death phenotype with FB1 using *Arabidopsis* T-DNA KO homozygous lines. [a]Arabidopsis Genome Initiative (AGI) gene identifier. [b]SALK number of homozygous T-DNA insertion lines mapped to the specific gene locus. [c]Line number for homozygous lines available at NASC. [d]Predicted T-DNA insertion site in each SALK line. [e]Protein fraction the protein was identified as differentially expressed with FB1 treatment in chapter 3.

genes were tested during the course of this study (Table 5.2). All KO lines obtained were screened for an altered cell death phenotype with FB1 using the conductivity assay. Only the SALK_020808 and SALK_100183 lines, highlighted in grey in Table 5.2 and predicted to be knocked out for the UDP-glucose pyrophosphorylase (*UGP1)* gene (AT3G03250), displayed enhanced resistance to FB1-induced cell death. Evidence for this is presented bellow.

The lack of a cell death phenotype with FB1 in the KO lines for the other candidate genes can have two different explanations. Firstly, proteins regulated by FB1 participate in non-cell death related processes, such as growth retardation and slowing down of metabolism that precedes cell death (Chivasa *et al.,* 2005a). Secondly, even if the protein plays a role in cell death, high gene redundancy for a particular gene can prevent a cell death phenotype from being observed in single KO lines. For example, the high molecular weight heat shock protein (AT1G79930) has at least 25 family members and the putative cell division cycle protein 48 (AT5G03340) has at least 17 family members in *Arabidopsis*.

5.2.2 The effects of *UGP1* on FB1-induced cell death.

The *UGP1* knockout mutants used in this study, SALK_020808 and SALK_100183, have predicted T-DNA inserted into an intron and exon, respectively, as is schematically depicted in Figure 5.2A. Inhibition of *UGP1* expression in the KO lines was confirmed by sqRT-PCR using the primers F-UGP1 and R-UGP1. A significant reduction in the level of PCR product in SALK_020808 indicated it to be a partial KO while the complete absence of the expected product in SALK_100183 confirmed it to be a complete KO (Figure 5.2B). The ability of cells to splice out T-DNA sequences inserted into introns during mRNA processing can lead to varying levels of reduced expression of the targeted gene (Ulker *et al.,* 2008). The low level of *UGP1* expression of SALK_020808 could therefore be related to inefficient splicing of the last intron containing the T-DNA insert (Figure 5.2B). The cell death kinetics of leaf tissue of the *ugp1* mutant lines in comparison wildtype plants was established using the conductivity assay. Using this assay, it was observed that the extent of FB1-induced cell death was significantly diminished in both *ugp1* lines (Figure 5.2C), showing that they were resistant to FB1 treatment. The low expression level of *UGP1* in the SALK_020808 knockdown line produced the same effect in its cell death response as the complete KO, showing that the residual levels of this protein are not sufficient to

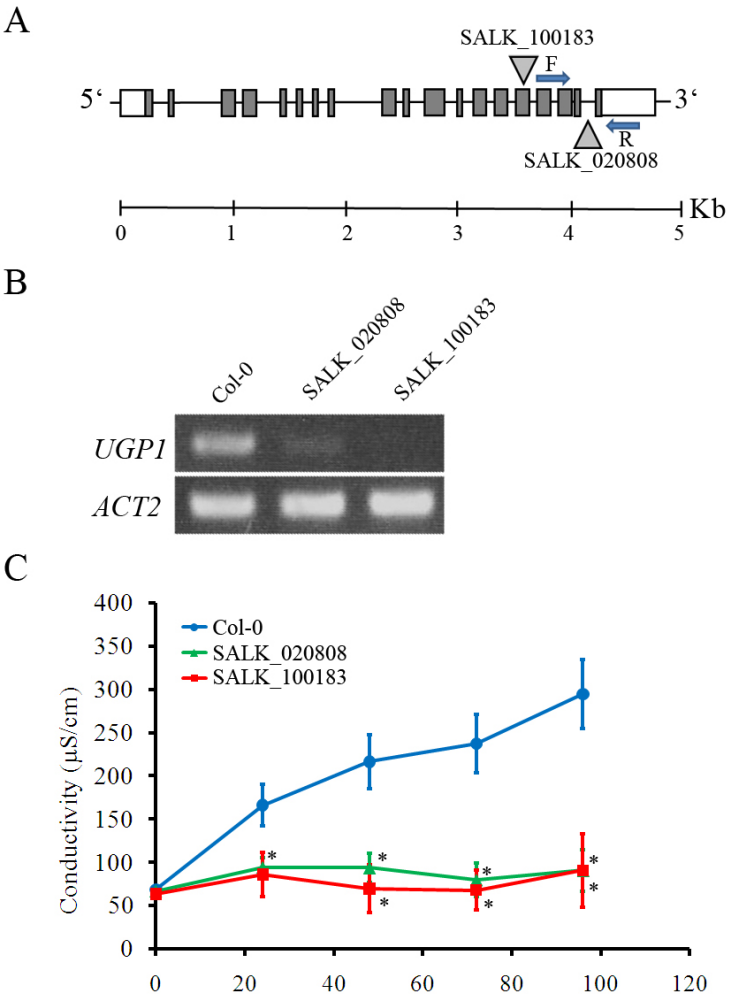

Figure 5.2 *UGP1* is required for FB1-induced cell death. (A) Schematic diagram showing predicted T-DNA insertion sites of *UGP1* KO mutants SALK_020808 and SALK_100183. The insertion sites are indicated by the triangles and grey and white boxes denote exons and untranslated regions, respectively. The locations of F-UGP1 (F) and R-UGP1 (R) primers are indicated by arrows. The kilobase (Kb) scale shows the relative lengths of the different element of the gene. (B) sqRT-PCR amplification of the 307 bp *UGP1*-specific gene product from cDNA samples derived from Col-0 and the two T-DNA lines using F-UGP1 and R-UGP1. SALK_100183 is shown to be a complete knockout whereas SALK_020808 a partial knockout. Actin-2 (*ACT2*) was used as a constitutive reference control. (C) Cell death timecourse of leaf disks floated on 10 µM FB1 solutions. The conductivity of the solution was measured every 24 h after a 48 h dark incubation and numbers indicate hours after light exposure. Values and error bars represent means ± SE (n = 3). An asterisk denotes data points at which mutant lines are significantly ($p \leq 0.01$) lower than Col-0.

enable normal cell death initiation. These results demonstrate that the UDP-glucose pyrophosphorylase is an essential factor that enables FB1 to trigger cell death.

Genotyping of the T-DNA insertions was performed to show that both lines are homozygous for the annotated T-DNA insert. It was important to perform genotyping of the lines, especially the SALK_020808 knockdown line as its knockdown of the *UGP1* transcript (Figure 5.2B) could indicate that the line was actually heterozygous for the T-DNA insert. New primers were designed to specifically flank each insertion site and were used for genotyping of each line. Primers L1 and R1 were designed to flank the insertion site in the SALK_100183 line and primers L2 and R2 designed to flank the insertion site in the SALK_020808. PCR analysis on genomic DNA revealed that Col-0 successfully amplified both gene-specific sequences. Each mutant line failed to amplify the gene specific product containing the T-DNA insert, but successfully amplified the T-DNA specific sequence product using the T-DNA specific primer LBa1 with its respective gene specific primer (Figure 5.3). This confirmed that both lines were homozygous for the reported insertion and that the low expression of *UGP1* in the SALK_020808 is most likely due to a small proportion of the intron harbouring the T-DNA insert being successfully excised from the mature mRNA.

In addition to the conductivity assay, the *UGP1* KO line SALK_100183 was tested for an altered cell death phenotype using two qualitative cell death assays: leaf infiltration assay and Evans Blue staining assay. The SALK_100183 line was chosen for these assays because this one is the complete KO line (Figure 5.2B). In the leaf infiltration assay, 4-5 week old *Arabidopsis* leaves of Col-0 and SALK_100183 were completely infiltrated with a 10 μM FB1 solution using a syringe without a needle and cell death symptom development monitored daily. 4 days after infiltration, Col-0 tissue was dead and shrivelled whereas the SALK_100183 leaves only showed very small patches of chlorosis in the infiltrated tissue (Figure 5.4A). Additionally, Evans Blue staining, a dye that infiltrates dead cells killed by FB1 but is kept out of living cells due to their intact plasma membrane, was used to directly visualize cell death in the tissue (Chivasa *et al.,* 2005a). Due to these characteristics, Evans Blue can be used as a means of direct visualization of cell death at the individual cell scale i.e. death of isolated cells surrounded by living cells. Undetached leaves from Col-0 and SALK_100183 were infiltrated with 5 μM FB1 and left for 48 hours in normal growth conditions, a length of time that under the growth conditions used no cell

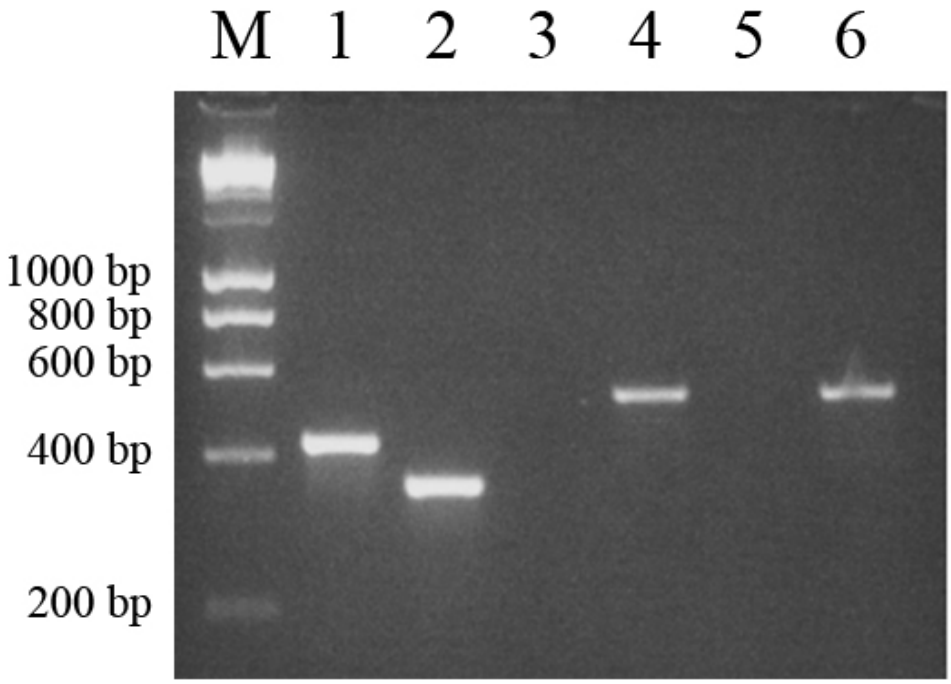

Figure 5.3 Genotyping of *UGP1* KO mutants. SALK_020808 and SALK_100183 successfully amplified a T-DNA left boarder-gene specific PCR product (Lanes 4 and 6) and failed to amplify the gene specific product (Lanes 3 and 5) that was successfully amplified in the Col-0 (Lanes 1 and 2), confirming they are homozygous for the T-DNA insertion. Legend: M- Hyperladder I Marker, 1- L2+R2 Col-0 DNA, 2- L1+R1 Col-0 DNA, 3- L2+R2 SALK_020808 DNA, 4- L2+LBa1 SALK_020808 DNA, 5- L1+R1 SALK_100183 DNA, 6- R1+LBa1 SALK_100183 DNA. The predicted band sizes for the primer combinations used are: L2+R2 - 432 bp; L1+R1 – 354 bp; L2+LBa1 – 558 bp; R1+LBa1 – 547 bp.

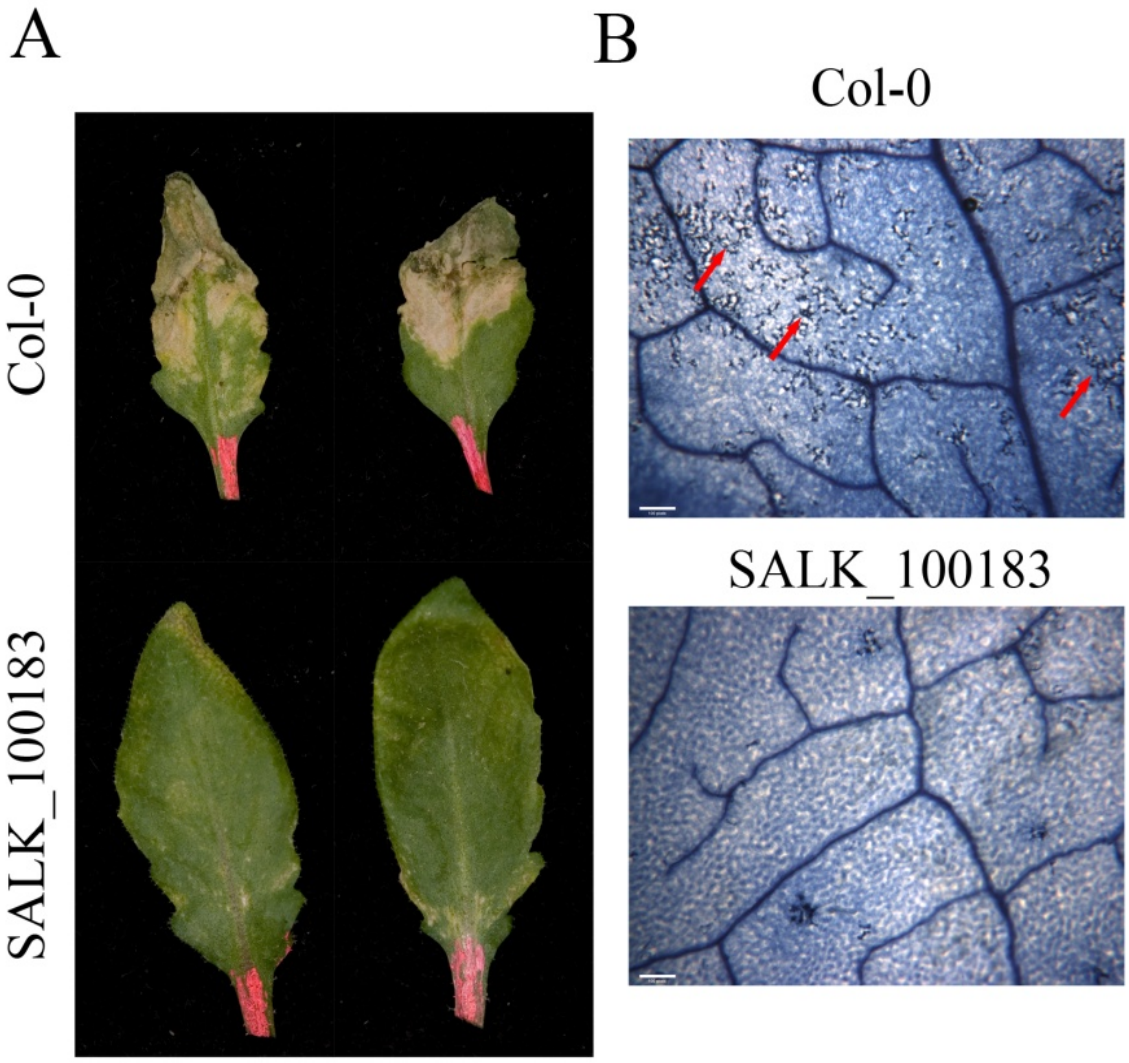

Figure 5.4 *UGP1* KO lines are resistant to FB1-induced PCD. (A) Appearance of leaves 4 days after infiltration with 10 µM FB1. The red colour in the petiole is from the markers used to label the infiltrated leaves. (B) Cell death of individual cells visualized by Evans blue staining. Leaves were infiltrated with 5 µM FB1 and stained with Evans blue 48 hours later. Cell death is visible in mesophyll cells located between vascular tissue bundles and is only seen in the Col-0 (red arrows). Mock infiltrated controls showed no visible cell death. The 3 patches of stained cells in the SALK_100183 are dead cells that make up the trichome pedestal. Scale bar indicates 0.1 mm.

death symptoms are visible in Col-0. Leaf disk were then corked from the infiltrated tissue and stained with Evans Blue. It was observed that Col-0 already showed significant numbers of dead mesophyll cells. These are visible as strong accumulations of Evans blue dye in between the vascular tissues (Figure 5.4B). As expected, SALK_100183 showed no visible cell death in mesophyll cells apart from the trichome pedestals (Figure 5.4B). Both these results are in agreement with the conductivity data (Figure 5.2C) and further demonstrate the resistant cell death phenotype of *ugp1* mutants.

5.2.3 The UDP-glucose pyrophosphorylase is a novel cell death regulator

Using a combination of proteomics, reverse genetics and FB1 treatments, *UGP1* was identified as a previously unknown regulator of FB1-induced cell death. *UGP1* is a key cytosolic enzyme in carbohydrate metabolism and plays an important role in the synthesis of UDP-glucose, a precursor of cellulose, calose and sucrose (Amor *et al.,* 1995; Kleczkowski *et al.,* 2004). In mature leaves, it is primarily involved in generating sucrose for export whereas in non-photosynthetic tissues it synthesizes UDP-glucose from sucrose (Huber and Akazawa 1986). The production of UDP-glucose by *UGP1,* and its highly homologous family member *UGP2*, is essential for normal growth and development of *Arabidopsis*. Although single knockout mutants for either *UGP1* or *UGP2* display normal development (Meng *et al.,* 2009; Park *et al.,* 2010), a double knockout mutant for both genes had a reduction of 52% in UDP-glucose content and displays a severe reduction in growth, delayed flowering and male sterility (Park *et al.,* 2010). The double KO phenotype could be rescued by gene complementation or UDP-glucose feeding, indicating that reduced levels of UDP-glucose are responsible for the growth phenotype observed (Park *et al.,* 2010). Results from this chapter (Figure 5.2 and 5.4) now reveal that, in addition to its primary metabolic function, *UGP1* has a cell death regulatory role in *Arabidopsis*.

5.2.3.1 UGP1 does not play a role in eATP signalling in cell death

The resistant phenotypes of the *ugp1* mutants to FB1 clearly show *UGP1* is required for FB1-induced cell death. They do not, however, show if this cell death role is connected with eATP signalling events that are critical during FB1-induced cell death. I was curious to investigate if *UGP1* could be involved in eATP-mediated signalling. From the 2D-DiGE data obtained in chapter 3, it is clear that the UGP1 protein is not regulated by ATP treatment at the protein abundance level and this suggests *UGP1* is not located downstream

of eATP signalling events during cell death elicitation. Instead, *UGP1* might be located upstream of eATP signalling events or belong of a completely different pathway specifically required by FB1 during FB1-induced cell death. Depletion of eATP using exogenous ATP degrading enzymes or treatment with the non-hydrolysable ATP analogue, AMP-PCP, causes cell death in *Arabidopsis* (Chivasa *et al.,* 2005a). Due to the recalcitrant nature of its gamma phosphate, AMP-PCP inhibits eATP-mediated signalling initiated by ATP hydrolysis. AMP-PCP could be initiating cell death by blocking reactions in the ECM that require ATP hydrolysis, or by a different mechanism. It is not entirely clear if AMP-PCP causes cell death exclusively by inhibiting eATP-mediated signalling that requires ATP hydrolysis, but this is likely be an important component in the mechanism. Therefore, the analogue can be used as a quick and easy tool to determine if a cell death regulator is required in downstream signalling events that lead to AMP-PCP induced cell death. The rational for this is the following. If a gene is required for PCD progression downstream of signalling events controlled by eATP levels, KO mutants for this gene should produce an altered cell death phenotype following AMP-PCP treatment as well as FB1 treatment. If the gene operates independently of eATP signalling events in FB1-induced cell death, it should not affect signalling initiated by AMP-PCP treatment and so KO mutants for the gene won't display an altered cell death phenotype following AMP-PCP treatment.

The effects of AMP-PCP treatment on cell death induction were tested in hydroponically grown seedlings, using Evans blue staining to visualize cell death. Col-0 and SALK_100183 seedlings were grown in hydroponic conditions for 5 days. When grown in high humidity conditions, such as in liquid medium, cuticle development is suppressed (Thomas *et al.,* 2000), making their ECM accessible to the liquid medium they are growing in. Therefore, treatments applied to the medium come in direct contact with the plasma membrane of the seedling's tissues. The seedlings were treated with increasing concentrations of AMP-PCP in order to determine the concentration at which AMP-PCP starts to cause cell death in Col-0 and SALK_100183 seedlings. The concentration range between 0 μM and 800 μM AMP-PCP was used. Evans blue was used to stain for dead cells in the cotyledons of seedlings and multiple seedlings per treatment were used for increased confidence in the results. At concentrations of 200 and 300 μM, no lesions were visible in either Col-0 or SALK_100183 (Table 5.3). At 400 μM, the analogue was causing extensive cell death lesions in all cotyledons in both Col-0 and SALK_100183 seedlings (Table 5.3). These results clearly show that *UGP1* does not mediated cell death signalling

	AMP-PCP concentrations		
Line	**200 µM**	**300 µM**	**400 µM**
Col-0	0 out of 12	0 out of 14	12 out of 12
SALK_100183	0 out of 14	0 out of 14	16 out of 16

Table 5.3 *UGP1* KO line SALK_100183 shows no significant altered cell death phenotype with AMP-PCP treatment in *Arabidopsis* seedlings. Cell death was monitored by Evans Blue staining as in Figure 5.4B. Cotyledons were scored as positive for cell death if one or more lesions were visible. A total of 8 seeds were sterilized and grown in 2 flasks containing half strength MS10 media. Numbers of total cotyledons observed per treatment in Col-0 and SALK_100183 are shown on the right of each cell.

initiated by exposure to AMP-PCP, suggesting it is not a component of the cell death signalling cascade initiated by eATP depletion. Therefore *UGP1* is either a component of an FB1-specific signalling pathway or is invoked before eATP depletion in FB1-induced cell death.

5.2.4 Further characterization *UGP1* KO mutants

In order to gain further insight into the mechanism of *UGP1* in cell death, I was curious to test if eATP-mediated signalling is affected in the KO lines using the eATP molecular markers identified from chapter 4. Additionally, I was curious to see if *UGP1* plays a role in pathogen-induced cell death using *Pseudomonas syringae* DC3000, a natural pathogen of *Arabidopsis* (Katagiri *et al.,* 2002), in order to establish if it is important in HR cell death in addition to its role in FB1-induced cell death.

5.2.4.1 UGP1 KO mutants show altered eATP-mediated signalling

A possible function for *UGP1* during FB1-induced cell death could be related to a secondary gene expression role, particularly in eATP regulated genes that could play a role in cell death signalling. Semi-quantitative PCR analysis was used to determine the expression levels of the eATP molecular markers identified previously in chapter 4. Leaf tissue from 4-week soil grown Col-0, SALK_100183 and SALK_020808 were collected for RNA extraction. Leaf samples consisted of 3 leaves of equal size from 3 independent plants to prevent skewing of the results if a single plant that had previously been subject to stress during growth, such as drought stress, was unintentionally used. The basal expression of levels of 5 markers identified in chapter 4 were measured and 3 of them (AT3G28210, AT4G01360 and AT3G22910) showed differences in the SALK_100183 line (Figure 5.5). For the markers AT4G01360 and AT3G22910, no differences were detected between Col-0 and SALK_020808. This might be related to the fact that this line is not a complete KO of *UGP1* (Figure 5.2B). Although a reduction of *UGP1* still blocks FB1-induced cell death, it is enough to enable normal expression of these genes. Only for the AT3G28210 gene did its basal expression level correlate with the abundance of *UGP1* transcript, with its expression in the SALK_020808 line being in-between Col-0 (highest abundance) and SALK_100183 (lowest abundance) (Figure 5.5). Although the gene expression changes reported here are not dramatic, the results provide preliminary evidence for a novel gene expression role for *UGP1*.

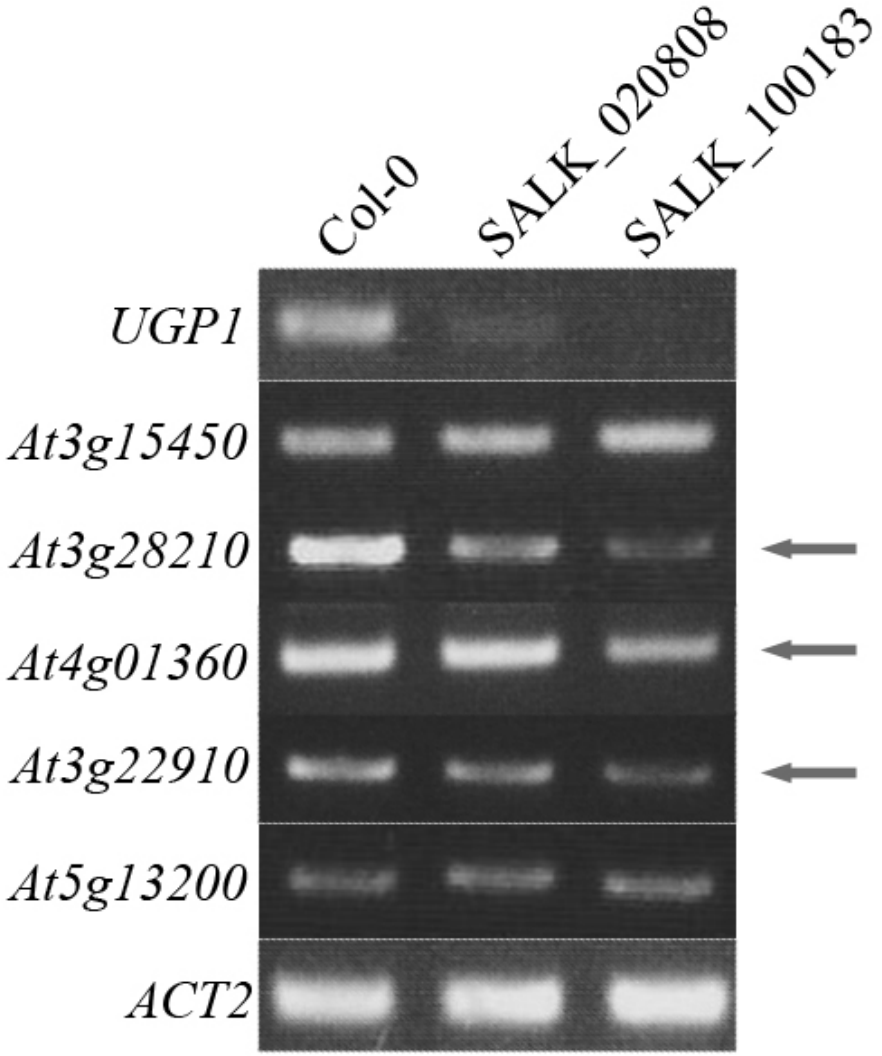

Figure 5.5 Basal expression levels of 5 extracellular ATP molecular markers in Col-0, SALK_020808 and SALK_100183. Expression levels were analysed by sqRT-PCR and the 3 that are showing significant changes in the SALK_100183 line are indicated by arrows. Actin-2 (*ACT2*) was used as a constitutive reference control. Experiment was performed twice with similar results.

The significance of this gene expression role of *UGP1* in FB1-induced cell death remains to be investigated.

The eATP molecular markers were identified solely because they are regulated by eATP signalling and it is not known if they play a role in cell death. Of these three genes that are downregulated in the *UGP1* complete KO line, (AT3G28210, AT4G01360 and AT3G22910), only the AT4G01360 was previously tested for an altered cell death phenotype in chapter 4, but showed no significant cell death phenotype following FB1 treatment. At least for this gene, it is clear that it does not have a role in cell death, but for the other this remains to be seen. Overall, these results show that these eATP markers are downstream of *UGP1*, providing evidence that *UGP1* can regulate gene expression that could overlap with eATP-mediated signalling events. It remains to be shown if *UGP1*- and eATP-mediated signalling can converge on cell death regulators during cell death and if this is related to the resistant phenotype of *ugp1* mutants to FB1.

5.2.4.2 UGP1 is involved in pathogen-induced HR

Since *UGP1* KO lines are resistant to the pathogen-derived toxin FB1, I was curious to test if this gene is also important in cell death directly elicited by a living plant pathogen. The *Pseudomonas syringae* pv. tomato DC3000 expressing the *avrRpm1* avirulence gene was selected because it activates HR cell death due to the recognition of the pathogen avirulence gene by the *RPM1* plant resistance gene in a incompatible interaction (Jones *et al.,* 2006), revealing if *UGP1* plays a role in HR during effector-triggered immunity. 1-day old bacteria colonies grown on a plate were used to make a solution containing 10^7 cfu/ml. This solution was then infiltrated into 10 independent 4-week old Col-0 and SALK_100183 plants. Four leaf disks were immediately taken from the infiltrated leaf of each plant and grouped into 4 replicas, each containing 1 disk from one of the 10 plants. The conductivity of the MQ water where the leaf disks were floated was measured every hour (Figure 5.6). Cell death initiated approximately 3 hours after infiltration and at 8 hours the ion leakage was starting to stabilize in both lines. Cell death in the SALK_100183 line was significantly ($p \leq 0.01$) lower than in Col-0 from 3 hours onwards (Figure 5.6) and was most obvious at the 3 hour timepoint, where the conductivity of SALK_100183 was 63% of Col-0, possibly indicating a delay in HR initiation. The extent of cell death in the SALK_100183 line was also lower than in Col-0, since 8 hours after infiltration SALK_100183 conductivity stabilized at 90% of Col-0 (Figure 5.6).

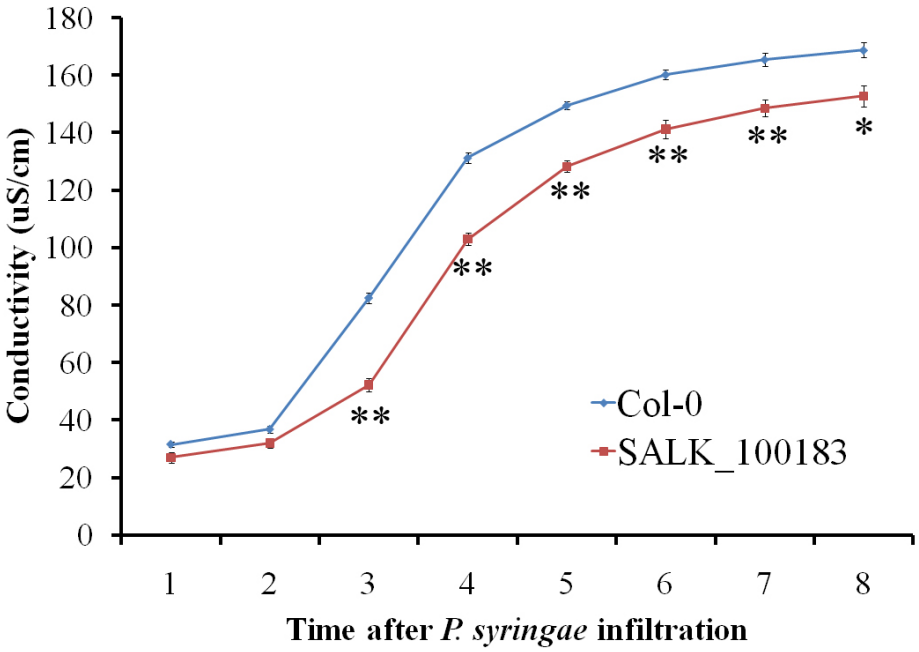

Figure 5.6 *UGP1* functions in the hypersensitive response. Partial pathogen resistance is achieved through elimination of *UGP1* function. Avirulent *Pseudomonas syringae* solution containing 10^7 cfu/ml was infiltrated into leaves and leaf discs were immediately taken and floated on MQ water. Thereafter, conductivity of the MQ water was measured every hour up to 8 hours. Mean conductivity values are shown and error bars indicate ± SE (n = 4). An asterisk denotes data points at which mutants are significantly ($p \leq 0.05$) lower than Col-0 and two asterisks indicate a stronger significance ($p \leq 0.01$).

Overall, the results show that *UGP1* can contribute to the HR response in *Arabidopsis* Col-0 induced by *Pseudomonas syringae* expressing the *avrRpm1* gene. How *UGP1* plays a role in effector-triggered HR cannot be inferred from the conductivity assay. It could be that UDP-glucose production by *UGP1* is necessary for efficient recognition of the pathogen effector or bacterial effector delivery.

5.2.4.3 Possible mechanisms of UGP1 regulation of FB1-induced cell death

UGP1 could function in cell death in two possible ways. Firstly, *UGP1* could have an unknown biochemical activity or signalling property conferring its secondary function in cell death control. Other proteins have previously been shown to have a secondary function in PCD. Cytochrome *c* is an essential component of the mitochondrial electron transport chain transferring electrons between complex III and IV (Garrett *et al.,* 2010). In animals, it also has a secondary function when it translocates from mitochondria to the cytosol in order to participate in the assembly of the apoptosome together with Apaf-1 and caspase-9 initiating apoptosis (Li *et al.,* 1997). The hexokinase protein phosphorylates glucose into glucose-6-phosphate in the initial step of glycolysis. Additionally to this function, hexokinase has an anti-PCD function when it associates itself with the mitochondrial membranes in plants (Kim *et al.,* 2006a). Evidence suggesting a secondary function specific to *UGP1* in FB1-induced cell death is the absence of gene redundancy between *UGP1* and its other family member *UGP2*. Although *UGP2* is constitutively expressed in leaf tissues (Meng *et al.,* 2009), it is unable to replace *UGP1* in the *ugp1* mutants (Figure 5.2C), even though it bears similar metabolic functions to *UGP1*. Both genes code for proteins with conserved amino acid residues essential for their catalytic activity (McCoy *et al.,* 2007) and have specific UDP-glucose pyrophosphorylase activity with slight differences in substrate affinity and reaction kinetics (Meng *et al.,* 2008). Both *UGP1* and *UGP2* are simultaneously expressed in all plant tissues and genetic studies on *ugp1* and *ugp2* loss-of function mutants found no differences in their levels of soluble sugars (Meng *et al.,* 2009). Additionally, no differential morphological phenotype relative to wildtype was observed at any stage of development (Park *et al.,* 2010), demonstrating metabolic redundancy between the two genes. There are some differences between these genes at the protein level that could account for a secondary function specific to *UGP1*. *UGP1* and *UGP2* have a 92% identity at the aminoacid levels and this difference resulted in only 5

out of 8 putative phosphorylation motifs being shared between the two proteins (Meng *et al.,* 2008). The existence of unique phosphorylation putative motifs in *UGP1* opens the possibility for a secondary function involved in the promotion of cell death that is not present in *UGP2*, but this hypothesis requires further characterization of the putative sites and their possible role in cell death.

Second, *UGP1* might be involved in regulating SA signalling. SA is required for FB1 cell death (Asai *et al.,* 2000) and plants with altered SA levels display altered cell death kinetics that correlate with the amount of SA in the tissue (Greenberg *et al.,* 1994; Lawton *et al.,* 1995). Studies on transgenic hybrid poplar have shown that overexpression of a UDP-glucose pyrophosphorylase resulted in a 270-fold accumulation of the glycoside of salicylic acid, an inactive form of SA, and these plants displayed a typical defence response phenotype consisting of impaired growth rates, substantially smaller leaves and increase in cellulose content (Coleman *et al.,* 2007). The glycoside of salicylic acid has been shown to accumulate in the presence of SA after pathogen attack (Lee and Raskin 1999). It is reasonable to speculate that the opposite scenario could be happening in the FB1-resistant *ugp1* mutants – the absence of the *UGP1* protein could reduce the accumulation of SA required for FB1-induced cell death. If this is the case, such a phenotype would impair SA signalling during FB1 treatment and result in a FB1-resistant phenotype. Because SA mediates defence responses to pathogens (Gaffney *et al.,* 1993; Delaney *et al.,* 1994), the SA connection could indicate *UGP1* also plays a putative function in pathogen-induced cell death, which was found to be the case for *Pseudomonas syringae* DC3000 expressing the *avrRpm1* gene (Figure 5.6). In further support of this hypothesis, other FB1-resistant mutants with enhanced resistance to bacterial pathogens have been previously reported (Stone *et al.,* 2000). This indicates communality between the signalling events in HR and FB1-induced cell death.

5.3 Accidental discovery of the effect of sucrose on FB1-induced cell death

During the course of this study, it was noticed that in one experiment with cell cultures treated with FB1 the cells were dying much faster than they normally did when viability was measured by the MTT assay. This was intriguing and I decided to follow it up and try to determine if this was a real result. The culture media used in the experiment came from a new batch of media, suggesting something was different in that media. This was tested by subcultering a culture into two flasks: one containing media from previous batches, which produced the normal cell death response, and one containing the new media. The

cells were then treated with FB1 and the new media culture died faster than the old media culture. This indicated the new batch media had a different composition.

5.3.1 Sucrose promotes FB1-induced cell death

After observing unusually fast cell death kinetics in a new batch of cell culture media, examination of the records on the procedures used to make up the media showed that the new batch had been accidentally prepared with elevated sucrose. Normal sucrose concentration in *Arabidopsis* growth media is 3% (w/v), which corresponds to 87.64 mM, but the new batch had been made up with 5% (w/v), which corresponds to 146 mM. This is an extra 58.36 mM of sucrose. Cell cultures with higher levels of sucrose were more sensitive to FB1 than those with normal levels of sucrose and this effect was more pronounced at high (4 μM) FB1 concentrations (Figure 5.7). These results show that in cell cultures sucrose levels are important during FB1-induced cell death. Because these initial observations were performed in the cell culture system, there was concern that it could be an artefact of the system. Subsequent experiments were designed to test if this observation was a cell culture artefact or if it was a true biological response of plants. Therefore, leaves of 4-5 week old *Arabidopsis* plants were infiltrated with 10 μM FB1, 150 mM sucrose and a combined treatment of both, with cell death symptom development monitored overtime. On exposure to FB1, *Arabidopsis* leaves gradually developed symptoms that start off as chlorosis, followed by severe water loss leading to shrivelling and death of the entire leaf, whereas mock and sucrose infiltrated remained symptomless (Figure 5.8). However, leaves treated with a combination of FB1 and sucrose rapidly developed severe symptoms and were completely dead within 4 days of treatment (Figure 5.8). These results show that increased sucrose availability in the plant ECM accelerates FB1-induced cell death, a connection that had not been previously established before.

There are at least 3 ways in which sucrose can be accelerating cell death. First, it could be due to sucrose directly modulating FB1 signalling. Second, sucrose levels could be altering the expression levels of sucrose-responsive genes that play a role in cell death. Finally, it could be the result of sucrose-induced changes in carbohydrate metabolism/composition of the cells. The significance of the novel effect of sucrose is discussed bellow in light of the role of sugar signalling in cell death, the requirement of light for FB1-induced cell death and a possible role of sucrose in age related resistance to pathogens in nature.

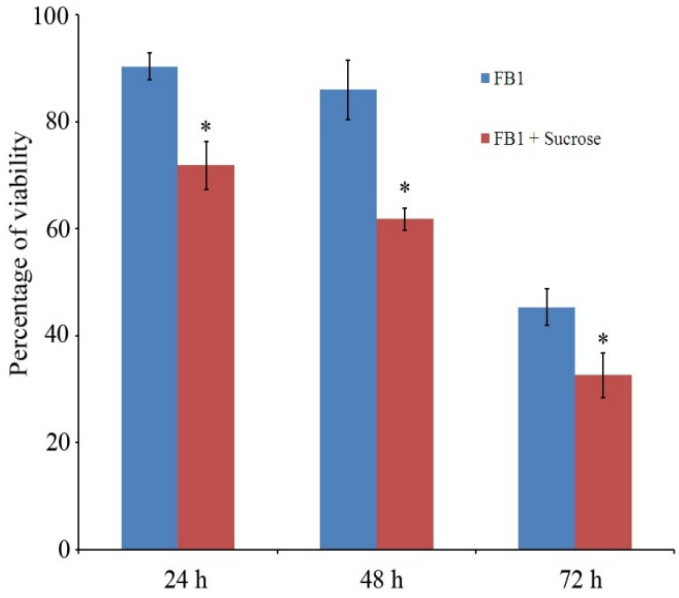

Figure 5.7 The effects of sucrose on the viability of *Arabidopsis* cell cultures. 3-day old cultures treated with 4 µM FB1 only or 4 µM FB1 + 2% (w/v) sucrose, in addition to the sucrose already present in the media which is 3% (w/v). The gradual decrease of viability is shown as a percentage to their controls (mock and 2% (w/v) sucrose treated, respectively) measured by the MTT assay. An asterisk denotes a significant ($p \leq 0.01$) change between FB1 and FB1 + sucrose treatments according to Student's *t*-test. Values and error bars represent means ± SE ($n = 3$).

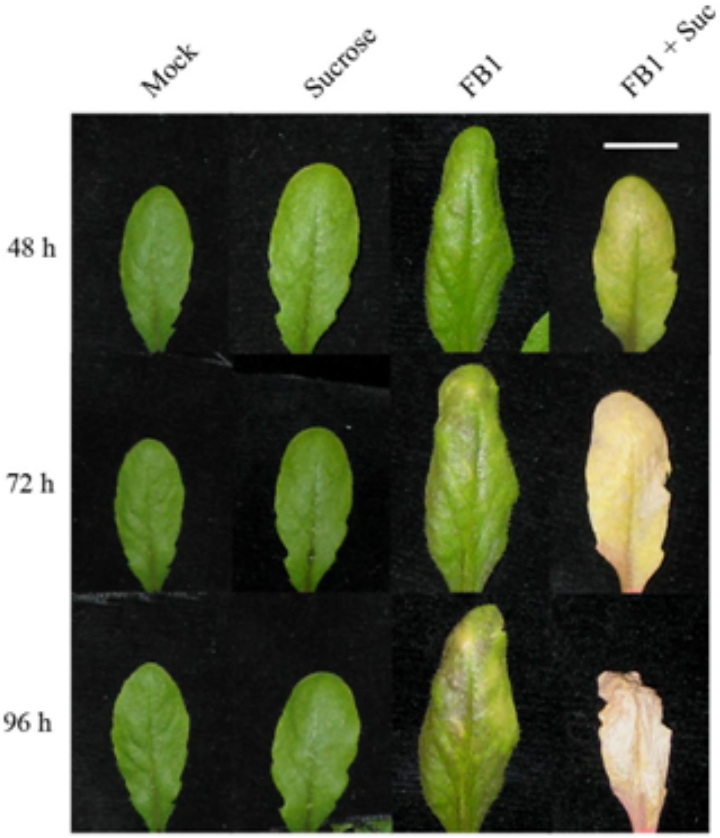

Figure 5.8 The effects of sucrose on FB1-induced cell death in whole plants. 4-week old *Arabidopsis* leaves were infiltrated with 150 mM sucrose, 10 µM FB1 or both treatments (FB1+Suc) and photographed at 48, 72 and 96 hours after infiltration. Scale bar indicates 1 cm.

5.3.2 The role of sucrose in FB1-induced cell death

The data from Figure 5.7 and 5.8 reveals that sucrose levels influence the response of *Arabidopsis* to FB1 treatment – higher levels of sucrose promoted cell death. Although soluble sugars, such as sucrose, provide cellular energy and the building blocks for cell growth, they also serve a signalling role in controlling growth and development in plants (Rolland *et al.,* 2006). In *Arabidopsis*, a signalling role for sugars in the regulation of cell death has been proposed based on genetic studies showing a link between altered sugar signalling/perception and PCD. Hexokinase 1 (*HXK1*), a protein involved in sugar metabolism, is a well characterized sugar sensor that mediates sugar signalling during senescence independently of its primary metabolic function (Moore *et al.,* 2003). Transgenic tomato plants overexpressing the *Arabidopsis HXK1* gene display an early senescence phenotype (Dai *et al.,* 1999) whereas *Arabidopsis HXK1* loss-of-function mutants display a delayed senescence phenotype (Moore *et al.,* 2003). These studies demonstrate that sugars are important signalling molecules and clearly show that sugar signalling positively regulates PCD via *HXK1*. In another study, the *Arabidopsis* hypersenescing mutant *hys1*, is hyper-responsive to exogenously applied sugars and displays an early senescence phenotype as well as upregulation of senescence-associated genes (Yoshida *et al.,* 2002). The early senescence phenotype in *hys1* is independent of *HXK1*-mediated signalling (Aki *et al.,* 2007), suggesting multiple pathways mediate sugar sensing and PCD. These reports implicate sugar signalling as an important component in cell death whereas the specific sucrose-FB1 connection is shown in this chapter.

The observation of the novel effects of sucrose on FB1-induced cell death provides a new explanation for the effects of light on plant PCD reported in the literature. The requirement for light in PCD has been previously connected to the light-dependent accumulation of toxic chlorophyll products in the chloroplast such as pheophorbide, red chlorophyll catabolite and uroporphyrinogen III that cause oxidative damage (Hu *et al.,* 1998; Mach *et al.,* 2001; Pruzinska *et al.,* 2003). Some PCD elicitors induce a light-dependent production of excess excitation energy in the chloroplast that could play a role in generation of ROS and activation of PCD in plants (Allen *et al.,* 1999; Boccara *et al.,* 2007). The results from Figure 5.7 and 5.8 suggest that at least part of the light requirement could also be governed by sucrose concentrations present in the tissue during cell death elicitation. In the light, photosynthetic tissues accumulate higher amounts of sucrose than non-photosynthetic ones and this correlates with the fact that light treated leaves are more susceptible to FB1 than

the same leaves placed in the dark (Stone *et al.,* 2000). The caveat of reduced levels of sucrose in dark treated tissue is that sucrose signalling is reduced and that could play a significant part in dark-induced resistance to FB1 and other forms of PCD. Further investigation of this possibility is beyond the scope of this thesis.

Interestingly, the link between sucrose levels and plant PCD could be used in nature as a regulatory mechanism of HR cell death in response to pathogens. In normally developing plants, older leaves are more resistant to plant pathogens than younger leaves due to age-related resistance (ARR) that has been observed in many plants (Reuveni *et al.,* 1986; Kus *et al.,* 2002). However, in vertical growing plants, young leaves are at their highest photosynthetic output due to reduced shading by the plant's canopy. Therefore, higher levels of sucrose production in younger leaves promote the activation of HR cell death upon pathogen attack. As the leaf ages, sucrose production decreases, the dependence on sucrose-promoted HR cell death decreases as ARR becomes prominent. This has been observed in tobacco plants, where younger leaves more efficiently activate PCD than older leaves in response to *Agrobacterium* (Pruss *et al.,* 2008) and *Phytophthora infestans* (Shibata *et al.,* 2010) pathogen attack, but a direct link with sucrose concentrations has yet to be tested.

5.3.3 *UGP1* might mediate sucrose-induced increase in FB1 susceptibility

In this chapter *UGP1* was identified as a novel cell death regulator. There is precedence for a specific upregulation of *UGP1* by as little as 50 mM sucrose in whole plants (Ciereszko *et al.,* 2001). Since sucrose accelerates FB1-induced cell death (Figure 5.7 and 5.8) and simultaneously upregulates *UGP1* expression, it was hypothesised that the upregulation of *UGP1* could be a critical step in mediating the effects of sucrose on the response of *Arabidopsis* to FB1. Assuming that FB1 cell death progression exclusively signals downstream through UGP1 protein, KO lines for *UGP1* should not be affected by sucrose in their response to FB1. First, it was necessary to establish if the extra sucrose added to cell cultures, that already have 3% (w/v) sucrose in them, can result in an upregulation of *UGP1* expression. Indeed, within 3 hours of sucrose addition, *UGP1* transcript was upregulated as measured by sqRT-PCR (Figure 5.9). Next, Col-0 and SALK_100183 leaves were infiltrated with FB1 only and FB1+sucrose, similarly to Figure 5.8, and the progression of cell death symptoms monitored daily (Figure 5.10).

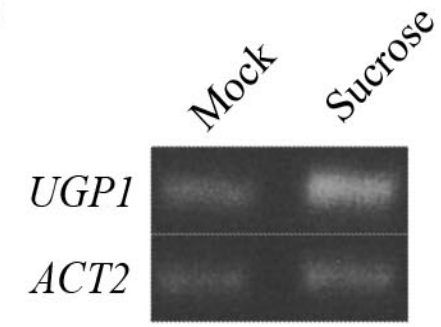

Figure 5.9 Induction of *UGP1* gene expression by sucrose. Cell cultures, containing 3% (w/v) sucrose, were mock treated or treated with extra 2% (w/v) sucrose and samples for sqRT-PCR harvested 3 hours later. Actin-2 (*ACT2*) was used as a constitutive reference control.

Sucrose addition failed to accelerate cell death in the SALK_100183 line. The lack of a functional copy of this gene in the *ugp1* mutant obviously prevents its sucrose-dependent upregulation, with the result that the symptoms of FB1 and the FB1+sucrose treatments in infiltrated leaves become indistinguishable (Figure 5.10). The results show that *UGP1* is a critical regulator in FB1 cell death and suggest that the sucrose effect on FB1 cell death requires the activity of this protein in detriment of using a separate pathway/mechanism, although a possible causal relationship between sucrose and *UGP1* cannot be derived from these results alone. More data is required to test this possibility, such as analysing the FB1 cell death kinetics in *UGP1*-overexpressing lines.

Additionally, I was interested in investigating if the mechanism of *UGP1* is related to changes in the levels of UDP-glucose, since *UGP1* is the main producer of UDP-glucose in the plant cell. The hypothesis being that reduced levels of UGP-glucose result in resistance to FB1 and that increased levels of UGP-glucose result in susceptibility to FB1. This is a reasonable hypothesis since UDP-glucose in its own right is capable of modulating gene expression in bacteria (Bohringer *et al.,* 1995) and is a potent agonist of $P2Y_{11}$ purinoreceptors in mammals (Harden *et al.,* 2010). Two separate lines of evidence support this hypothesis. Firstly, the resistant cell death phenotype of *UGP1* KO lines suggests that a decrease in the concentration of UDP-glucose could be related to the observed resistance to FB1, since *ugp1* mutants have reduced UDP-glucose levels relative to wild type plants (Park *et al.,* 2010). Secondly, sucrose treatment is likely to be causing an increase in UDP-glucose content *in vivo*. The main metabolic pathways for synthesis of UDP-glucose are via *UGP1* and sucrose synthase (SuSy) (Figure 5.11A). Sucrose treatment simultaneously increases both these pathways, by upregulating *UGP1* and by increasing the substrate for SuSy to generate UDP-glucose. It is therefore likely that UDP-glucose levels increase following sucrose treatment, even if only transiently, altering the response to FB1. With these considerations in mind, there could be a possible correlation between UDP-glucose levels during FB1 treatment and the extent of FB1-induced cell death.

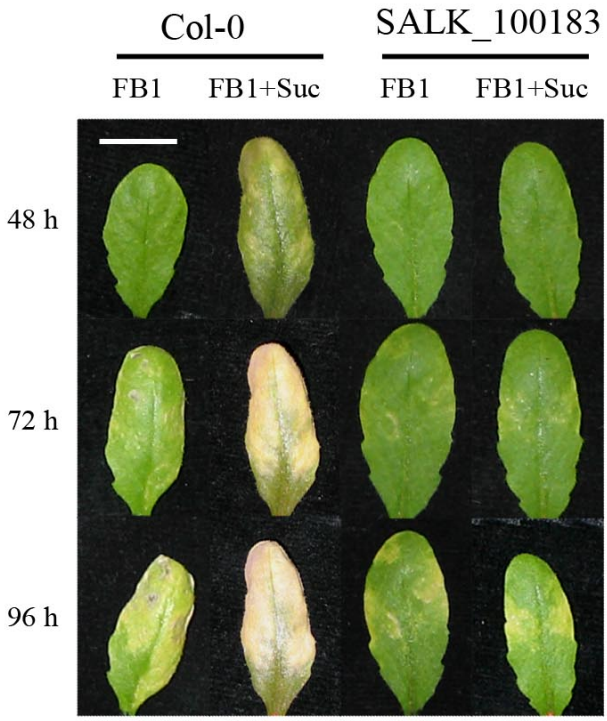

Figure 5.10 Sucrose fails to enhance FB1-induced cell death in the *UGP1* KO mutant. 4-day old Col-0 and SALK_100183 leaves were infiltrated with either 10 µM FB1 or 10 µM FB1 + 150 mM sucrose and photographed 48, 72 and 96 hours post infiltration. Scale bar indicates 1 cm.

A

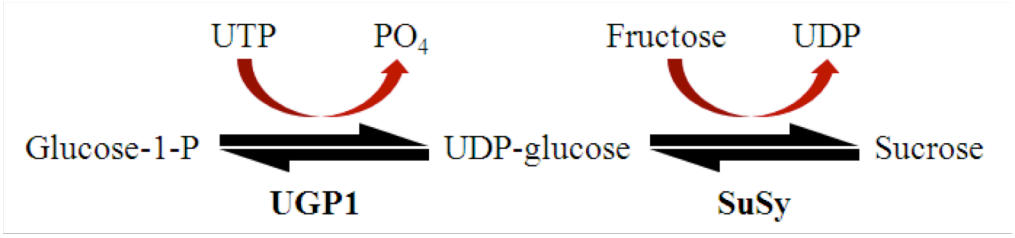

B

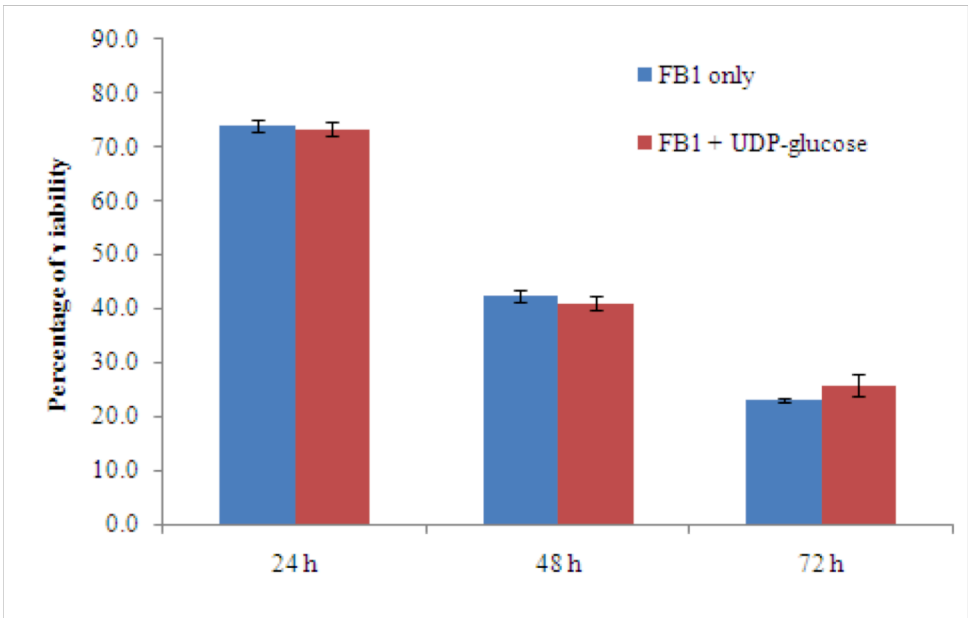

Figure 5.11 UDP-glucose does not modulate FB1-induced cell death. (A) Schematic showing the two main metabolic routes for UDP-glucose synthesis in plants. UTP-Uridine tri-phosphate, UDP–Uridine diphosphate. (B) The effects of UDP-glucose on FB1 induced cell death. 3-day old cultures were treated with 1 µM FB1 and 100 µM UDP-glucose or mock treated (FB1 only). Their effects on the viability of cultures in response to FB1 are shown as a percentage to their respective controls (no FB1 treatment) measured by the MTT assay. Values and error bars represent means ± SE (n = 3).

The effects of UDP-glucose on FB1-induced cell death were investigated in suspension cell cultures and the effects on culture viability measured using the MTT assay (Figure 5.11B). UDP-glucose was added to the final concentration of 100 µM to cell cultures, which is equivalent to 2 µMol/g of fresh weight of cells. This concentration is two orders of magnitude higher than the reported physiological concentrations of UGP-glucose of 20 nMol/g of fresh weight (Park *et al.,* 2010). The results clearly show that, unlike sucrose, 100 µM UDP-glucose did not alter the response of cell cultures to FB1-induced cell death. Cultures treated with UDP-glucose or FB1+UDP-glucose were statistically indistinguishable from each other via an independent Student's *t*-test, showing UDP-glucose concentrations are not an important factor during cell death inception. However, it is possible that reduced levels of UDP-glucose present during FB1 treatment might account for the resistant phenotype of in the *ugp1* mutants, since these have lower levels of UDP-glucose than wildtype plants (Park *et al.,* 2010). If this is the case then increasing the concentrations of UDP-glucose during FB1 treatment in the *ugp1* mutant should revert its resistant phenotype to FB1. The effects of increasing the concentrations of UDP-glucose on the *UGP1* KO line SALK_100183 were tested using the conductivity assay (Figure 5.12). Leaf disks were floated on solutions containing 2,5 µM FB1 and 2,5 µM FB1 + 100 µM UDP-glucose to compare the extent of cell death as a percentage to their mock and 100 µM UDP-glucose only controls, respectively. Both controls were necessary because UDP-glucose on its own significantly increases the conductivity of the underlying solution. Unsurprisingly, UDP-glucose had no significant effect on Col-0 (Figure 5.12A) as would be expected from the cell culture experiment (Figure 5.11B). As expected, SALK_100183 line died significantly slower than Col-0 and the addition of UDP-glucose did not significantly change its response to FB1 (Figure 5.12B). This shows that the death kinetics in response to FB1 is not complemented by the addition of UDP-glucose to the SALK_100183 line. These results show that the requirement of *UGP1* for FB1 induced cell death is not connected to its primary metabolic function in the synthesis of UDP-glucose.

5.4 Conclusions

The aim of this chapter was to identify cell death regulators that are directly regulated by FB1 using a proteomics and reverse genetics approach. Candidate genes specifically regulated by FB1 signalling were identified by proteomics from the 2D-DiGE experiment

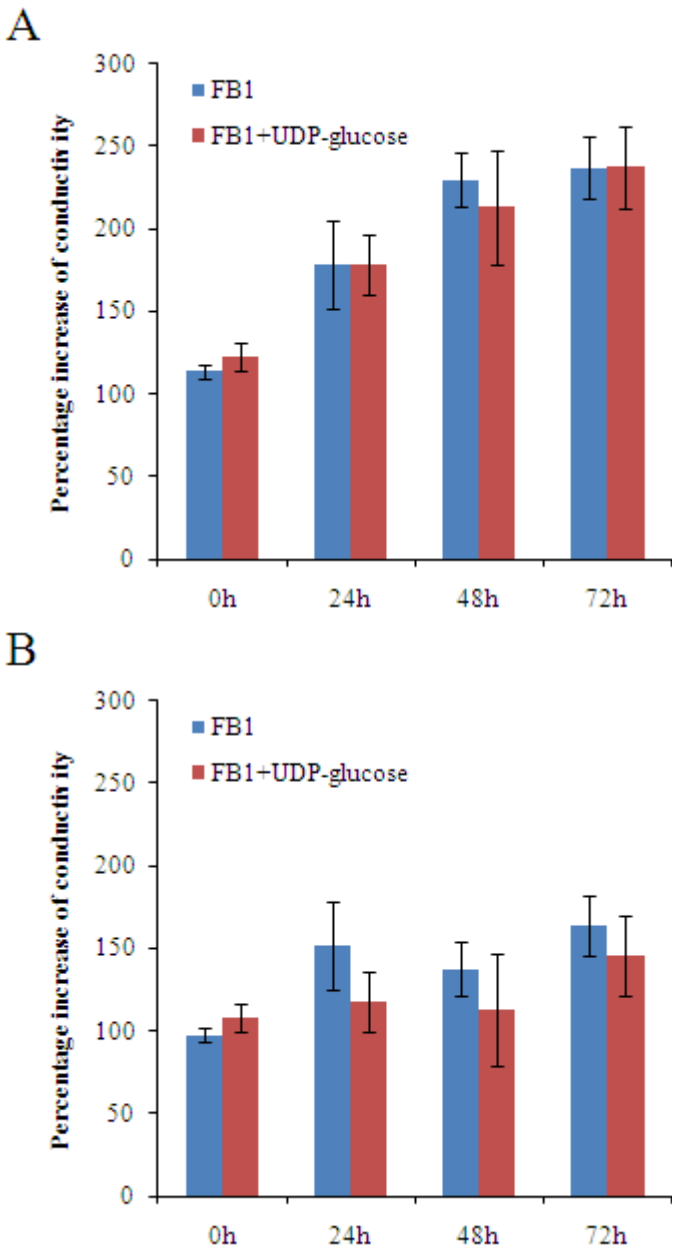

Figure 5.12 Increased UDP-glucose does not modulate FB1-induced cell death in the *ugp1* mutant. Cell death time-course of (A) Col-0 and (B) SALK_100183 leaf disks floated on containing 2,5 µM FB1 or 2,5 µM FB1 and 100 µM UDP-glucose. The conductivity of the solution was measured every 24 h after a 48 h dark incubation and numbers indicate hours after light exposure. The increase in conductivity of the solution is shown as a percentage to their respective controls (MQ water and 100 µM UDP-glucose). Values and error bars represent means ± SE (n = 4). No significant differences were observed between the extent of FB1-induced cell death with or without UDP-glucose in either Col-0 or SALK_100183.

from chapter 3. *UGP1* gene was among this list and the 2 KO lines obtained for *UGP1* showed a remarkable resistant cell death phenotype to FB1-induced cell death, even though one of the lines was not a complete KO for the *UGP1* gene (Figure 5.2B). This was also observed in the complete KO line SALK_100183 by leaf infiltration with FB1 and Evans Blue staining of seedlings. The lack of cell death symptoms in the *UGP1* KO line was in agreement with its resistance to FB1 treatment in the conductivity assay.

UGP1 KO line showed no altered cell death phenotype following AMP-PCP treatment, suggesting that *UGP1* does not play a role in eATP signalling events controlling cell death, at least for signalling events requiring ATP hydrolysis. Further characterization of *UGP1* KO mutants by sqRT-PCR revealed it to play a role in gene expression, possibly by interfering with eATP-mediated signalling. Pathogen cell death assays on the SALK_100183 line revealed *UGP1* to play a role in pathogen-induced cell death, suggesting this protein is a core cell death regulator. The identification of *UGP1* as a FB1-responsive cell death regulator adds another gene to the FB1 signalling pathway and opens the door for further testing for a cell death role of the remaining 31 FB1-responsive genes identified in this study that were not tested due to no KO line being available (Table 5.1), making this a useful resource for future studies.

A connection between sucrose and FB1 cell death was accidentally discovered and confirmed as a real biological phenomenon. Increased sucrose levels were found to accelerate FB1-induced cell death in both cell cultures and whole plants. SALK_100183 plants failed to show increased susceptibility to FB1, possibly because of its failure to upregulated the *UGP1* gene following sucrose treatment. Additionally, the requirement of *UGP1* in FB1-induced cell death does not appear to be related to its ability to produce UDP-glucose.

Chapter 6 General discussion

Plant growth, development and responses to biotic and abiotic stresses are the result of precise and complex interactions between multiple cellular signalling pathways. Intracellular signalling then modulates gene expression, protein and metabolite abundances that result in a favourable response of the organism to the situation it is currently at in its life cycle. Studies looking at gene expression, protein and metabolite abundance changes provide insight into the signalling events that control different aspects of growth and development. The area of extracellular ATP signalling, as well as the physiological processes it governs, is now emerging as an important area of research in plant biology (Clark *et al.,* 2009). The work presented in this thesis is focused on understanding the signalling components that underlie the physiological roles of eATP in plants.

One of the physiological functions of eATP is the regulation of plant viability (Chivasa *et al.,* 2005a). Although this physiological role has been elegantly demonstrated using ATP degrading systems and the mycotoxin FB1, the signalling components downstream of eATP that regulate cell death are unknown. In this thesis, I successfully employed a 2D-DiGE proteomic approach to identify several putative proteins that might account for the toxic effects of FB1 on *Arabidopsis thaliana* (*Arabidopsis*), as well as the specific effects of eATP on this particular type of cell death. Two of these candidates were subsequently shown by reverse genetics to be critical components of FB1 cell death signalling. In addition to its role in regulating viability, the global effects of eATP modulation were investigated using large-scale analysis of gene expression and protein abundance changes. The findings presented in this thesis indicate a wide effect of eATP on cell metabolism, suggesting more as yet uncharacterized physiological roles under eATP control in addition to the roles already reported (Thomas *et al.,* 2000; Tang *et al.,* 2003; Chivasa *et al.,* 2005a; Roux *et al.,* 2007; Chivasa *et al.,* 2009a; Weerasinghe *et al.,* 2009). The new findings presented in this thesis, as well as their relative positions to FB1 and eATP, are summarized in Figure 6.1.

6.1 Extracellular ATP regulated cell death genes

The main objective of this thesis was to identify genes which mediate the eATP signalling cascade controlling plant cell death using a combination of proteomics and reverse genetics. The use of the ATP filter screen reduced the number of candidate genes from over 25.000 predicted genes in the *Arabidopsis* genome (AGSC 2000) to a smaller and

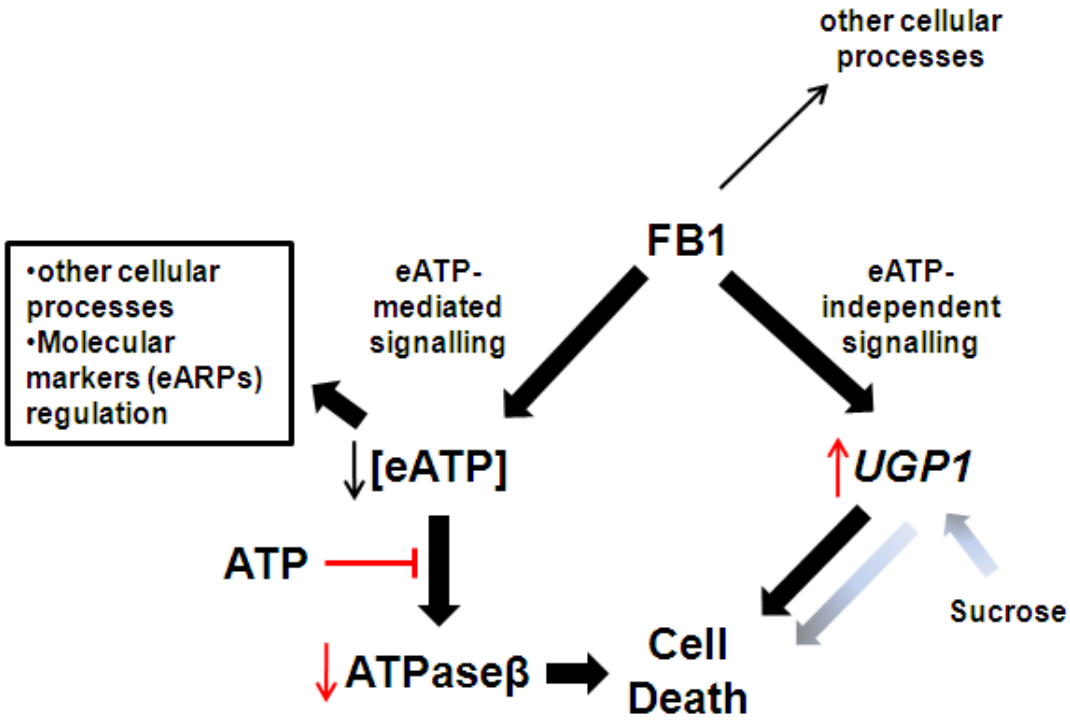

Figure 6.1 FB1 causes cell death in plants by a poorly characterized mechanism. FB1 treatment initiates cell-death related signalling events downstream and independent of eATP, both essential for cell death inception, as well as affecting other cellular processes. It is not clear if these two separate pathways intersect with each other before cell death. The two novel cell death genes identified in this thesis as critical for FB1-induced cell death are ATPaseβ and *UGP1,* and they are components of the eATP-mediated and eATP-independent signalling cascades, respectively. FB1 treatment results in downregulation of ATPaseβ and upregulation of *UGP1*. The mechanism by which ATP treatment rescues cell from FB1-induced cell death might require the blocking of ATPaseβ downregulation. The function of *UGP1* on cell death might be related to its abundance during cell death elicitation because increased levels of *UGP1,* brought about by sucrose treatment, accelerate cell death progression (gradient arrows). Increasing eATP levels regulates other cellular processes unrelated to cell death. Several genes and proteins were found to be directly regulated by ATP. Until they are linked to a known or novel physiological process, they can be used as molecular markers of eATP-mediated signalling called extracellular ATP regulated proteins [eARPs, (Chivasa *et al.,* 2009b)].

manageable number before testing KO lines for altered cell death phenotypes. By using this approach, the chances of finding a cell death regulator should increase, although there is no certainty that one will be discovered. An experimental approach was developed based on previous research showing that the PCD inducing mycotoxin FB1 causes cell death by depleting eATP levels (Chivasa *et al.,* 2005a). FB1 was utilized because: i) it gradually depletes eATP, giving plant cells time to modify their metabolism and proteome; ii) it is a natural toxin that several plants, including *Arabidopsis* (Urban *et al.,* 2002), encounter in nature; and iii) *Arabidopsis* cell cultures treated with FB1 can be rescued from cell death commitment by exogenous ATP addition, whereas cell cultures treated with ATP degrading enzymes cannot. Therefore, since FB1-induced cell death in cell cultures can be blocked by adding ATP, the central premises of the experimental approach predicted that some cell death regulators could change in protein abundance in accordance with eATP availability. Being this the case, then a proteomics approach would be suitable for identifying them. Using 2D-DiGE analysis of protein abundance, many proteins were found to change in abundance following FB1 treatment and a subset of these were controlled by levels of ATP, demonstrating that they were directly regulated by eATP-mediated signalling. This response formed the basis for a filter for selecting putative cell death genes from the bulk of FB1-regulated genes that might be involved in other physiological processes such as growth retardation (Chivasa *et al.,* 2005a) and defence gene expression (Stone *et al.,* 2000). Testing for a role of these genes in cell death was performed on T-DNA KO mutants for each gene available by looking for an altered cell death phenotype following FB1 treatment. The availability of KO lines from the SALK collection, together with a quantitative and reproducible cell death assay, made it possible to test many of the putative cell death genes identified in this thesis. Finally, the whole experimental approach was shown to work by the identification of the first eATP-regulated cell death gene – the ATPaseβ. This gene is required for successful FB1-induced cell death progression. Its function in cell death is probably secondary to its main role in energy production, as the catalytic subunit of the mitochondrial ATP synthase complex. The different possibilities of how ATPaseβ could play a role in cell death were discussed in chapter 3.

There exist reports in the literature that could suggest a link between ATPaseβ and cell death. In animal systems, ATPaseβ has been shown to be differentially regulated during different cell death-inducing treatments including digoxin-induced apoptosis in human

endothelial cells (Qi *et al.,* 2001), in d-galactosamine-induced apoptosis in cultured human hepatocytes (Rodriguez-Ariza *et al.,* 2005), in anthrax lethal toxin-induced apoptosis in mouse macrophage cells (Chandra *et al.,* 2005) and in cerulean-induced apoptosis in pancreatic acinar AR42J cells (Yu *et al.,* 2003), although its function, if any, in these forms of cell death remains unclear. A more direct connection between this protein and cell death has been established in yeast and recently in humans. In yeast, ATPaseβ is required in BAX-induced apoptosis, but not during BAX-induced growth arrest, suggesting a specific cell death function (Gross *et al.,* 2000). In humans, it has been recently identified as an auto-antigen of the auto-immune component of Alzheimer's disease (Vacirca *et al.,* 2010). These authors show that anti-ATP synthase antibodies were present in the serum of a significant number of Alzheimer patients, and such antibodies are capable of inducing apoptosis in the SH-SY5Y neuroblastoma cell line (Vacirca *et al.,* 2010), possibly by blocking ATP synthesis of cell surface ATP synthase and consequent eATP depletion. These reports from different tissues and different PCD-inducing treatments provide a link between ATPaseβ and cell death in animals, although the nature of this connection is unclear. ATPaseβ could be playing a central role in the later stages of cell death or simply change in abundance as a consequence of metabolic shutdown prior to cell death. In plants, altered abundance of this protein has been previously shown to occur following salt stress-induced PCD in rice root tip cells (Chen *et al.,* 2009a) but an active role in plant cell death regulation had never been established until now.

The results from this thesis clearly show that the ATP filter can identify genes which are essential in cell death regulation. Of the 12 genes tested using homozygous KO lines only one gene, ATPaseβ, was conclusively shown to play a role in FB1-induced cell death. This was not unexpected since modulation of protein abundance is only one mechanism by which eATP can block cell death. Other mechanisms include activation of an expressed protein, such as the catalytically inactive form of caspase-9, the pro-caspase-9 (Srinivasula *et al.,* 1998), and protein translocation, such as cytochrome *c* translocation from the mitochondrial inner membrane to the cytosol (Li *et al.,* 1997). This ATP filter was also capable of identifying putative cell death candidates from FB1-regulated functionally related proteins. The ATP synthase D chain (AT3G52300) was one of the FB1 regulated genes identified that was not regulated by eATP levels. This protein forms part of the peripheral stalk in the mitochondrial F_1-F_0 ATP synthase that also harbours ATPaseβ. Unlike the KO lines for the ATPaseβ subunit, the 2 KO lines for this gene did not produce

an altered cell death phenotype. This result cannot be explained by gene redundancy issues because this gene has no other family members in *Arabidopsis*. Although ATP synthase D chain belong to the same protein complex as ATPaseβ, these results show that it is not essential in FB1-induced cell death. Moreover, these results illustrates how eATP-mediated signalling specifically targets genes involved in regulating cell death, such as ATPaseβ, whereas others that are functionally related and even present in the same protein complex, but don't have a role in cell death, are not.

6.2 Cell death genes regulated solely by Fumonisin B1

One of the objectives of this thesis was to identify cell death genes not regulated by eATP that are required for FB1-induced cell death using a 2D-DiGE and reverse genetics approach. The exact mechanism of FB1 induced-cell death in plants is not fully understood, primarily because the main FB1 target(s) in plants is not known. FB1-induced cell death has at least two separate signalling components (Figure 6.1), one dependent on eATP signalling events and one independent of them, with the eATP-dependent pathway having a clear role in cell death regulation (Chivasa *et al.,* 2005a). The toxic effects of FB1 not related to eATP signalling could also be essential for cell death inception if these two pathways intersect with each other in some way.

Using 2D-DiGE, putative candidates in the FB1-specific pathway were selected based on their proteomic profile showing differential expression with FB1 independently of its ability to trigger eATP depletion (inverse ATP filter). Reverse genetics validated this approach with the identification of UDP-glucose pyrophosphorylase (*UGP1*) as a cell death gene directly regulated by FB1. A KO and a knockdown T-DNA line for this gene both showed significant resistance to FB1-induced cell death. The *UGP1* KO line showed no altered cell death phenotype when treated with AMP-PCP. This clearly showed that the signalling cascade initiated by eATP depletion, that might be mimicked by AMP-PCP treatment, is unaffected by the absence of *UGP1*. However, because the exact mechanism of AMP-PCP is not fully understood, conclusive evidence for a cell death role of *UGP1* in eATP-triggered cell death will only be achieved by observing the cell death response of the *UGP1* KO mutants initiated by ATP degrading enzymes (Chivasa *et al.,* 2005a). *UGP1* appears to be, at least partly, required in nature for some types of pathogen-induced HR, since *UGP1* KO line showed less effector-mediated HR-cell death initiated by avirulent *Pseudomonas syringae* expressing the *avrRpm1* effector. The role of *UGP1* is not clear but

it would be interesting to test if SA signalling is disrupted in the KO line which could explain the reduced HR-cell death. This could be achieved by looking at the kinetics of PR protein induction in the *UGP1* KO line triggered by exogenous SA infiltration or by pathogen attack. To better understand the mechanism of FB1 cell death in *Arabidopsis*, a possible connection between *UGP1* and the other genes critical to FB1 cell death (Kuroyanagi *et al.,* 2005; Stone *et al.,* 2005; Shi *et al.,* 2007) warrants further research.

The accidental finding that high sucrose levels accelerate FB1-induced cell death could be explained by two separate mechanisms. Firstly, sucrose might be upregulating genes required by FB1 for cell death inception. *UGP1* is a candidate for this category since it is upregulated by FB1 at the protein level, is required for FB1-induced cell death and sucrose levels specifically regulate its expression. Secondly, changes in sucrose metabolism due to increased sucrose concentrations during FB1 treatment could cause plant cells to die faster with FB1. It is possible that *UGP1* could also play a role here, since it is metabolically very close to sucrose breadonw/synthesis. This hypothesis might be tested using a non-hydrolysable sucrose analogue, such as palatinose, on FB1-induced cell death. This analogue only activates sucrose signalling without affecting the carbohydrate pool and can therefore be used to separate sucrose-induced signalling from sucrose-induced metabolic alterations. The sucrose effect does not appear to be related to changes in UDP-glucose content, the main product of *UGP1* activity. Results showed that increased UDP-glucose concentrations did not affect to cell death response of Col-0 or *ugp1* mutant to FB1, showing that UDP-glucose does not modulate FB1-induced cell death. Although there is some correlative evidence between the levels of *UGP1* and FB1-induced cell death, such as the resistance of dark treated plants that show reduced *UGP1* expression (Ciereszko *et al*., 2001, Stone *et al*., 2000), this relationship, and the possible role of sucrose, remains to be properly tested.

6.3 Metabolic consequences of eATP modulation

The extracellular ATP area in plants is still relatively new, with very few genes identified as specifically responding to exogenous ATP addition, and the full scope of genes and proteins regulated by eATP-mediated signalling has still not been compiled. One of the objectives of this thesis was to identify novel genes and proteins regulated by eATP

employing large-scale proteomic and transcriptomic approaches. A 2D-DiGE experiment looking at protein abundance changes following ATP treatment in cell cultures identified 35 unique proteins as differentially regulated by ATP. Bioinformatics analysis revealed a strong effect of ATP on photosynthetic proteins, which suggests that this physiological process might be under eATP regulation. Only one other study has used 2D-DiGE to look at the effects of increasing eATP concentrations on the plant proteome (Chivasa *et al.,* 2010). This study was performed in tobacco using long-term ATP treatment and identified 37 proteins whose protein abundance is modulated by eATP signalling. Some of those proteins were also identified in this thesis, but many were not. These differences could be explained by the different plant species used, unavailability of the tobacco genome or the different sampling timepoints between these studies.

Many genes were shown to be modulated by eATP, but the physiological significance of each individual gene can only be tested by reverse genetics. Unfortunately, this becomes a tedious task if there is no clear idea about which physiological processes to test. It becomes imperative to first identify putative physiological processes regulated by ATP based on proteomics or transcriptomic high-throughput studies. Taking all the results of this thesis into account, a more global view of the physiological significance of ATP treatment can be achieved when combining all early eATP-regulated proteins and genes to possibly provide clues for future research. A total of 64 unique genes were shown to be regulated by eATP and can be regarded as molecular markers of eATP-mediated signalling. These included reversed proteins from chapter 3, eATP-regulated proteins and the 10 confirmed eATP molecular markers from chapter 4. Analysis of the metabolic pathways these genes are annotated as being involved in using DAVID bioinformatics analysis tool shows a significant enrichment for genes involved in glycolysis/gluconeogenesis, carbon fixation in photosynthetic organism, biosynthesis of phenylpropanoids, RNA degradation and the pentose phosphate pathway. Such enrichments could provide clues for novel physiological processes under eATP control, but no firm conclusions should be drawn from these results alone. Confirmation of a connection between eATP and these metabolic pathways can only be established by performing experiments specifically designed for such purpose and such experiments were beyond the scope of this thesis. For example, the effects or eATP on glycolysis can be predicted using metabolomics and then tested by using sub-lethal doses of AMP-PCP to simulated elevated eATP levels and measuring the concentration of glycolysis-related metabolites over time.

Careful bioinformatic analysis of this data results in at least one prediction of the effects of ATP on metabolism that is in agreement with published results. When considering the genes identified as belonging to the KEGG pathway of biosynthesis of phenylpropanoids (KEGG pathway ID: ath01061), a total of 8 genes regulated by eATP were annotated as having a role in that pathway: AT3G52930, AT5G19550, AT1G79550, AT4G34050, AT3G04120, AT3G60750, AT3G29200, AT2G36530. The proteomic data for these genes provides a clear indication that eATP-mediated signalling is restricting the metabolic flux through this pathway, as 6 out of the 8 genes are significantly downregulated following ATP treatment. Such an effect could indicate a reduction in metabolites derived from this pathway, such as SA. However, the main SA producing enzymes *ics1* and *ics2* were not identified as eATP-regulated by either proteomics or transcriptomics, leaving open to speculation how exactly eATP antagonizes SA signalling/accumulation (Chivasa *et al.,* 2009a). The results presented in this thesis certainly did not identify all the eATP-regulated genes in *Arabidopsis,* due to inherent limitations of 2D proteomics and the nature of the DNA chip data used, and therefore provide an incomplete picture of the global effects of eATP modulation but the phenylpropanoid metabolism example shows they can be useful. Ultimately, once a DNA chip designed to look at ATP-induced changes in the plant transcriptome is published will the full scope of physiological processes under eATP control be known.

Re-examination of one timepoint of a previously acquired DNA chip experiment in the Slabas group identified 100 genes that are potentially regulated by eATP. The chip predictions of the ATP only effects for 10 of these genes were validated by sqRT-PCR using new RNA samples derived from cell cultures treated with ATP. Although they are clearly regulated by ATP, their physiological significance remains to be discovered, making them novel molecular markers for eATP signalling. Four of these genes were tested for a cell death role using KO lines but none were involved. These markers were then used as a tool to search for possible alterations in eATP-mediated signalling in the KO mutant background of genes found to have a role in cell death in this thesis, ATPaseβ and *UGP1*. Although both genes are required for successful FB1-induced cell death inception, their absence in the KO lines produced different effects on the expression levels of 5 eATP molecular markers tested. The *UGP1* complete KO line showed reduced basal expression levels of 3 markers: AT3G28210, AT4G01360 and AT3G22910. The ATPaseβ KO lines

only showed a reduction in expression of AT3G22910, a putative calcium-transporting ATPase. This difference in the number of markers showing altered basal expression could be related to the position of each cell death gene in the FB1 signalling pathway. ATPaseβ is downstream of eATP signalling whereas *UGP1* is not (Figure 6.1). Therefore, the expression profile of these markers in a KO background of a cell death gene can potentially be used as a "marker fingerprint", providing clues for the position of this gene in the signalling pathway relative to others. The earlier a gene is located in a signalling cascade, the more markers it can potentially modulate, ultimately with the eATP receptor(s) controlling all of them.

The molecular markers identified from the DNA chip re-examination in this thesis were also used to test a hypothesis on how eATP signalling negatively regulated defence responses in plants (Chivasa *et al.,* 2009a). As eATP and SA antagonistically regulate each other and defence gene expression, it was purposed that the proteins mediating these effects, extracellular ATP regulated proteins (eARPs), are oppositely regulated by ATP and SA treatments (Chivasa *et al.,* 2009b). One of the eATP markers identified in this thesis, AT3G15450, showed an ATP and SA treatment gene expression profile consistent with the hypothesis. This gene was upregulated following ATP treatment and downregulated following SA treatment in suspension cell cultures, showing that ATP and SA can antagonistically regulated the expression of downstream genes. Testing the possible role for this gene in defence using a KO mutant is still required. These findings now make it possible to identify the genes that could mediated the physiological role of eATP signalling in plant defences. Similarly to the ATP filter used in this thesis to identify cell death genes that mediate eATP control of cell viability, an ATP + SA filter can now be used to identify genes that mediate eATP-mediated suppression of defence responses. This can be performed using a whole genome transcriptomic or a proteomics based approach. It might also be possible to use this ATP + SA filter to identify cell death genes. Genes that respond in the same direction with both ATP and SA treatment could play a role in cell death regulation (Chivasa *et al.,* 2009b). The expression profile of AT3G22910 confirmed the existence of eATP- and SA-specific signalling cascades that alter its gene expression in the same direction. Although it remains to be tested using KO mutants if AT3G22910 does indeed play a role in cell death, the fact that this gene was downregulated in two different mutant backgrounds that are resistant to FB1-induced cell death (ATPaseβ and *UGP1*) makes it a promising candidate for future research.

In addition to the example shown above, it can be envisaged many other ways of using these molecular markers for research in the eATP field. For example, the markers can possibly be used as a tool to investigate the degree of overlap between cell death signalling controlled by eATP and cell death signalling controlled by well known cell death regulators, such as *acd2* (Mach *et al.,* 2001), *lsd1* (Jabs *et al.,* 1996) and *dnd1* (Clough *et al.,* 2000). Such research might provide clues as to the possible ubiquitous nature of eATP in the control of plant cell death.

6.4 Future Work

The 2D-DiGE proteomic approach employed in this thesis is not final and a number of refinements can still be made. For example, increased spot resolution can be achieved by the use of narrower range IPG strips of 1 pI unit during first dimension separation of the protein sample. This would allow the separation of mixtures spots identified in this thesis, providing more candidate cell death genes. Limitations of gel-based proteomics always reduce the number of candidate proteins that can possibly by identified. In this thesis, proteins not soluble in LB or outside the pI range employed (4-7) were not identified. Other proteomic methodologies can be applied for more refined results. For example, because of the poor representation of low-abundance and hydrophobic proteins in gel-based proteomics, the use of MS-based proteomic approaches, such as isobaric tags for relative and absolute quantitation [iTRAQ, (Rowland *et al.,* 2010)] could allow a more complete analysis of the protein fractions. This is especially true for the microsomal fraction, where membrane-bound proteins were poorly represented, even though the fraction was enriched for them. Sub-cellular fractionation for enrichment of specific compartments and organelles can yield further targets not identified in the bulk fractions analysed due to their low abundance. Of special interest are the protein fractions enriched for cell wall-bound and plasma membrane-bound proteins, where the primary eATP target(s) are expected to be located. Future studies should focus on these protein fractions. Notwithstanding the limitations described above, this work has shown the usefulness of gel-based proteomics techniques for identifying proteins regulated by eATP signalling.

ATPaseβ was shown to play a role in cell death and possible mechanisms for the ATPaseβ cell death function were discussed, but the exact nature of it remains to be shown. In testing for a secondary role of this protein in cell death, it would be interesting to identify

putative binding partners for this protein using a high throughput yeast-two-hybrid assay for the *Arabidopsis* proteome, since ATPaseβ could be regulating cell death via a protein complex similarly to cytochrome *c* (Li *et al.,* 1997). Additionally, the control of gene expression function of this gene could be studied using whole genome DNA chips by comparing the transcriptomes of Col-0 and ATPaseβ mutant lines during FB1 elicitation. Such an approach might identify novel components of the eATP cell death signalling cascade downstream of ATPaseβ.

Besides ATPaseβ, reverse genetics results revealed preliminary evidence for a cell death role of 3 other eATP-regulated genes. Further experiments are required to confirm the putative cell death role of the eATP-regulated genes *PDIL*, AT3G18130 and AT4G34050 in FB1-induced cell death. *PDIL* (AT1G77510), member of the thioredoxin superfamily that catalyse the rearrangement of protein disulfide bonds, only had one knockdown homozygous T-DNA line available that showed a significant altered cell death phenotype. AT3G18130, *Arabidopsis RACK1C*, showed an altered cell death phenotype in only one of the two predicted KO lines tested, but the KO status of these lines needs to be confirmed. *RACK1C* belongs to a 3-member gene family in *Arabidopsis* involved in plant development (Guo and Chen 2008). The identification of a second KO line for these genes will permit further testing to conclusively show if *PDIL* and *RACK1C* have a role in eATP-mediated cell death. Alternatively, complementation of the KO mutants by transforming them with a wildtype copy of the genes can also be done if not extra KO lines are available. SALK homozygous lines for AT4G34050, a putative caffeoyl-CoA 3-O-methyltransferase, showed a small decrease in cell death that could be related to gene redundancy issues, since AT4G34050 is part of a 6 member gene family. Although the change was statistically significant, it was so small that it suggested a minor role for this gene in cell death. An RNA silencing approach could be used to lower the expression of all family members (Herr and Baulcombe 2004) and test if their metabolic activity plays an important role in cell death. In addition to these 3 genes, a further 12 putative cell death genes that are reversed with ATP treatment were not tested for an altered cell death phenotype due to the absence of homozygous KO lines in the SALK collection. Future studies aimed at elucidating eATP signalling in cell death should make use of this resource, particularly as new KO lines become available. In fact, as this thesis was being compiled, three homozygous KO lines (SALK_134934, SALK_009963 and SALK_041331) for AT1G64520 and AT1G79690 were added to the SALK collection.

Finally, a connection between FB1-resistant phenotype of *UGP1* KO mutants and eATP signalling is open to future investigations and, if found to exist, would illustrate the interdependence of the eATP-dependent and eATP-independent signalling cascades in FB1-induced cell death (Figure 6.1). Although the results of the AMP-PCP experiment suggest *UGP1* is not required downstream of eATP depletion, it is possible that the resistant phenotype of *UGP1* KO lines could be related to altered eATP depletion kinetics following FB1 treatment. This possibility could be tested by directly measuring eATP levels in Col-0 and *ugp1* mutants during FB1 elicitation using the firefly luciferase assay, a very sensitive luminescence assay that specifically measures ATP concentrations. ATP concentrations would be measured in apoplastic fluid obtained from Col-0 and *ugp1* mutant plants by forcing plants to secrete guttation fluid in high humidity conditions during FB1 treatment (Chivasa *et al.,* 2010). Alternatively, a high concentration of hydroponically grown seedlings could be used. If these produce enough eATP in the medium to be detected by the luciferase assay, it would be possible to measure the eATP depletion kinetics in the Col-0 and *UGP1* KO mutant line during FB1 elicitation. If *UGP1* plays a role in eATP depletion, it would be the first gene to be shown to play a critical role in the FB1 mechanism of eATP depletion.

6.5 Final conclusions

Overall, work presented in this thesis has demonstrated a successful experimental approach employing proteomics and reverse genetics for identifying novel plant cell death regulators using the cell death inducing toxin FB1 and *Arabidopsis* suspension cell culture system (Figure 6.1). An ATP filter was used to identify putative cell death genes that are being regulated by ATP levels at the protein abundance levels. This approach reduced the number of genes to be tested by reverse genetics to a manageable level and resulted in the identification of several candidates, with one of them, ATPaseβ, being validated as a cell death regulator by reverse genetics. Additionally, a proteomics approach for identifying putative cell death genes that mediate the toxic effects of FB1 independently of its ability to trigger eATP depletion resulted in the identification of another cell death regulator *UGP1* as well as several other candidates. Knowledge of the eATP field in plants was expanded with the identification of several new genes and proteins modulated by eATP-mediated signalling using 2D-DiGE proteomics and re-examination of a DNA chip

experiment, providing indirect evidence for new physiological roles for eATP signalling in plants. Early extracellular ATP molecular marker genes were established and utilized as a tool for probing the eATP signalling cascade in the KO mutants and for testing a hypothesis relating to eATP control of defence responses. The potential of these markers in the area of eATP signalling will undoubtedly make them useful tools in future studies.

References

Abbracchio, M. P., G. Burnstock, J. M. Boeynaems, E. A. Barnard, J. L. Boyer, C. Kennedy, G. E. Knight, M. Fumagalli, C. Gachet, K. A. Jacobson and G. A. Weisman (2006). "International Union of Pharmacology LVIII: update on the P2Y G protein-coupled nucleotide receptors: from molecular mechanisms and pathophysiology to therapy." Pharmacological Reviews **58**(3): 281-341.

Abraham, E. H., A. G. Prat, L. Gerweck, T. Seneveratne, R. J. Arceci, R. Kramer, G. Guidotti and H. F. Cantiello (1993). "The multidrug resistance (mdr1) gene product functions as an ATP channel." Proc Natl Acad Sci U S A **90**(1): 312-6.

Agboh, K. C., T. E. Webb, R. J. Evans and S. J. Ennion (2004). "Functional characterization of a P2X receptor from Schistosoma mansoni." Journal of Biological Chemistry **279**(40): 41650-7.

AGSC, A. g. s. c. (2000). "Analysis of the genome sequence of the flowering plant Arabidopsis thaliana." Nature **408**(6814): 796-815.

Aki, T., M. Konishi, T. Kikuchi, T. Fujimori, T. Yoneyama and S. Yanagisawa (2007). "Distinct modulations of the hexokinase1-mediated glucose response and hexokinase1-independent processes by HYS1/CPR5 in Arabidopsis." Journal of Experimental Botany **58**(12): 3239-3248.

Allen, L. J., K. B. MacGregor, R. S. Koop, D. H. Bruce, J. Karner and A. W. Bown (1999). "The relationship between photosynthesis and a mastoparan-induced hypersensitive response in isolated mesophyll cells." Plant Physiology **119**(4): 1233-42.

Alonso, J. M. and J. R. Ecker (2006). "Moving forward in reverse: genetic technologies to enable genome-wide phenomic screens in Arabidopsis." Nat Rev Genet **7**(7): 524-36.

Alonso, J. M., A. N. Stepanova, T. J. Leisse, C. J. Kim, H. M. Chen, P. Shinn, D. K. Stevenson, J. Zimmerman, P. Barajas, R. Cheuk and a. l. et. (2003). "Genome-wide Insertional mutagenesis of Arabidopsis thaliana." Science **301**(5633): 653-657.

Amor, Y., C. H. Haigler, S. Johnson, M. Wainscott and D. P. Delmer (1995). "A Membrane-Associated Form of Sucrose Synthase and Its Potential Role in Synthesis of Cellulose and Callose in Plants." Proc Natl Acad Sci U S A **92**(20): 9353-9357.

Apel, K. and H. Hirt (2004). "Reactive oxygen species: Metabolism, oxidative stress, and signal transduction." Annual Review of Plant Biology **55**: 373-399.

Asai, T., J. M. Stone, J. E. Heard, Y. Kovtun, P. Yorgey, J. Sheen and F. M. Ausubel (2000). "Fumonisin B1-induced cell death in Arabidopsis protoplasts requires jasmonate-, ethylene-, and salicylate-dependent signaling pathways." Plant Cell **12**(10): 1823-1835.

Ascencio-Ibanez, J. T., R. Sozzani, T. J. Lee, T. M. Chu, R. D. Wolfinger, R. Cella and L. Hanley-Bowdoin (2008). "Global analysis of Arabidopsis gene expression uncovers a complex array of changes impacting pathogen response and cell cycle during geminivirus infection." Plant Physiology **148**(1): 436-54.

Ashburner, M., C. A. Ball, J. A. Blake, D. Botstein, H. Butler, J. M. Cherry, A. P. Davis, K. Dolinski, S. S. Dwight, J. T. Eppig, M. A. Harris, D. P. Hill, L. Issel-Tarver, A. Kasarskis, S. Lewis, J. C. Matese, J. E. Richardson, M. Ringwald, G. M. Rubin and G. Sherlock (2000). "Gene ontology: tool for the unification of biology. The Gene Ontology Consortium." Nature Genetics **25**(1): 25-9.

Ausubel, F. M. (2005). "Are innate immune signaling pathways in plants and animals conserved?" Nature Immunology **6**(10): 973-9.

Avni, A., J. D. Anderson, N. Holland, J. D. Rochaix, Z. Gromet-Elhanan and M. Edelman (1992). "Tentoxin sensitivity of chloroplasts determined by codon 83 of beta subunit of proton-ATPase." Science **257**(5074): 1245-7.

Baulcombe, D. C., G. R. Saunders, M. W. Bevan, M. A. Mayo and B. D. Harrison (1986). "Expression of biologically-active viral satellite RNA from the nuclear genome of transformed plants." Nature **321**(6068): 446-449.

Becker, K. G., D. A. Hosack, G. Dennis, Jr., R. A. Lempicki, T. J. Bright, C. Cheadle and J. Engel (2003). "PubMatrix: a tool for multiplex literature mining." BMC Bioinformatics **4**: 61.

Benschop, J. J., S. Mohammed, M. O'Flaherty, A. J. Heck, M. Slijper and F. L. Menke (2007). "Quantitative phosphoproteomics of early elicitor signaling in Arabidopsis." Molecular & Cellular Proteomics **6**(7): 1198-214.

Boccara, M., W. Schwartz, E. Guiot, G. Vidal, R. De Paepe, A. Dubois and A. C. Boccara (2007). "Early chloroplastic alterations analysed by optical coherence tomography during a harpin-induced hypersensitive response." Plant Journal **50**(2): 338-346.

Bodin, P. and G. Burnstock (2001). "Purinergic signalling: ATP release." Neurochemical Research **26**(8-9): 959-69.

Bohringer, J., D. Fischer, G. Mosler and R. Hengge-Aronis (1995). "UDP-glucose is a potential intracellular signal molecule in the control of expression of sigma S and sigma S-dependent genes in Escherichia coli." Journal of Bacteriology **177**(2): 413-22.

Boyum, R. and G. Guidotti (1997). "Glucose-dependent, cAMP-mediated ATP efflux from Saccharomyces cerevisiae." Microbiology **143 (Pt 6)**: 1901-8.

Burnstock, G. (1972). "Purinergic nerves." Pharmacological Reviews **24**(3): 509-81.

Burnstock, G. (2009). "Purinergic signalling: past, present and future." Brazilian Journal of Medical and Biological Research **42**(1): 3-8.

Cao, D., J. E. Froehlich, H. Zhang and C. L. Cheng (2003). "The chlorate-resistant and photomorphogenesis-defective mutant cr88 encodes a chloroplast-targeted HSP90." Plant Journal **33**(1): 107-18.

Chandra, H., P. K. Gupta, K. Sharma, A. R. Mattoo, S. K. Garg, W. N. Gade, R. Sirdeshmukh, K. Maithal and Y. Singh (2005). "Proteome analysis of mouse macrophages treated with anthrax lethal toxin." Biochimica Et Biophysica Acta **1747**(2): 151-9.

Chaudry, I. H. (1982). "Does ATP cross the cell plasma membrane." Yale J Biol Med **55**(1): 1-10.

Chen, L. and C. F. Brosnan (2006). "Regulation of immune response by P2X7 receptor." Crit Rev Immunol **26**(6): 499-513.

Chen, X., Y. Wang, J. Li, A. Jiang, Y. Cheng and W. Zhang (2009a). "Mitochondrial proteome during salt stress-induced programmed cell death in rice." Plant Physiol Biochem **47**(5): 407-15.

Chen, Z., Z. Zheng, J. Huang, Z. Lai and B. Fan (2009b). "Biosynthesis of salicylic acid in plants." Plant Signaling & Behavior **4**(6): 493-496.

Chessell, I. P., J. P. Hatcher, C. Bountra, A. D. Michel, J. P. Hughes, P. Green, J. Egerton, M. Murfin, J. Richardson, W. L. Peck, C. B. Grahames, M. A. Casula, Y. Yiangou, R. Birch, P. Anand and G. N. Buell (2005). "Disruption of the P2X7 purinoceptor gene abolishes chronic inflammatory and neuropathic pain." Pain **114**(3): 386-96.

Chivasa, S., A. M. Murphy, J. M. Hamilton, K. Lindsey, J. P. Carr and A. R. Slabas (2009a). "Extracellular ATP is a regulator of pathogen defence in plants." Plant Journal **60**(3): 436-448.

Chivasa, S., B. K. Ndimba, W. J. Simon, K. Lindsey and A. R. Slabas (2005a). "Extracellular ATP functions as an endogenous external metabolite regulating plant cell viability." Plant Cell **17**(11): 3019-3034.

Chivasa, S., B. K. Ndimba, W. J. Simon, D. Robertson, X. L. Yu, X. L. Yu, J. P. Knox, P. Bolwell and A. R. Slabas (2002). "Proteomic analysis of the Arabidopsis thaliana cell wall." Electrophoresis **23**(11): 1754-1765.

Chivasa, S., W. J. Simon, J. M. Hamilton, K. Lindsey and A. R. Slabas (2007). Discovery via proteomics of a novel cell signalling pathway in plants involving extracellular ATP. Plant proteomics. J. Šamaj and J. J. Thelen, Springer.

Chivasa, S., W. J. Simon, A. M. Murphy, K. Lindsey, J. P. Carr and A. R. Slabas (2010). "The effects of extracellular adenosine 5 '-triphosphate on the tobacco proteome." Proteomics **10**(2): 235-244.

Chivasa, S., W. J. Simon, X. L. Yu, N. Yalpani and A. R. Slabas (2005b). "Pathogen elicitor-induced changes in the maize extracellular matrix proteome." Proteomics **5**(18): 4894-4904.

Chivasa, S., D. F. Tome, J. M. Hamilton and A. R. Slabas (2011). "Proteomic analysis of extracellular ATP-regulated proteins identifies ATP synthase beta-subunit as a novel plant cell death regulator." Molecular & Cellular Proteomics **10**(3): M110 003905.

Chivasa, S., D. F. Tome, A. M. Murphy, J. M. Hamilton, K. Lindsey and J. P. Carr (2009b). "Extracellular ATP: a modulator of cell death and pathogen defense in plants." Plant Signal Behav **4**(11): 1078-80.

Ciereszko, I., H. Johansson and L. A. Kleczkowski (2001). "Sucrose and light regulation of a cold-inducible UDP-glucose pyrophosphorylase gene via a hexokinase-independent and abscisic acid-insensitive pathway in Arabidopsis." Biochemical Journal **354**(Pt 1): 67-72.

Clapham, D. E. (2007). "Calcium signaling." Cell **131**(6): 1047-58.

Clark, G. and S. J. Roux (2009). "Extracellular nucleotides: Ancient signaling molecules." Plant Science **177**(4): 239-244.

Clark, G., J. Torres, S. Finlayson, X. Guan, C. Handley, J. Lee, J. E. Kays, Z. J. Chen and S. J. Roux (2010a). "Apyrase (nucleoside triphosphate-diphosphohydrolase) and extracellular nucleotides regulate cotton fiber elongation in cultured ovules." Plant Physiology **152**(2): 1073-83.

Clark, G., M. Wu, N. Wat, J. Onyirimba, T. Pham, N. Herz, J. Ogoti, D. Gomez, A. A. Canales, G. Aranda, M. Blizard, T. Nyberg, A. Terry, J. Torres, J. Wu and S. J. Roux (2010b). "Both the stimulation and inhibition of root hair growth induced by extracellular nucleotides in Arabidopsis are mediated by nitric oxide and reactive oxygen species." Plant Molecular Biology **74**(4-5): 423-35.

Claros, M. G. and P. Vincens (1996). "Computational method to predict mitochondrially imported proteins and their targeting sequences." European Journal of Biochemistry **241**(3): 779-86.

Clough, S. J., K. A. Fengler, I. C. Yu, B. Lippok, R. K. Smith and A. F. Bent (2000). "The Arabidopsis dnd1 "defense, no death" gene encodes a mutated cyclic nucleotide-gated ion channel." Proc Natl Acad Sci U S A **97**(16): 9323-9328.

Coleman, H. D., T. Canam, K. Y. Kang, D. D. Ellis and S. D. Mansfield (2007). "Over-expression of UDP-glucose pyrophosphorylase in hybrid poplar affects carbon allocation." Journal of Experimental Botany **58**(15-16): 4257-68.

Communi, D., C. Govaerts, M. Parmentier and J. M. Boeynaems (1997). "Cloning of a human purinergic P2Y receptor coupled to phospholipase C and adenylyl cyclase." Journal of Biological Chemistry **272**(51): 31969-73.

Communi, D., N. Suarez-Huerta, D. Dussossoy, P. Savi and J. M. Boeynaems (2001). "Cotranscription and intergenic splicing of human P2Y11 and SSF1 genes." Journal of Biological Chemistry **276**(19): 16561-6.

Conigrave, A. D., J. Y. Lee, L. van der Weyden, L. Jiang, P. Ward, V. Tasevski, B. M. Luttrell and M. B. Morris (1998). "Pharmacological profile of a novel cyclic AMP-linked P2 receptor on undifferentiated HL-60 leukemia cells." Br J Pharmacol **124**(7): 1580-5.

Consonni, C., M. E. Humphry, H. A. Hartmann, M. Livaja, J. Durner, L. Westphal, J. Vogel, V. Lipka, B. Kemmerling, P. Schulze-Lefert, S. C. Somerville and R. Panstruga (2006). "Conserved requirement for a plant host cell protein in powdery mildew pathogenesis." Nature Genetics **38**(6): 716-720.

Curtis, M. J. and T. J. Wolpert (2002). "The oat mitochondrial permeability transition and its implication in victorin binding and induced cell death." Plant Journal **29**(3): 295-312.

D'Silva, I., G. G. Poirier and M. C. Heath (1998). "Activation of cysteine proteases in cowpea plants during the hypersensitive response--a form of programmed cell death." Experimental Cell Research **245**(2): 389-99.

Dai, N., A. Schaffer, M. Petreikov, Y. Shahak, Y. Giller, K. Ratner, A. Levine and D. Granot (1999). "Overexpression of Arabidopsis hexokinase in tomato plants inhibits growth, reduces photosynthesis, and induces rapid senescence." Plant Cell **11**(7): 1253-1266.

Danon, A. and P. Gallois (1998). "UV-C radiation induces apoptotic-like changes in Arabidopsis thaliana." Febs Letters **437**(1-2): 131-6.

Day, R. B., C. B. McAlvin, J. T. Loh, R. L. Denny, T. C. Wood, N. D. Young and G. Stacey (2000). "Differential expression of two soybean apyrases, one of which is an early nodulin." Mol Plant Microbe Interact **13**(10): 1053-70.

Delaney, T. P., S. Uknes, B. Vernooij, L. Friedrich, K. Weymann, D. Negrotto, T. Gaffney, M. Gut-Rella, H. Kessmann, E. Ward and J. Ryals (1994). "A central role of salicylic Acid in plant disease resistance." Science **266**(5188): 1247-50.

Demidchik, V., C. Nichols, M. Oliynyk, A. Dark, B. J. Glover and J. M. Davies (2003). "Is ATP a signaling agent in plants?" Plant Physiology **133**(2): 456-461.

Demidchik, V., Z. Shang, R. Shin, E. Thompson, L. Rubio, A. Laohavisit, J. C. Mortimer, S. Chivasa, A. R. Slabas, B. J. Glover, D. P. Schachtman, S. N. Shabala and J. M. Davies (2009). "Plant extracellular ATP signalling by plasma membrane NADPH oxidase and Ca2+ channels." Plant Journal **58**(6): 903-13.

Derelle, E., C. Ferraz, S. Rombauts, P. Rouze, A. Z. Worden, S. Robbens, F. Partensky, S. Degroeve, S. Echeynie, R. Cooke, Y. Saeys, J. Wuyts, K. Jabbari, C. Bowler, O. Panaud, B. Piegu, S. G. Ball, J. P. Ral, F. Y. Bouget, G. Piganeau, B. De Baets, A. Picard, M. Delseny, J. Demaille, Y. Van de Peer and H. Moreau (2006). "Genome analysis of the smallest free-living eukaryote Ostreococcus tauri unveils many unique features." Proc Natl Acad Sci U S A **103**(31): 11647-52.

Downward, J. (2003). "Cell biology: metabolism meets death." Nature **424**(6951): 896-7.

Drury, A. N. and A. Szent-Gyorgyi (1929). "The physiological activity of adenine compounds with especial reference to their action upon the mammalian heart." J Physiol **68**(3): 213-37.

Dutta, A. K., R. Z. Sabirov, H. Uramoto and Y. Okada (2004). "Role of ATP-conductive anion channel in ATP release from neonatal rat cardiomyocytes in ischaemic or hypoxic conditions." J Physiol **559**(Pt 3): 799-812.

Elliott, J. I., A. Surprenant, F. M. Marelli-Berg, J. C. Cooper, R. L. Cassady-Cain, C. Wooding, K. Linton, D. R. Alexander and C. F. Higgins (2005). "Membrane phosphatidylserine distribution as a non-apoptotic signalling mechanism in lymphocytes." Nat Cell Biol **7**(8): 808-16.

Etzler, M. E., G. Kalsi, N. N. Ewing, N. J. Roberts, R. B. Day and J. B. Murphy (1999). "A nod factor binding lectin with apyrase activity from legume roots." Proc Natl Acad Sci U S A **96**(10): 5856-61.

Ferrer, J. L., M. B. Austin, C. Stewart, Jr. and J. P. Noel (2008). "Structure and function of enzymes involved in the biosynthesis of phenylpropanoids." Plant Physiol Biochem **46**(3): 356-70.

Feys, B. J. and J. E. Parker (2000). "Interplay of signaling pathways in plant disease resistance." Trends in Genetics **16**(10): 449-55.

Finger, T. E., V. Danilova, J. Barrows, D. L. Bartel, A. J. Vigers, L. Stone, G. Hellekant and S. C. Kinnamon (2005). "ATP signaling is crucial for communication from taste buds to gustatory nerves." Science **310**(5753): 1495-9.

Foresi, N. P., A. M. Laxalt, C. V. Tonon, C. A. Casalongue and L. Lamattina (2007). "Extracellular ATP induces nitric oxide production in tomato cell suspensions." Plant Physiology **145**(3): 589-592.

Fountain, S. J., L. Cao, M. T. Young and R. A. North (2008). "Permeation properties of a P2X receptor in the green algae Ostreococcus tauri." Journal of Biological Chemistry **283**(22): 15122-6.

Fountain, S. J., K. Parkinson, M. T. Young, L. S. Cao, C. R. L. Thompson and R. A. North (2007). "An intracellular P2X receptor required for osmoregulation in Dictyostelium discoideum." Nature **448**(7150): 200-203.

Franklin-Tong, V. E. and C. W. Gourlay (2008). "A role for actin in regulating apoptosis/programmed cell death: evidence spanning yeast, plants and animals." Biochemical Journal **413**: 389-404.

Fukuda, H. (1997). "Tracheary Element Differentiation." Plant Cell **9**(7): 1147-1156.

Gaffney, T., L. Friedrich, B. Vernooij, D. Negrotto, G. Nye, S. Uknes, E. Ward, H. Kessmann and J. Ryals (1993). "Requirement of salicylic Acid for the induction of systemic acquired resistance." Science **261**(5122): 754-6.

Garrett, R. H. and C. M. Grisham (2010). *Biochemistry*. Boston USA, Brooks/Cole, Boston, MA.

Gilchrist, D. G. (1997). "Mycotoxins reveal connections between plants and animals in apoptosis and ceramide signaling." Cell Death and Differentiation **4**(8): 689-698.

Gomez-Gomez, L. and T. Boller (2002). "Flagellin perception: a paradigm for innate immunity." Trends in Plant Science **7**(6): 251-6.

Gookin, T. E., J. Kim and S. M. Assmann (2008). "Whole proteome identification of plant candidate G-protein coupled receptors in Arabidopsis, rice, and poplar: computational prediction and in-vivo protein coupling." Genome Biology **9**(7): R120.

Gorodeski, G. I. (2009). "P2X7-mediated chemoprevention of epithelial cancers." Expert Opin Ther Targets **13**(11): 1313-32.

Gottesman, M. M. and I. Pastan (1988). "The multidrug transporter, a double-edged sword." Journal of Biological Chemistry **263**(25): 12163-6.

Govindarajulu, M., S. Y. Kim, M. Libault, R. H. Berg, K. Tanaka, G. Stacey and C. G. Taylor (2009). "GS52 ecto-apyrase plays a critical role during soybean nodulation." Plant Physiology **149**(2): 994-1004.

Greenberg, J. T., A. L. Guo, D. F. Klessig and F. M. Ausubel (1994). "Programmed Cell-Death in Plants - a Pathogen-Triggered Response Activated Coordinately with Multiple Defense Functions." Cell **77**(4): 551-563.

Gross, A., K. Pilcher, E. Blachly-Dyson, E. Basso, J. Jockel, M. C. Bassik, S. J. Korsmeyer and M. Forte (2000). "Biochemical and genetic analysis of the mitochondrial

response of yeast to BAX and BCL-X(L)." Molecular and Cellular Biology **20**(9): 3125-36.

Groth, G., T. Hisabori, H. Lill and D. Bald (2002). "Substitution of a single amino acid switches the tentoxin-resistant thermophilic F1-ATPase into a tentoxin-sensitive enzyme." Journal of Biological Chemistry **277**(23): 20117-9.

Guo, J. and J. G. Chen (2008). "RACK1 genes regulate plant development with unequal genetic redundancy in Arabidopsis." BMC Plant Biol **8**: 108.

Gygi, S. P., Y. Rochon, B. R. Franza and R. Aebersold (1999). "Correlation between protein and mRNA abundance in yeast." Molecular and Cellular Biology **19**(3): 1720-30.

Hajduch, M., L. B. Hearne, J. A. Miernyk, J. E. Casteel, T. Joshi, G. K. Agrawal, Z. Song, M. Zhou, D. Xu and J. J. Thelen (2010). "Systems analysis of seed filling in Arabidopsis: using general linear modeling to assess concordance of transcript and protein expression." Plant Physiology **152**(4): 2078-87.

Handa, M. and G. Guidotti (1996). "Purification and cloning of a soluble ATP-diphosphohydrolase (apyrase) from potato tubers (Solanum tuberosum)." Biochem Biophys Res Commun **218**(3): 916-23.

Harden, T. K., J. I. Sesma, I. P. Fricks and E. R. Lazarowski (2010). "Signalling and pharmacological properties of the P2Y receptor." Acta Physiol (Oxf) **199**(2): 149-60.

Haynes, P. A., S. P. Gygi, D. Figeys and R. Aebersold (1998). "Proteome analysis: biological assay or data archive?" Electrophoresis **19**(11): 1862-71.

Hennessey, T. M. (2005). "Responses of the ciliates Tetrahymena and Paramecium to external ATP and GTP." Purinergic Signal **1**(2): 101-10.

Herr, A. J. and D. C. Baulcombe (2004). "RNA silencing pathways in plants." Cold Spring Harb Symp Quant Biol **69**: 363-70.

Holmgren, A. (1989). "Thioredoxin and glutaredoxin systems." Journal of Biological Chemistry **264**(24): 13963-6.

Holton, P. (1959). "The liberation of adenosine triphosphate on antidromic stimulation of sensory nerves." J Physiol **145**(3): 494-504.

Horton, P., K. J. Park, T. Obayashi and K. Nakai (2006). "Protein subcellular localization prediction with WOLF PSORT." Proceedings of the 4th Asia-Pacific Bioinformatics Conference **3**: 39-48

363.

Hu, G. S., N. Yalpani, S. P. Briggs and G. S. Johal (1998). "A porphyrin pathway impairment is responsible for the phenotype of a dominant disease lesion mimic mutant of maize." Plant Cell **10**(7): 1095-1105.

Huang da, W., B. T. Sherman and R. A. Lempicki (2009). "Systematic and integrative analysis of large gene lists using DAVID bioinformatics resources." Nat Protoc **4**(1): 44-57.

Huang da, W., B. T. Sherman, Q. Tan, J. Kir, D. Liu, D. Bryant, Y. Guo, R. Stephens, M. W. Baseler, H. C. Lane and R. A. Lempicki (2007). "DAVID Bioinformatics Resources: expanded annotation database and novel algorithms to better extract biology from large gene lists." Nucleic Acids Research **35**(Web Server issue): W169-75.

Huang, J., M. Gu, Z. Lai, B. Fan, K. Shi, Y. H. Zhou, J. Q. Yu and Z. Chen (2010). "Functional analysis of the Arabidopsis PAL gene family in plant growth, development, and response to environmental stress." Plant Physiology **153**(4): 1526-38.

Huber, S. C. and T. Akazawa (1986). "A novel sucrose synthase pathway for sucrose degradation in cultured sycamore cells." Plant Physiology **81**(4): 1008-13.

Ishitani, R. and D. M. Chuang (1996). "Glyceraldehyde-3-phosphate dehydrogenase antisense oligodeoxynucleotides protect against cytosine arabinonucleoside-induced apoptosis in cultured cerebellar neurons." Proc Natl Acad Sci U S A **93**(18): 9937-41.

Ivanova, E. P., Y. V. Alexeeva, D. K. Pham, J. P. Wright and D. V. Nicolau (2006). "ATP level variations in heterotrophic bacteria during attachment on hydrophilic and hydrophobic surfaces." International Microbiology **9**(1): 37-46.

Jabs, T., R. A. Dietrich and J. L. Dangl (1996). "Initiation of runaway cell death in an Arabidopsis mutant by extracellular superoxide." Science **273**(5283): 1853-1856.

Jacobson, M. D., M. Weil and M. C. Raff (1997). "Programmed cell death in animal development." Cell **88**(3): 347-354.

Jaffe, M. J. (1973). "Role of Atp in Mechanically Stimulated Rapid Closure of Venus-Flytrap." Plant Physiology **51**(1): 17-18.

Jeter, C. R. and S. J. Roux (2006). "Plant responses to extracellular nucleotides: Cellular processes and biological effects." Purinergic Signal **2**(3): 443-9.

Jeter, C. R., W. Q. Tang, E. Henaff, T. Butterfield and S. J. Roux (2004). "Evidence of a novel cell signaling role for extracellular adenosine triphosphates and diphosphates in Arabidopsis." Plant Cell **16**(10): 2652-2664.

Jones, J. D. and J. L. Dangl (2006). "The plant immune system." Nature **444**(7117): 323-9.

Kanehisa, M. and S. Goto (2000). "KEGG: kyoto encyclopedia of genes and genomes." Nucleic Acids Research **28**(1): 27-30.

Karp, N. A., J. L. Griffin and K. S. Lilley (2005). "Application of partial least squares discriminant analysis to two-dimensional difference gel studies in expression proteomics." Proteomics **5**(1): 81-90.

Katagiri, F., R. Thilmony and S. Y. He (**2002**). The Arabidopsis Thaliana-Pseudomonas Syringae

Interaction. The Arabidopsis book, America Society of Plant Biologists.

Khakh, B. S. and G. Burnstock (2009). "The double life of ATP." Sci Am **301**(6): 84-90, 92.

Kim, M., J. H. Lim, C. S. Ahn, K. Park, G. T. Kim, W. T. Kim and H. S. Pai (2006a). "Mitochondria-associated hexokinases play a role in the control of programmed cell death in Nicotiana benthamiana." Plant Cell **18**(9): 2341-55.

Kim, S. H., S. H. Yang, T. J. Kim, J. S. Han and J. W. Suh (2009). "Hypertonic stress increased extracellular ATP levels and the expression of stress-responsive genes in Arabidopsis thaliana seedlings." Biosci Biotechnol Biochem **73**(6): 1252-6.

Kim, S. Y., M. Sivaguru and G. Stacey (2006b). "Extracellular ATP in plants. Visualization, localization, and analysis of physiological significance in growth and signaling." Plant Physiology **142**(3): 984-992.

Kleczkowski, L. A., M. Geisler, I. Ciereszko and H. Johansson (2004). "UDP-glucose pyrophosphorylase. An old protein with new tricks." Plant Physiology **134**(3): 912-8.

Knight, G. E. (2009). Purinergic receptors. Encyclopedia of Neuroscience. L. R. Squire, Elsevier.

Komoszynski, M. and A. Wojtczak (1996). "Apyrases (ATP diphosphohydrolases, EC 3.6.1.5): Function and relationship to ATPases." Biochimica Et Biophysica Acta-Molecular Cell Research **1310**(2): 233-241.

Koukalova, B., A. Kovarik, J. Fajkus and J. Siroky (1997). "Chromatin fragmentation associated with apoptotic changes in tobacco cells exposed to cold stress." Febs Letters **414**(2): 289-92.

Krause, M. and J. Durner (2004). "Harpin inactivates mitochondria in Arabidopsis suspension cells." Mol Plant Microbe Interact **17**(2): 131-9.

Krishna, P. and G. Gloor (2001). "The Hsp90 family of proteins in Arabidopsis thaliana." Cell Stress Chaperones **6**(3): 238-46.

Krysan, P. J., J. C. Young and M. R. Sussman (1999). "T-DNA as an insertional mutagen in Arabidopsis." Plant Cell **11**(12): 2283-90.

Kunze, G., C. Zipfel, S. Robatzek, K. Niehaus, T. Boller and G. Felix (2004). "The N terminus of bacterial elongation factor Tu elicits innate immunity in Arabidopsis plants." Plant Cell **16**(12): 3496-507.

Kuroyanagi, M., K. Yamada, N. Hatsugai, M. Kondo, M. Nishimura and I. Hara-Nishimura (2005). "Vacuolar processing enzyme is essential for mycotoxin-induced cell death in Arabidopsis thaliana." Journal of Biological Chemistry **280**(38): 32914-20.

Kus, J. V., K. Zaton, R. Sarkar and R. K. Cameron (2002). "Age-related resistance in Arabidopsis is a developmentally regulated defense response to Pseudomonas syringae." Plant Cell **14**(2): 479-490.

Laemmli, U. K. (1970). "Cleavage of structural proteins during the assembly of the head of bacteriophage T4." Nature **227**(5259): 680-5.

Lam, E. (2004). "Controlled cell death, plant survival and development." Nat Rev Mol Cell Biol **5**(4): 305-15.

Lawton, K., K. Weymann, L. Friedrich, B. Vernooij, S. Uknes and J. Ryals (1995). "Systemic acquired resistance in Arabidopsis requires salicylic acid but not ethylene." Molecular Plant-Microbe Interactions **8**(6): 863-870.

Lazarowski, E. R., R. C. Boucher and T. K. Harden (2003). "Mechanisms of release of nucleotides and integration of their action as P2X- and P2Y-receptor activating molecules." Molecular Pharmacology **64**(4): 785-95.

Lee, H., Y. Guo, M. Ohta, L. Xiong, B. Stevenson and J. K. Zhu (2002). "LOS2, a genetic locus required for cold-responsive gene transcription encodes a bi-functional enolase." Embo Journal **21**(11): 2692-702.

Lee, H. I., J. León and I. Raskin (1995). "Biosynthesis and metabolism of salicylic acid." Proceedings of the National Academy of Sciences **92**(10): 4076-4079.

Lee, H. I. and I. Raskin (1999). "Purification, cloning, and expression of a pathogen inducible UDP-glucose:Salicylic acid glucosyltransferase from tobacco." Journal of Biological Chemistry **274**(51): 36637-42.

Lew, R. R. and J. D. W. Dearnaley (2000). "Extracellular nucleotide effects on the electrical properties of growing Arabidopsis thaliana root hairs." Plant Science **153**(1): 1-6.

Li, L. Y., X. Luo and X. Wang (2001). "Endonuclease G is an apoptotic DNase when released from mitochondria." Nature **412**(6842): 95-9.

Li, M., T. J. Kim, H. J. Kwon and J. W. Suh (2008). "Effects of extracellular ATP on the physiology of Streptomyces coelicolor A3(2)." Fems Microbiology Letters **286**(1): 24-31.

Li, P., D. Nijhawan, I. Budihardjo, S. M. Srinivasula, M. Ahmad, E. S. Alnemri and X. Wang (1997). "Cytochrome c and dATP-dependent formation of Apaf-1/caspase-9 complex initiates an apoptotic protease cascade." Cell **91**(4): 479-89.

Libault, M., J. Wan, T. Czechowski, M. Udvardi and G. Stacey (2007). "Identification of 118 Arabidopsis transcription factor and 30 ubiquitin-ligase genes responding to chitin, a plant-defense elicitor." Mol Plant Microbe Interact **20**(8): 900-11.

Lim, P. O., H. J. Kim and H. G. Nam (2007). "Leaf senescence." Annual Review of Plant Biology **58**: 115-136.

Lin, S. S., R. Martin, S. Mongrand, S. Vandenabeele, K. C. Chen, I. C. Jang and N. H. Chua (2008). "RING1 E3 ligase localizes to plasma membrane lipid rafts to trigger FB1-induced programmed cell death in Arabidopsis." Plant Journal **56**(4): 550-561.

Liu, X., C. N. Kim, J. Yang, R. Jemmerson and X. Wang (1996). "Induction of apoptotic program in cell-free extracts: requirement for dATP and cytochrome c." Cell **86**(1): 147-57.

Ludlow, M., D. Traynor, P. Fisher and S. Ennion (2008). "Extracellular ATP and ADP mediate Ca2+ influx in Dictyostelium discoideum." Purinergic Signalling **4**: S5-S6.

Lustig, K. D., A. K. Shiau, A. J. Brake and D. Julius (1993). "Expression cloning of an ATP receptor from mouse neuroblastoma cells." Proc Natl Acad Sci U S A **90**(11): 5113-7.

Lüttge, U., E. V. Schöch and E. Ball (1974). "Can Externally Applied Atp Supply Energy to Active Ion Uptake Mechanisms of Intact Plant Cells?" Functional Plant Biology **1**(2): 211-220.

Mach, J. M., A. R. Castillo, R. Hoogstraten and J. T. Greenberg (2001). "The Arabidopsis-accelerated cell death gene ACD2 encodes red chlorophyll catabolite reductase and suppresses the spread of disease symptoms." Proc Natl Acad Sci U S A **98**(2): 771-776.

Majewski, N., V. Nogueira, P. Bhaskar, P. E. Coy, J. E. Skeen, K. Gottlob, N. S. Chandel, C. B. Thompson, R. B. Robey and N. Hay (2004). "Hexokinase-mitochondria interaction mediated by Akt is required to inhibit apoptosis in the presence or absence of Bax and Bak." Molecular Cell **16**(5): 819-30.

Mann, M. and O. N. Jensen (2003). "Proteomic analysis of post-translational modifications." Nature Biotechnology **21**(3): 255-61.

Mano, J., E. Belles-Boix, E. Babiychuk, D. Inze, Y. Torii, E. Hiraoka, K. Takimoto, L. Slooten, K. Asada and S. Kushnir (2005). "Protection against photooxidative injury of tobacco leaves by 2-alkenal reductase. Detoxication of lipid peroxide-derived reactive carbonyls." Plant Physiology **139**(4): 1773-83.

Marrs, K. A. (1996). "The Functions and Regulation of Glutathione S-Transferases in Plants." Annu Rev Plant Physiol Plant Mol Biol **47**: 127-158.

Marteau, F., N. S. Gonzalez, D. Communi, M. Goldman and J. M. Boeynaems (2005). "Thrombospondin-1 and indoleamine 2,3-dioxygenase are major targets of extracellular ATP in human dendritic cells." Blood **106**(12): 3860-6.

Mattevi, A. (2006). "To be or not to be an oxidase: challenging the oxygen reactivity of flavoenzymes." Trends in Biochemical Sciences **31**(5): 276-83.

May, M. J. and C. J. Leaver (1993). "Oxidative Stimulation of Glutathione Synthesis in Arabidopsis thaliana Suspension Cultures." Plant Physiology **103**(2): 621-627.

McAlvin, C. B. and G. Stacey (2005). "Transgenic expression of the soybean apyrase in Lotus japonicus enhances nodulation." Plant Physiology **137**(4): 1456-62.

McCabe, P. F., A. Levine, P. J. Meijer, N. A. Tapon and R. I. Pennell (1997). "A programmed cell death pathway activated in carrot cells cultured at low cell density." Plant Journal **12**(2): 267-280.

McCoy, J. G., E. Bitto, C. A. Bingman, G. E. Wesenberg, R. M. Bannen, D. A. Kondrashov and G. N. Phillips, Jr. (2007). "Structure and dynamics of UDP-

glucose pyrophosphorylase from Arabidopsis thaliana with bound UDP-glucose and UTP." Journal of Molecular Biology **366**(3): 830-41.

Mega, R., M. Manzoku, A. Shinkai, N. Nakagawa, S. Kuramitsu and R. Masui (2010). "Very rapid induction of a cold shock protein by temperature downshift in Thermus thermophilus." Biochem Biophys Res Commun **399**(3): 336-40.

Meng, M., M. Geisler, H. Johansson, J. Harholt, H. V. Scheller, E. J. Mellerowicz and L. A. Kleczkowski (2009). "UDP-glucose pyrophosphorylase is not rate limiting, but is essential in Arabidopsis." Plant and Cell Physiology **50**(5): 998-1011.

Meng, M., M. Wilczynska and L. A. Kleczkowski (2008). "Molecular and kinetic characterization of two UDP-glucose pyrophosphorylases, products of distinct genes, from Arabidopsis." Biochimica Et Biophysica Acta **1784**(6): 967-72.

Mengiste, T., P. Amedeo and J. Paszkowski (1997). "High-efficiency transformation of Arabidopsis thaliana with a selectable marker gene regulated by the T-DNA 1' promoter." Plant Journal **12**(4): 945-8.

Miernyk, J. A. (1999). "Protein folding in the plant cell." Plant Physiology **121**(3): 695-703.

Millson, S. H., A. W. Truman, V. King, C. Prodromou, L. H. Pearl and P. W. Piper (2005). "A two-hybrid screen of the yeast proteome for Hsp90 interactors uncovers a novel Hsp90 chaperone requirement in the activity of a stress-activated mitogen-activated protein kinase, Slt2p (Mpk1p)." Eukaryotic Cell **4**(5): 849-60.

Mizukami-Murata, S., H. Iwahashi, S. Kimura, K. Nojima, Y. Sakurai, T. Saitou, N. Fujii, Y. Murata, S. Suga, K. Kitagawa, K. Tanaka, S. Endo and M. Hoshi (2010). "Genome-wide expression changes in Saccharomyces cerevisiae in response to high-LET ionizing radiation." Appl Biochem Biotechnol **162**(3): 855-70.

Montillet, J. L., S. Chamnongpol, C. Rusterucci, J. Dat, B. van de Cotte, J. P. Agnel, C. Battesti, D. Inze, F. Van Breusegem and C. Triantaphylides (2005). "Fatty acid hydroperoxides and H2O2 in the execution of hypersensitive cell death in tobacco leaves." Plant Physiology **138**(3): 1516-26.

Moore, B., L. Zhou, F. Rolland, Q. Hall, W. H. Cheng, Y. X. Liu, I. Hwang, T. Jones and J. Sheen (2003). "Role of the Arabidopsis glucose sensor HXK1 in nutrient, light, and hormonal signaling." Science **300**(5617): 332-6.

Moriyama, E. N., P. K. Strope, S. O. Opiyo, Z. Chen and A. M. Jones (2006). "Mining the Arabidopsis thaliana genome for highly-divergent seven transmembrane receptors." Genome Biology **7**(10): R96.

Ndimba, B. K., S. Chivasa, J. M. Hamilton, W. J. Simon and A. R. Slabas (2003). "Proteomic analysis of changes in the extracellular matrix of Arabidopsis cell suspension cultures induced by fungal elicitors." Proteomics **3**(6): 1047-1059.

Noctor, G. and C. H. Foyer (1998). "Ascorbate and Glutathione: Keeping Active Oxygen Under Control." Annu Rev Plant Physiol Plant Mol Biol **49**: 249-279.

Noel, L. D., G. Cagna, J. Stuttmann, L. Wirthmuller, S. Betsuyaku, C. P. Witte, R. Bhat, N. Pochon, T. Colby and J. E. Parker (2007). "Interaction between SGT1 and cytosolic/nuclear HSC70 chaperones regulates Arabidopsis immune responses." Plant Cell **19**(12): 4061-76.

Noh, Y. S. and R. M. Amasino (1999). "Identification of a promoter region responsible for the senescence-specific expression of SAG12." Plant Molecular Biology **41**(2): 181-194.

North, R. A. (2002). "Molecular physiology of P2X receptors." Physiological Reviews **82**(4): 1013-1067.

Oh, S. A., S. Y. Lee, I. K. Chung, C. H. Lee and H. G. Nam (1996). "A senescence-associated gene of Arabidopsis thaliana is distinctively regulated during natural and artificially induced leaf senescence." Plant Molecular Biology **30**(4): 739-54.

Osbourn, A. (2010). "Gene clusters for secondary metabolic pathways: an emerging theme in plant biology." Plant Physiology **154**(2): 531-5.

Packham, D. E., L. Jiang and A. D. Conigrave (1996). "ATP-induced beta-glucuronidase release from undifferentiated HL-60 cells is dependent on Ca2+ ions." Cellular Signalling **8**(1): 67-73.

Parish, R. W. and M. Weibel (1980). "Extracellular ATP, ecto-ATPase and calcium influx in Dictyostelium discoideum cells." Febs Letters **118**(2): 263-6.

Park, J. I., T. Ishimizu, K. Suwabe, K. Sudo, H. Masuko, H. Hakozaki, I. S. Nou, G. Suzuki and M. Watanabe (2010). "UDP-Glucose Pyrophosphorylase is Rate Limiting in Vegetative and Reproductive Phases in Arabidopsis thaliana." Plant and Cell Physiology **51**(6): 981-996.

Pennington, S. R. and M. J. Dunn (2001). Proteomics: From protein sequence to function.

Perkins, D. N., D. J. Pappin, D. M. Creasy and J. S. Cottrell (1999). "Probability-based protein identification by searching sequence databases using mass spectrometry data." Electrophoresis **20**(18): 3551-67.

Plesner, L. (1995). "Ecto-ATPases: identities and functions." International Review of Cytology - a Survey of Cell Biology **158**: 141-214.

Potucek, Y. D., J. M. Crain and J. J. Watters (2006). "Purinergic receptors modulate MAP kinases and transcription factors that control microglial inflammatory gene expression." Neurochemistry International **49**(2): 204-14.

Pruss, G. J., E. W. Nester and V. Vance (2008). "Infiltration with Agrobacterium tumefaciens induces host defense and development-dependent responses in the infiltrated zone." Mol Plant Microbe Interact **21**(12): 1528-38.

Pruzinska, A., G. Tanner, I. Anders, M. Roca and S. Hortensteiner (2003). "Chlorophyll breakdown: Pheophorbide a oxygenase is a Rieske-type iron-sulfur protein, encoded by the accelerated cell death 1 gene." Proc Natl Acad Sci U S A **100**(25): 15259-15264.

Qi, A. D., C. Kennedy, T. K. Harden and R. A. Nicholas (2001). "Differential coupling of the human P2Y(11) receptor to phospholipase C and adenylyl cyclase." Br J Pharmacol **132**(1): 318-26.

Queitsch, C., T. A. Sangster and S. Lindquist (2002). "Hsp90 as a capacitor of phenotypic variation." Nature **417**(6889): 618-24.

Rabilloud, T., C. Valette and J. J. Lawrence (1994). "Sample application by in-gel rehydration improves the resolution of two-dimensional electrophoresis with immobilized pH gradients in the first dimension." Electrophoresis **15**(12): 1552-8.

Ramagli, L. S., S. Capetillo, F. F. Becker and L. V. Rodriguez (1985). "Alterations in nonhistone chromatin proteins during hepatocarcinogenesis induced by diverse acting carcinogens." Carcinogenesis **6**(3): 367-75.

Rao, M. V. and K. R. Davis (2001). "The physiology of ozone induced cell death." Planta **213**(5): 682-90.

Reape, T. J. and P. F. McCabe (2010). "Apoptotic-like regulation of programmed cell death in plants." Apoptosis **15**(3): 249-56.

Reichler, S. A., J. Torres, A. L. Rivera, V. A. Cintolesi, G. Clark and S. J. Roux (2009). "Intersection of two signalling pathways: extracellular nucleotides regulate pollen germination and pollen tube growth via nitric oxide." Journal of Experimental Botany **60**(7): 2129-38.

Reuveni, M., S. Tuzun, J. S. Cole, M. R. Siegel and J. Kuc (1986). "The Effects of Plant-Age and Leaf Position on the Susceptibility of Tobacco to Blue Mold Caused by Peronospora-Tabacina." Phytopathology **76**(4): 455-458.

Ribnicky, D. M., V. Shulaev and I. Raskin (1998). "Intermediates of Salicylic Acid Biosynthesis in Tobacco." Plant Physiology **118**(2): 565-572.

Riewe, D., L. Grosman, A. R. Fernie, C. Wucke and P. Geigenberger (2008a). "The potato-specific apyrase is apoplastically localized and has influence on gene expression, growth, and development." Plant Physiology **147**(3): 1092-109.

Riewe, D., L. Grosman, A. R. Fernie, H. Zauber, C. Wucke and P. Geigenberger (2008b). "A Cell Wall-Bound Adenosine Nucleosidase is Involved in the Salvage of Extracellular ATP in Solanum tuberosum (vol 49, pg 1572, 2008)." Plant and Cell Physiology **49**(11): 1765-1765.

Rocha, E. P. (2008). "The organization of the bacterial genome." Annual Review of Genetics **42**: 211-33.

Rodriguez-Ariza, A., L. M. Lopez-Sanchez, R. Gonzalez, F. J. Corrales, P. Lopez, A. Bernardos and J. Muntane (2005). "Altered protein expression and protein nitration pattern during d-galactosamine-induced cell death in human hepatocytes: a proteomic analysis." Liver Int **25**(6): 1259-69.

Rolland, F., E. Baena-Gonzalez and J. Sheen (2006). "Sugar sensing and signaling in plants: conserved and novel mechanisms." Annual Review of Plant Biology **57**: 675-709.

Rosso, M. G., Y. Li, N. Strizhov, B. Reiss, K. Dekker and B. Weisshaar (2003). "An Arabidopsis thaliana T-DNA mutagenized population (GABI-Kat) for flanking sequence tag-based reverse genetics." Plant Molecular Biology **53**(1-2): 247-59.

Roux, S. J. and I. Steinebrunner (2007). "Extracellular ATP: an unexpected role as a signaler in plants." Trends in Plant Science **12**(11): 522-527.

Rowland, J. (2006). Analysis of the Androgen-regulated Proteome
in Human Prostate Cancer. Urology Research Group. Newcastle-upon-Tyne, University of Newcastle. **Doctor of Philosophy:** 399.

Rowland, J. G., W. J. Simon, Y. Nishiyama and A. R. Slabas (2010). "Differential proteomic analysis using iTRAQ reveals changes in thylakoids associated with Photosystem II-acquired thermotolerance in Synechocystis sp. PCC 6803." Proteomics **10**(10): 1917-29.

Rozen, S. and H. Skaletsky (2000). "Primer3 on the WWW for general users and for biologist programmers." Methods Mol Biol **132**: 365-86.

Sambrook, J., E. F. Fritsch and T. Maniatis (1989). Molecular Cloning: A Laboratory Manual. Cold Spring Harbor, New York, Cold Spring Harbor Laboratory Press.

Sanchez, J. C., V. Rouge, M. Pisteur, F. Ravier, L. Tonella, M. Moosmayer, M. R. Wilkins and D. F. Hochstrasser (1997). "Improved and simplified in-gel sample application using reswelling of dry immobilized pH gradients." Electrophoresis **18**(3-4): 324-7.

Sangster, T. A., A. Bahrami, A. Wilczek, E. Watanabe, K. Schellenberg, C. McLellan, A. Kelley, S. W. Kong, C. Queitsch and S. Lindquist (2007). "Phenotypic diversity and altered environmental plasticity in Arabidopsis thaliana with reduced Hsp90 levels." Plos One **2**(7): e648.

Saunders, P. A., R. W. Chen and D. M. Chuang (1999). "Nuclear translocation of glyceraldehyde-3-phosphate dehydrogenase isoforms during neuronal apoptosis." Journal of Neurochemistry **72**(3): 925-32.

Scott, I. and D. C. Logan (2008). "Mitochondrial morphology transition is an early indicator of subsequent cell death in Arabidopsis." New Phytologist **177**(1): 90-101.

Seefelder, W., H. U. Humpf, G. Schwerdt, R. Freudinger and M. Gekle (2003). "Induction of apoptosis in cultured human proximal tubule cells by fumonisins and fumonisin metabolites." Toxicol Appl Pharmacol **192**(2): 146-53.

Shang, Z., A. Laohavisit and J. M. Davies (2009). "Extracellular ATP activates an Arabidopsis plasma membrane Ca(2+)-permeable conductance." Plant Signal Behav **4**(10): 989-91.

Shi, L. H., J. Bielawski, J. Y. Mu, H. L. Dong, C. Teng, J. Zhang, X. H. Yang, N. Tomishige, K. Hanada, Y. A. Hannun and J. R. Zuo (2007). "Involvement of sphingoid bases in mediating reactive oxygen intermediate production and programmed cell death in Arabidopsis." Cell Research **17**(12): 1030-1040.

Shibata, Y., K. Kawakita and D. Takemoto (2010). "Age-Related Resistance of Nicotiana benthamiana Against Hemibiotrophic Pathogen Phytophthora infestans Requires Both Ethylene- and Salicylic Acid-Mediated Signaling Pathways." Molecular Plant-Microbe Interactions **23**(9): 1130-1142.

Skalamera, D. and M. C. Heath (1998). "Changes in the cytoskeleton accompanying infection-induced nuclear movements and the hypersensitive response in plant cells invaded by rust fungi." Plant Journal **16**(2): 191-200.

Smith-Becker, J., E. Marois, E. J. Huguet, S. L. Midland, J. J. Sims and N. T. Keen (1998). "Accumulation of salicylic acid and 4-hydroxybenzoic acid in phloem fluids of cucumber during systemic acquired resistance is preceded by a transient increase in phenylalanine ammonia-lyase activity in petioles and stems." Plant Physiology **116**(1): 231-8.

Song, C. J., I. Steinebrunner, X. Z. Wang, S. C. Stout and S. J. Roux (2006). "Extracellular ATP induces the accumulation of superoxide via NADPH oxidases in Arabidopsis." Plant Physiology **140**(4): 1222-1232.

Song, H., R. Zhao, P. Fan, X. Wang, X. Chen and Y. Li (2009). "Overexpression of AtHsp90.2, AtHsp90.5 and AtHsp90.7 in Arabidopsis thaliana enhances plant sensitivity to salt and drought stresses." Planta **229**(4): 955-64.

Sorensen, C. E. and I. Novak (2001). "Visualization of ATP release in pancreatic acini in response to cholinergic stimulus. Use of fluorescent probes and confocal microscopy." Journal of Biological Chemistry **276**(35): 32925-32.

Srinivasula, S. M., M. Ahmad, T. Fernandes-Alnemri and E. S. Alnemri (1998). "Autoactivation of procaspase-9 by Apaf-1-mediated oligomerization." Molecular Cell **1**(7): 949-57.

Srobarova, A., J. A. da Silva, G. Kogan, A. Ritieni and A. Santini (2009). "Beauvericin decreases cell viability of wheat." Chem Biodivers **6**(8): 1208-15.

Steele, J. A., T. F. Uchytil, R. D. Durbin, P. Bhatnagar and D. H. Rich (1976). "Chloroplast coupling factor 1: A species-specific receptor for tentoxin." Proc Natl Acad Sci U S A **73**(7): 2245-8.

Steinebrunner, I., C. Jeter, C. Song and S. J. Roux (2000). "Molecular and biochemical comparison of two different apyrases from Arabidopsis thaliana." Plant Physiology and Biochemistry **38**(12): 913-922.

Steinebrunner, I., J. Wu, Y. Sun, A. Corbett and S. J. Roux (2003). "Disruption of apyrases inhibits pollen germination in arabidopsis." Plant Physiology **131**(4): 1638-1647.

Stockmann-Juvala, H., J. Mikkola, J. Naarala, J. Loikkanen, E. Elovaara and K. Savolainen (2004). "Fumonisin B-1-induced toxicity and oxidative damage in U-118MG glioblastoma cells." Toxicology **202**(3): 173-183.

Stockmann-Juvala, H. and K. Savolainen (2008). "A review of the toxic effects and mechanisms of action of fumonisin B1." Human & Experimental Toxicology **27**(11): 799-809.

Stone, J. M., J. E. Heard, T. Asai and F. M. Ausubel (2000). "Simulation of fungal-mediated cell death by fumonisin B1 and selection of fumonisin B1-resistant (fbr) Arabidopsis mutants." Plant Cell **12**(10): 1811-1822.

Stone, J. M., X. Liang, E. R. Nekl and J. J. Stiers (2005). "Arabidopsis AtSPL14, a plant-specific SBP-domain transcription factor, participates in plant development and sensitivity to fumonisin B1." Plant Journal **41**(5): 744-754.

Suarez, M. F., L. H. Filonova, A. Smertenko, E. I. Savenkov, D. H. Clapham, S. von Arnold, B. Zhivotovsky and P. V. Bozhkov (2004). "Metacaspase-dependent programmed cell death is essential for plant embryogenesis." Current Biology **14**(9): R339-40.

Sueldo, D. J., N. P. Foresi, C. A. Casalongue, L. Lamattina and A. M. Laxalt (2010). "Phosphatidic acid formation is required for extracellular ATP-mediated nitric oxide production in suspension-cultured tomato cells." New Phytologist **185**(4): 909-16.

Sundstrom, J. F., A. Vaculova, A. P. Smertenko, E. I. Savenkov, A. Golovko, E. Minina, B. S. Tiwari, S. Rodriguez-Nieto, A. A. Zamyatnin, Jr., T. Valineva and a. l. et. (2009). "Tudor staphylococcal nuclease is an evolutionarily conserved component of the programmed cell death degradome." Nat Cell Biol **11**(11): 1347-54.

Susin, S. A., H. K. Lorenzo, N. Zamzami, I. Marzo, B. E. Snow, G. M. Brothers, J. Mangion, E. Jacotot, P. Costantini, M. Loeffler, N. Larochette, D. R. Goodlett, R. Aebersold, D. P. Siderovski, J. M. Penninger and G. Kroemer (1999). "Molecular characterization of mitochondrial apoptosis-inducing factor." Nature **397**(6718): 441-6.

Tanaka, K., S. J. Swanson, S. Gilroy and G. Stacey (2010). "Extracellular nucleotides elicit cytosolic free calcium oscillations in Arabidopsis." Plant Physiology **154**(2): 705-19.

Tang, W. Q., S. R. Brady, Y. Sun, G. K. Muday and S. J. Roux (2003). "Extracellular ATP inhibits root gravitropism at concentrations that inhibit polar auxin transport." Plant Physiology **131**(1): 147-154.

Tax, F. E. and D. M. Vernon (2001). "T-DNA-associated duplication/translocations in Arabidopsis. Implications for mutant analysis and functional genomics." Plant Physiology **126**(4): 1527-38.

Terrile, M. C., C. V. Tonon, M. J. Iglesias, L. Lamattina and C. A. Casalongue (2010). "Extracellular ATP and nitric oxide signaling pathways regulate redox-dependent responses associated to root hair growth in etiolated Arabidopsis seedlings." Plant Signal Behav **5**(6): 698-701.

Thomas, C., A. Rajagopal, B. Windsor, R. Dudler, A. Lloyd and S. J. Roux (2000). "A role for ectophosphatase in xenobiotic resistance." Plant Cell **12**(4): 519-533.

Thomas, C., Y. Sun, K. Naus, A. Lloyd and S. Roux (1999). "Apyrase functions in plant phosphate nutrition and mobilizes phosphate from extracellular ATP." Plant Physiology **119**(2): 543-551.

Tiwari, B. S., B. Belenghi and A. Levine (2002). "Oxidative stress increased respiration and generation of reactive oxygen species, resulting in ATP depletion, opening of mitochondrial permeability transition, and programmed cell death." Plant Physiology **128**(4): 1271-1281.

Tonge, R., J. Shaw, B. Middleton, R. Rowlinson, S. Rayner, J. Young, F. Pognan, E. Hawkins, I. Currie and M. Davison (2001). "Validation and development of fluorescence two-dimensional differential gel electrophoresis proteomics technology." Proteomics **1**(3): 377-96.

Tonon, C., M. Cecilia Terrile, M. Jose Iglesias, L. Lamattina and C. Casalongue (2010). "Extracellular ATP, nitric oxide and superoxide act coordinately to regulate hypocotyl growth in etiolated Arabidopsis seedlings." Journal of Plant Physiology **167**(7): 540-6.

Torres, J., A. Rivera, G. Clark and S. J. Roux (2008). "Participation of extracellular nucleotides in the wound response of Dasycladus vermicularis and Acetabularia acetabulum (Dasycladales, Chlorophyta)." Journal of Phycology **44**(6): 1504-1511.

Torres, M. A., J. D. Jones and J. L. Dangl (2006). "Reactive oxygen species signaling in response to pathogens." Plant Physiology **141**(2): 373-8.

Tsuda, M., Y. Shigemoto-Mogami, S. Koizumi, A. Mizokoshi, S. Kohsaka, M. W. Salter and K. Inoue (2003). "P2X4 receptors induced in spinal microglia gate tactile allodynia after nerve injury." Nature **424**(6950): 778-83.

Udvardy, J. and G. L. Farkas (1973). "ATP stimulates formation of nucleases in excised Avena leaves." Zeitschrift Fur Pflanzenphysiologie **69**(5): 394-401.

Ulker, B., E. Peiter, D. P. Dixon, C. Moffat, R. Capper, N. Bouche, R. Edwards, D. Sanders, H. Knight and M. R. Knight (2008). "Getting the most out of publicly available T-DNA insertion lines." Plant Journal **56**(4): 665-77.

Unlu, M., M. E. Morgan and J. S. Minden (1997). "Difference gel electrophoresis: a single gel method for detecting changes in protein extracts." Electrophoresis **18**(11): 2071-7.

Urbach, V., N. Helix, B. Renaudon and B. J. Harvey (2002). "Cellular mechanisms for apical ATP effects on intracellular pH in human bronchial epithelium." J Physiol **543**(Pt 1): 13-21.

Urban, M., S. Daniels, E. Mott and K. Hammond-Kosack (2002). "Arabidopsis is susceptible to the cereal ear blight fungal pathogens Fusarium graminearum and Fusarium culmorum." Plant Journal **32**(6): 961-73.

Vacirca, D., F. Delunardo, P. Matarrese, T. Colasanti, P. Margutti, A. Siracusano, S. Pontecorvo, A. Capozzi, M. Sorice, A. Francia, W. Malorni and E. Ortona (2010). "Autoantibodies to the adenosine triphosphate synthase play a pathogenetic role in Alzheimer's disease." Neurobiol Aging.

Virginio, C., A. MacKenzie, R. A. North and A. Surprenant (1999). "Kinetics of cell lysis, dye uptake and permeability changes in cells expressing the rat P2X7 receptor." J Physiol **519 Pt 2**: 335-46.

Visconti, A., M. B. Doko, C. Bottalico, B. Schurer and A. Boenke (1994). "Stability of fumonisins (FB1 and FB2) in solution." Food Additives and Contaminants **11**(4): 427-31.

Wang, D., N. D. Weaver, M. Kesarwani and X. Dong (2005). "Induction of protein secretory pathway is required for systemic acquired resistance." Science **308**(5724): 1036-40.

Wang, E., W. P. Norred, C. W. Bacon, R. T. Riley and A. H. Merrill, Jr. (1991). "Inhibition of sphingolipid biosynthesis by fumonisins. Implications for diseases associated with Fusarium moniliforme." Journal of Biological Chemistry **266**(22): 14486-90.

Wang, E., P. F. Ross, T. M. Wilson, R. T. Riley and A. H. Merrill, Jr. (1992). "Increases in serum sphingosine and sphinganine and decreases in complex sphingolipids in ponies given feed containing fumonisins, mycotoxins produced by Fusarium moniliforme." Journal of Nutrition **122**(8): 1706-16.

Wang, W., B. Vinocur, O. Shoseyov and A. Altman (2004). "Role of plant heat-shock proteins and molecular chaperones in the abiotic stress response." Trends in Plant Science **9**(5): 244-52.

Watanabe, N. and E. Lam (2004). "Recent advance in the study of caspase-like proteases and Bax inhibitor-1 in plants: their possible roles as regulator of programmed cell death." Molecular Plant Pathology **5**(1): 65-70.

Weerasinghe, R. R., S. J. Swanson, S. F. Okada, M. B. Garrett, S. Y. Kim, G. Stacey, R. C. Boucher, S. Gilroy and A. M. Jones (2009). "Touch induces ATP release in Arabidopsis roots that is modulated by the heterotrimeric G-protein complex." Febs Letters **583**(15): 2521-6.

White, C. and J. G. McGeown (2003). "Inositol 1,4,5-trisphosphate receptors modulate Ca2+ sparks and Ca2+ store content in vas deferens myocytes." Am J Physiol Cell Physiol **285**(1): C195-204.

Wieraszko, A. and W. Seifert (1984). "Evidence for a functional role of gangliosides in synaptic transmission: studies on rat brain striatal slices." Neuroscience Letters **52**(1-2): 123-8.

Wildermuth, M. C., J. Dewdney, G. Wu and F. M. Ausubel (2001). "Isochorismate synthase is required to synthesize salicylic acid for plant defence." Nature **414**(6863): 562-565.

Wilkin, F., X. Duhant, C. Bruyns, N. Suarez-Huerta, J. M. Boeynaems and B. Robaye (2001). "The P2Y11 receptor mediates the ATP-induced maturation of human monocyte-derived dendritic cells." Journal of Immunology **166**(12): 7172-7.

Wolf, C., M. Hennig, D. Romanovicz and I. Steinebrunner (2007). "Developmental defects and seedling lethality in apyrase AtAPY1 and AtAPY2 double knockout mutants." Plant Molecular Biology **64**(6): 657-72.

Wu, J., I. Steinebrunner, Y. Sun, T. Butterfield, J. Torres, D. Arnold, A. Gonzalez, F. Jacob, S. Reichler and S. J. Roux (2007). "Apyrases (nucleoside triphosphate-diphosphohydrolases) play a key role in growth control in Arabidopsis." Plant Physiology **144**(2): 961-75.

Wu, S. J., Y. S. Liu and J. Y. Wu (2008a). "The signaling role of extracellular ATP and its dependence on Ca2+ flux in elicitation of Salvia miltiorrhiza hairy root cultures." Plant and Cell Physiology **49**(4): 617-24.

Wu, S. J. and J. Y. Wu (2008b). "Extracellular ATP-induced NO production and its dependence on membrane Ca2+ flux in Salvia miltiorrhiza hairy roots." Journal of Experimental Botany **59**(14): 4007-16.

Xie, Z. and Z. Chen (2000). "Harpin-induced hypersensitive cell death is associated with altered mitochondrial functions in tobacco cells." Mol Plant Microbe Interact **13**(2): 183-90.

Yegutkin, G. G., A. Mikhailov, S. S. Samburski and S. Jalkanen (2006). "The detection of micromolar pericellular ATP pool on lymphocyte surface by using lymphoid ecto-adenylate kinase as intrinsic ATP sensor." Molecular Biology of the Cell **17**(8): 3378-85.

Yoshida, S., M. Ito, I. Nishida and A. Watanabe (2002). "Identification of a novel gene HYS1/CPR5 that has a repressive role in the induction of leaf senescence and pathogen-defence responses in Arabidopsis thaliana." Plant Journal **29**(4): 427-437.

Yu, J. H., S. Y. Yun, J. W. Lim, H. Kim and K. H. Kim (2003). "Proteome analysis of rat pancreatic acinar cells: implication for cerulein-induced acute pancreatitis." Proteomics **3**(12): 2446-53.

Zipfel, C., S. Robatzek, L. Navarro, E. J. Oakeley, J. D. Jones, G. Felix and T. Boller (2004). "Bacterial disease resistance in Arabidopsis through flagellin perception." Nature **428**(6984): 764-7.

Appendix A Complete proteomics expression data

Table 1A Proteins differentially expressed with FB1 in the TSP fraction. [a]Sequence accession number in the non-redundant NCBInr database version 20070713. [b]Arabidopsis Genome Initiative (AGI) gene identifier. [c]MOWSE, for a significant ($p \leq 0.05$) positive protein identification, cut-off threshold was 71. [d]Number of peptides matched to the protein sequence. [e]Number of unmatched peptides matched to the protein sequence. [f]Ratio represents fold-change of FB1 relative to the control. [g]Ratio represents fold-change of FB1+ATP signal relative to FB1 signal. Statistically significant ($p \leq 0.05$) ratios that exhibit a minimum 20% fold change are highlighted in grey.

											FB1/Control		FB1+ATP/FB1	
Master number	Database accession[a]	Gene locus[b]	Annotation	molecular weight (Da)	pI	MOWSE score[c]	sequence coverage (%)	peptides[d]	unassigned peptides[e]	total peptides	Fold change[f]	*p*-value	Fold change[g]	*p*-value
370											1.86	0.00046	1.05	0.95
581											-1.5	0.023	1.78	0.055
755			No significant hit								-1.3	0.025	1.53	0.0053
759	gi|15912329	AT1G79690	Nudix hydrolase homolog 3 (atnudt3)	36767	5.28	74	39	12	60	72	-1.37	0.0085	1.52	0.046
786	gi|18402264	AT2G30110	ubiquitin-activating enzyme (E1)	121202	5.11	91	17	16	37	53	-1.33	0.019	1.29	0.13
874	gi|450880	AT5G02500	heat shock cognate protein 70-1	71712	5.03	85	31	15	62	77	1.21	0.0022	1.05	0.24
943	gi|15230534	AT3G12580	heat shock protein 70 (HSP70)	71456	5.14	146	36	25	41	66	1.22	0.036	1.22	0.27
976	gi|4467097	AT5G03340	putative cell division cycle protein 48	93559	5.37	80	26	16	49	65	1.18	0.0048	1.05	0.9
1038											1.33	0.0012	-1.1	0.21
1039	gi|15231702	AT3G52880	peroxisomal monodehydroascorbate reductase	46629	6.41	100	33	11	30	41	-1.53	1.20E-05	1.23	0.24
1043	gi|15223226	AT1G70730	putative phosphoglucomutase	63442	5.56	181	44	23	42	65	-1.41	0.025	1.38	0.042
1044	gi|15220668	AT1G23190	putative phosphoglucomutase	63131	5.92	169	37	21	36	57	-1.75	0.00021	1.73	0.021
1045	gi|15227940	AT2G17980	ATSLY1 protein transporter	69393	5.99	102	36	21	103	124	-1.5	0.0019	1.29	0.042
1047	gi|15242459	AT5G09590	heat shock protein 70 (Hsc70-5)	73174	5.63	250	49	35	62	97	1.24	0.0071	-1.15	0.011
1049	gi|18411711	AT3G60750	putative transketolase	80374	5.94	92	20	12	26	38	1.35	0.0037	-1.08	0.31
1052	gi|15232776	AT3G09840	cell division cycle protein	90079	5.13	92	29	16	60	76	1.26	0.011	1.09	0.23
1054	gi|62321694	AT5G53460	NADH-dependent glutamate synthase	53573	5.29	130	41	16	42	58	1.52	0.00099	-1.14	0.16
1068			No significant hit								1.36	0.0051	-1.06	0.38
1071			No significant hit								1.26	0.014	-1.15	0.064
1090	gi|15241849	AT5G02500	heat shock cognate protein 70-1	71712	5.03	89	28	20	45	65	1.24	0.013	-1.13	0.19
1097	gi|15231939	AT3G08590	putative 2,3-biphosphoglycerate-independent	60897	5.53	142	52	19	60	79	-1.22	0.023	1.33	0.14

			phosphoglycerate mutase											
1102	gi|15241849	AT5G02500	heat shock cognate protein 70-1	71712	5.03	126	40	18	79	97	1.26	0.015	-1.13	0.2
1103	gi|15241849	AT5G02500	heat shock cognate protein 70-1	71712	5.03	123	33	20	43	63	1.36	0.0033	-1.1	0.27
1124	gi|15230534	AT3G12580	heat shock protein 70 (HSP70)	71456	5.14	129	33	22	49	71	1.42	5.60E-05	-1.02	0.66
1127	gi|15230534	AT3G12580	heat shock protein 70 (HSP70)	71456	5.14	80	19	13	35	48	1.52	3.00E-05	1.04	0.84
1152			No significant hit								-1.38	0.0062	1.33	0.042
1153	gi|15223975	AT1G77510	protein disulfide isomerase-like (PDIL)	56614	4.9	148	51	19	63	82	-1.26	0.015	1.23	0.025
1170	gi|4467097	AT4G37910	mitochondrial heat shock protein 70-1 (mtHsc70-1)	71130	5.31	177	38	25	40	65	-1.26	0.0095	-1.19	0.12
1172			No significant hit								-1.22	0.016	-1.14	0.14
1201											1.28	3.60E-05	-1	0.85
1205	gi|15230534	AT3G12580	heat shock protein 70 (HSP70)	63702	5.6	112	26	22	38	60	1.78	8.30E-05	-1.19	0.16
1210			No significant hit								1.74	3.20E-05	-1.05	0.65
1233	gi|15231092	AT3G58610	ketol-acid reductoisomerase	64172	6.36	189	30	18	19	37	-1.29	0.017	1.31	0.1
1240	gi|15238686	AT5G17920	cobalamin-independent methionine synthase	84646	6.09	90	17	11	25	36	1.27	0.014	-1.13	0.12
1355	gi|15236376	AT4G13940	S-adenosyl-L-homocysteine hydrolase	53971	5.6	125	46	21	78	99	1.35	0.027	1.65	0.009
1395	gi|18414006	AT4G13430	Isopropyl malate isomerase large subunit 1 (IIL1)	54979	8.08	98	35	16	49	65	-1.24	0.015	1.31	0.13
1436	gi|15220329	AT1G04820	alpha tubulin isoform	50194	4.93	135	45	16	26	42	-1.28	0.023	1.33	0.26
1437	gi|15220329	AT1G04820	alpha tubulin isoform	50194	4.93	178	47	15	19	34	-1.27	0.042	1.3	0.29
1495			No significant hit								-1.28	0.0069	1.5	0.017
1508											1.33	9.60E-05	-1.19	0.0043
1509			No significant hit								1.37	0.00065	-1.13	0.14
1514	gi|62320318	AT4G24190	heat shock 90.7 like protein	36954	4.7	104	30	11	24	35	1.34	0.00066	-1.38	0.00082
1515	gi|217855	AT5G52640	heat shock protein AtHSP90.1	80870	4.97	76	15	11	22	33	1.38	5.80E-06	-1.26	0.014
1518	gi|42573019	AT4G24190	heat shock 90.7 like protein	94148	4.92	95	22	15	33	48	1.23	0.0083	-1.38	0.00042
1583	gi|18406515 & gi|4210332	AT2G44350 & AT5G55070	ATCS (citrate synthase 4); 2-oxoglutarate dehydrogenase	N/A	N/A	Mix: 327 + 230	N.A.	N.A.	N.A.	N.A.	1.4	0.0016	1.14	0.1
1584											1.34	0.016	-1.28	0.062
1594			No significant hit								1.49	0.0049	1.22	0.00091
1796			No significant hit								-1.25	0.012	1.35	0.1
1805	gi|15223838	AT1G77120	alcohol dehydrogenase	41836	5.83	81	24	9	21	30	-1.45	0.007	1.56	0.051
1817	gi|18415911	AT5G08690	ATP synthase beta-subunit	59847	6.18	138	42	21	61	82	1.27	3.40E-05	-1.14	0.023

1853	gi|21618158	AT3G29360	putative UDP-glucose 6-dehydrogenase	53709	5.69	162	58	28	99	127	1.27	1.70E-05	-1.05	0.4
1883	gi|21954073 & gi|15231715	AT4G09670 & AT3G52930	putative AX110P protein; fructose-bisphosphate aldolase, putative	N/A	N/A	Mix: 89 + 86	N.A.	N.A.	N.A.	N.A.	-1.25	0.016	1.07	0.4
1904	gi|18411737	AT3G60830	actin-related protein	40278	4.81	84	33	9	31	40	-1.5	0.0056	-1.12	0.18
1905	gi|15229530	AT3G17820	glutamine synthetase	38798	5.72	108	29	13	38	51	1.32	0.00015	1.2	0.16
1906	gi|15229530	AT3G17820	glutamine synthetase	38798	5.72	219	76	27	57	84	1.47	9.60E-06	1.16	0.05
1930	gi|15231715	AT3G52930	putative fructose-bisphosphate aldolase	38858	6.05	95	42	10	34	44	-1.21	0.025	1.35	0.006
1944	gi|15237214	AT5G52640	heat shock protein AtHSP90.1	81414	4.95	123	27	19	54	73	1.2	0.028	-1.7	0.0043
1945			No significant hit								-1.79	6.70E-05	1.27	0.24
1946	gi|15220770	AT1G62380	1-aminocyclopropane-1-carboxylic oxidase (ACC oxidase)	36388	4.98	85	43	12	58	70	-1.59	0.0027	1.19	0.12
1951	gi|15232455	AT3G14990	putative 4-methyl-5(b-hydroxyethyl)-thiazole monophosphate biosynthesis protein	42230	5.31	95	45	19	151	170	-1.58	4.00E-05	1.15	0.14
1957											1.45	0.026	1.03	0.7
1975	gi|15229231	AT3G04120	GAPDH (C subunit)	37005	6.62	104	45	16	76	92	-1.24	0.019	1.68	0.0008
1999											1.21	0.01	-1.04	0.45
2012	gi|15229231	AT3G04120	GAPDH (C subunit)	37005	6.62	141	43	15	23	38	-1.22	9.10E-07	-1.06	0.13
2050	gi|240254000	AT1G03475	coproporphyrinogen III oxidase	43769	6.24	140	46	18	47	65	-1.29	0.022	1.32	0.0056
2060											-1.4	0.0072	1.27	0.094
2069			No significant hit								-1.32	0.002	1.07	0.91
2110	gi|23397307	AT5G08670	ATP synthase beta-subunit	59847	6.18	90	49	20	141	161	1.27	0.0057	-1.06	0.42
2140	gi|15224810	AT2G44060	late embryogenesis abundant family protein (LEA)	36185	4.69	137	61	21	93	114	1.28	0.00013	-1.13	0.024
2152			No significant hit								1.46	0.0014	-1.08	0.41
2157	gi|15231841	AT3G53580	diaminopimelate epimerase	39473	5.45	153	57	21	57	78	-1.22	0.00078	-1.26	0.00062
2173	gi|15229589	AT3G18130	similarity to mammalian RACKs	35805	6.66	111	46	14	51	65	-1.51	0.016	1.88	0.011
2197											-1.4	0.00036	-1.07	0.43
2200	gi|18414298	AT5G03630	monodehydroascorbate reductase	47507	5.24	116	45	18	72	90	-1.49	2.80E-05	-1.26	0.015
2203			No significant hit								-1.31	0.0013	-1.2	0.11
2215	gi|15219412	AT1G79550	phosphoglycerate kinase (PGK)	42162	5.49	124	62	19	95	114	-1.38	0.0036	-1.41	0.0027
2253	gi|15228498	AT3G03250	UGP1 (UDP-glucose pyrophosphorylase 1)	51877	5.8	71	30	12	74	86	1.29	0.014	-1.3	0.067
2256	gi|15227981	AT2G36460	putative fructose-bisphosphate aldolase	38705	7.01	85	45	9	37	46	-1.44	0.00094	-1.08	0.21
2275	gi|15231715	AT3G52930	putative fructose-bisphosphate aldolase	38858	6.05	146	57	14	40	54	-1.22	0.014	-1.17	0.045

2287	gi|18407710 & gi|21593226	AT1G63000 & AT2G41530	NRS/ER (nucleotide-rhamnose synthase/epimerase-reductase); putative esterase D	N/A	N/A	Mix: 143 + 93	N.A.	N.A.	N.A.	N.A.	-1.24	0.017	1.04	0.67
2306			No significant hit								1.49	0.0084	-1.71	0.018
2327											1.26	0.0072	-1.07	0.36
2345	gi|15237888	AT5G16970	2-alkenal reductase (EC 1.3.1.74)	38394	5.81	96	48	14	72	86	1.26	0.0013	-1.13	0.2
2379	gi|15239741 & ...	AT5G19440 & ...	cinnamyl-alcohol dehydrogenase; putative (CAD) & and many more	N/A	N/A	Mix: 255 and many more	N.A.	N.A.	N.A.	N.A.	1.47	0.00075	-1.37	0.043
2404	gi|15241472 & gi|15235213	AT5G44340 & AT4G34050	TUB4 (tubulin beta-4 chain); caffeoyl-CoA 3-O-methyltransferase, putative	N/A	N/A	Mix: 114 + 101	N.A.	N.A.	N.A.	N.A.	1.59	1.50E-06	-1.25	0.007
2405	gi|15235213	AT4G34050	putative caffeoyl-CoA 3-O-methyltransferase	29251	5.13	136	61	21	99	120	1.87	1.90E-06	-1.33	0.0018
2423			No significant hit								1.22	0.00053	-1.31	0.0019
2431			No significant hit								-1.28	2.90E-05	-1.08	0.17
2465	gi|14916970	ATMG01190	ATPase subunit 1	55296	6.23	282	52	27	33	60	-1.21	0.0003	-1.19	0.0033
2477	gi|145333043	AT4G13940	S-adenosyl-L-homocysteine hydrolase	36022	5.05	82	38	10	39	49	1.29	0.0006	-1.2	0.011
2553	gi|15241849	AT5G02500	heat shock cognate protein 70-1	71712	5.03	83	18	15	34	49	-1.57	0.0018	-1.2	0.15
2563											-1.67	0.00094	-1.02	0.67
2564			No significant hit								-1.39	0.015	-1.29	0.045
2571	gi|15221116 & …	AT1G11840 & …	ATGLX1 (glyoxalase I homolog); and many more	N/A	N/A	Mix : 614 and many more	N.A.	N.A.	N.A.	N.A.	1.39	0.00061	-1.48	0.00022
2577	gi|15221116 & gi|15227987	AT1G11840 & AT2G36530	LOS2; ATGLX1 (glyozylase I homolog)	N/A	N/A	Mix: 202 + 205	N.A.	N.A.	N.A.	N.A.	1.22	0.0023	-1.47	0.0067
2597	gi|145333043	AT4G13940	S-adenosyl-L-homocysteine hydrolase	36022	5.05	137	57	17	45	62	1.22	0.0051	-1.26	0.059
2630	gi|15225839	AT2G27020	20S proteasome subunit PAG1	27645	5.93	117	39	14	37	51	1.21	0.0056	-1.13	0.069
2640	gi|15226489	AT2G21250	putative NADPH-dependent mannose 6-phosphate reductase	34988	6.61	77	37	11	54	65	-1.48	0.00024	1.02	0.91
2658	gi|15242351	AT5G15650	reversibly glycosylated polypeptide-2	41377	5.76	123	26	10	11	21	1.38	0.014	-1.51	0.023
2688	gi|15233268	AT3G22110	alpha-3 subunit of 20s proteasome	27458	6.6	89	47	11	54	65	-1.36	1.50E-06	1.18	0.36
2703	gi|15217661	AT1G64520	regulatory particle non-ATPase 12a (RPN12a)	30915	4.81	116	51	15	70	85	1.2	0.027	-1.45	0.0087
2718	gi|15242516	AT5G09810	actin 7	41937	5.31	80	45	15	128	143	1.29	0.00041	1.1	0.31

2728	gi|15231715	AT3G52930	putative fructose-bisphosphate aldolase	38858	6.05	86	48	11	69	80	1.25	0.01	-1.58	0.0024
2759	gi|15231715 & gi|436792	AT3G52930 & AT5G20830	fructose-bisphosphate aldolase; sucrose synthase	N/A	N/A	Mix: 306 + 252	N.A.	N.A.	N.A.	N.A.	1.42	9.20E-05	-1.49	0.0091
2798											-1.26	0.0041	1.46	0.00019
2816											1.3	0.00044	1	1
2822											-1.26	0.014	1.22	0.15
2828											-1.25	0.00011	1.03	0.62
2854	gi|15232965	AT3G60820	20S proteasome beta subunit PBF1	24856	6.95	156	60	15	37	52	1.38	0.00064	-1.02	0.69
2881	gi|15223576	AT1G19570	dehydroascorbate reductase	23740	5.56	109	66	10	47	57	-1.25	0.00016	-1.05	0.1
2921	gi|15242045 &...	AT5G20720 &...	CPN20 (chaperonin 20); and many more	N/A	N/A	Mix: 543 and many more	N.A.	N.A.	N.A.	N.A.	1.23	0.024	-1.31	0.005
2929			No significant hit								1.36	0.0045	-1.52	0.046
2888	gi|15228818	AT3G56090	ferritin 3 AtFER3	64172	6.36	123	52	17	88	105	1.26	0.013	-1.5	0.015
2952			No significant hit								-1.23	0.0048	1.09	0.42
2987	gi|15220832	AT1G53540	17.6 kDa class I small heat shock protein (HSP17.6C-CI)	17593	5.36	90	38	10	49	59	1.3	0.0045	-1.04	0.52
2989			No significant hit								-1.3	0.00039	-1.32	0.002
2997			No significant hit								1.25	0.029	-1.43	0.015
3003											-1.3	0.0051	1.11	0.45
3008			No significant hit								1.42	0.047	-1.6	0.03
3036	gi|166717	AT5G38480	general regulatory factor 3	28587	4.82	108	34	12	26	38	1.25	0.0092	-1.3	0.015
3041											1.52	2.30E-06	1.12	0.026
3056	gi|15218640	AT1G02930	glutathione transferase	23471	5.8	114	38	11	44	55	1.53	0.00029	-1.58	0.009
3079											-1.45	0.0013	-1.01	0.94
3105											1.4	0.0032	-1.02	0.82
3118	gi|15239136	AT5G42980	thioredoxin	13101	5.06	99	72	11	54	65	-1.49	0.00065	-1.38	0.025
3133											-1.37	0.036	-1.23	0.092
3158			No significant hit								1.25	0.0083	-1.15	0.16
3160			No significant hit								-1.88	0.0015	1.08	0.47
3184											-1.25	0.0028	-1.01	0.91
3275											-1.27	0.012	-1.06	0.48

3280	gi|30697295	AT5G59880	actin depolymerizing factor 3	16026	5.93	111	75	12	72	84	-1.21	0.0019	1.08	0.11
3303											-1.36	1.20E-05	-1.06	0.36
3354			No significant hit								-1.37	2.10E-05	-1.09	0.11
3479											1.31	0.02	-1.49	0.021
3486			No significant hit								1.24	0.05	-1.35	0.043
3563											1.35	0.007	-1.58	0.012
3690											-1.29	0.011	-1.09	0.069
3770											-1.29	0.0073	1.07	0.21
4003	gi|15232682	AT3G09440	heat shock cognate 70 kDa protein 3 (HSC70-3)	71559	4.97	97	32	21	62	83	1.25	0.031	-1.22	0.051
4004			No significant hit								-1.22	0.031	1.44	0.11
4018											1.34	0.0031	-1.18	0.11
4064	gi|15230534 & gi|30693966	AT3G12580 & AT5G42020	HSP70 (heat shock protein 70); ATP binding & BIP (luminal binding protein)	N/A	N/A	Mix: 166 + 140	N.A.	N.A.	N.A.	N.A.	1.29	0.0012	1.19	0.083
4066	gi|15230534	AT3G12580	heat shock protein 70 (HSP70)	71456	5.14	249	56	37	59	96	1.27	0.0072	1.16	0.011
4077			No significant hit								-1.28	0.0047	-1.06	0.3
4088			No significant hit								1.33	3.10E-05	-1.08	0.043
4088			No significant hit								1.33	3.10E-05	-1.08	0.043

Table 1B Proteins differentially expressed with FB1 in the Microsomal protein fraction. [a]Sequence accession number in the non-redundant NCBInr database version 20070713. [b]Arabidopsis Genome Initiative (AGI) gene identifier. [c]MOWSE, for a significant ($p \leq 0.05$) positive protein identification, cut-off threshold was 71. [d]Number of peptides matched to the protein sequence. [e]Number of unmatched peptides matched to the protein sequence. [f]Ratio represents fold-change of FB1 relative to the control. [g]Ratio represents fold-change of FB1+ATP signal relative to FB1 signal. Statistically significant ($p \leq 0.05$) ratios that exhibit a minimum 20% fold change are highlighted in grey.

											FB1/Control		FB1+ATP/FB1	
Master number	Database accession[a]	Gene locus[b]	Annotation	molecular weight (Da)	pI	MOWSE score[c]	sequence coverage (%)	peptides[d]	unassigned peptides[e]	total peptides	Fold change[f]	*p*-value	Fold change[g]	*p*-value
269	gi|79321519	AT1G79930	high molecular weight heat shock protein 70 (HSP91)	88060	5.19	128	36	27	96	123	1.93	2.40E-07	-1.09	0.22
326	gi|30696056	AT1G56070	translation elongation factor 2-like protein	94743	5.89	88	38	28	134	162	2.28	2.20E-05	1.04	0.82
327	gi|30696056	AT1G56070	translation elongation factor 2-like protein	94743	5.89	125	46	30	116	146	2.24	6.40E-09	1.09	0.17
335	gi|15232776	AT3G09840	cell division cycle protein	90079	5.13	91	14	14	23	37	3.35	9.40E-09	-1.09	0.34
370			No significant hit								-1.79	0.0009	1.13	0.18
371	gi|18417676	AT5G15450	chloroplast-targeted Hsp101 homologue	106047	5.93	90	32	31	128	159	-1.59	0.0035	1.14	0.15
471	gi|47600741	AT5G17920	cobalamin-independent methionine synthase	84646	6.09	94	38	22	133	155	5.18	9.10E-10	1.11	0.5
485	gi|15241115	AT5G56030	heat shock protein 90 (HSP90)	80299	4.95	218	39	36	67	103	1.78	1.10E-06	1	0.99
567			No significant hit								2.35	6.40E-08	-1.14	0.089
570			No significant hit								2.37	7.10E-09	-1.15	0.028
574	gi|15233779	AT4G24280	chloroplast heat shock protein 70-1 (cpHsc70-1)	76461	5.07	74	21	15	50	65	2.19	4.50E-09	-1.2	0.0097
581	gi|15233779	AT4G24280	chloroplast heat shock protein 70-1 (cpHsc70-1)	76461	5.07	137	31	21	44	65	2.09	5.10E-07	-1.18	0.014
586			No significant hit								1.67	0.0079	1.16	0.45
594	gi|15241849	AT5G02500	heat shock cognate protein 70-1	71712	5.03	214	56	29	63	92	1.79	9.30E-07	-1.1	0.077
604			No significant hit								1.7	0.0013	1.33	0.32
605	gi|15241849	AT5G02500	heat shock cognate protein 70-1	71712	5.03	187	48	27	62	89	2.13	2.30E-08	-1.08	0.27
612	gi|15230534	AT3G12580	heat shock protein 70 (HSP70)	71456	5.14	218	48	26	35	61	2.13	3.60E-07	-1.17	0.059
637	gi|15219234	AT1G78900	catalytic subunit A of the vacuolar ATP synthase	69111	5.11	156	47	25	93	118	-1.8	7.00E-05	1.19	0.17
640	gi|15219234	AT1G78900	catalytic subunit A of the vacuolar ATP synthase	69111	5.11	192	39	22	37	59	-1.63	0.00019	1.19	0.11
649	gi|4467097	AT4G37910	mitochondrial heat shock protein 70-1 (mtHsc70-1)	73315	5.51	113	47	29	158	187	-1.54	0.00023	1.21	0.065
742	gi|30691626	AT4G37910	mitochondrial heat shock protein 70-1 (mtHsc70-1)	73315	5.51	98	34	20	89	109	2.04	9.90E-05	-1.31	0.025
743	gi|15232845	AT3G02090	metalloendopeptidase (MPPBETA)	59180	6.3	137	37	15	23	38	-1.92	9.40E-05	1.21	0.14

746	gi|110740617	AT3G02090	metalloendopeptidase (MPPBETA)	51555	5.71	209	59	26	66	92	-1.94	1.40E-05	1.19	0.094
747	gi|110740617	AT3G02090	metalloendopeptidase (MPPBETA)	51555	5.71	184	57	22	54	76	-1.9	0.00015	1.23	0.13
749	gi|110740617	AT3G02090	metalloendopeptidase (MPPBETA)	51555	5.71	224	59	25	56	81	-1.8	0.00024	1.26	0.11
752	gi|110740617	AT3G02090	metalloendopeptidase (MPPBETA)	51555	5.71	87	17	9	20	29	-1.61	0.00067	1.2	0.092
760	gi|30691626	AT4G37910	mitochondrial heat shock protein 70-1 (mtHsc70-1)	73315	5.51	106	47	29	167	196	3.14	1.10E-05	-1.65	0.0096
761	gi|30691626	AT4G37910	mitochondrial heat shock protein 70-1 (mtHsc70-1)	73315	5.51	101	26	16	41	57	4.34	8.30E-08	-1.6	0.0032
788	gi|14916970	ATMG01190	ATPase subunit 1	55296	6.23	207	41	20	26	46	-2.01	5.50E-06	1.3	0.041
793	gi|14916970	ATMG01190	ATPase subunit 1	55296	6.23	213	51	27	71	98	-1.96	2.20E-06	1.28	0.051
799	gi|14916970	ATMG01190	ATPase subunit 1	55296	6.23	235	60	29	65	94	-2.81	4.00E-06	1.29	0.058
802	gi|7525018	ATCG00120	ATPase CF1 alpha subunit	55351	5.19	216	37	20	20	40	-1.7	0.00019	1.29	0.034
803	gi|14916970	ATMG01190	ATPase subunit 1	55296	6.23	164	35	16	22	38	-2.31	4.40E-08	1.17	0.13
810			No significant hit								-2.1	0.00013	1.24	0.19
812	gi|14916970	ATMG01190	ATPase subunit 1	55296	6.23	207	51	24	52	76	-1.93	2.00E-05	1.26	0.056
832	gi|18415911	AT5G08690	Encodes the mitochondrial ATP synthase beta-subunit	59847	6.18	225	63	28	63	91	-1.88	4.10E-07	1.24	0.016
837	gi|14916970	ATMG01190	ATPase subunit 1	55296	6.23	197	36	18	19	37	-1.69	0.00059	1.21	0.065
839	gi|18415911	AT5G08690	Encodes the mitochondrial ATP synthase beta-subunit	59847	6.18	248	63	28	56	84	-2.17	5.30E-08	1.23	0.014
840	gi|18415911	AT5G08690	Encodes the mitochondrial ATP synthase beta-subunit	59847	6.18	250	62	28	55	83	-1.86	8.20E-07	1.32	0.025
841	gi|14916970	ATMG01190	ATPase subunit 1	55296	6.23	79	23	10	32	42	-1.69	0.00083	1.22	0.026
844	gi|18415911	AT5G08690	Encodes the mitochondrial ATP synthase beta-subunit	59847	6.18	251	64	25	36	61	-1.72	3.00E-05	1.34	0.029
846	gi|18415911	AT5G08690	Encodes the mitochondrial ATP synthase beta-subunit	59847	6.18	249	60	25	36	61	-1.74	0.00029	1.38	0.018
849	gi|18415911	AT5G08690	Encodes the mitochondrial ATP synthase beta-subunit	59847	6.18	217	58	27	61	88	-2.04	5.90E-06	1.28	0.099
857	gi|18415911	AT5G08690	Encodes the mitochondrial ATP synthase beta-subunit	59847	6.18	112	33	14	39	53	-1.78	1.80E-06	1.13	0.022
963			No significant hit								2.3	1.80E-06	1.25	0.053
964	gi|18415911	AT5G08690	Encodes the mitochondrial ATP synthase beta-subunit	59847	6.18	206	55	27	77	104	3.07	1.60E-07	1.16	0.38
976	gi|15234354	AT4G01850	S-adenosylmethionine synthetase 2 (SAM-2)	43627	5.67	92	47	17	131	148	2.66	1.30E-09	1.12	0.19
1054											1.86	4.90E-06	-1.08	0.19
1079	gi|15242516	AT5G09810	Actin 7	41937	5.31	203	62	23	66	89	2.3	4.50E-08	-1.03	0.65
1085	gi|15242516	AT5G09810	Actin 7	41937	5.31	187	59	22	70	92	2.3	5.90E-08	-1.07	0.38
1087			No significant hit								-1.6	0.00063	1.09	0.38
1154	gi|15231715	AT3G52930	putative fructose-bisphosphate aldolase	38858	6.05	121	48	13	42	55	1.58	5.50E-06	-1.09	0.28

1163	gi|21536853	AT1G79550	cytosolic phosphoglycerate kinase (PGK)	42162	5.49	129	58	16	68	84	2.62	1.40E-08	-1.04	0.54
1176	gi|21536853	AT1G79550	cytosolic phosphoglycerate kinase (PGK)	42178	5.49	145	48	16	44	60	3.29	1.20E-10	-1.01	0.87
1178			No significant hit								2.45	4.30E-05	-1.42	0.046
1182	gi|15237214	AT5G52640	heat shock protein AtHSP90.1	81414	4.95	98	23	16	45	61	2.85	4.50E-05	-1.41	0.12
1189	gi|15215642	AT5G56010	heat shock protein 90 (HSP90)	60921	5.11	85	27	14	51	65	2.87	3.80E-05	-1.43	0.12
1234			No significant hit								-1.75	1.40E-05	-1.02	0.98
1359			No significant hit								-1.55	0.001	1.15	0.027
1389			No significant hit								1.6	1.50E-05	1.14	0.065
1496	gi|15237488	AT5G40770	prohibitin 3	30381	6.99	121	38	11	27	38	-1.74	9.80E-05	1.1	0.3
1506											-1.73	5.10E-07	1.07	0.33
1531	gi|18403751	AT3G23400	plastid-lipid associated protein	30493	5.82	142	53	14	42	56	-1.63	1.90E-06	-1.01	0.83
1546											3.08	1.10E-06	-1.03	0.83
1569											2.33	1.90E-10	1.04	0.31
1574											2.55	1.20E-09	1.02	0.65
1604	gi|15227104	AT2G21870	unknown protein mitochondrial	27579	6.28	137	65	19	68	87	-2.03	2.10E-05	1.23	0.15
1632											-1.74	4.00E-07	1.21	0.023
1653	gi|18403751	AT3G23400	plastid-lipid associated protein	30493	5.82	106	38	9	19	28	-1.58	1.90E-06	1.07	0.26
1655	gi|15219412 & gi|15227104	AT1G79550 & AT2G21870	unknown protein; putative ATP synthase PGK	N/A	N/A	Mix: 293 & 332	N.A.	N.A.	N.A.	N.A.	-1.55	0.00035	1.04	0.52
1663	gi|15219265 & gi|15219311	AT1G79010 & AT1G16700	NADH-ubiquinone oxidoreductase; ATMLO15	N/A	N/A	Mix: 175 & 177	N.A.	N.A.	N.A.	N.A.	-1.59	2.60E-07	1.08	0.099
1753	gi|15240628	AT5G13450	ATP synthase delta chain	26362	9.25	185	63	18	42	60	-1.83	3.50E-06	1.23	0.034
1767	gi|23397307	AT5G08670	mitochondrial ATP synthase beta-subunit	48284	5.41	124	59	22	138	160	-1.7	3.20E-06	1.12	0.31
1799	gi|2326361	AT4G25200	AtHSP23.6-mito	23595	6.45	93	61	10	46	56	-2.29	1.40E-06	-1.03	0.73
1803			No significant hit								-2.23	6.50E-08	-1.19	0.012
1810	gi|15228276	AT3G16640	putative translationally controlled tumor protein (TCTP)	18898	4.52	93	54	10	55	65	2.73	2.20E-10	1.03	0.66
1813	gi|15231176	AT3G52300	ATP synthase D chain	19574	5.09	212	83	20	45	65	-2.32	3.60E-06	-1.12	0.32
1862			No significant hit								-2	1.30E-06	1.25	0.066
1867			No significant hit								-1.57	2.10E-08	1.15	0.023
2049			No significant hit								-1.75	1.60E-08	1.09	0.29
2118			No significant hit								-1.87	3.00E-06	1.03	0.82
2335											-1.59	0.00012	1.09	0.28
2337	gi|15240628	AT5G13450	ATP synthase delta chain	26362	9.25	133	53	14	41	55	-1.68	8.60E-06	1.23	0.027

Table 1C Proteins differentially expressed with ATP in the TSP fraction. [a]Sequence accession number in the non-redundant NCBInr database version 20090901. [b]Arabidopsis Genome Initiative (AGI) gene identifier. [c]MOWSE, for a significant ($p \leq 0.05$) positive protein identification, cut-off threshold was 71. [d]Number of peptides matched to the protein sequence. [e]Number of unmatched peptides matched to the protein sequence. [f]Number of sequenced peptides used for MS/MS identification. [g]Ratio represents fold-change of ATP relative to the control.

Master number	Database accession[a]	Gene locus[b]	Annotation	molecular weight (Da)	pI	Identification method	MOWSE score[c]	sequence coverage (%)	peptides[d]	unassigned peptides[e]	total peptides	Sequenced peptides[f]	Fold change[g]	*p*-value
480													2.23	0.0023
481													2.5	0.0021
483													3.08	0.0016
484													2.6	0.0012
501													3	1.10E-05
504													4.26	1.50E-05
505	gi|27363244	At1g79930	encodes high molecular weight heat shock protein 70	91692	5.15	MS/MS	92	18	19	23	42	0	3.21	3.00E-05
510													3.5	7.20E-05
511	gi|17473863	At1g79920	putative heat-shock protein, ATP binding	91653	5.09	MS/MS	278	30	33	26	59	5	4.04	2.00E-05
512	gi|17473863	At1g79920	putative heat-shock protein, ATP binding	91653	5.09	MS/MS	195	25	30	35	65	5	3.81	4.20E-05
513	gi|17473863	At1g79920	putative heat-shock protein, ATP binding	91653	5.09	MS/MS	286	29	31	34	65	5	3.47	8.60E-05
514													3.32	2.20E-05
517	gi|27363244	At1g79930	encodes high molecular weight heat shock protein 70	91692	5.15	MS/MS	199	28	32	21	53	2	3.48	2.30E-05
523													2.56	0.00091
524	gi|27363244	At1g79930	encodes high molecular weight heat shock protein 70	91692	5.15	MS/MS	163	21	23	13	36	4	2.88	5.80E-06
555													2.09	2.20E-05
559													2.09	2.30E-04
562													2.18	0.00044
564													2.13	0.00064
576	gi|6056373	At1g56070	encodes a translation elongation factor 2-like protein	94185	5.89	MS/MS	270	36	35	22	57	3	2.32	0.00071
580													2.19	0.0013

582	gi|6056373	At1g56070	encodes a translation elongation factor 2-like protein	94185	5.89	MS/MS	305	37	39	21	60	4	2.58	0.0003
584			No significant hit			MS/MS							2.15	0.0012
587													2.4	0.00031
588													2.34	0.00022
589													2.37	0.0005
590	gi|6056373	At1g56070	encodes a translation elongation factor 2-like protein	94185	5.89	MS/MS	329	36	37	10	47	4	2.6	0.00026
624	gi|34098843	At1g63770	peptidase M1 family protein	99096	5.43	MS/MS	74	11	15	21	36	1	3.25	3.40E-05
634			No significant hit			MS/MS							2.97	2.30E-05
638			No significant hit			MS/MS							2.7	0.00019
681	gi|27363244	At1g79930	encodes high molecular weight heat shock protein 70	91692	5.15	MS/MS	157	24	29	30	59	3	2.2	0.0017
687			No significant hit			MS/MS							2.02	1.10E-03
718			No significant hit			MS/MS							2.16	0.00025
741	gi|30678090	At2g04030	Encodes a chloroplast-targeted 90-kDa heat shock protein	88202	4.93	MS/MS	338	42	37	22	59	4	2.54	0.00011
742													2.24	0.00033
743	gi|30678090	At2g04030	Encodes a chloroplast-targeted 90-kDa heat shock protein	88202	4.93	MS/MS	219	33	27	34	61	3	2.26	0.00032
990													2.08	0.00027
1008													2.32	0.00034
1030	gi|30725440	At1g78900	Encodes catalytic subunit A of the vacuolar AtP synthase	68769	5.11	MS/MS	227	36	26	35	61	4	2.23	0.00046
1114	gi|21689675	At4g33070	pyruvate decarboxylase, putative	66170	5.7	MS/MS	138	17	19	29	48	5	2.02	8.80E-08
1161	gi|34098917	At3g23990	mitochondrial chaperonin HSP	61312	5.66	MS/MS	313	40	29	34	63	5	2.26	3.90E-05
1163	gi|34098917	At3g23990	mitochondrial chaperonin HSP	61312	5.66	MS/MS	372	44	33	32	65	5	2.36	3.10E-05
1166	gi|34098917	At3g23990	mitochondrial chaperonin HSP	61312	5.66	MS/MS	364	37	31	34	65	5	2.13	0.00029
1177													2.38	3.70E-06
1182	gi|23197790	At2g33210	heat shock protein 60-2	61939	6.37	MS/MS	102	26	18	47	65	1	2.27	0.0007
1189			No significant hit			MS/MS							2.36	0.00012
1199													2.35	0.00071
1227													2.04	9.30E-05
1250													2.1	4.30E-06
1253													2.29	5.40E-07
1258													2.07	0.00011

1272													2.68	0.0001
1347	gi|7269543	At4g26900	encodes a glutamine amidotransferase and cyclase	64153	6.31	MS/MS	147	35	26	39	65	0	2.53	2.90E-06
1355	gi|15236376	At4g13940	S-adenosyl-L-homocysteine hydrolase	53971	5.66	MALDI-ToF	125	46	21	78	99	N.A.	2.68	1.20E-06
1383	gi|21281109	At5g08690	Encodes the mitochondrial AtP synthase beta-subunit	59676	6.18	MS/MS	389	55	33	32	65	6	2.08	8.10E-06
1384	gi|23297411	At2g36530	Involved in cold tolerance and encodes an enolase	47689	5.54	MS/MS	572	62	31	34	65	7	2.22	9.40E-05
1479													2.25	9.50E-06
1605	gi|19699164	At5g20070	NUDIX HYDROLASE HOMOLOG 19	48316	5.69	MS/MS	167	26	16	49	65	4	2.18	0.00027
1829	gi|1515105	At5g52640	Encodes a cytosolic heat shock protein AtHSP90.1	81013	4.98	MS/MS	212	20	23	42	65	4	-2.03	0.00012
1842	gi|30678090	At2g04030	Encodes a chloroplast-targeted 90-kDa heat shock protein	88202	4.93	MS/MS	248	26	23	42	65	3	-2.22	4.10E-05
1860	gi|15215642	At5g56010	A member of heat shock protein 90 gene family	60807	5.11	MS/MS	688	42	35	30	65	7	-2.04	1.50E-08
1868	gi|15215642	At5g56010	A member of heat shock protein 90 gene family	60807	5.11	MS/MS	556	38	31	34	65	6	-2.07	4.90E-06
1933	gi|2462763	At1g60730	aldo/keto reductase family protein	37450	5.68	MS/MS	94	16	7	19	26	1	2.52	3.60E-05
1944	gi|15237214	At5g52640	heat shock protein AtHSP90.1	81414	4.95	MALDI-ToF	123	27	19	54	73	N.A.	-2.48	6.60E-09
2200	gi|18414298	At5g03630	monodehydroascorbate reductase	47507	5.24	MALDI-ToF	116	45	18	72	90	N.A.	-2.14	1.60E-06
2243	gi|23297085	At5g35360	acetyl-CoA carboxylase	58350	6.85	MS/MS	179	23	16	34	50	4	-2.14	1.80E-05
2275	gi|15231715	At3g52930	putative fructose-bisphosphate aldolase	38858	6.15	MALDI-ToF	146	57	14	40	54	N.A.	-2.08	8.70E-05
2362	gi|16974511	At1g35160	gF14 protein phi chain member of 14-3-3 protein family	30160	4.79	MS/MS	133	42	14	47	61	2	-2.37	1.20E-05
2457													-2.15	5.90E-06
2468	gi|28393681	At3g17820	encodes a cytosolic glutamine synthetase	38628	5.59	MS/MS	212	22	15	50	65	4	-2.45	8.80E-07
2577	gi|15227987 & gi|15221116	At1g11840 & At2g36530	Mixture: LOS2 (low exp. osmotically resp. genes); AtgLX1 (gLYOXALASE I HOMOLOg)	N.A.	N.A.	MS/MS	205+202	N.A.	N.A.	N.A.	N.A.	N.A.	-2.06	1.00E-06
2658	gi|15242351	At5g15650	Reversibly glycosylated Polypeptide-2	41377	5.76	MALDI-ToF	123	26	10	11	21	N.A.	-3.35	2.30E-05
2672	gi|21554322	At3g29200	L-ascorbate peroxidase	27544	5.72	MS/MS	88	42	11	32	43	1	2.48	5.90E-06
2703	gi|15217661	At1g64520	regulatory particle non-ATPase 12a (RPN12a)	30915	4.81	MALDI-ToF	116	51	15	70	85	N.A.	-2.09	7.50E-07
2736	gi|11270444	At2g21170	Encodes a plastidic triose phosphate isomerase	27138	5.24	MS/MS	467	44	15	50	65	5	-2.18	5.10E-07
2747	gi|11270444	At2g21170	Encodes a plastidic triose phosphate isomerase	27138	5.24	MS/MS	190	36	12	53	65	3	-2.89	2.10E-06
2759	gi|15231715 & gi|436792	At3g52930 & At5g20830	Mixture: fructose-bisphosphate aldolase; sucrose synthase	N.A.	N.A.	MS/MS	306+252	N.A.	N.A.	N.A.	N.A.	N.A.	-2.18	5.50E-06
2888	gi|15228818	At3g56090	ferritin 3 AtFER3	28876	5.54	MALDI-ToF	123	52	17	88	105	N.A.	-2.29	4.70E-05
2904			No significant hit			MS/MS							-2.31	1.00E-07

2921	gi|17065646	At5g20720	Encodes a chloroplast co-chaperonin	26785	8.86	MS/MS	141	37	13	33	46	4	-2.05	7.00E-06
2929													-2.07	1.90E-07
2938													-2.14	1.50E-07
2989	gi|436792	At5g20830	sucrose synthase (SUS1)	92866	5.66	MS/MS	388	11	8	57	65	5	-2.06	8.40E-05
2997													-2.06	5.90E-05
3005													-2.33	5.80E-06
3009													-2.86	1.60E-07
3063	gi|15239772	At5g19550	aspartate aminotransferase 2	44269	6.8	MS/MS	142	20	13	27	40	4	-2.01	4.40E-05
3133													-2.4	3.70E-05
3147													-2.23	1.30E-05
3151	gi|23505949	At5g19770	tubulin 3	49622	4.95	MS/MS	73	12	6	53	59	1	-2.24	0.00021
3360	gi|21553673	At3g60750	putative transketolase	79875	5.88	MS/MS	343	12	13	49	62	5	-2.36	3.90E-06
3387	gi|16396	At4g09320	nucleoside diphosphate kinase type 1	16229	7.03	MS/MS	233	55	15	24	39	4	2.25	6.60E-05
3479			No significant hit			MS/MS							-2.44	3.10E-06
3486	gi|13899069	At4g09320	nucleoside diphosphate kinase type 1	15797	6.84	MALDI-ToF	102	43	8	23	31	N.A.	-2.66	6.80E-05
3726													-2.06	1.40E-06
3739													-2.77	6.10E-05
3740													-2.95	4.90E-05
3756			No significant Hit			MS/MS							-2.37	7.40E-05
3757	gi|6721173	At3g04120	encodes cytosolic GAPDH (C subunit)	36891	6.62	MS/MS	330	25	11	50	61	5	-2.65	5.90E-07
3758													-2.35	1.80E-06
3761													-2.27	6.20E-05
3777													-2.23	2.20E-06
3909													-2.26	0.00026
4006	gi|60266727	At4g13940	Encodes a S-adenosyl-L-homocysteine hydrolase	53356	5.66	MS/MS	229	29	23	34	57	5	2.65	2.20E-07
4008	gi|23297411	At2g36530	enolase 2	47689	5.54	MS/MS	523	58	29	36	65	7	2.06	0.00077
4040	gi|21436091	At2g37760	aldo/keto reductase family protein	34663	6.52	MS/MS	382	48	24	36	60	4	2.52	9.60E-06
4062	gi|20260174	At2g36530	enolase 2	47747	5.45	MS/MS	360	57	25	40	65	6	2.08	1.50E-06

Appendix B Publications resulting from this thesis

This paper is available on line at http://www.mcponline.org

Proteomic Analysis of Extracellular ATP-Regulated Proteins Identifies ATP Synthase β-Subunit as a Novel Plant Cell Death Regulator*[S]

Stephen Chivasa‡¶, Daniel F. A. Tomé‡¶, John M. Hamilton‡, and Antoni R. Slabas‡§

Extracellular ATP is an important signal molecule required to cue plant growth and developmental programs, interactions with other organisms, and responses to environmental stimuli. The molecular targets mediating the physiological effects of extracellular ATP in plants have not yet been identified. We developed a well characterized experimental system that depletes *Arabidopsis* cell suspension culture extracellular ATP via treatment with the cell death-inducing mycotoxin fumonisin B1. This provided a platform for protein profile comparison between extracellular ATP-depleted cells and fumonisin B1-treated cells replenished with exogenous ATP, thus enabling the identification of proteins regulated by extracellular ATP signaling. Using two-dimensional difference in-gel electrophoresis and matrix-assisted laser desorption-time of flight MS analysis of microsomal membrane and total soluble protein fractions, we identified 26 distinct proteins whose gene expression is controlled by the level of extracellular ATP. An additional 48 proteins that responded to fumonisin B1 were unaffected by extracellular ATP levels, confirming that this mycotoxin has physiological effects on *Arabidopsis* that are independent of its ability to trigger extracellular ATP depletion. Molecular chaperones, cellular redox control enzymes, glycolytic enzymes, and components of the cellular protein degradation machinery were among the extracellular ATP-responsive proteins. A major category of proteins highly regulated by extracellular ATP were components of ATP metabolism enzymes. We selected one of these, the mitochondrial ATP synthase β-subunit, for further analysis using reverse genetics. Plants in which the gene for this protein was knocked out by insertion of a transfer-DNA sequence became resistant to fumonisin B1-induced cell death. Therefore, in addition to its function in mitochondrial oxidative phosphorylation, our study defines a new role for ATP synthase β-subunit as a pro-cell death protein. More significantly, this protein is a novel target for extracellular ATP in its function as a key negative regulator of plant cell death. ***Molecular & Cellular Proteomics 10: 10.1074/mcp.M110.003905, 1–13, 2011.***

ATP is a ubiquitous, energy-rich molecule of fundamental importance in living organisms. It is a key substrate and vital cofactor in many biochemical reactions and is thus conserved by all cells. However, in addition to its localization and functions inside cells, ATP is actively secreted to the extracellular matrix where it forms a halo around the external cell surface. The existence of this extracellular ATP (eATP)[1] has been reported in several organisms including bacteria (1), primitive eukaryotes (2), animals (3), and plants (4–6). This eATP is not wasted, but harnessed at the cell surface as a potent signaling molecule enabling cells to communicate with their neighbors and regulate crucial growth and developmental processes.

In animals, eATP is a crucial signal molecule in several physiological processes such as neurotransmission (7, 8), regulation of blood pressure (9), enhanced production of reactive oxygen species (ROS) (10), protein translocation (11), and apoptosis (12). Extracellular ATP signal perception at the animal cell surface is mediated by P2X and P2Y receptors, which bind ATP extracellularly and recruit intracellular second messengers (13, 14). P2X receptors are ligand-gated ion channels that provide extracellular Ca^{2+} a corridor for cell entry after binding eATP, facilitating a surge in cytosolic [Ca^{2+}] that is essential in activating down-stream signaling. P2Y receptors transduce the eATP signal by marshalling heteromeric G-proteins on the cytosolic face of the plasma membrane and activating appropriate downstream effectors.

Although eATP exists in plants, homologous P2X/P2Y receptors for eATP signal perception have not yet been identified, even in plant species with fully sequenced genomes. Notwithstanding the obscurity of plant eATP signal sensors, some of the key downstream messengers recruited by eATP-mediated signaling are known. For example, eATP triggers a surge in cytosolic Ca^{2+} concentration (15–17) and a heightened production of nitric oxide (18–20) and reactive oxygen

From the ‡School of Biological and Biomedical Sciences, Durham University, Durham DH1 3LE, United Kingdom

Received August 3, 2010, and in revised form, November 24, 2010
Published, MCP Papers in Press, December 14, 2010, DOI 10.1074/mcp.M110.003905

[1] The abbreviations used are: eATP, extracellular ATP; FB1, fumonisin B1; ROS, reactive oxygen species; TSP, total soluble protein.

species (17, 21, 22). Altering eATP levels is attended by activation of plant gene expression (16, 21) and changes in protein abundance (5, 23), indicating that eATP-mediated signaling impacts on plant physiology. Indeed eATP has been demonstrated to regulate plant growth (20, 24–26), gravitropic responses (27), xenobiotic resistance (4), plant-symbiont interactions (28), and plant-pathogen interactions (23, 29). However, the mechanism by which eATP regulates these processes remains unclear, largely because the eATP signal sensors and downstream signal regulatory genes and proteins have not been identified.

We previously reported that eATP plays a central regulatory role in plant cell death processes (5). Therefore, an understanding of the signaling components galvanized by eATP in cell death regulation might serve a useful purpose in providing mechanistic detail of how eATP signals in plant physiological processes. We found that eATP-mediated signaling negatively regulates cell death as its removal by application of ATP-degrading enzymes to the apoplast activates plant cell death (5). Remarkably, fumonisin B1 (FB1), a pathogen-derived molecule that activates defense gene expression in *Arabidopsis* (30), commandeers this eATP-regulated signaling to trigger programmed cell death (5). FB1 is a mycotoxin secreted by fungi in the genus *Fusarium* and initiates programmed cell death in both animal and plant cells (31, 32). In *Arabidopsis*, FB1 inaugurates cell death by inactivating eATP-mediated signaling via triggering a drastic collapse in the levels of eATP (5). FB1-induced *Arabidopsis* programmed cell death is dependent on the plant signaling hormone salicylic acid (33), which is a key regulator of eATP levels (29). Because concurrent application of FB1 and exogenous ATP to remedy the FB1-induced eATP deficit blocks death, FB1 and exogenous ATP treatments can therefore be used as probes to identify the key signal regulators downstream of eATP in cell death control. This is vital for achieving the global objective of elucidating the mechanism of eATP signaling in plant physiology.

Gel-based proteomic analyses have been previously applied to successfully identify the novel role of eATP in the regulation of plant defense gene expression and disease resistance (23, 29). We have now employed FB1 and ATP treatments together with two-dimensional difference in-gel electrophoresis (DIGE) and matrix-assisted laser desorption-time of flight MS (MALDI-TOF MS) to identify the changes in *Arabidopsis* protein profiles associated with a shift from normal to cell death-inception metabolism. Additional reverse genetic analyses enabled us to definitively identify a putative ATP synthase β-subunit as a target for eATP-mediated signaling with an unexpected function in the regulation of plant programmed cell death.

EXPERIMENTAL PROCEDURES

Plant Material and Growth Conditions—Cell suspension cultures of *Arabidopsis thaliana* var. Landsberg erecta (34) were grown at 22 °C under a 16 h photoperiod (100 μmol/m^2/s) regimen. Cell cultures were used for experiments in mid-exponential growth phase (3–4 days postsubculturing). Soil grown-plants were incubated in a growth chamber with a 16 h photoperiod (100–120 μmol.m^{-2}.s^{-1}) maintained at 20 °C during the light phase and 15 °C during the dark phase. Plants were used for experiments 4–5 weeks following sowing.

Cell Culture Treatment—Stock solutions of FB1 (Sigma, Haverhill, UK) were prepared in 70% methanol and filter-sterilized before using to treat cell cultures. Mock treatments were performed with an equivalent dilution of 70% methanol. Stocks of filter-sterilized 100 mM ATP, pH 6.5 (adjusted with KOH) were prepared fresh every time. Samples for proteomic analysis were prepared by treating 3 days old *Arabidopsis* cell cultures adjusted to a cell density of 5% (w/v) in a 100 ml culture volume. One set of cultures (FB1) was treated with 1 μM FB1 at the beginning of the experiment, whereas the second set of cultures (FB1+ATP) was similarly treated with FB1, but 1 mM ATP was added 40 h later. The controls were mock-treated with methanol, the carrier solution for FB1. Each treatment had 4 independent biological replicates. The cells were harvested 48 h following the start of the experiment and frozen in liquid nitrogen.

Protein Sample Preparation—Cells were pulverised at 4 °C in a homogenization buffer (1 mM EDTA/10 mM Tris-HCl, pH 8.0) using a French Press (Constant systems Ltd., Warwick, UK) and the homogenate centrifuged (20,000 × *g*, 30 min, 4 °C). The supernatant, containing microsomal membranes and the total soluble protein fraction, was centrifuged (100,000 × *g*, 1 h, 4 °C) to separate these fractions. Total soluble protein (TSP) was recovered from the supernatant by precipitation (80% [v/v] acetone, −20 °C, 12 h) and extracted from the precipitate with a protein solubilization solution (9 M urea, 2 M thiourea, 4%[w/v] CHAPS). The microsomal membrane pellets were washed three times with homogenization buffer and protein extracted using the protein solubilization solution.

Protein Labeling and Gel Electrophoresis—Protein samples from four biological replicates of each treatment were labeled with CyDyes (GE Healthcare, Buckinghamshire, UK) as described before (35). Each biological replicate sample was split into two and one labeled with Cy3 and the other with Cy5 in a dye swap experimental design to preclude dye-specific artifacts (36). The pooled standard consisting of equal amounts of all the samples was labeled with Cy2. Protein mixtures containing 12.5 μg each of Cy3-and Cy5-labeled samples plus the Cy2-labeled pooled standard were resolved in 24 cm linear gradient pI 4–7 IPG strips for 70kVh as previously described (35). Second dimension separation was performed on an Ettan DALT Twelve System (GE Healthcare, Buckinghamshire, UK) in custom made 10–20% gradient polyacrylamide gels cast using the automated 2DE Optimizer gel caster (NextGen sciences, Cambridge, UK). Following resolution, the gels were immediately scanned using a Typhoon 9400 variable mode imager (GE Healthcare, Buckinghamshire, UK).

Image Analysis—Gel images were analyzed using DeCyder Differential Analysis Software version 6.5 (GE Healthcare, Buckinghamshire, UK) as described previously (35). Briefly, four biological and two technical replicates (from the dye-swap) comprised a total of 8 images per treatment. Spot detection, quantification and normalization of spot volume against the internal standard were performed automatically using the Differential In-Gel analysis module with estimated number of spots set to 5000. The Biological Variation Analysis module was used for spot matching and differential protein analysis. Matched spots were manually checked between gels to minimize false spot matching and exclude spot artifacts. The software automatically generated a ratio of sample spot volume to the pooled standard spot volume and normalized these ratios across all gels to generate standardized spot abundance values. The standardized spot abundance

values from the four biological replicates and two technical replicates were then averaged and the means subjected to Student's *t* test to check for statistically significant differences. Only manually inspected spots present in all replicate gels and displaying a significant ($p \leq 0.05$) FB1-induced change in abundance of a minimum of 20% (TSP) or 50% (microsomal protein) were selected for further analyses. The response of these spots to ATP added after FB1 was analyzed by statistical comparison of FB1+ATP average with FB1 only average. Only spots with an average standardized abundance that significantly ($p \leq 0.05$) shifted from the FB1 treatment average in response to the FB1+ATP treatment were selected for further analyses as ATP-responsive proteins. Probability values associated with the comparison of means were calculated using Student's *t* test.

MALDI-TOf MS Protein Identification—Preparative gels for protein identification loaded with 200 μg of unlabeled protein were stained with Sypro Ruby™ total protein stain (Genomic Solutions, Huntington, UK) according to the manufacturer's instructions. Differentially expressed spots were robotically excised using a ProPick Work station (Genomic Solutions, Huntington, UK) for identification by MALDI-TOF using a Voyager DE-STR Biospectrometry work station (Applied Biosystems, Warrington, Cheshire, UK) as described previously (37). Briefly, spot plugs of 2.0 mm diameter were digested with modified trypsin (Promega, Madison, WI) in a ProGest work station (Genomic Solutions, Huntington, UK) using the standard overnight digestion protocol supplied with the instrument. A total of 0.5 μl of each digest was spotted together with 0.5 μl of a saturated solution of α-cyano-4-hydroxycinnamic acid matrix directly onto a MALDI target plate using an Applied Biosystems Symbiot robot (Boston, MA). Instrument calibration was carried out for each sample using PE Sequazyme calibration mixture I (containing des-Arg-bradykinin, angiotensin I, Glu-fibrinopeptide B, and neurotensin). After each spot's spectra were acquired, automated peak detection, peak de-isotoping and noise reduction was carried out using Applied Biosystems Data Explorer 2.1.0 to generate peak mass tables. Trypsin peptide peaks (842.5 + 2211.1) were used as internal calibrants and were excluded from database searches. The peptide mass fingerprint for each spot was used to search *Viridiplantae* (green plants) sequences in the nonredundant NCBInr database version 20070713 (5269953 sequences; 1825351362 residues) using the Mascot 4.0 search engine (Matrix Science, London, UK). The following search parameters were used: peptide mass tolerance: ± 50 ppm, maximum number of missed cleavages: 1, fixed modifications: carbamidomethylation of cysteine residues, variable modifications: oxidation of methionine residues. The Mascot software probability-based MOWSE score cut-off for a significant ($p \leq 0.05$) positive protein identification of 71 was applied. Where more than one database entry was obtained from a single spot, the spots were excluded because it was impossible to know which of the proteins in the mixture were differentially regulated.

RNA Analysis and PCR Reactions—Total RNA was extracted using RNeasy Plant kit (Qiagen, Crawley, UK), with on-column DNase treatment, according to the manufacturer's instructions. First-strand cDNA synthesis was performed as previously described (35) using oligo-$(dT)_{15}$ (Progema, Southampton, UK), 3 μg of total RNA and SuperScript III reverse transcriptase (Invitrogen, Paisley, UK). For PCR reactions, the following primer pairs were used: *ATP SYNTHASE β-SUBUNIT* (At5g08690) 5′-TCCACACACCCACTCATGGCG-3′ and 5′-TCACAATGCCTCAGCAGACAACC-3′; *ACTIN 2* (At3g18780) 5′-GGATCGGTGGTTCCATTCTTG-3′ and 5′-AGAGTTGTCACACACAAGTG-3′, *SEN1* (At4g35770) 5′-TTAAAATTCCTACGTCAGTACCAG-3′ and 5′-TCTCTGTCCAAGCGACGTATCC-3′.

Cell Death Assays—Discs of 8 mm diameter were cored from leaves of 4-week-old plants and floated on 10 μM FB1 solutions in triplicate Petri-dishes. Each replicate had 10 leaf discs each originating from one of 10 replicate plants. The discs were incubated in the dark for 48 h to allow uptake of FB1 prior to the onset of cell death. After the dark incubation, the discs were placed under a 16 h photoperiod regime and the conductivity of the underlying solution measured at 24 h intervals using a Jenway conductivity meter (Jenway Ltd., Felsted, UK). In addition, 10 μM FB1 was also infiltrated into the apoplast of attached leaves from the abaxial surface using a syringe without a needle. Symptom development was visually monitored and photographs taken 4 days following infiltration.

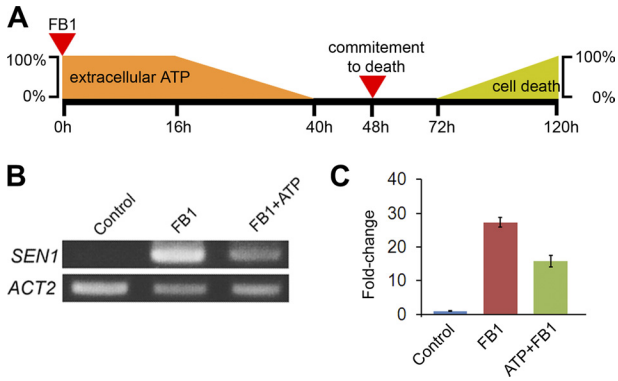

FIG. 1. **Schematic representation of FB1-induced events and the effects of exogenous ATP.** *A*, addition of FB1 to cell cultures triggers eATP depletion commencing ~16 h later and disappearing below detection at ~40 h. Cells irreversibly commit to die at ~48 h and cell death starts at ~72 h. Exogenous ATP added at 40 h attenuates FB1-induced signaling and gene expression, thereby blocking cell death. Note that the decline of eATP from 100–0% and the increase of cell death from 0–100% do not progress at rates indicated by the gradients on the diagram. *B*, induction by FB1 of a cell death marker, *senescence-associated 1* (*SEN1*), is attenuated by exogenous ATP. Samples for RT-PCR were harvested at 42 h. *Actin-2* (*ACT2*) was used as a constitutive reference control. *C*, densitometric analysis of *SEN1* PCR bands from (*B*) expressed as fold-change relative to the control sample. Data and error bars are means ± se ($n = 3$).

RESULTS

Establishing the Experimental System—To identify eATP-regulated proteins with a putative function in cell death regulation, we used *Arabidopsis* cell cultures treated with FB1 or FB1+ATP. FB1 inactivates eATP-mediated signaling by triggering removal of the input signal (eATP), thereby initiating cell death (5). Exogenous ATP supplied back to the FB1-treated cultures rescues the cells from death, most probably by re-establishing the eATP-mediated signaling. Thus, exogenous ATP treatment can be used as a filter to identify the subset of FB1-induced genes/proteins whose expression and abundance is altered in response to the specific depletion of eATP. We used the cell death marker *SEN1* (At4g35770), a gene activated during senescence-associated programmed cell death (38), to validate the utility of the exogenous ATP filter in this experimental system. FB1 treatment up-regulated *SEN1* expression, but, in accordance with its ability to blockade FB1-induced cell death (5), exogenous ATP attenuated the response of this gene to FB1 treatment (Fig. 1). Because exogenous ATP effectively blocked FB1 effects at the transcript level, it is most likely that this is reflected at the protein

level as well. Therefore, a comparative analysis of protein profiles of mock-treated cultures with FB1- and FB1+ATP-treated cultures can reveal eATP-regulated proteins that mediate its physiological effects, including cell death control.

We have previously shown that exogenous ATP rescues cells from death if added concurrently with FB1 or any time up to ~40 h later, but fails to rescue the cells if added ~48 h or thereafter (5). Although 40 h coincides with the time when eATP levels have diminished below detection (5), these findings indicate that the cells' metabolism irreversibly commits to cell death at ~48 h, with cell death symptoms appearing ~24 h later (5). Therefore, we chose to perform proteomic analyses at the 48 h time point in order to detect the changes that switch normal metabolism to a death program, but that precede actual cell death. The timing of events triggered by FB1 addition to *Arabidopsis* cell cultures is illustrated schematically in Fig. 1.

Protein Gel Analysis and Protein Identification—Fractions enriched for total soluble protein (TSP) and microsomal membrane protein were prepared from *Arabidopsis* cell cultures exposed to FB1 or a combination of FB1+ATP treatments. In the latter, ATP was added to the cell cultures 40 h after FB1. Treated cells were harvested for protein extraction at the 48 h time point. Images of the protein gels revealed big differences in the profiles of TSP and microsomal membrane proteins (Fig. 2), indicating that analysis of the two separate fractions enabled the coverage of a wider range of proteins than would be achievable if only one of the protein fractions was targeted for analysis. As we used a gel-based approach, it is obvious that only a fraction of the membrane-associated proteins are represented in this study because highly hydrophobic proteins do not easily enter two-dimensional gels. However, this inadvertently helped to simplify the protein profile by reducing the number of proteins.

Quantitative analysis was performed using two-dimensional DIGE on four independent biological replicates of each treatment and two technical replicates of each sample. Average standardized spot volumes of the control and FB1 treatments were compared using Student's *t* test and the fold-change in protein abundance calculated by generating the ratio [FB1/control] for up-regulated spots or [control/FB1] for down-regulated spots (Tables I and II). To quantify the effects of ATP on FB1-induced changes in protein abundance, average spot volumes of the FB1 and FB1+ATP treatments were compared using the Student's *t* test and the ratio [FB1+ATP/FB1] or [FB1/FB1+ATP] generated for up-regulated or down-regulated spots, respectively (Tables I and II). The ratio of down-regulated spots is indicated by a minus sign in both Tables I and II.

Approximately 5000 features, including both authentic protein spots and some artifacts, were automatically detected on the pooled standard master gels. The majority of protein spots in both the TSP and microsomal protein fractions did not respond to FB1 treatment. The abundance of 145 protein

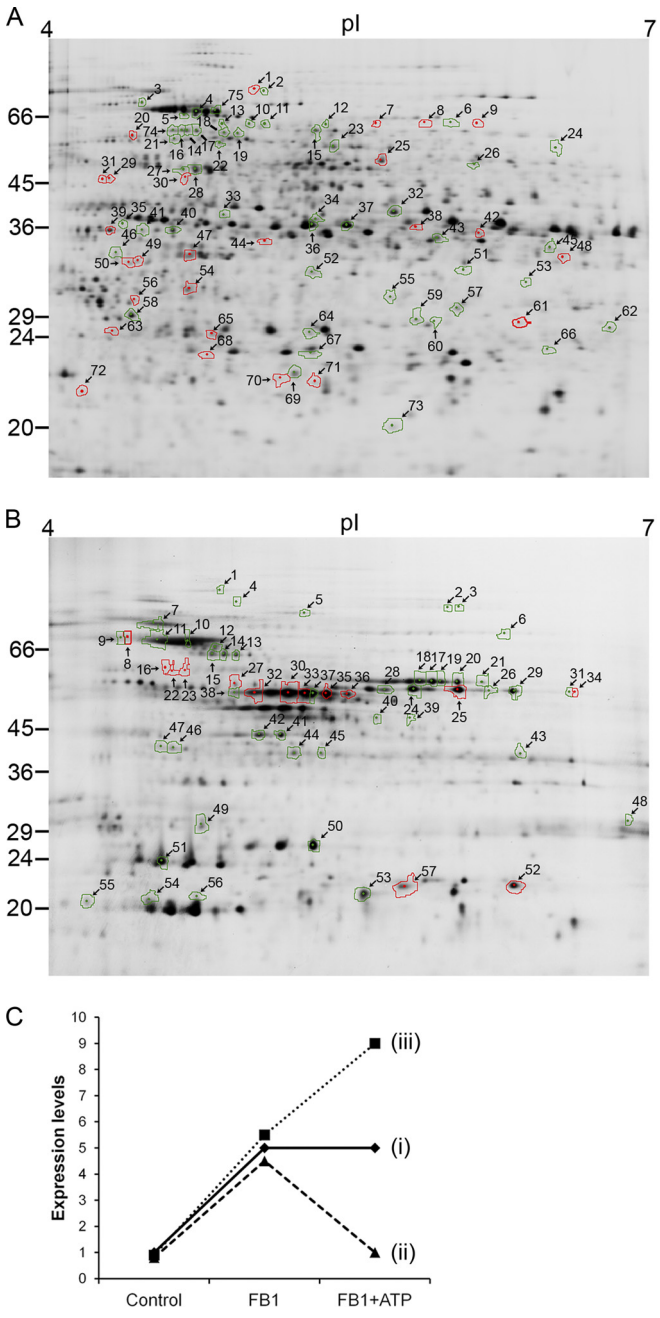

FIG. 2. **2-D DIGE analysis of *Arabidopsis* proteins and their response profile.** Total soluble protein (*A*) and microsomal membrane protein (*B*) fractions were analyzed by 2-D DIGE and protein spots responding to FB1 alone (*green boundary*) or to both FB1 and exogenous ATP (*red boundaries*) were identified by MALDI-TOF MS. *C*, protein response profiles: some proteins responded only to FB1 (*profile i*), and others to both FB1 and ATP (*profiles ii and iii*). Reciprocals of these profiles are also considered to belong to the same response group.

spots in the TSP fraction was significantly ($p \leq 0.05$) altered in response to FB1 treatment by at least 20%. Of these 145 TSP spots, only 75 were positively identified (Table I). The remaining 70 could not be positively identified - the majority being

TABLE I
TSP fraction proteins differentially expressed in response to FB1 and FB1+ATP

Spot	Gene locus	Protein name	Score[a]	Sequence coverage	Peptides[b]	FB1/Control		FB1+ATP/FB1	
						Ratio[c]	*p* value	Ratio[d]	*p* value[e]
				%					
Molecular chaperones									
3	At5g02500	heat shock cognate protein 70–1	85	31	15	1.21	2.2e-3	1.05	nss
4	At3g12580	heat shock protein 70 (HSP70)	146	36	24	1.22	3.6e-2	1.22	nss
10	At5g09590	heat shock protein 70 (Hsc70–5)	250	49	35	1.24	7.1e-3	−1.15	1.1e-2
14	At5g02500	heat shock cognate protein 70–1	89	28	20	1.24	1.3e-2	−1.13	nss
16	At5g02500	heat shock cognate protein 70–1	126	40	18	1.26	1.5e-2	−1.13	nss
17	At5g02500	heat shock cognate protein 70–1	123	33	20	1.36	3.3e-3	−1.10	nss
18	At3g12580	heat shock protein 70 (HSP70)	129	33	22	1.42	5.6e-5	−1.02	nss
19	At3g12580	heat shock protein 70 (HSP70)	80	19	13	1.52	3.0e-5	1.04	nss
20	At1g77510	protein disulfide isomerase-like	148	51	19	−1.26	1.5e-2	1.23	2.5e-2
21	At4g37910	mitochondrial heat shock protein 70–1	177	38	25	−1.26	9.5e-3	−1.19	nss
22	At3g12580	heat shock protein 70 (HSP70)	112	26	22	1.78	8.3e-5	−1.19	nss
29	At4g24190	heat shock 90.7 like protein	104	30	11	1.34	6.6e-4	−1.38	8.0e-4
30	At5g52640	heat shock protein AtHSP90.1	76	15	11	1.38	5.8e-6	−1.26	1.4e-2
31	At4g24190	heat shock 90.7 like protein	95	22	15	1.23	8.3e-3	−1.38	4.0e-4
39	At5g52640	heat shock protein AtHSP90.1	123	27	19	1.20	2.8e-2	−1.70	4.3e-3
57	At5g02500	heat shock cognate protein 70–1	83	18	15	−1.57	1.8e-3	−1.20	nss
69	At1g53540	17.6 kDa class I small heat shock protein	90	38	10	1.3	4.5e-3	−1.04	nss
74	At3g09440	heat shock cognate 70 kDa protein 3	97	32	21	1.25	3.1e-2	−1.22	nss
75	At3g12580	heat shock protein 70 (HSP70)	249	56	37	1.27	7.2e-3	1.16	1.1e-2
Glycolytic enzymes									
7	At1g70730	putative phosphoglucomutase	181	44	23	−1.41	2.5e-2	1.38	4.2e-2
8	At1g23190	putative phosphoglucomutase	169	37	21	−1.75	2.1e-4	1.73	2.1e-2
15	At3g08590	putative phosphoglycerate mutase	142	52	19	−1.22	2.3e-2	1.33	nss
38	At3g52930	fructose-bisphosphate aldolase	95	42	10	−1.21	2.5e-2	1.35	6.0e-3
42	At3g04120	GAPDH (C subunit)	104	45	16	−1.24	1.9e-2	1.68	8.0e-4
43	At3g04120	GAPDH (C subunit)	141	43	15	−1.22	9.1e-7	−1.06	nss
50	At1g79550	phosphoglycerate kinase (PGK)	124	62	19	−1.38	3.6e-3	−1.41	2.7e-3
51	At2g36460	fructose-bisphosphate aldolase	85	45	9	−1.44	9.4e-4	−1.08	nss
52	At3g52930	fructose-bisphosphate aldolase	146	57	14	−1.22	1.4e-2	−1.17	4.5e-2
65	At3g52930	fructose-bisphosphate aldolase	86	48	11	1.25	1.0e-2	−1.58	2.4e-3
Antioxidant enzymes									
6	At3g52880	monodehydroascorbate reductase	100	33	11	−1.53	1.2e-5	1.23	nss
49	At5g03630	monodehydroascorbate reductase	116	45	18	−1.49	2.8e-5	−1.26	1.5e-2
53	At5g16970	2-alkenal reductase (EC 1.3.1.74)	96	48	14	1.26	1.3e-3	−1.13	nss
67	At1g19570	dehydroascorbate reductase	109	66	10	−1.25	1.6e-4	−1.05	nss
71	At1g02930	glutathione transferase	114	38	11	1.53	2.9e-4	−1.58	9.0e-3
72	At5g42980	thioredoxin	99	72	11	−1.49	6.5e-4	−1.38	2.5e-2
Cytoskeleton-related proteins									
27	At1g04820	alpha tubulin isoform	135	45	16	−1.28	2.3e-2	1.33	nss
38	At1g04820	alpha tubulin isoform	178	47	15	−1.27	4.2e-2	1.30	nss
35	At3g60830	actin-related protein	84	33	9	−1.5	5.6e-3	−1.12	nss
64	At5g09810	actin 7	80	45	15	1.29	4.1e-4	1.10	nss
73	At5g59880	actin depolymerizing factor 3	111	75	12	−1.21	1.9e-3	1.08	nss
Protein degradation									
2	At2g30110	ubiquitin-activating enzyme (E1)	91	17	16	−1.33	1.9e-2	1.29	nss
59	At2g27020	20S proteasome subunit PAG1	117	39	14	1.21	5.6e-3	−1.13	nss
62	At3g22110	α-3 subunit of 20s proteasome	89	47	11	−1.36	1.5e-6	1.18	nss
63	At1g64520	regulatory particle non-ATPase 12a	116	51	15	1.20	2.7e-2	−1.45	8.7e-3
66	At3g60820	20S proteasome β-subunit PBF1	156	60	15	1.38	6.4e-4	−1.02	nss
Amino acid metabolism									
13	At5g53460	NADH-dependent glutamate synthase	130	41	16	1.52	9.9e-4	−1.14	nss
23	At3g58610	ketol-acid reductoisomerase	189	30	18	−1.29	1.7e-2	1.31	nss
24	At5g17920	cobalamin-independent methionine synthase	90	17	11	1.27	1.4e-2	−1.13	nss
36	At3g17820	glutamine synthetase	108	29	13	1.32	1.5e-4	1.20	nss
37	At3g17820	glutamine synthetase	219	76	27	1.47	9.6e-6	1.16	nss
47	At3g53580	diaminopimelate epimerase	153	57	21	−1.22	7.8e-4	−1.26	6.0e-4
Unclassified									
1	At1g79690	Nudix hydrolase homolog 3	74	39	12	−1.37	8.5e-3	1.52	4.6e-2
5	At5g03340	putative cell division cycle protein 48	80	26	16	1.18	4.8e-3	1.05	nss
9	At2g17980	ATSLY1 protein transporter	102	36	21	−1.5	1.9e-3	1.29	4.2e-2
11	At3g60750	putative transketolase	92	20	12	1.35	3.7e-3	−1.08	nss
12	At3g09840	cell division cycle protein	92	29	16	1.26	1.1e-2	1.09	nss
25	At4g13940	S-adenosyl-L-homocysteine hydrolase	125	46	21	1.35	2.7e-2	1.65	9.0e-3

TABLE I—*continued*

Spot	Gene locus	Protein name	Score[a]	Sequence coverage	Peptides[b]	FB1/Control		FB1+ATP/FB1	
						Ratio[c]	*p* value	Ratio[d]	*p* value[e]
				%					
26	At4g13430	Isopropyl malate isomerase large subunit 1	98	35	16	−1.24	1.5e-2	1.31	nss
32	At1g77120	alcohol dehydrogenase	81	24	9	−1.45	7.0e-3	1.56	nss
33	At5g08690	ATP synthase β-subunit	138	42	21	1.27	3.4e-5	−1.14	2.3e-2
34	At3g29360	putative UDP-glucose 6-dehydrogenase	162	58	28	1.27	1.7e-5	−1.05	nss
40	At1g62380	ACC oxidase	85	43	12	−1.59	2.7e-3	1.19	nss
41	At3g14990	thiazole monophosphate biosynthesis protein	95	45	19	−1.58	4.0e-5	1.15	nss
44	At1g03475	coproporphyrinogen III oxidase	140	46	18	−1.29	2.2e-2	1.32	5.6e-3
45	At5g08670	ATP synthase β-subunit	90	49	20	1.27	5.7e-3	−1.06	nss
46	At2g44060	late embryogenesis abundant family protein	137	61	21	1.28	1.3e-4	−1.13	2.4e-2
48	At3g18130	similarity to mammalian RACKs	111	46	14	−1.51	1.6e-2	1.88	1.1e-2
54	At4g34050	putative caffeoyl-CoA 3-O-methyltransferase	136	61	21	1.87	1.9e-6	−1.33	1.8e-3
55	Atmg01190	ATPase subunit 1	282	52	27	−1.21	3.0e-4	−1.19	3.3e-3
56	At4g13940	S-adenosyl-L-homocysteine hydrolase	82	38	10	1.29	6.0e-4	−1.20	1.1e-2
58	At4g13940	S-adenosyl-L-homocysteine hydrolase	137	57	17	1.22	5.1e-3	−1.26	nss
60	At2g21250	mannose 6-phosphate reductase	77	37	11	−1.48	24e-4	1.02	nss
61	At5g15650	reversibly glycosylated polypeptide-2	123	26	10	1.38	1.4e-2	−1.51	2.3e-2
68	At3g56090	ferritin 3 AtFER3	123	52	17	1.26	1.3e-2	−1.5	5.0e-3
70	At5g38480	general regulatory factor 3	108	34	12	1.25	9.2e-3	−1.3	1.5e-2

[a] Mowse score, for a significant ($p < 0.05$) positive protein identification, cut-off threshold was 71.

[b] Number of peptides matched to the protein sequence.

[c] Ratio represents fold-change of FB1 relative to the control treatment.

[d] Ratio represents fold-change of FB1+ATP relative to FB1 *i.e.* comparison of the FB1+ATP average with the FB1 average to check if ATP addition significantly altered protein response to FB1 alone.

[e] Probability value was replaced by nss when the difference between the treatments being compared was not statistically significant (*i.e.* *p* value >0.05).

low abundance spots, from which inadequate sample was present in the preparative gel to enable identification, whereas a few were in protein mixtures. Spots with protein mixtures were excluded because it was not possible to determine which of the proteins was changing in abundance in response to the treatments. A total of 83 protein spots significantly ($p \leq 0.05$) responded to FB1 by at least a 50% change in abundance in the microsomal membrane fraction. Only 57 of these were positively identified (Table II) whereas identification of the rest was similarly hindered by low abundance or existence as multiple protein mixtures on the gels. The total number of positively identified protein spots in both the TSP and microsomal membrane fractions was 132 (Tables I and II), but this represented 74 unique proteins. The redundancy revealed by the inequality between the number of protein spots and unique proteins arises from the existence of post-translationally modified polypeptides and an overlap of 13 proteins that were identified in both protein fractions. Additional data relating to protein identification is presented in supplemental Table 1 and supplemental Protein Mass Spectra.

The exogenous ATP filter revealed the subset of FB1-responsive proteins, which is regulated by the level of eATP. The response of 24 TSP spots and 16 microsomal membrane protein spots to FB1 was attenuated by exogenous ATP (Fig. 2*C profile ii*). These are the proteins most likely to mediate the physiological effects of eATP. A total of 26 unique proteins were in this category. However, the majority of the FB1-responsive proteins remained unaffected by exogenous ATP (Fig. 2*C profile i*), indicating that FB1 has other targets and physiological effects that are independent of its ability to trigger eATP depletion. A minority of the spots (eight spots) had their response to FB1 enhanced by the addition of exogenous ATP (Fig. 2*C profile iii*). This result suggests that FB1 and exogenous ATP activate common, but as yet uncharacterized, plant signaling cascades where a combination of the two compounds has a synergistic effect.

Classification of Differentially Expressed Proteins—The identified proteins were classified into several functional categories (Tables I and II). Molecular chaperones and heat shock proteins were highly represented in the data sets and they were largely up-regulated in response to FB1. Remarkably, exogenous ATP attenuated this heightened increase in molecular chaperones, indicating that FB1-induced depletion of eATP is the central cue for the deployment of this protein response. Many subunits of the ATP synthesis machinery were down-regulated by FB1 treatment, but again this response was dependent on the level of eATP because exogenous ATP impeded this response. Although the majority of spots in this category were from the mitochondrial ATP synthase, vacuolar and chloroplastic ATP synthase subunits were also identified. Several cellular redox control proteins were suppressed in response to FB1. These included a glutathione *S*-transferase, dehydroascorbate reductase, and thioredoxin. Curiously, exogenous ATP enhanced the suppression of these proteins, indicating that eATP depletion *per ser* is not the cue for this response. Central metabolic pathways, such as glycolysis and amino acid synthesis were also affected by

TABLE II
Microsomal proteins differentially expressed in response to FB1 and FB1+ATP

Spot	Gene locus	Protein name	Score[a]	Sequence coverage	Peptides[b]	FB1/Control		FB1+ATP/FB1	
						Ratio[c]	*p* value	Ratio[d]	*p* value[e]
				%					
Molecular chaperones									
1	At1g79930	high molecular weight heat shock protein	128	36	27	1.93	2.4e-7	−1.09	nss
5	At5g15450	chloroplast-targeted Hsp101 homologue	90	32	31	−1.59	3.5e-3	1.14	nss
7	At5g56030	heat shock protein 90 (HSP90)	218	39	36	1.78	1.1e-6	1.00	nss
8	At4g24280	chloroplast heat shock protein 70–1	74	21	15	2.19	4.5e-9	−1.20	9.7e-3
9	At4g24280	chloroplast heat shock protein 70–1	137	31	21	2.09	5.1e-7	−1.18	0.014
10	At5g02500	heat shock cognate protein 70–1	214	56	29	1.79	9.3e-7	−1.10	nss
11	At5g02500	heat shock cognate protein 70–1	187	48	27	2.13	2.3e-8	−1.08	nss
12	At3g12580	heat shock protein 70 (HSP70)	218	48	26	2.13	3.6e-7	−1.17	nss
15	At4g37910	mitochondrial heat shock protein 70–1	102	44	28	−1.54	2.3e-4	1.21	nss
16	At4g37910	mitochondrial heat shock protein 70–1	98	34	20	2.04	9.9e-5	−1.31	2.5e-2
22	At4g37910	mitochondrial heat shock protein 70–1	106	47	29	3.14	1.1e-5	−1.65	9.6e-3
23	At4g37910	mitochondrial heat shock protein 70–1	101	26	16	4.34	8.3e-8	−1.6	3.2e-3
46	At5g52640	heat shock protein AtHSP90.1	98	23	16	2.85	4.5e-5	−1.41	nss
47	At5g56010	heat shock protein 90 (HSP90)	85	27	14	2.87	3.8e-5	−1.43	nss
54	At4g25200	AtHSP23.6-mito	84	52	10	−2.29	1.4e-6	−1.03	nss
ATP synthesis machinery									
13	At1g78900	vacuolar ATP synthase subunit A	156	47	25	−1.80	7.0e-5	1.19	nss
14	At1g78900	vacuolar ATP synthase subunit A	192	39	22	−1.63	1.9e-4	1.19	nss
24	Atmg01190	ATPase subunit 1	207	41	20	−2.01	5.5e-6	1.30	4.1e-2
25	Atmg01190	ATPase subunit 1	213	51	27	−1.96	2.2e-6	1.28	nss
26	Atmg01190	ATPase subunit 1	235	60	29	−2.81	4.0e-6	1.29	nss
27	Atcg00120	ATPase CF1 α-subunit	216	37	20	−1.70	1.9e-4	1.29	3.4e-2
28	Atmg01190	ATPase subunit 1	164	35	16	−2.31	4.4e-8	1.17	nss
29	Atmg01190	ATPase subunit 1	207	51	24	−1.93	2.0e-5	1.26	nss
30	At5g08690	mitochondrial ATP synthase β-subunit	217	58	27	−1.88	4.1e-7	1.24	1.6e-2
31	Atmg01190	ATPase subunit 1	197	36	18	−1.69	5.9e-4	1.21	nss
32	At5g08690	mitochondrial ATP synthase β-subunit	248	63	28	−2.17	5.3e-8	1.23	1.4e-2
33	At5g08690	mitochondrial ATP synthase β-subunit	250	62	28	−1.86	8.2e-7	1.32	2.5e-2
34	Atmg01190	ATPase subunit 1	79	23	10	−1.69	8.3e-4	1.22	2.6e-2
35	At5g08690	mitochondrial ATP synthase β-subunit	251	64	25	−1.72	3.0e-5	1.34	2.9e-2
36	At5g08690	mitochondrial ATP synthase β-subunit	249	60	25	−1.74	2.9e-4	1.38	1.8e-2
37	At5g08690	mitochondrial ATP synthase β-subunit	217	58	27	−2.04	5.9e-6	1.28	nss
38	At5g08690	mitochondrial ATP synthase β-subunit	112	33	14	−1.78	1.8e-6	1.13	2.2e-2
39	At5g08690	mitochondrial ATP synthase β-subunit	206	55	27	3.07	1.6e-7	1.16	nss
50	At2g21870	unknown protein mitochondrial	137	65	19	−2.03	2.1e-5	1.23	nss
52	At5g13450	ATP synthase delta chain	185	63	18	−1.83	3.5e-6	1.23	3.4e-2
53	At5g08670	mitochondrial ATP synthase β-subunit	124	59	22	−1.7	3.2e-6	1.12	nss
56	At3g52300	ATP synthase D chain	212	83	20	−2.32	3.6e-6	−1.12	nss
57	At5g13450	ATP synthase delta chain	133	53	14	−1.68	8.6e-6	1.23	2.7e-2
Unclassified									
2	At1g56070	translation elongation factor 2-like	88	38	28	2.28	2.2e-5	1.04	nss
3	At1g56070	translation elongation factor 2-like	125	46	30	2.24	6.4e-9	1.09	nss
4	At3g09840	cell division cycle protein	91	14	14	3.35	9.4e-9	−1.09	nss
6	At5g17920	cobalamin-independent methionine synthase	88	37	21	5.18	9.1e-10	1.11	nss
17	At3g02090	metalloendopeptidase (MPPBETA)	137	37	15	−1.92	9.4e-5	1.21	nss
18	At3g02090	metalloendopeptidase (MPPBETA)	209	59	26	−1.94	1.4e-5	1.19	nss
19	At3g02090	metalloendopeptidase (MPPBETA)	184	57	22	−1.9	1.5e-4	1.23	nss
20	At3g02090	metalloendopeptidase (MPPBETA)	224	59	25	−1.8	2.4e-4	1.26	nss
21	At3g02090	metalloendopeptidase (MPPBETA)	87	17	9	−1.61	6.7e-4	1.20	nss
40	At4g01850	S-adenosylmethionine synthetase 2	92	47	17	2.66	1.3e-9	1.12	nss
41	At5g09810	Actin 7	203	62	23	2.3	4.5e-8	−1.03	nss
42	At5g09810	Actin 7	187	59	22	2.3	5.9e-8	−1.07	nss
43	At3g52930	fructose-bisphosphate aldolase	121	48	13	1.58	5.5e-6	−1.09	nss
44	At1g79550	cytosolic phosphoglycerate kinase	118	55	18	2.62	1.4e-8	−1.04	nss
45	At1g79550	cytosolic phosphoglycerate kinase	132	44	15	3.29	1.2e-10	−1.01	nss
48	At5g40770	prohibitin 3	121	38	11	−1.74	9.8e-5	1.10	nss
49	At3g23400	plastid-lipid associated protein	142	53	14	−1.63	1.9e-6	−1.01	nss
51	At3g23400	plastid-lipid associated protein	106	38	9	−1.58	1.9e-6	1.07	nss
55	At3g16640	translationally controlled tumor protein	93	54	10	2.73	2.2e-10	1.03	nss

[a] Mowse score, for a significant ($p < 0.05$) positive protein identification, cut-off threshold was 71.

[b] Number of peptides matched to the protein sequence.

[c] Ratio represents fold-change of FB1 relative to the control treatment.

[d] Ratio represents fold-change of FB1+ATP relative to FB1 *i.e.* comparison of the FB1+ATP average with the FB1 average to check if ATP addition significantly altered protein response to FB1 alone.

[e] Probability value was replaced by nss when the difference between the treatments being compared was not statistically significant (*i.e.* *p* value >0.05).

FB1 treatment. Other functional categories of FB1-responsive proteins included members of the cell's protein degradation machinery, cytoskeleton-associated proteins with a structural role, and various enzymes involved in several other cellular and metabolic processes.

ATP Synthase β-subunit is a Cell Death Regulator—After identifying eATP-regulated proteins using FB1 treatments and the exogenous ATP filter, we initiated a systematic investigation of their possible role in plant cell death control. From the list of 28 proteins identified in this category, we selected candidates for which *Arabidopsis* transfer-DNA (T-DNA) gene knockout mutants from the SALK T-DNA collection (39) existed. We searched the *Arabidopsis* genome database for gene family members and relegated to the bottom of the list candidates from large gene families, whose function is unlikely to be obtained via reverse genetic studies owing to the high likelihood of gene redundancy. The response of the knockout mutants to FB1 treatment was examined using qualitative and quantitative cell death assays and any mutant with cell death kinetics and phenotype different from wild-type plants clearly defined novel cell death signal regulatory proteins under eATP control.

At the top of our candidate protein list was ATP synthase β-subunit (AT5G08690), a dominant microsomal membrane fraction eATP-regulated protein found in spots 30, 32, 33, and 35–39 (Fig. 2*B*; Table II). Although seven of the spots appeared as a charge train of ~55 kDa, one spot (spot 39) had a lower molecular weight of ~49 kDa (Fig. 2*B*). The same ATP synthase β-subunit protein was identified in the TSP fraction as a ~38 kDa spot (spot 33) (Fig. 2*A*). Distribution of the identified peptides from the two low molecular weight species was predominantly in the central region of the primary sequence of ATP synthase β-subunit (Fig. 3), suggesting the possibility that they arise from N- and/or C-terminal cleavage of the ~55 kDa protein.

We obtained three independent homozygous gene knockout mutants of ATP synthase β-subunit (SALK_005252, SALK_024990, and SALK_135351) with a single T-DNA inserted into predicted exonal regions of the gene (Fig. 4*A*). Gene knockout status was confirmed by RT-PCR. Primers designed to straddle the insertion sites successfully amplified the expected 1795 bp gene-specific product in wild-type Columbia-0 plants whereas the absence of this product in all knockout lines confirmed the lack of a functional copy of the gene (Fig. 4*B*). Next we established the cell death kinetics of leaf tissue obtained from the knockout plant lines against wild-type plant tissues. The assay involves floating leaf discs on FB1 solutions and measuring the conductivity of the solution, which rises as dying cells release their contents. Measured over time, the conductivity profile reflects the relative rates and extent of FB1-induced cell death. The rate and extent of cell death were significantly diminished in all three knockout lines (Fig. 4*C,* 4*E*), indicating that they were resistant to FB1. Leaf discs from the ion leakage assay photographed 96 h post-treatment revealed advanced stages of chlorosis, that accompany cell death, in wild-type tissues (Fig. 4*F*). Corresponding tissues from SALK_135351 and SALK_005252 did not have these symptoms (Fig. 4*F*), displaying the resistance engendered by disruption ATP synthase β-chain subunit gene expression. Moreover, cell death symptom development was also suppressed in the SALK_024990 knockout line when FB1 was infiltrated into leaves left attached to growing plants (Fig. 4*D*). Overall, these results demonstrate that the ATP synthase β-subunit is a novel cell death regulator identified via proteomics.

A

```
  1 MASRRVLSSL LRSSSGRSAA KLVNRNPRLP SPSPARHAAP CSYLLGRVAE
 51 YATSSPASSA APSSAPAKDE GKKTYDYGGK GAIGRVCQVI GAIVDVRFED
101 QEGLPPIMTS LEVQDHPTRL VLEVSHHLGQ NVVRTIAMDG TEGLVRGRKV
151 LNTGAPITVP VGRATLGRIM NVLGEPIDER GEIKTEHYLP IHRDAPALVD
201 LATGQEILAT GIKVVDLLAP YQRGGKIGLF GGAGVGKTVL IMELINNVAK
251 AHGGFSVFAG VGERTREGND LYREMIESGV IKLGEKQSES KCALVYGQMN
301 EPPGARARVG LTGLTVAEYF RDAEGQDVLL FIDNIFRFTQ ANSEVSALLG
351 RIPSAVGYQP TLASDLGALQ ERITTTKKGS ITSVQAIYVP ADDLTDPAPA
401 TTFAHLDATT VLSRQISELG IYPAVDPLDS TSRMLSPHIL GEEHYNTARG
451 VQKVLQNYKN LQDIIAILGM DELSEDDKLT VARARKIQRF LSQPFHVAEI
501 FTGAPGKYVD LKENINSFQG LLDGKYDDLS EQSFYMVGGI DEVVAKAEKI
551 AKESAA
```

B

```
  1 MASRRVLSSL LRSSSGRSAA KLVNRNPRLP SPSPARHAAP CSYLLGRVAE
 51 YATSSPASSA APSSAPAKDE GKKTYDYGGK GAIGRVCQVI GAIVDVRFED
101 QEGLPPIMTS LEVQDHPTRL VLEVSHHLGQ NVVRTIAMDG TEGLVRGRKV
151 LNTGAPITVP VGRATLGRIM NVLGEPIDER GEIKTEHYLP IHRDAPALVD
201 LATGQEILAT GIKVVDLLAP YQRGGKIGLF GGAGVGKTVL IMELINNVAK
251 AHGGFSVFAG VGERTREGND LYREMIESGV IKLGEKQSES KCALVYGQMN
301 EPPGARARVG LTGLTVAEYF RDAEGQDVLL FIDNIFRFTQ ANSEVSALLG
351 RIPSAVGYQP TLASDLGALQ ERITTTKKGS ITSVQAIYVP ADDLTDPAPA
401 TTFAHLDATT VLSRQISELG IYPAVDPLDS TSRMLSPHIL GEEHYNTARG
451 VQKVLQNYKN LQDIIAILGM DELSEDDKLT VARARKIQRF LSQPFHVAEI
501 FTGAPGKYVD LKENINSFQG LLDGKYDDLS EQSFYMVGGI DEVVAKAEKI
551 AKESAA
```

FIG. 3. **ATP synthase β-subunit sequence and sequence coverage.** *A*, sequence coverage by peptides identified from ATP synthase β-subunit in spot 33 (shown in Fig. 2*A*) of the TSP fraction. *B*, sequence coverage by peptides identified from ATP synthase β-subunit in spot 39 (shown in Fig. 2*B*) of the microsomal protein fraction. Residues in bold constitute the trypsin-generated peptides identified by mass spectrometry. Underlined residues form the cleavable predicted mitochondrial targeting sequence.

DISCUSSION

Rationale of using FB1 and an ATP Filter to Identify eATP-regulated Proteins—In order to identify eATP effectors and target proteins, we sought to use an experimental system in which endogenous eATP is depleted so as to trigger changes in the abundance of proteins whose gene expression is tightly regulated by the presence of eATP. This could easily be achieved using enzymatic eATP-sequestering systems such as exogenous apyrase or a glucose/hexokinase mixture. However, we chose to use FB1 treatments, which have been shown to activate progressive depletion of eATP prior to the onset of cell death (5). The advantage of this system is twofold. First, eATP diminishes gradually, which enables the reverse treatment of replenishing eATP in FB1-treated cultures by addition of exogenous ATP. Such a treatment would filter out proteins responding to FB1 only from those responding to FB1-induced eATP removal. Second, FB1 is linked to a physiologically relevant process because it is a pathogen-derived

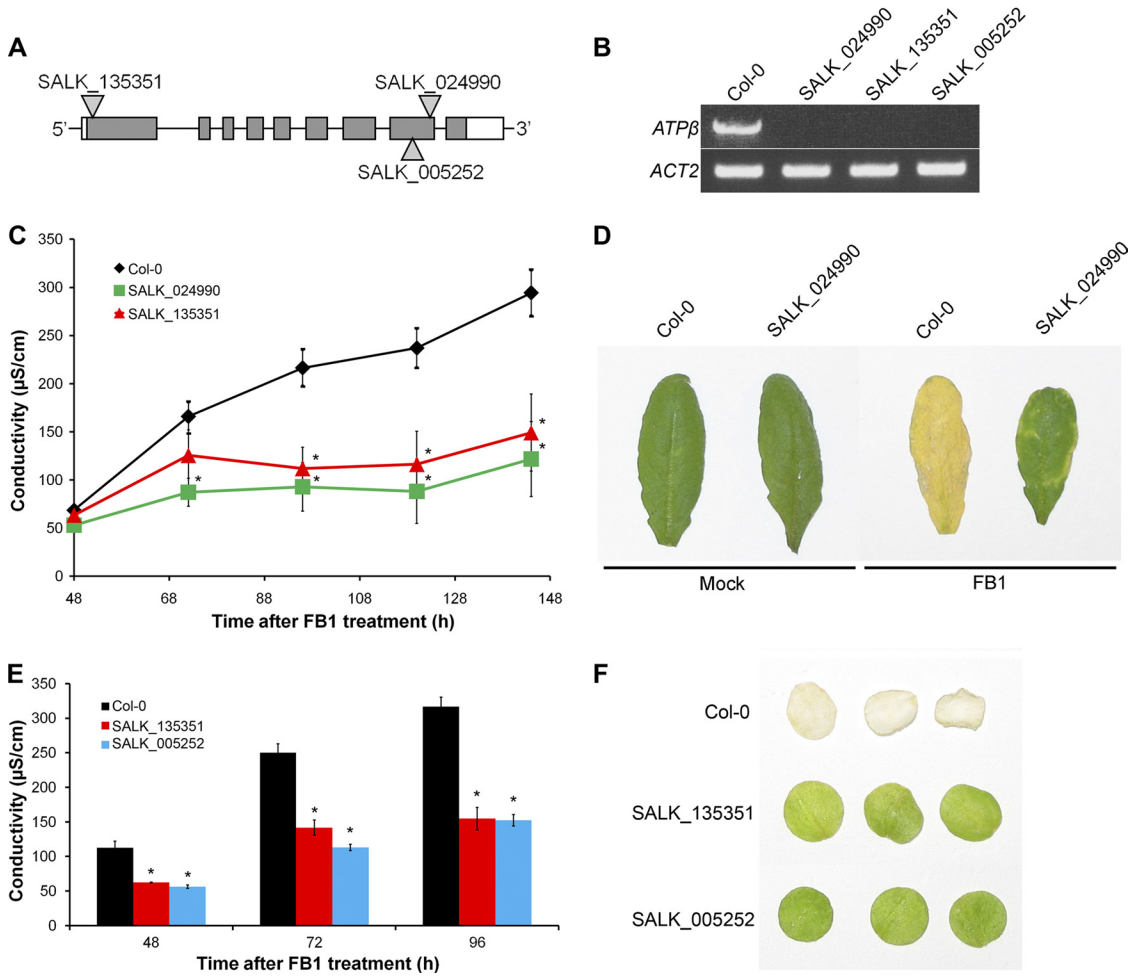

FIG. 4. **ATP synthase β-subunit gene knockout mutant plants are resistant to FB1.** *A*, schematic diagram showing T-DNA insertion sites in three independent knockout mutants (SALK_024990, SALK_135351, and SALK_005252). Inverted triangles indicate insertion sites and gray boxes represent exons. *B*, RT-PCR amplification of *ATP β-synthase subunit* (*ATPase-β*) in RNA samples derived from Columbia-0 (Col-0) plants and the three independent T-DNA insertion mutants. *Actin-2* (*ACT2*) was used as a constitutive reference control. *C,* cell death profiles of leaf disc tissues. Leaf discs were treated with FB1 and incubated in the dark for 48 h and then exposed to light. The conductivity of FB1 solutions on which discs were floating was measured at 48 h and every 24 h thereafter. Values and error bars represent means ± se ($n = 3$). An asterisk indicates data points at which the mutants are significantly ($p < 0.05$) lower that the wildtype (Col-0). *D,* appearance of Col-0 and SALK_024990 leaves 4 days after infiltration with FB1. *E*, leaf disc cell death assay with SALK_135351 and SALK_005252 as described in (*C*). *F*, leaf discs treated as described in (*E*) and photographed at 96 h.

toxin whose use could result in a better understanding of events surrounding cell death processes triggered by certain plant pathogens. Presently it is not clear how endogenous eATP is depleted, but using FB1 can provide clues that may lead to discovery of the mechanism by which pathogens deplete eATP. Because cell cultures treated with FB1 are primed for eATP depletion, we used an excessive concentration of exogenous ATP, as high as 1 mM, to ensure that the FB1-induced eATP deficit was cancelled for the duration of the treatment.

Proteomic Changes Underlying the Switch to FB1-induced Cell Death—There was a clear up-surge in the abundance of molecular chaperones in response to FB1 treatment (Table I and II). This group of proteins is important for maintaining cellular homeostasis by regulating protein folding, assembly, translocation, and degradation (40). Heightened expression of chaperone genes during stress is designed to re-establish normal protein conformation, thereby mitigating the adverse effects of stress (41). Because FB1 activates programmed cell death preceded by a shift in cellular metabolism underpinned by drastic changes in global gene expression, it is not surprising that chaperone proteins are deployed to accommodate the accompanying increased traffic through protein synthesis, translocation and degradation pathways. Not only does FB1 activate cell death processes, but also triggers pathogen defense systems that include synthesis of an array of pathogenesis-related proteins (30), most of which transit through the endoplasmic reticulum and increase the demand for chaperones. Similar chaperone increases occur in *Arabidopsis* responding to programmed cell death-eliciting patho-

gens (42) or exogenous plant hormones (43, 44), which activate enormous changes in the transcriptome. Remarkably, exogenous ATP blocked the rise in chaperone levels, indicating that this response was triggered by the cell death signal depletion of eATP.

Our study has revealed that a prime target for FB1 is cellular ATP synthesis. We identified subunits of the vacuolar and chloroplastic ATP synthase proteins as responsive to FB1, with the great majority belonging to the mitochondrial F_1F_0-ATP synthase machinery. The mitochondrial F_1F_0-ATP synthase has two main parts; the hydrophilic catalytic F_1 complex and the transmembrane proton-transporting F_0 subcomplex. We identified subunits α, β, and δ of the F_1 complex and subunit-D of the F_0 complex. Consistent with our findings, other cell death treatments, such as oxidative stress, have been reported to suppress expression of α-subunit and β-subunit genes (45). Though not determined experimentally in this study, the repression of ATP synthase proteins by FB1 is likely to disrupt oxidative phosphorylation and lead to a significant depression in cellular ATP levels. Harpin, a pathogen-derived cell death-activating elicitor, disrupts oxidative phosphorylation by triggering cytochrome *c* release (46), thereby inhibiting mitochondrial ATP production prior to onset of cell death (46, 47). Reduction in cellular ATP could likely account for growth retardation imposed by FB1 on *Arabidopsis* (5) as general metabolism is slowed. However, the fact that exogenous ATP blocked the suppression of ATP synthase genes by FB1 provides a profoundly fascinating insight. Extracellular ATP appears to positively regulate mitochondrial ATP synthesis, directly linking the cell death trigger—eATP depletion—to the key organelle now established as a central hub for programmed cell death control (48). Thus eATP depletion, driven by FB1 treatment (5), negatively regulates intracellular ATP production, which may lead to decreased ATP secretion that further reduces eATP. This step could serve as a signal amplification loop to ensure the onset of cell death in response to FB1 treatment.

Among the proteins differentially expressed following FB1 treatment were several enzymes involved in protecting cells from oxidative damage. Glutathione transferase and 2-alkenal reductase play significant roles in plant detoxification of lipid peroxide-derived cytotoxic compounds (49, 50). Monodehydroascorbate reductase and dehydroascorbate reductase (Table I) function in the anti-oxidant glutathione-ascorbate cycle (51) whereas thioredoxin (Table I) together with thioredoxin reductase constitute the thioredoxin anti-oxidant system (52). Except for glutathione transferase and 2-alkenal reductase that increased, all the other anti-oxidative enzymes were down-regulated by FB1 (Table I). An overall reduction of these enzymes may account for the observed accumulation of ROS in *Arabidopsis* plants exposed to FB1 (30). ROS can function as signaling molecules (53) or triggers of cell death by attacking membrane lipids to give rise to phytotoxic lipid peroxides (54). Shutdown of some anti-oxidative enzymes and up-regulation of others by FB1 (Table I) could be indicative of a finely tuned balance between harnessing the signaling capability of ROS and tightly controlling their propensity to trigger membrane damage and cell death. Attenuation of FB1 effects on these proteins by exogenous ATP (Table I) implicates them as regulatory or effector elements downstream of eATP signaling in cell death control.

Glycolysis proved to be a major target for FB1 suppression as reflected by seven different proteins belonging to the pathway that were identified as down-regulated proteins (Table I). The reduction in these proteins inevitably constricts flux through the pathway, a strategy that could be useful to divert energy and metabolites toward essential processes required for the response to FB1. For example, up-regulation of components of the amino acid biosynthetic pathways (Table I) could provide building blocks for pathogenesis-related protein synthesis that is triggered by FB1 (30). In addition, slowing down central metabolic pathways could also starve the cells of energy in preparation for programmed cell death. In rescuing the cells from death, exogenous ATP did not attenuate the response of all the glycolytic proteins to FB1, but it enhanced the suppression of some (Table I). This possibly indicates the need for ATP to reset the global metabolic processes in a highly ordered fashion before the full switch back to normal metabolism can be achieved. Reasons for the targeting of glycolytic enzymes by FB1 and exogenous ATP in this study may not be simplistic. It is now known that hexokinase, which catalyzes the first commitment step of glycolysis, is a critical regulator of programmed cell death in plants (55) and animals (56, 57). Glyceraldehyde-3-phosphate dehydrogenase (GAPDH) is now known to translocate to the nucleus of neuronal cells (58) where it activates apoptosis (58, 59). In view of this, a possible role for GAPDH, and the other glycolytic proteins identified in this study, in FB1-induced cell death warrants investigation.

Enzymes of the protein degradation machinery also responded to FB1 treatment (Table I). Changes in protein abundance in response to treatment may entail synthesis of new proteins, for up-regulation, and degradation of existing proteins, for down-regulation. Thus, it is not surprising that the cellular protein degradation machinery was invoked by FB1. A previous study reported that an E3 ubiquitin ligase is a critical regulator of FB1-induced cell death in *Arabidopsis* (60), revealing a crucial function of the ubiquitin-dependent protein degradation pathway in this response. However, an interesting observation is that exogenous ATP did not significantly attenuate the FB1 effects on 4 of the 5 protein spots in this category (Table I). This probably implies that in resetting metabolism from inception of cell death to normal growth metabolism, exogenous ATP requires the action of the protein degradation machinery to eradicate prodeath proteins that had accumulated prior to its addition. Thus, both FB1 and exogenous ATP may recruit the same processes, but for different purposes.

Finally, the rest of the unclassified proteins differentially expressed in response to FB1 reveal that the toxin effects are widespread. The significance of a majority of these proteome changes is not yet clear to us, but when more data on the physiological effects of FB1 on *Arabidopsis* become available in the future, our data sets could prove useful in understanding the basis for FB1 action.

ATP Synthase β-subunit is a Novel Cell Death Signal Regulator—Reverse genetics, using T-DNA insertional mutants from the SALK collection, in combination with FB1 treatments revealed a new role for ATP synthase β-subunit in the regulation of cell death. Although the use of sequence-indexed T-DNA mutants accelerates gene discovery, occasionally the observed phenotype is caused by a secondary mutation and not by the T-DNA-tagged gene indexed in the mutant collection database. Therefore, confirmation of the observed phenotype with either a second independent mutant line or complementation of mutant plants with a copy of the native gene is required (61–63). In this study, we used three independent T-DNA mutant lines and all gave the same phenotype, confirming that ATP synthase β-subunit has a pro-cell death function in *Arabidopsis*.

In two-dimensional gels of microsomal membrane fractions, ATP synthase β-subunit existed as a charge train of seven spots of ~55 kDa and an extra spot (spot 39) of ~49 kDa (Fig. 2*B*). Another ATP synthase β-subunit spot (spot 33) of ~38 kDa was identified in the TSP fraction (Fig. 2*A*). ATP synthase β-subunit has 566 amino acid residues and, according to MitoProt II prediction algorithm (64), the first 38 residues on the N terminus constitute the cleavable mitochondrial targeting sequence. Therefore, the mature sequence with 528 residues has a predicted molecular weight of 54,586.03 Da, which is very close to the experimentally determined molecular weight of ~55 kDa we observed for the charge train (Fig. 2*B*). All the seven ~55 kDa spots in the charge train were down-regulated in response to FB1 whereas the ~38 kDa and ~49 kDa were up-regulated (Tables I and II). The basis for the appearance of these lower molecular weight species is still unclear, but they possibly could arise from proteolytic processing of the ~55 kDa protein spots. If all the amino acids upstream of the identified most extreme N-terminal peptide and downstream of the identified most extreme C-terminal peptide (Fig. 3*A*) were cleaved off from the protein sequence, the predicted size of the truncated sequence becomes ~38.7 kDa, which almost matches the experimentally determined size of the ~38 kDa TSP low molecular weight spot (spot 33, Fig. 2*A*). Doing the same for the ~49 kDa microsomal spot based on the identified peptides (Fig. 3*B*) yields a putative product whose predicted size of ~47.6 kDa is close to the low molecular weight observed on gels (Fig. 2*B*). Therefore, the increase in the abundance of the low molecular weight spots, which is reciprocated by a decrease in the ~55 kDa charge train, could be accounted for by post-translational cleavage of the mature protein. The protein could be proteolytically processed in response to FB1 and ATP treatment protects it from degradation. The respective contribution to cell death regulation of the intact and truncated protein forms and the responsible proteases await further investigation.

The finding that FB1-induced eATP depletion down-regulates the abundance of *Arabidopsis* ATP synthase β-chain subunit agrees with our previous findings in tobacco. Treatment of tobacco with β,γ-methylene adenosine 5′-triphosphate (AMP-PCP), a nonhydrolysable ATP analog that interferes with eATP signaling, causes a dramatic suppression of several subunits of mitochondrial and chloroplast ATP synthase proteins (23). Therefore, eATP depletion achieved by FB1 treatment or by competitive exclusion from its binding sites with excess amounts of AMP-PCP have the same effect on mitochondrial and chloroplast ATP synthase proteins. Given that the γ phosphate of AMP-PCP is recalcitrant to cleavage, we can conclude that eATP-mediated regulation of ATP synthase proteins in *Arabidopsis* may similarly require cleavage of the γ phosphate as in tobacco (23). The nature of this reaction will become clear once the primary eATP target or receptor protein(s) in the extracellular matrix are identified. Although ATP synthase proteins had been identified as eATP-regulated proteins in tobacco (23), we still did not know which eATP controlled physiological processes these proteins mediated. Therefore, in addition to confirming the previous findings in tobacco (23), the current study has now revealed a novel function of the *Arabidopsis* ATP synthase β-subunit in cell death regulation.

The mechanism by which ATP synthase β-subunit promotes death is the focus of current research in our laboratory. Nevertheless, we envisage three possible ways by which ATP synthase β-subunit could perform this function. First, it could directly interact with other core cell death factors in a protein complex that is independent from its classical function in ATP production. This would be similar to cytochrome *c*, a mitochondrial oxidative phosphorylation protein, which translocates to the cytosol, following exposure to a cell death stimulus, and forms a complex with caspase-9 and Apaf-1 to initiate apoptosis (65). Second, ATP synthase β-subunit might be capable of influencing gene expression directly or indirectly, thereby activating cell death genes. Cytosolic proteins such as gluceraldehyde-3-phosphate dehydrogenase (58) and enolase (66) are now known to translocate to the nucleus to affect gene expression, though they are classical glycolytic enzymes. ATP synthase β-subunit could have a similar secondary function in regulation of gene expression as revealed by altered basal expression of several genes in the knockout mutant plants (data not shown). Finally, ATP synthase β-subunit within the F_1 complex could be targeted for direct binding by FB1 or another prodeath protein/signal, leading to an inhibition of mitochondrial ATP production. Likewise, the basis for phytotoxicity of tentoxin, another fungal-derived toxin, is cellular depletion of ATP caused by inhibition of chloroplastic photophosphorylation (67). In this scenario, FB1 resistance

in the At5g08690 knockout mutants could result from the lack of a binding site in the mitochondrial F_1 complex as the target At5g08690 gene product would be absent and replaced by products from one of the two other family members, At5g08680 and At5g08670. The *Arabidopsis* ATP synthase β-subunit protein belongs to a multigene family consisting of three members having 98% sequence similarity at the amino acid level, with differences only in the first 61 amino acids, making this region an ideal focal point for future genetic analyses to determine the basis for its cell death promotional function. Certain residues of the chloroplastic ATP synthase β-subunit were found to be critical for binding of the cell death-inducing tentoxin to the chloroplast F_1-ATP synthase (68). Mutagenesis of a specific chloroplastic ATP synthase β-subunit gene codon of tentoxin-resistant *Chlamydomonas reinhardtii* to match the corresponding codon of tentoxin-sensitive *Nicotiana* species rendered the alga tentoxin-sensitive (68), demonstrating very specific structural requirements for chloroplastic ATP synthase β-subunit function in cell death promotion. Similarly, a single amino acid substitution in the chloroplastic β-subunit switched tentoxin-resistant F_1-ATP synthase of thermophilic *Bacillus* PS3 to a tentoxin-sensitive enzyme (69). A similar situation could account for the nonredundant function of At5g08690 gene product in cell death as revealed by FB1 resistance in the gene knockout plants.

Acknowledgments—We thank Bill Simon and Joanne Robson for help with MALDI-TOF MS analyses.

* This work was supported by BBSRC grant BBH0002831, and a Portuguese government FCT scholarship (SFRH/BD/28814/2006) awarded to D. F. A. T.

S This article contains supplemental Table 1.

§ To whom correspondence should be addressed: School of Biological and Biomedical Sciences, Durham University, Durham DH1 3LE, United Kingdom. Tel.: +44-191-3341253; Fax: +44-191-3341295; E-mail: a.r.slabas@durham.ac.uk.

¶ Both authors contributed equally to this work.

REFERENCES

1. Ivanova, E. P., Alexeeva, Y. V., Pham, D. K., Wright, J. P., and Nicolau, D. V. (2006) ATP level variations in heterotrophic bacteria during attachment on hydrophilic and hydrophobic surfaces. *Int. Microbiol.* **9,** 37–46
2. Ludlow, M., Traynor, D., Fisher, P., and Ennion, S. (2008) Extracellular ATP and ADP mediate Ca^{2+} influx in *Dictyostelium discoideum*. *Purinergic Signalling* **4,** S5–S6
3. Surprenant, A., and Evans, R. J. (1993) ATP in Synapses. *Nature* **362,** 211–212
4. Thomas, C., Sun, Y., Naus, K., Lloyd, A., and Roux, S. (1999) Apyrase functions in plant phosphate nutrition and mobilizes phosphate from extracellular ATP. *Plant Physiol.* **119,** 543–552
5. Chivasa, S., Ndimba, B. K., Simon, W. J., Lindsey, K., and Slabas, A. R. (2005) Extracellular ATP functions as an endogenous external metabolite regulating plant cell viability. *Plant Cell* **17,** 3019–3034
6. Kim, S. Y., Sivaguru, M., and Stacey, G. (2006) Extracellular ATP in plants. Visualization, localization, and analysis of physiological significance in growth and signaling. *Plant Physiol.* **142,** 984–992
7. Zimmermann, H. (2000) Extracellular metabolism of ATP and other nucleotides. *Naunyn-Schmiedebergs Arch. Pharmacol.* **362,** 299–309
8. Housley, G. D., Bringmann, A., and Reichenbach, A. (2009) Purinergic signaling in special senses. *Trends Neurosci.* **32,** 128–141
9. Komoszynski, M., and Wojtczak, A. (1996) Apyrases (ATP diphosphohydrolases, EC 3.6.1.5): Function and relationship to ATPases. *Biochim. Biophys. Acta.* **1310,** 233–241
10. Dichmann, S., Idzko, M., Zimpfer, U., Hofmann, C., Ferrari, D., Luttmann, W., Virchow, C., Jr, Di, Virgilio, F., and Norgauer, J. (2000) Adenosine triphosphate-induced oxygen radical production and CD11b up-regulation: Ca++ mobilization and actin reorganization in human eosinophils. *Blood* **95,** 973–978
11. Pines, A., Perrone, L., Bivi, N., Romanello, M., Damante, G., Gulisano, M., Kelley, M. R., Quadrifoglio, F., and Tell, G. (2005) Activation of APE1/Ref-1 is dependent on reactive oxygen species generated after purinergic receptor stimulation by ATP. *Nucleic Acids Res.* **33,** 4379–4394
12. Resta, V., Novelli, E., Di, Virgilio, F., and Galli-Resta, L. (2005) Neuronal death induced by endogenous extracellular ATP in retinal cholinergic neuron density control. *Development* **132,** 2873–2882
13. North, R. A., and Surprenant, A. (2000) Pharmacology of cloned P2X receptors. *Ann. Rev. Pharmacol. Toxicol.* **40,** 563–580
14. North, R. A. (2002) Molecular physiology of P2X receptors. *Physiol. Rev.* **82,** 1013–1067
15. Demidchik, V., Nichols, C., Oliynyk, M., Dark, A., Glover, B. J., and Davies, J. M. (2003) Is ATP a signaling agent in plants? *Plant Physiol.* **133,** 456–461
16. Jeter, C. R., Tang, W., Henaff, E., Butterfield, T., and Roux, S. J. (2004) Evidence of a novel cell signaling role for extracellular adenosine triphosphates and diphosphates in Arabidopsis. *Plant Cell* **16,** 2652–2664
17. Demidchik, V., Shang, Z. L., Shin, R., Thompson, E., Rubio, L., Laohavisit, A., Mortimer, J. C., Chivasa, S., Slabas, A. R., Glover, B. J., Schachtman, D. P., Shabala, S. N., and Davies, J. M. (2009) Plant extracellular ATP signalling by plasma membrane NADPH oxidase and Ca2+ channels. *Plant J.* **58,** 903–913
18. Foresi, N. P., Laxalt, A. M., Tonón, C. V., Casalongué, C. A., and Lamattina, L. (2007) Extracellular ATP induces nitric oxide production in tomato cell suspensions. *Plant Physiol.* **145,** 589–592
19. Wu, S. J., and Wu, J. Y. (2008) Extracellular ATP-induced NO production and its dependence on membrane Ca^{2+} flux in *Salvia miltiorrhiza* hairy roots. *J. Exp. Bot.* **59,** 4007–4016
20. Reichler, S. A., Torres, J., Rivera, A. L., Cintolesi, V. A., Clark, G., and Roux, S. J. (2009) Intersection of two signalling pathways: extracellular nucleotides regulate pollen germination and pollen tube growth via nitric oxide. *J. Exp. Bot.* **60,** 2129–2138
21. Song, C. J., Steinebrunner, I., Wang, X., Stout, S. C., and Roux, S. J. (2006) Extracellular ATP induces the accumulation of superoxide via NADPH oxidases in Arabidopsis. *Plant Physiol.* **140,** 1222–1232
22. Wu, S. J., Liu, Y. S., and Wu, J. Y. (2008) The signaling role of extracellular ATP and its dependence on Ca-2 flux in elicitation of Salvia miltiorrhiza hairy root cultures. *Plant Cell Physiol.* **49,** 617–624
23. Chivasa, S., Simon, W. J., Murphy, A. M., Lindsey, K., Carr, J. P., and Slabas, A. R. (2010) The effects of extracellular adenosine 5′-triphosphate on the tobacco proteome. *Proteomics* **10,** 235–244
24. Steinebrunner, I., Wu, J., Sun, Y., Corbett, A., and Roux, S. J. (2003) Disruption of apyrases inhibits pollen germination in Arabidopsis. *Plant Physiol.* **131,** 1638–1647
25. Tonón, C., Cecilia, Terrile, M., José, Iglesias, M., Lamattina, L., and Casalongué, C. (2010) Extracellular ATP, nitric oxide and superoxide act co-ordinately to regulate hypocotyl growth in etiolated Arabidopsis seedlings. *J. Plant Physiol.* **167,** 540–546
26. Clark, G., Torres, J., Finlayson, S., Guan, X., Handley, C., Lee, J., Kays, J. E., Chen, Z. J., and Roux, S. J. (2010) Apyrase (nucleoside triphosphate-diphosphohydrolase) and extracellular nucleotides regulate cotton fibre elongation in cultured ovules. *Plant Physiol.* **152,** 1073–1083
27. Tang, W., Brady, S. R., Sun, Y., Muday, G. K., and Roux, S. J. (2003) Extracellular ATP inhibits root gravitropism at concentrations that inhibit polar auxin transport. *Plant Physiol.* **131,** 147–154
28. McAlvin, C. B., and Stacey, G. (2005) Transgenic expression of the soybean apyrase in *Lotus japonicus* enhances nodulation. *Plant Physiol.* **137,** 1456–1462
29. Chivasa, S., Murphy, A. M., Hamilton, J. M., Lindsey, K., Carr, J. P., and Slabas, A. R. (2009) Extracellular ATP is a regulator of pathogen defence in plants. *Plant J.* **60,** 436–448
30. Stone, J. M., Heard, J. E., Asai, T., and Ausubel, F. M. (2000) Simulation of fungal-mediated cell death by fumonisin B1 and selection of fumonisin B1-resistant (fbr) Arabidopsis mutants. *Plant Cell* **12,** 1811–1822

31. Wang, H., Jones, C., Ciacci-Zanella, J., Holt, T., Gilchrist, D. G., and Dickman, M. B. (1996) Fumonisins and *Alternaria alternata lycopersici* toxins: Sphinganine analog mycotoxins induce apoptosis in monkey kidney cells. *Proc. Natl. Acad. Sci. U.S.A.* **93,** 3461–3465
32. Gilchrist, D. G. (1997) Mycotoxins reveal connections between plants and animals in apoptosis and ceramide signaling. *Cell Death Differ.* **4,** 689–698
33. Asai, T., Stone, J. M., Heard, J. E., Kovtun, Y., Yorgey, P., Sheen, J., and Ausubel, F. M. (2000) Fumonisin B1-induced cell death in Arabidopsis protoplasts requires jasmonate-, ethylene-, and salicylate-dependent signaling pathways. *Plant Cell* **12,** 1823–1836
34. May, M. J., and Leaver, C. J. (1993) Oxidative stimulation of glutathione synthesis in *Arabidopsis thaliana* suspension cultures. *Plant Physiol.* **103,** 621–627
35. Chivasa, S., Hamilton, J. M., Pringle, R. S., Ndimba, B. K., Simon, W. J., Lindsey, K., and Slabas, A. R. (2006) Proteomic analysis of differentially expressed proteins in fungal elicitor-treated Arabidopsis cell cultures. *J. Exp. Bot.* **57,** 1553–1562
36. Karp, N. A., Griffin, J. L., and Lilley, K. S. (2005) Application of partial least squares discriminant analysis to two dimensional difference gel studies in expression proteomics. *Proteomics* **5,** 81–90
37. Chivasa, S., Ndimba, B. K., Simon, W. J., Robertson, D., Yu, X. L., Knox, J. P., Bolwell, P., and Slabas, A. R. (2002) Proteomic analysis of the *Arabidopsis thaliana* cell wall. *Electrophoresis* **23,** 1754–1765
38. Oh, S. A., Lee, S. Y., Chung, I. K., Lee, C. H., and Nam, H. G. (1996) A senescence-associated gene of *Arabidopsis thaliana* is distinctively regulated during natural and artificially induced leaf senescence. *Plant Mol. Biol.* **30,** 739–754
39. Alonso, J. M., Stepanova, A. N., Leisse, T. J., Kim, C. J., Chen, H., Shinn, P., Stevenson, D. K., Zimmerman, J., Barajas, P., Cheuk, R., Gadrinab, C., Heller, C., Jeske, A., Koesema, E., Meyers, C. C., Parker, H., Prednis, L., Ansari, Y., Choy, N., Deen, H., Geralt, M., Hazari, N., Hom, E., Karnes, M., Mulholland, C., Ndubaku, R., Schmidt, I., Guzman, P., Aguilar-Henonin, L., Schmid, M., Weigel, D., Carter, D. E., Marchand, T., Risseeuw, E., Brogden, D., Zeko, A., Crosby, W. L., Berry, C. C., and Ecker, J. R. (2003) Genome-wide Insertional mutagenesis of *Arabidopsis thaliana. Science* **301,** 653–657
40. Miernyk, J. A. (1999) Protein folding in the plant cell. *Plant Physiol.* **121,** 695–703
41. Wang, W., Vinocur, B., Shoseyov, O., and Altman, A. (2004) Role of plant heat-shock proteins and molecular chaperones in the abiotic stress response. *Trends Plant Sci.* **9,** 244–252
42. Noël, L. D., Cagna, G., Stuttmann, J., Wirthmüller, L., Betsuyaku, S., Witte, C. P., Bhat, R., Pochon, N., Colby, T., and Parker, J. E. (2007) Interaction between SGT1 and cytosolic/nuclear HSC70 chaperones regulates Arabidopsis immune responses. *Plant Cell* **19,** 4061–4076
43. Schenk, P. M., Kazan, K., Wilson, I., Anderson, J. P., Richmond, T., Somerville, S. C., and Manners, J. M. (2000) Coordinated plant defense responses in Arabidopsis revealed by microarray analysis. *Proc. Natl. Acad. Sci. U.S.A.* **97,** 11655–11660
44. Wang, D., Weaver, N. D., Kesarwani, M., and Dong, X. (2005) Induction of protein secretory pathway is required for systemic acquired resistance. *Science* **308,** 1036–1040
45. Sweetlove, L. J., Heazlewood, J. L., Herald, V., Holtzapffel, R., Day, D. A., Leaver, C. J., and Millar, A. H. (2002) The impact of oxidative stress on Arabidopsis mitochondria. *Plant J.* **32,** 891–904
46. Krause, M., and Durner, J. (2004) Harpin inactivates mitochondria in Arabidopsis suspension cells. *Mol. Plant-Microbe Interact.* **17,** 131–139
47. Xie, Z., and Chen, Z. (2000) Harpin-induced hypersensitive cell death is associated with altered mitochondrial functions in tobacco cells. *Mol. Plant-Microbe Interact.* **13,** 183–190
48. Lam, E. Kato, N., and Lawton, M. (2001) Programmed cell death, mitochondria and the plant hypersensitive response. *Nature* **411,** 848–853
49. Marrs, K. A. (1996) The functions and regulation of glutathione S-transferases in plants. *Annu. Rev. Plant Physiol. Plant Mol. Biol.* **47,** 127–158
50. Mano, J., Belles-Boix, E., Babiychuk, E., Inzé, D., Torii, Y., Hiraoka, E., Takimoto, K., Slooten, L., Asada K., and Kushnir, S. (2005) Protection against photooxidative injury of tobacco leaves by 2-alkenal reductase. Detoxication of lipid peroxide-derived reactive carbonyls. *Plant Physiol.* **139,** 1773–1783
51. Noctor, G., and Foyer, C. H. (1998) Ascorbate and glutathione: keeping active oxygen under control. *Annu. Rev. Plant Physiol. Plant Mol. Biol.* **49,** 249–279
52. Holmgren, A. (1989) Thioredoxin and glutaredoxin systems. *J. Biol. Chem.* **264,** 13963–13966
53. Apel, K., and Hirt, H. (2004) Reactive oxygen species: Metabolism, oxidative stress, and signal transduction. *Ann. Rev. Plant Biol.* **55,** 373–399
54. Montillet, J. L., Chamnongpol, S., Rustérucci, C., Dat, J., van, de, Cotte, B., Agnel, J. P., Battesti, C., Inzé, D., Van, Breusegem, F., and Triantaphylidès, C. (2005) Fatty acid hydroperoxides and H_2O_2 in the execution of hypersensitive cell death in tobacco leaves. *Plant Physiol.* **138,** 1516–1526
55. Kim, M., Lim, J.-H., Ahn, C. S., Park, K., Kim, G. T., Kim, W. T., and Pai, H.-S. (2006) Mitochondria-associated hexokinases play a role in the control of programmed cell death in. *Nicotiana benthamiana. Plant Cell* **18,** 2341–2355
56. Downward, J. (2003) Metabolism meets death. *Nature* **424,** 896–897
57. Majewski, N., Noqueira, V., Bhaskar, P., Coy, P. E., Skeen, J. E., Gottlob, K., Chandel, N. S., Thompson, C. B., Robey, R. B., and Hay, N. (2004) Hexokinase-mitochondria interaction mediated by Akt is required to inhibit apoptosis in the presence or absence of Bax and Bak. *Mol. Cell* **16,** 819–830
58. Saunders, P. A., Chen, R. W., and Chuang, D. M. (1999) Nuclear translocation of glyceralaldehyde-3-phosphate dehydrogenase isoforms during neuronal apoptosis. *J. Neurochem.* **72,** 925–932
59. Ishitani, R., and Chuang, D. M. (1996) Glyceralaldehyde-3-phosphate dehydrogenase antisense oligonucleotides protect against cytosine arabinonucleoside-induced apoptosis in cultured cerebellar neurons. *Proc. Natl. Acad. Sci. U.S.A.* **93,** 9937–9941
60. Lin, S. S., Martin, R., Mongrand, S., Vandenabeele, S., Chen, K. C., Jang, I. C., and Chua, N. H. (2008) RING1 E3 ligase localizes to plasma membrane lipid rafts to trigger FB1-induced programmed cell death in Arabidopsis. *Plant J.* **56,** 550–561
61. Krysan, P. J., Young, J. C., and Sussman, M. R. (1999) T-DNA as an insertional mutagen in Arabidopsis. *Plant Cell* **11,** 2283–2290
62. Tax, F. E., and Vernon, D. M. (2001) T-DNA-associated duplications/translocations in Arabidopsis. Implications for mutant analysis and functional genomics. *Plant Physiol.* **126,** 1527–1538
63. Ajjawi, I., Lu, Y., Savage, L. J., Bell, S. M., and Last, R. L. (2010) Large-scale reverse genetics in Arabidopsis: case studies from the Chloroplast 2010 Project. *Plant Physiol.* **152,** 529–540
64. Claros, M. G., and Vincens, P. (1996) Computational method to predict mitochondrially imported proteins and their targeting sequences. *Eur. J. Biochem*. **241,** 779–786.
65. Li, P., Nijhawan, D., Budihardjo, I., Srinivasula, S. M., Ahmad, M., Alnemri, E. S., and Wang, X. (1997) Cytochrome *c* and dATP-dependent formation of Apaf-1/Caspase-9 complex initiates an apoptotic protease cascade. *Cell* **91,** 479–489
66. Lee, H., Guo, Y., Ohta, M., Xiong, L., Stevenson, B., and Zhu, J. K. (2002) LOS2, a genetic locus required for cold-responsive gene transcription encodes a bi-functional enolase. *EMBO J.* **21,** 2692–2702
67. Steele, J. A., Uchytil, T. F., Durbin, R. D., Bhatnagar, P., and Rich, D. H. (1976) Chloroplast coupling factor 1: A species-specific receptor for tentoxin. *Proc. Natl. Acad. Sci. U.S.A.* **73,** 2245–2248
68. Avni, A., Anderson, J. D., Holland, N., Rochaix, J. D., Gromet-Elhanan, Z., and Edelman, M. (1992) Tentoxin sensitivity of chloroplasts determined by codon 83 of beta subunit of proton-ATPase. *Science* **257,** 1245–1247
69. Groth, G., Hisabori, T., Lill, H., and Bald, D. (2002) Substitution of a single amino acid switches the tentoxin-resistant thermophilic F_1-ATPase into a tentoxin-sensitive enzyme. *J. Biol. Chem.* **277,** 20117–20119

Plant Signaling & Behavior 4:11, 1-3; November 2009; © 2009 Landes Bioscience

Extracellular ATP

A modulator of cell death and pathogen defence in plants

Stephen Chivasa,[1,2] Daniel F.A. Tomé,[2] Alex M. Murphy,[3] John M. Hamilton,[1,2] Keith Lindsey,[1,2] John P. Carr[3] and Antoni R. Slabas[1,2,*]

[1]Creative Gene Technology Ltd; The Integrative Cell Biology Laboratory; and [2]School of Biological and Biomedical Sciences; Durham University; Durham, UK; [3]Department of Plant Sciences; University of Cambridge; Cambridge, UK

Key words: extracellular ATP, pathogen defence, cell death, salicylic acid, tobacco

Submitted: 08/07/09

Accepted: 08/07/09

Previously published online: www.landesbioscience.com/journals/psb/article/9784

*Correspondence to:
Antoni R. Slabas; Email: a.r.slabas@durham.ac.uk

Addendum to: Chivasa S, Murphy AM, Hamilton JM, Lindsey K, Carr JP, Slabas AR. Extracellular ATP is a regulator of pathogen defence in plants. Plant J 2009; PMID: 19594709; DOI:10.1111/j.1365-313X.2009.03968.x.

Living organisms acquire or synthesize high energy molecules, which they frugally conserve and use to meet their cellular metabolic demands. Therefore, it is surprising that ATP, the most accessible and commonly utilised chemical energy carrier, is actively secreted to the extracellular matrix of cells. It is now becoming clear that in plants this extracellular ATP (eATP) is not wasted, but harnessed at the cell surface to signal across the plasma membrane of the secreting cell and neighbouring cells to control gene expression and influence plant development. Identification of the gene/protein networks regulated by eATP-mediated signalling should provide insight into the physiological roles of eATP in plants. By disrupting eATP-mediated signalling, we have identified pathogen defence genes as part of the eATP-regulated gene circuitry, leading us to the discovery that eATP is a negative regulator of pathogen defence in plants.[1] Previously, we reported that eATP is a key signal molecule that modulates programmed cell death in plants.[2] A complex picture is now emerging, in which eATP-mediated signalling cross-talks with signalling mediated by the major plant defence hormone, salicylic acid, in the regulation of pathogen defence and cell death.

The occurrence of eATP appears to be widespread across the plant kingdom—it has been directly or indirectly detected in many plant species including *Arabidopsis thaliana,*[2-5] *Zea mays,*[2] *Phaseolus vulgaris,*[2] *Nicotiana tabacum,*[1,2] *Medicago truncatula*[6] and *Salvia miltiorrhiza.*[7] The existence of eATP in all plant species investigated to date suggests that it likely has fundamental roles in plant growth and development. Although eATP is also found in vertebrate,[8,9] Drosophila[10] and microbial cells,[11] transcriptional induction of genes coding for key enzymes of plant hormone biosynthesis by eATP[4] points to the possibility that eATP-mediated signalling might have signalling functions unique to the plant kingdom. In our recent article[1] we indeed demonstrated a unique function of plant eATP—it is a negative regulator of pathogen defence gene expression and disease resistance. Here, we propose a model that predicts the existence of a new class of genes/proteins mediating eATP effects on defence gene expression and cell death. We call these eARPs for extracellular ATP regulated proteins (eARPs). We also discuss the complex relationship between eATP and salicylic acid (SA)-mediated signalling in the context of eARP regulation.

Extracellular ATP has been detected on the surfaces of intact plant leaves on which cuticle development has been suppressed by high humidity,[3] in the extracellular fluids of cell suspension cultures,[1,2] germinating pollen[5] and hydroponic plants,[2,4,12,13] on surfaces of root cells,[6] and in guttation fluids collected from intact leaves (Chivasa S, unpublished data). We previously demonstrated that enzymatic removal of eATP from these tissues or disruption of its signalling via competitive exclusion from target binding sites with the non-hydrolysable analogue β, γ-methyleneadenosine 5'-triphosphate (AMP-PCP), activates cell death.[2] Our recent results reveal that this cell death response is strongly regulated by light intensity.[1] This is reminiscent of

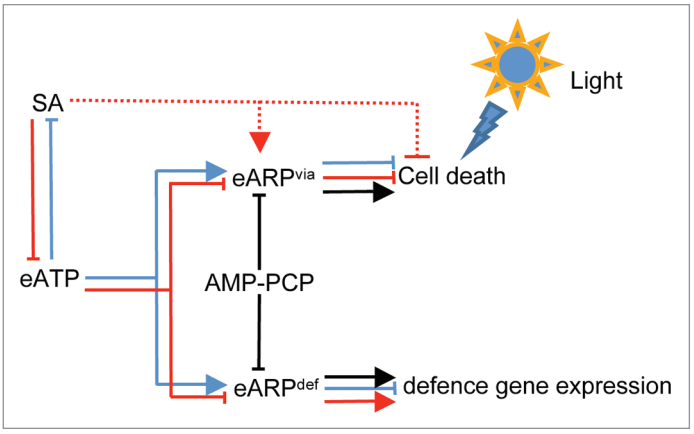

Figure 1. Model of how eATP- and SA-mediated signalling interconnect. Under normal growth conditions, basal SA levels do not deplete eATP. Basal eATP negatively regulates cell death and defence gene expression through eARP^{via} and eARP^{def} activity, respectively (blue lines). The red lines represent signalling activated by increases in tissue SA levels, caused by either exogenous application or elicitor/pathogen-induced biosynthesis. Inhibition of cell death by SA could involve signalling through eARP^{via} activity or another independent pathway (represented by dotted red lines). Black lines represent the outcome in response to addition of the non-hydrolysable ATP analogue, AMP-PCP. Cell death occurs in the presence of high light (~200 µmol.m^{-2}.s^{-1}). Pointed arrows denote activation; blunt-ending lines denote downregulation.

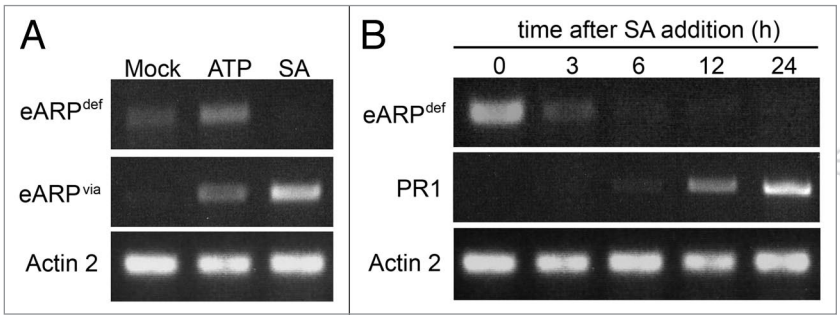

Figure 2. Gene expression in response to SA and ATP treatments. (A) RT-PCR analysis of putative Arabidopsis eARPs in cell culture samples treated with 1 mM ATP or 200 µM SA for 30 minutes or 24 h, respectively. (B) RT-PCR analysis of a putative eARP^{def} and PR1, an archetypal SA-inducible defence gene. Arabidopsis cell cultures were treated with 200 µM SA for the indicated time. Actin 2 served as a constitutive reference gene.

the requirement of light for hypersensitive cell death induced by certain incompatible pathogens.[14] This may indicate a possible involvement of chloroplasts in the cell death response as it has now been demonstrated that porphyrin/chlorophyll catabolites act as pro-death signals in plants[15,16] and are the basis for the spontaneous cell death in some lesion-mimic mutants.[17,18]

Although the initial receptor or target protein that directly interacts with eATP in the extracellular matrix or plasma membrane is unknown, downstream second messengers recruited for intracellular signalling include Ca^{2+} ions,[4,19,20] reactive oxygen species,[21,22] and nitric oxide.[20,23] A model of what we envisage to happen during eATP-mediated suppression of cell death and defence gene expression, based on our results in tobacco, is schematically depicted in **Figure 1**. We suggest that eATP signalling controls the expression of two sets of *eARP* genes, (i) *eARP* genes regulating cell death/viability (designated in our model as *eARP*^{via}) and (ii) *eARP* genes negatively-regulating pathogen defence genes (designated *eARP*^{def}). Under normal growth conditions, eATP-mediated signalling controls *eARP*^{via} genes, whose expression is required to suppress a default cell death pathway. Removal of eATP using glucose-hexokinase treatment disrupts expression of these genes, thereby triggering the onset of cell death. Impairment of eATP signalling via competitive exclusion with AMP-PCP will have a similar effect to that activated by glucose-hexokinase treatment. However, even though exogenous SA treatments cause eATP depletion, cell death does not occur because SA activates a separate signalling that protects against cell death.[1,15] The protective effects of SA may be mediated by positive regulation of *eARP*^{via} genes or different sets of genes/proteins that are not under eATP regulation.

Increases in SA via exogenous SA application, treatments with pathogen-derived elicitors,[24] or inoculation with incompatible pathogens,[25] will diminish the level of eATP.[1] Ablation of eATP downregulates *eARP*^{def} gene expression, which switches on expression of defence genes such as pathogenesis-related (*PR*) genes. Likewise, depletion of eATP by glucose-hexokinase or impairment of eATP signalling using AMP-PCP also disrupts expression of *eARP*^{def} genes—this switches on defence gene expression. Remarkably, increasing eATP by addition of exogenous ATP enhances the expression of *eARP*^{def} genes, which hinders basal disease resistance and renders the treated tissues more susceptible to pathogens. However, we acknowledge the possibility that regulation of eARPs by both eATP and SA could be post-transcriptional. We also note that the relationship between ATP and eATP is complex. Increasing eATP by infiltrating leaves with exogenous ATP triggers a decrease in the levels of SA. Exogenous SA also leads to a reduction in eATP. Therefore, these two signalling molecules mutually regulate their steady-state levels. Their effects on defence gene expression are antagonistic, while they both support cell viability.

We have investigated ATP-induced gene expression in Arabidopsis using whole genome DNA chips and identified several putative *eARP* genes. They fall into two categories with distinct expression profiles; (i) putative eARP^{via}, which respond similarly to both ATP or SA treatments, and (ii) putative eARP^{def}, which respond to SA in the opposite direction to their response to ATP (**Fig. 2A**). Our hypothesis states that exogenous SA treatment depletes eATP and should dismantle *eARP*^{def} gene expression in order to activate defence genes. In accordance with this, the putative

eARP^{def} is downregulated by SA (**Fig. 2A**) and its reduction precedes *PR*-1 transcript accumulation (**Fig. 2B**). Thus, Arabidopsis has putative eARPs whose gene expression profile fits our prediction of components involved in eATP regulatory functions. Current research in our group focuses on eARP identification and finding the subset that has a role in mediating eATP signalling in defence and cell death regulation.

In conclusion, our study has revealed a novel function of eATP—as a negative regulator of defence gene expression. The modulation of eATP levels by AMP-PCP, glucose-hexokinase, SA, and some pathogens mediates defence gene expression in tobacco. We have also proposed a model predicting the expression profiles of signalling genes downstream of eATP, which feed into inhibition of cell death or suppression of defence genes. We are currently testing this model in on-going research.

Acknowledgements

This work was supported by BBSRC grants to the A.R.S. (BB/D015987/1) and J.P.C. (BB/F014376/1) groups.

References

1. Chivasa S, Murphy AM, Hamilton JM, Lindsey K, Carr JP, Slabas AR. Extracellular ATP is a regulator of pathogen defence in plants. Plant J 2009; doi:10.1111/j.1365-313X.2009.03968.x.
2. Chivasa S, Ndimba BK, Simon JW, Lindsey K, Slabas AR. Extracellular ATP functions as an endogenous external metabolite regulating plant cell viability. Plant Cell 2005; 17:3019-34.
3. Thomas C, Rajagopal A, Windsor B, Dudler R, Lloyd A, Roux SJ. A role for ectophosphatase in xenobiotic resistance. Plant Cell 2000; 12:519-33.
4. Jeter CR, Tang W, Henaff E, Butterfield T, Roux SJ. Evidence of a novel cell signalling role for extracellular adenosine triphosphates and diphosphates in Arabidopsis. Plant Cell 2004; 16:2652-64.
5. Wu J, Steinebrunner I, Su Y, Butterfield T, Torres J, Arnold D, et al. Apyrases (Nucleoside Triphosphate-Diphosphohydrolases) play a key role in growth control in Arabidopsis. Plant Physiol 2007; 144:961-75.
6. Kim S-Y, Sivaguru M, Stacey G. Extracellular ATP in Plants. Visualization, localization and analysis of physiological significance in growth and signalling**.** Plant Physiol 2006; 142:984-92.
7. Wu S-J, Liu Y-S, Wu J-Y. The signaling role of extracellular ATP and its dependence on Ca^{2+} flux in elicitation of *Salvia miltiorrhiza* hairy root cultures. Plant Cell Physiol 2008; 49:617-24.
8. Holton P. The liberation of adenosine triphosphate on antidromic stimulation of sensory nerves. J Physiol (Lond) 1959; 145:494-504.
9. Parish RW, Weibel M. Extracellular ATP, ecto-ATPase and calcium influx in *Dictyostelium discoideum* cells. FEBS Lett 1980; 118:263-6.
10. Masse K, Bhamra S, Eason R, Dale N, Jones EA. Purine-mediated signalling triggers eye development. Nature 2007; 449:1058-62.
11. Ivanova EP, Alexeeva YV, Pham DK, Wright JP, Nicolau DV. ATP level variations in heterotrophic bacteria during attachment on hydrophilic and hydrophobic surfaces. International Microbiol 2006; 9:37-46.
12. Kim S-H, Yang SH, Kim T-J, Han JS, Suh J-W. Hypertonic stress increased extracellular ATP levels and the expression of stress-responsive genes in *Arabidopsis thaliana* seedlings. Biosci Biotechnol Biochem 2009; 73:1252-6.
13. Weerasinghe RR, Swanson SJ, Okada SF, Garrett MB, Kim S-Y, Stacey G, et al. Touch induces ATP release in Arabidopsis roots that is modulated by the heterotrimeric G-protein complex. FEBS Lett 2009; doi:10.1016/j.febslet.2009.07.007.
14. Zeier J, Pink B, Mueller MJ, Berger S. Light conditions influence specific defence responses in incompatible plant-pathogen interactions: uncoupling systemic resistance from salicylic acid and PR-1 accumulation. Planta 2004; 219:673-83.
15. Mach JM, Castillo AR, Hoogstraten R, Greenberg JT. The Arabidopsis-accelerated cell death gene ACD2 encodes red chlorophyll catabolite reductase and suppresses the spread of disease symptoms. Proc Natl Acad Sci USA 2001; 98:771-6.
16. Yao N, Greenberg JT. Arabidopsis ACCELERATED CELL DEATH2 modulates programmed cell death. Plant Cell 2006; 18:397-411.
17. Hu G, Yalpani N, Briggs SP, Johal GS. A porphyrin pathway impairment is responsible for the phenotype of a dominant disease lesion mimic mutant of maize. Plant Cell 1998; 10:1095-105.
18. Pruzinská A, Tanner G, Anders I, Roca M, Hörtensteiner S. Chlorophyll breakdown: pheophorbide a oxygenase is a Rieske-type iron-sulfur protein, encoded by the accelerated cell death 1 gene. Proc Natl Acad Sci USA 2003; 100:15259-64.
19. Demidchik V, Nichols C, Oliynyk M, Dark A, Glover BJ, Davies JM. Is ATP a signalling agent in plants? Plant Physiol 2003; 133:456-61.
20. Wu S-J, Wu J-Y. Extracellular ATP-induced NO production and its dependence on membrane Ca^{2+} flux in *Salvia miltiorrhiza* hairy roots. J Exp Bot 2008; 59:4007-16.
21. Song CJ, Steinebrunner I, Wang X, Stout SC, Roux SJ. Extracellular ATP induces the accumulation of superoxide via NADPH oxidases in Arabidopsis. Plant Physiol 2006; 140:1222-32.
22. Demidchik V, Shang Z, Shin R, Thompson E, Rubio L, Laohavisit A, et al. Plant extracellular ATP signalling by plasma membrane NADPH oxidase and Ca^{2+} channels. Plant J 2009; 58:903-13.
23. Foresi NP, Laxalt AM, Tonón CV, Casalongué CA, Lamattina L. Extracellular ATP induces nitric oxide production in tomato cell suspensions. Plant Physiol 2007; 145:589-92.
24. Dorey S, Baillieul F, Pierrel M-A, Saindrenan P, Fritig B, Kauffmann S. Spatial and temporal tnduction of cell death, defense genes and accumulation of salicylic acid in tobacco leaves reacting hypersensitively to a fungal glycoprotein elicitor. Molec Plant Microbe Interact 1997; 10:646-55.
25. Malamy J, Carr JP, Klessig DF, Raskin I. Salicylic acid: a likely endogenous signal in the resistance response of tobacco to viral infection. Science 1990; 250:1002-4.